

**Study of the activation mechanisms of the CXC chemokine receptor 4  
(CXCR4) and the atypical chemokine receptor 3 (ACKR3)**

**Untersuchung zum Aktivierungsmechanismus des CXC Chemokin-Rezeptor 4  
(CXCR4) und des atypischen Chemokin-Rezeptor 3 (ACKR3)**

Doctoral thesis for a doctoral degree  
at the Graduate School of Life Sciences,  
Julius-Maximilians-Universität Würzburg,  
Section: Biomedicine

submitted by

**Cristina Perpiñá Viciano**

from

Valencia (Spain)

Würzburg, 2019

Submitted on: .....

Members of the *Promotionskomitee*:

Chairperson: Prof. Dr. Manfred Gessler

Primary Supervisor: Prof. Dr. Carsten Hoffmann

Supervisor (Second): Prof. Dr. Elke Butt-Dörje

Supervisor (Third): Prof. Dr. Martin J. Lohse

Date of Public Defense: .....

Date of Receipt of Certificates: .....

## **Affidavit**

I hereby confirm that my thesis entitled "Study of the activation mechanisms of the CXC chemokine receptor 4 (CXCR4) and the atypical chemokine receptor 3 (ACKR3)" is the result of my own work. I did not receive any help or support from commercial consultants. All sources and / or materials applied are listed and specified in the thesis.

Furthermore, I confirm that this thesis has not yet been submitted as part of another examination process neither in identical nor in similar form.

Place, Date

Signature

## **Eidesstattliche Erklärung**

Hiermit erkläre ich an Eides statt, die Dissertation „Untersuchung zum Aktivierungsmechanismus des CXC Chemokin-Rezeptor 4 (CXCR4) und des atypischen Chemokin-Rezeptor 3 (ACKR3)" eigenständig, d.h. insbesondere selbständig und ohne Hilfe eines kommerziellen Promotionsberaters, angefertigt und keine anderen als die von mir angegebenen Quellen und Hilfsmittel verwendet zu haben.

Ich erkläre außerdem, dass die Dissertation weder in gleicher noch in ähnlicher Form bereits in einem anderen Prüfungsverfahren vorgelegen hat.

Ort, Datum

Unterschrift

## TABLE OF CONTENTS

SUMMARY .....	10
ZUSAMMENFASSUNG .....	11
1. INTRODUCTION .....	13
1.1. G PROTEIN-COUPLED RECEPTORS .....	13
1.1.1. Structure of GPCRs .....	13
1.1.2. Classification of GPCRs .....	14
1.1.3. GPCR activation and signaling pathways .....	15
1.1.3.1. GPCR activation .....	15
1.1.3.2. G protein-dependent signaling .....	16
1.1.3.3. G protein-independent signaling .....	18
1.1.3.4. Kinetics of the early events in the GPCR signaling cascade .....	19
1.2. THE CHEMOKINE:CHEMOKINE RECEPTOR NETWORK .....	21
1.2.1. Chemokines .....	22
1.2.1.1. CXCL12 .....	23
1.2.2. Chemokine receptors .....	24
1.2.3. Chemokine:chemokine receptor interaction .....	25
1.3. CXCR4 .....	26
1.3.1. CXCR4-mediated signaling in response to CXCL12 .....	26
1.3.2. Structure of CXCR4 .....	28
1.3.3. Oligomerization of CXCR4 .....	29
1.3.4. Stoichiometry of the CXCL12: CXCR4 complex .....	29
1.3.5. Other CXCR4 ligands .....	30
1.3.5.1. Macrophage migration inhibitory factor .....	30
1.3.5.2. Lactoferrin .....	32
1.4. ACKR3/CXCR7 .....	33
1.4.1. Ligand binding to ACKR3 .....	34
1.4.2. ACKR3 function and signaling .....	34
1.4.2.1. Scavenging function .....	34
1.4.2.2. G protein-mediated signaling .....	35
1.4.2.3. $\beta$ -arrestin-mediated signaling .....	35
1.4.3. ACKR3 oligomerization .....	36
1.5. FLUORESCENCE-BASED IMAGING METHODS TO STUDY GPCRS .....	37
1.5.1. Fluorescence .....	37
1.5.2. Fluorescent labeling strategies .....	37
1.5.3. Förster Resonance Energy Transfer .....	39
1.5.4. FRET to study kinetics of the early steps of the GPCR signaling cascade .....	40
2. MOTIVATION AND OBJECTIVES .....	43
3. MATERIALS AND METHODS .....	44
3.1. MATERIALS .....	44
3.1.1. DNA .....	44
3.1.2. Consumables .....	46
3.1.3. Ligands .....	48
3.1.4. Cell lines .....	49

3.1.4.1. Eukaryotic cell lines.....	49
3.1.4.2. Prokaryotic cell lines.....	49
3.1.5. Media for cell culture.....	49
3.1.5.1. Eukaryotic cell culture.....	49
3.1.5.2. Prokaryotic cell culture.....	49
3.1.6. Primers for cloning.....	50
3.1.7. Software.....	50
3.2. METHODS.....	51
3.2.1. Development of the CXCR4 constructs.....	51
3.2.2. Development of the ACKR3 constructs.....	52
3.2.3. PCR protocol.....	54
3.2.4. Restriction enzyme digestion.....	54
3.2.5. Ligations.....	55
3.2.6. DNA plasmid amplification and purification.....	55
3.2.6.1. Transformation of chemically competent <i>E. coli</i> cells.....	55
3.2.6.2. Extraction and purification of DNA plasmids.....	56
3.2.6.3. Determination of the DNA plasmid concentration.....	56
3.2.7. Eukaryotic cell culture.....	56
3.2.7.1. Maintenance routine.....	56
3.2.7.2. Mycoplasma contamination test.....	57
3.2.7.3. Freezing cells.....	57
3.2.7.4. Thawing frozen cells.....	58
3.2.8. FIAsh labeling of living cells.....	58
3.2.9. Confocal microscopy.....	58
3.2.10. FRET measurements in single cells.....	59
3.2.10.1. Microscopic set-up for FRET experiments.....	59
3.2.10.2. Determination of the FRET efficiency.....	59
3.2.10.3. Biopen® microchannel pipette.....	60
3.2.10.4. Kinetic measurements.....	60
3.2.10.5. Acceptor photobleaching in receptor/G protein interaction studies.....	61
3.2.11. Concentration-response curves in 96-well plates.....	62
3.2.11.1. Microplate reader.....	62
3.2.11.2. Experimental procedure.....	62
3.2.11.3. Data analysis.....	64
3.2.12. G protein activity in 96-well plates.....	64
3.2.13. Membrane preparation.....	65
3.2.14. Radioligand competition binding assays.....	66
3.2.15. Luciferase reporter assay.....	66
4. RESULTS.....	67
4.1. CXCR4.....	67
4.1.1. Design of FRET-based CXCR4 sensors.....	67
4.1.2. Characterization of the FRET-based CXCR4 sensors.....	69
4.1.2.1. Expression and localization.....	69
4.1.2.2. FRET efficiency.....	70
4.1.2.3. Downstream signaling properties.....	73
4.1.3. Activation of CXCR4 in response to CXCL12.....	75

4.1.4. Interaction of CXCR4 with G <sub>i</sub> proteins. ....	77
4.1.5. G protein activation mediated by CXCR4 in response to CXCL12. ....	80
4.1.6. Structural rearrangements between CXCR4 protomers in response to CXCL12. ....	83
4.1.7. Investigating the stoichiometry of CXCR4 in complex with CXCL12. ....	85
4.1.8. Characterization of other CXCR4 ligands. ....	86
4.1.8.1. Macrophage migration inhibitory factor. ....	86
4.1.8.2. Lactoferrin. ....	90
4.2. ACKR3. ....	92
4.2.1. Design of FRET-based ACKR3 sensors. ....	93
4.2.2. Characterization of the FRET-based ACKR3 sensor. ....	93
4.2.2.1. Expression and localization. ....	93
4.2.2.2. FRET efficiency. ....	94
4.2.2.3. Ligand binding. ....	97
4.2.3. Activation of ACKR3 in response to CXCL12. ....	98
4.2.4. Activation of ACKR3 in response to other ligands. ....	98
4.2.5. G protein activation mediated by ACKR3 in response to CXCL12. ....	101
5. DISCUSSION. ....	102
5.1. The FRET-based CXCR4 sensors report ligand-induced conformational changes in the receptor and reveal slower kinetics of CXCR4 activation in comparison to other well-known class A GPCRs. ....	102
5.2. CXCR4 exhibits a complex activation mechanism in response to CXCL12 as revealed by analysis of its early signaling steps. ....	104
5.3. MIF induces distinct structural rearrangements than CXCL12 in CXCR4 and does not activate G <sub>i</sub> proteins via this receptor. ....	105
5.4. Iron-bound lactoferrin, but not iron-free lactoferrin, leads to the activation of G <sub>12</sub> and G <sub>13</sub> proteins but not G <sub>11</sub> via CXCR4. ....	106
5.5. CXCR4 exhibits some degree of ligand-independent constitutive activity. ....	107
5.6. The HA-ACKR3-FIAsH-CFP sensor in combination with K44A dynamin is a powerful tool to investigate the ligand-induced activation of the receptor. ....	109
5.7. Re-localization of ACKR3 to the plasma membrane by using K44A dynamin is not sufficient to activate G proteins. ....	110
5.8. The Biopen <sup>®</sup> microfluidic system is suitable for kinetic studies. ....	111
5.9. Conclusions and future directions. ....	111
6. ANNEXES. ....	113
6.1. ABBREVIATIONS. ....	113
6.2. DNA SEQUENCES. ....	115
7. REFERENCES. ....	122
8. CURRICULUM VITAE. ....	138
9. ACKNOWLEDGMENTS. ....	141

## LIST OF FIGURES

Figure 1. GPCR architecture. ....	13
Figure 2. Receptor conformations in active ( $G_s$ and $G_{i/o}$ -bound) and inactive states. ....	16
Figure 3. Classical G protein-mediated signaling pathways. ....	16
Figure 4. Classical GPCR transduction pathways. ....	18
Figure 5. Functions regulated by chemokines and chemokine receptors. ....	22
Figure 6. Chemokines structure and classification. ....	23
Figure 7. Crystal structure of CXCL12. ....	23
Figure 8. CXCR4-mediated signaling in response to CXCL12. ....	27
Figure 9. CXCR4 structure. ....	28
Figure 10. MIF monomer crystal structure. ....	31
Figure 11. Conformational states of lactoferrin. ....	32
Figure 12. ACKR3-mediated signaling in response to CXCL12. ....	36
Figure 13. Jablonski diagram. ....	37
Figure 14. GFP and FIAsh. ....	39
Figure 15. Main requirements for FRET to occur between two fluorophores. ....	40
Figure 16. FRET-based approach. ....	41
Figure 17. FRET-based approaches to study the early steps of GPCR signaling. ....	42
Figure 18. Procedure to perform concentration-response curves in 96-well plate assay format. ....	63
Figure 19. Procedure to measure G protein activity in 96-well plate assay format. ....	65
Figure 20. Protein sequence of the human CXCR4 depicting the insertion positions of the tags and fluorophores used. ....	68
Figure 21. The CXCR4 constructs are expressed in the plasma membrane of HEK293 cells. ....	69
Figure 22. The CXCR4 sensors exhibit basal intramolecular FRET. ....	71-72
Figure 23. The FRET-based CXCR4 constructs preserve the ability to signal via $G_i$ proteins. ....	74
Figure 24. The FRET-based CXCR4 sensors report the dynamics and kinetics of receptor activation and deactivation. ....	76
Figure 25. CXCL12 binding to CXCR4 induces rearrangements between the receptor and the $G_{i1}$ protein. ....	78
Figure 26. CXCR4 and $G_{i1}$ proteins remain within FRET distance in the absence of agonist. ....	79
Figure 27. CXCR4 activates $G_{i1}$ , $G_{i2}$ , and $G_{i3}$ , but not $G_q$ , in response to CXCL12. ....	81

Figure 28. CXCR4 activates G <sub>i2</sub> proteins in the absence of agonist. ....	83
Figure 29. CXCL12 induces rearrangements between CXCR4 protomers. ....	84
Figure 30. The two mutations W94 and D97 do not impair the activation of CXCR4 or the rearrangement between protomers upon CXCL12 binding. ....	85
Figure 31. MIF binding induces structural rearrangements in CXCR4 but does not lead to G <sub>i</sub> protein activation via this receptor. ....	88
Figure 32. The kinetics of CXCR4 activation, CXCR4/G <sub>i</sub> interaction, and CXCR4 dimer rearrangement in response to CXCL12 are not affected by prior stimulation of the cells with MIF. ....	89
Figure 33. Fe <sub>2</sub> -Lf induces G <sub>i2</sub> and G <sub>i3</sub> but not G <sub>i1</sub> activation via CXCR4, while apo-Lf does not lead to activation of any G <sub>i</sub> protein subtype. ....	91
Figure 34. Protein sequence of the human ACKR3 depicting the insertion positions of the tags and fluorophores used. ....	92
Figure 35. Expression and localization of the different ACKR3 constructs analyzed by confocal microscopy. ....	95
Figure 36. The ACKR3 sensors exhibit basal intramolecular FRET. ....	96
Figure 37. Addition of the HA tag, the FAsH-binding motif, and/or CFP into ACKR3 do not affect its ability to bind CXCL12. ....	97
Figure 38. The FRET-based ACKR3 sensor combined with K44A dynamin reports the CXCL12-induced conformational changes in the receptor. ....	99
Figure 39. The FRET-based ACKR3 sensor combined with K44A dynamin is a valid tool to investigate the dynamics and kinetics of receptor activation in response to different ligands. ....	100
Figure 40. Re-localization of ACKR3 to the plasma membrane by using K44A dynamin is not sufficient to activate G <sub>i</sub> proteins. ....	101
Figure 41. Kinetics of the early reactions in the signaling cascade of GPCRs. ....	103



## LIST OF TABLES

Table 1. A-F classification system. ....	14
Table 2. GRAFS classification system. ....	14
Table 3. Families of G proteins and their members. ....	17
Table 4. Intra- and intermolecular FRET efficiency values of the CXCR4 constructs. ....	70
Table 5. EC <sub>50</sub> values for G protein activation mediated by different CXCR4 constructs in response to increasing concentrations of CXCL12. ....	73
Table 6. EC <sub>50</sub> values for FSK-induced cAMP inhibition mediated by different CXCR4 constructs in response to increasing concentrations of CXCL12. ....	74
Table 7. Summary of the parameters determined using the FRET-based CXCR4 sensors. ....	75
Table 8. Summary of the parameters determined for G protein activation mediated by the axis CXCL12/CXCR4, norepinephrine/ $\alpha_{2A}$ -AR, or ACh/M <sub>3</sub> -AChR. ....	82
Table 9. Summary of the on-kinetics determined for each of the processes studied for the axis MIF/CXCR4. ....	87
Table 10. Intra- and intermolecular FRET efficiency values of the ACKR3 constructs. ....	94
Table 11. IC <sub>50</sub> values resulting from the competitive binding assays performed with the different ACKR3 constructs. ....	97

## SUMMARY

The CXC chemokine receptor 4 (CXCR4) and the atypical chemokine receptor 3 (ACKR3) are seven-transmembrane receptors that are involved in numerous pathologies, including several types of cancers. Both receptors bind the same chemokine, CXCL12, leading to significantly different outcomes. While CXCR4 activation generally leads to canonical GPCR signaling, involving  $G_i$  proteins and  $\beta$ -arrestins, ACKR3, which is predominantly found in intracellular vesicles, has been shown to signal via  $\beta$ -arrestin-dependent signaling pathways. Understanding the dynamics and kinetics of their activation in response to their ligands is of importance to understand how signaling proceeds via these two receptors. In this thesis, different Förster resonance energy transfer (FRET)-based approaches have been combined to individually investigate the early events of their signaling cascades. In order to investigate receptor activation, intramolecular FRET sensors for CXCR4 and ACKR3 were developed by using the pair of fluorophores cyan fluorescence protein and fluorescence arsenical hairpin binder. The sensors, which exhibited similar functional properties to their wild-type counterparts, allowed to monitor their ligand-induced conformational changes and represent the first RET-based receptor sensors in the field of chemokine receptors. Additional FRET-based settings were also established to investigate the coupling of receptors with G proteins, rearrangements within dimers, as well as G protein activation. On one hand, CXCR4 showed a complex activation mechanism in response to CXCL12 that involved rearrangements in the transmembrane domain of the receptor followed by rearrangements between the receptor and the G protein as well as rearrangements between CXCR4 protomers, suggesting a role of homodimers in the activation course of this receptor. This was followed by a prolonged activation of  $G_i$  proteins, but not  $G_q$  activation, via the axis CXCL12/CXCR4. In contrast, the structural rearrangements at each step of the signaling cascade in response to macrophage migration inhibitory factor (MIF) were dynamically and kinetically different and no  $G_i$  protein activation via this axis was detected. These findings suggest distinct mechanisms of action of CXCL12 and MIF on CXCR4 and provide evidence for a new type of sequential signaling events of a GPCR. Importantly, evidence in this work revealed that CXCR4 exhibits some degree of constitutive activity, a potentially important feature for drug development. On the other hand, by co-transfecting the ACKR3 sensor with K44A dynamin, it was possible to increase its presence in the plasma membrane and measure the ligand-induced activation of this receptor. Different kinetics of ACKR3 activation were observed in response to CXCL12 and three other agonists by means of using the receptor sensor developed in this thesis, showing that it is a valuable tool to study the activation of this atypical receptor and pharmacologically characterize ligands. No CXCL12-induced G protein activation via ACKR3 was observed even when the receptor was re-localized to the plasma membrane by means of using the mutant dynamin. Altogether, this thesis work provides the temporal resolution of signaling patterns of two chemokine receptors for the first time as well as valuable tools that can be applied to characterize their activation in response to pharmacologically relevant ligands.

## ZUSAMMENFASSUNG

Der CXC Chemokin-Rezeptor 4 (CXCR4) und der atypische Chemokin-Rezeptor 3 (ACKR3) sind heptatransmembranäre Rezeptoren, die in zahlreichen Krankheitsbildern eine Rolle spielen, wie in einigen Krebsarten. Beide Rezeptoren werden zwar von dem gleichen Chemokin CXCL12 aktiviert, allerdings mit unterschiedlichen Signalweiterleitungsmustern. Die Aktivierung von CXCR4 führt zu kanonischer GPCR Signaltransduktion über Gi-Proteine und  $\beta$ -Arrestine. Die Signalweiterleitung des Rezeptors ACKR3 hingegen, welcher hauptsächlich in intrazellulären Vesikeln vorliegt, erfolgt über  $\beta$ -Arrestin-abhängige Signalwege. Es ist von großer Wichtigkeit die Dynamik und Kinetik dieser beiden Rezeptoren hinsichtlich der Aktivierung durch ihre Liganden und der Signalweiterleitung zu verstehen. In dieser Arbeit wurden verschiedene Förster-Resonanzenergietransfer (FRET) Anwendungen kombiniert, um die frühen Phasen der Signal-Kaskade von CXCR4 und ACKR3 zu untersuchen. Zur genaueren Aufklärung der Rezeptoraktivierung wurden intramolekulare FRET-Sensoren entwickelt, hierzu wurden die Fluorophore Cyan-fluoreszierendes Protein und engl. fluorescence arsenical hairpin binder verwendet. Die generierten Sensoren zeigten ähnliche funktionelle Eigenschaften wie die unveränderten Rezeptoren. Liganden-induzierte Änderungen der Rezeptorkonformation können mittels dieser Sensoren beobachtet werden und stellen die ersten RET-basierten Sensoren auf dem Forschungsgebiet der Chemokin-Rezeptoren dar. Weitere FRET-basierte Methoden wurden zur Untersuchung von Interaktionen zwischen Rezeptor und G-Protein, Neuordnung von Dimeren, sowie der G-Protein Aktivierung eingesetzt und für beide Chemokin-Rezeptoren etabliert. CXCR4 zeigte einen komplexen Aktivierungsmechanismus nach Stimulation durch CXCL12, bei welchem zunächst eine Neuordnung der Rezeptor-Transmembrandomäne gefolgt von Neuordnungen zwischen Rezeptor und G-Protein und zuletzt eine Neuordnung zwischen CXCR4 Protomeren erfolgte. Dies impliziert, dass im Aktivierungsprozess des Rezeptors Homodimere eine Rolle spielen. Zudem wurde eine verlängerte Gi -Protein Aktivierung gegenüber der Gq-Protein Aktivierung bei CXCL12 stimuliertem CXCR4 beobachtet. Hingegen zeigte eine Stimulierung mit dem Macrophage Migration Inhibitory Factor (MIF) bei jedem Schritt der frühen Singal-Kaskade veränderte Dynamiken und Kinetiken im Vergleich zu CXCL12. Darüber hinaus konnte keine Gi -Protein Aktivierung festgestellt werden. Dieser Befund zeigt individuelle Mechanismen für MIF und CXCL12 am CXCR4-Rezeptor und liefert Belege für eine neuer Art von sequenziellen Signalweiterleitungen an GPCRs. Eine wichtige Beobachtung dieser Arbeit für eine potentielle Medikamentenentwicklung ist das CXCR4 liganden-unabhängige Aktivität zeigt. Um die Aktivierung des ACKR3 Sensors messen zu können wurde durch eine Co-Transfektion mit K44A Dynamin eine höhere Membranständigkeit erreicht. CXCL12 und drei weiteren Agonisten zeigten am hier entwickelten ACKR3-Sensor unterscheidbare Kinetiken. Mit diesem wertvollen Werkzeug können Liganden an diesem atypischen Rezeptor pharmakologisch

charakterisiert werden. Es konnte keine CXCL12-induzierte G-Protein Aktivierung gemessen werden, trotz der stärkeren Präsenz an der Plasmamembran mit Hilfe der Dynamin-Mutante. In Summe liefert diese Arbeit zum ersten Mal eine zeitliche Auflösung von Signalweiterleitungsmustern von zwei Chemokin-Rezeptoren sowie wertvolle Werkzeuge zur Charakterisierung der frühen Phase der Signal-Kaskade durch andere pharmakologisch relevanten Liganden.

## 1. INTRODUCTION

### 1.1. G PROTEIN-COUPLED RECEPTORS.

Guanine nucleotide binding protein-coupled receptors (GPCRs) are the largest class of membrane proteins in the human genome, with almost 1000 members identified to date. These receptor proteins transduce extracellular signals of diverse nature (pheromones, photons, neurotransmitters, hormones, lipids, ions, small chemical agents, etc.) into intracellular responses in the cells, ultimately triggering a variety of cellular events that are determinant for a large number of biological processes. Consequently, alterations in the function or expression of these receptors result in a diverse number of pathologies, such as cardiovascular diseases, central nervous system (CNS) and immune disorders, and cancer (Insel et al., 2007). For this reason, GPCRs represent important therapeutic targets: ~34% of drugs approved by the food and drugs administration (FDA) are estimated to exert their clinical effects via GPCRs (Hauser et al., 2018).

#### 1.1.1. Structure of GPCRs.

Generally, GPCRs present a common architecture consisting of a single polypeptide chain with seven transmembrane (TM)-spanning (TM1-TM7) helices connected by three intracellular loops (ICL-1, ICL-2 and ICL-3) and three extracellular loops (ECL-1, ECL-2 and ECL-3), an extracellular amino-terminus, and an intracellular carboxy-terminus (**Figure 1A**). The helices are arranged in a circular fashion within the membrane, which, in many cases, contains the ligand binding site, normally accessible from the extracellular side (**Figure 1B**). While each TM domain is generally composed of around 20-27 amino acids, the C- and N-terminal domains as well as the loops can significantly vary in size. Remarkably, despite the overall conserved structural similarities, GPCRs are able to respond to a large repertoire of stimuli and differentially regulate complex signaling pathways and biological processes.

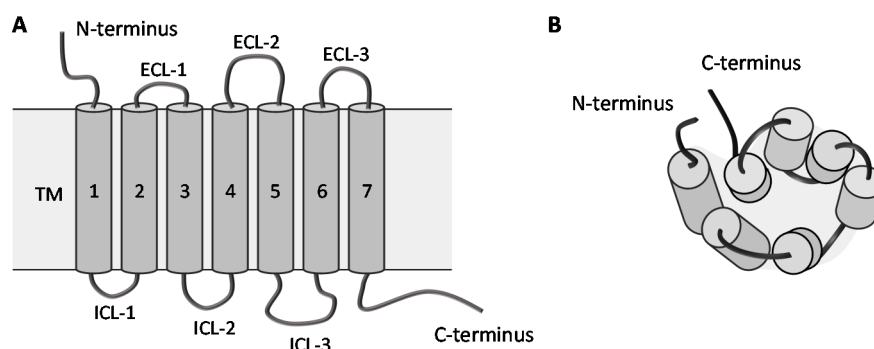


**Figure 1. GPCR architecture.** (A) Frontal view. (B) View from the extracellular side. Modified from Palmer, M. Biochemical Pharmacology, lecture notes, University of Waterloo.

### 1.1.2. Classification of GPCRs.

Over the years, several classification systems have been proposed in order to organize this superfamily of proteins. One of the most used classification systems is based on their amino acid sequences and functional similarities, and covers all known GPCRs from both vertebrates and invertebrates. This system presents 6 different classes, named from A to F, but class D and E do not exist in humans (Attwood and Findlay, 1994; Kolakowski, 1994; **Table 1**). Then, a novel classification system was proposed based on the phylogenetic analysis of approximately 800 human GPCR sequences. This system is called “GRAFS” and classifies the GPCRs into 5 families (Fredriksson et al., 2003; **Table 2**). The nomenclatures of both systems are partially overlapping. The main difference between these two is the subdivision of class B from the A-F system into two separate families in the GRAFS system, which gives rise to the adhesion family.

**Table 1. A-F classification system.**

Class	Family
A	Rhodopsin-like receptors
B	Secretin receptors
C	Metabotropic glutamate receptors
D	Fungal mating pheromone receptors
E	Cyclic AMP receptors
F	Frizzled/Smoothed receptors

**Table 2. GRAFS classification system.**

Class	Family
G	Glutamate
R	Rhodopsin
A	Adhesion
F	Frizzled/Taste2
S	Secretin

The rhodopsin family is the largest group of GPCRs (approximately 80% of GPCRs belong to this family) with four main groups named  $\alpha$ ,  $\beta$ ,  $\gamma$ , and  $\delta$ . It contains a diversity of GPCRs that transduce signals in response to a wide variety of stimuli. For instance, it includes the rhodopsin receptors, which are activated by light photons, and the chemokine receptors, which bind peptides of variable sizes. Most members share several structural characteristics, such as the NSxxNPxxY motif in TM7 and the DRY motif in the intracellular side of TM3, which are generally important determinants for the receptor conformational switch and G protein coupling (Ballesteros, Shi and Javitch, 2001; Kristiansen, 2004). Besides, some present an eighth helix in addition to the 7TM domain. Most GPCRs of this family bind their ligands directly in the TM cavity. In contrast, GPCRs from the other families often present long N-termini with specific domains that play a critical role in the binding of their ligands. For instance, many members of the secretin family present long N-termini stabilized by disulfide bonds and the binding mechanism of their ligands has been described to proceed via a “two-step mechanism” (Castro et al., 2005). Members of the glutamate family often present cysteine-rich domains in their long N-termini and form obligate dimers, which is crucial in their activation mechanism (El Moustaine et al., 2012).

### 1.1.3. GPCR activation and signaling pathways.

Upon activation in response to extracellular stimuli, GPCRs undergo conformational changes in their structures that allow them to interact with a variety of intracellular effectors, ultimately regulating a number of signaling cascades, including G protein-dependent and -independent.

#### 1.1.3.1. GPCR activation.

GPCR dynamics have been traditionally described by two-state models, in which receptors existed in either active or inactive conformations. Nevertheless, advances in crystallography, spectroscopy, and computer simulations in recent years have shown that GPCRs are highly dynamic entities that can adopt an infinite number of conformations (the term *conformation* refers to a particular three-dimensional snapshot of the protein at a single time point). Similar conformations can be clustered into groups, which are referred to as conformational states. This topic has been extensively reviewed by Manglik et al. (2015) and Latorraca, Venkatakrisnan and Dror (2017).

In the absence of ligand, receptors exist in equilibrium between multiple discrete conformational states. Binding of different ligands affects the dynamics of GPCRs in different manners. The largest effect is to shift the receptor population towards specific conformational states. Agonist binding shifts the equilibrium towards an active conformational state, increasing the level of activity. In contrast, binding of inverse agonists shifts the equilibrium towards an inactive conformational state and decreases the level of activity. Antagonists are neutral ligands that block ligand binding into the receptor without changing its activity. Some GPCRs intrinsically display high basal activity, also known as constitutive activity. This means that they undergo agonist-independent isomerization from inactive to active conformational states, which results in the agonist-independent activation of downstream signaling pathways. This has been described for more than 60 wild-type (wt) GPCRs. In addition, naturally-occurring mutations in GPCRs can also generate constitutively active receptors with increased basal activity in comparison to their wt counterparts, which is the cause of numerous diseases (Seifert and Wenzel-Seifert, 2002; Fukami et al., 2018).

GPCR activation involves conformational changes within the receptor that allow it to elicit an intracellular response. Crystal structures of many receptors in both inactive and active states indicate that the global conformational changes that occur upon activation are similar, particularly on the cytoplasmic side. The most common feature is a large outward shift of TM6 (ranging from 6 to 14Å, depending on the receptor/G protein pair studied) and small inward rotations and movements of TM5 and TM7 (**Figure 2**; Latorraca et al., 2017). This, combined with rearrangements of the loops, uncovers an intracellular site for the engagement of intracellular partners, such as G proteins or  $\beta$ -arrestins. The binding of the G protein to the agonist-bound GPCR further stabilizes the receptor in a fully active state (Mahoney and Sunahara, 2016).

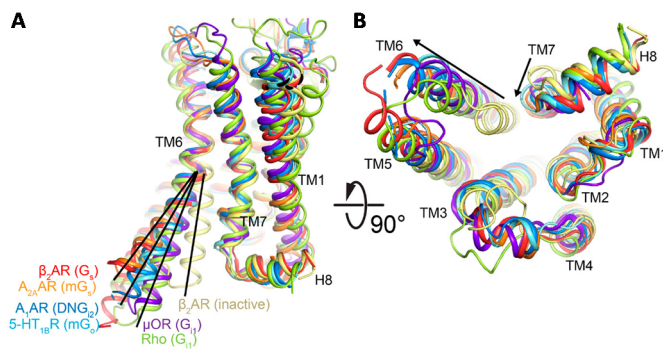


**Figure 2. Receptor conformations in active ( $G_s$ - and  $G_{i/o}$ -bound) and inactive states. (A) Side view. The position of TM6 is depicted with black lines. (B) View from the intracellular side. Arrows indicate the movement of TM6 and TM7 upon receptor activation. Adapted from Glukhova et al. (2018) with permission via RightsLink.**

### 1.1.3.2. G protein-dependent signaling.

Most GPCRs are able to signal through G proteins upon activation by a ligand. Heterotrimeric G proteins are composed of three subunits:  $G\alpha$ ,  $G\beta$ , and  $G\gamma$ . The two latter subunits can form a stable dimeric complex known as “ $G\beta\gamma$  complex”. There are 21 identified  $G\alpha$  isoforms in humans and at least 5 and 12 different  $G\beta$  and  $G\gamma$  subunits, respectively (Downes and Gautam, 1999). The formation of different combinations might depend on the expression pattern of the different subunits in specific cell types and, although specific combinations have been observed to not form, a large number of pairings is still possible.

G proteins are classified in four major families based on sequence homology between the identified  $G\alpha$  isoforms in the human genome:  $G_s$ ,  $G_{i/o}$ ,  $G_q$ , and  $G_{12/13}$ . These G protein subtypes regulate different downstream pathways.  $G_s$  proteins stimulate the activity of the enzyme adenylyl cyclase (AC), increasing cAMP levels, and thus the activity of cAMP-dependent protein kinases (PK), such as PKA. In contrast,  $G_{i/o}$  proteins have the opposite effect by inhibiting the activity of AC. The fact that  $G_{i/o}$  proteins are sensitive to pertussis toxin (PTX) facilitates the recognition of  $G_{i/o}$ -dependent responses. The  $G_q$  proteins stimulate the activation of phospholipase C (PLC)- $\beta$ , which in turn produces  $Ca^{2+}$  release and activation of PKC. Last, the  $G_{12/13}$  proteins regulate the activity of Rho GTPases. The  $G\beta\gamma$  complex can recruit G protein receptor kinases (GRKs) to the membrane, regulate the activity of channels, such as G protein-coupled, inwardly rectifying  $K^+$  (GIRK) channels or  $Ca^{2+}$  channels, or the activity of kinases and phospholipases (Milligan and Kostenis, 2006). The main G protein-mediated pathways are displayed in **figure 3**. The families and subtypes of G proteins are displayed in **table 3**.

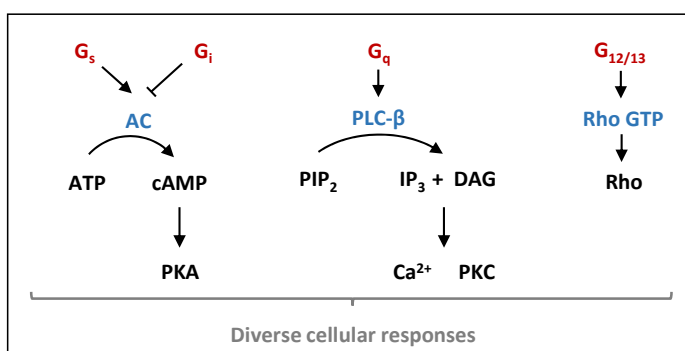


**Figure 3. Classical G protein-mediated signaling pathways.** The G protein families are shown in red and the downstream effector proteins in blue.



**Table 3. Families of G proteins and their members.**

Family	Members
<b>G<sub>s</sub></b>	G <sub>s</sub> , G <sub>olf</sub>
<b>G<sub>i/o</sub></b>	G <sub>i1</sub> , G <sub>i2</sub> , G <sub>i3</sub> , G <sub>oA</sub> , G <sub>oB</sub> , G <sub>t</sub> , G <sub>g</sub> , G <sub>z</sub>
<b>G<sub>q</sub></b>	G <sub>q</sub> , G <sub>11</sub> , G <sub>14</sub> , G <sub>15/16</sub>
<b>G<sub>12/13</sub></b>	G <sub>12</sub> , G <sub>13</sub>

In the inactive state, the G $\alpha$  subunit is bound to GDP and associates with the G $\beta\gamma$  complex, forming the inactive heterotrimer. Activation of the receptor promotes the engagement of the G protein on its intracellular side and triggers the dissociation of GDP from the G $\alpha$  subunit. The nucleotide-binding site is rapidly occupied by GTP due its high intracellular concentration. Subsequently, the G $\alpha$  and G $\beta\gamma$  subunits dissociate due to induced conformational changes within the G $\alpha$  subunit and can further interact with or modulate different downstream effectors. G protein-mediated signaling is terminated when the G $\alpha$  subunit, which has intrinsic GTPase activity, hydrolyzes GTP to GDP. At this point, it reassociates with the G $\beta\gamma$  complex to form the inactive heterotrimer. This process is known as the G protein activation cycle (**Figure 4**; Oldham and Hamm, 2008). Some studies have proposed that some G $\alpha$  and G $\beta\gamma$  subunits do not completely dissociate upon activation but rather rearrange (Bünemann, Frank and Lohse, 2003; Galés et al., 2006).

Two major models have been proposed to explain the coupling mode of receptors and G proteins, which have been review by Hein and Bünemann (2009). On one hand, the “free-collision coupling” model postulates that receptors and G proteins freely diffuse and interact, but only active receptors couple productively to G proteins, leading to their activation. This model is supported by the observed signal amplification between receptors and G proteins (also referred to as “receptor reserve”), which could be explained by the fact that one receptor has free access to multiple G proteins and that they couple catalytically. On the other hand, the “pre-coupling” model postulates that G proteins form a stable complex with receptors regardless of their activation state. Activation of the receptor produces a conformational change in the pre-assembled complex that would immediately lead to G protein activation. Theoretically, pre-coupled complexes would contribute to fast activation kinetics. There are many observations coming from different type of studies that support each of these models. However, alternative models have also been proposed to explain or reconcile discrepant observations. For example, the existence of small limiting regions where receptors have free but limited access to G proteins has been proposed (Patel, Murray and Insel, 2008; Sungkaworn et al., 2017). Also, the possibility that receptors are pre-assembled with G proteins and switch to a collision mode after initial stimulation. It is also important to consider that the expression levels and mobility of the individual components in the different contexts studied might influence the outcomes and interpretation, or that the coupling mode might depend on the receptor/G protein pair considered or the context.

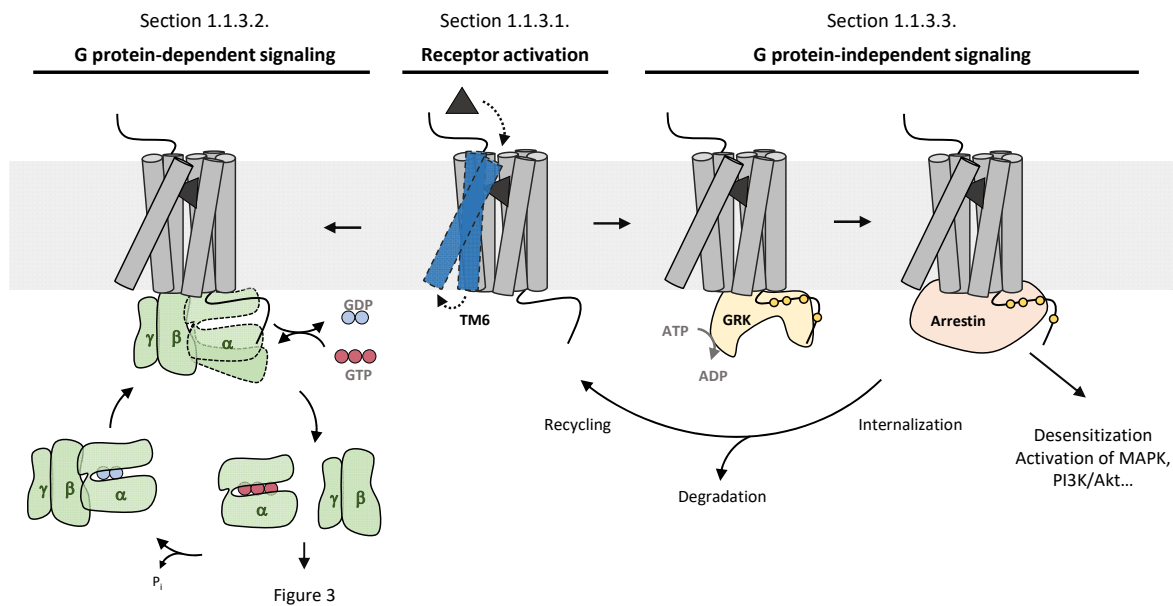


**Figure 4. Classical GPCR transduction pathways.** GPCRs can regulate diverse signaling pathways that can be G protein-dependent or -independent. Activation of the receptor leads to a conformational rearrangement which most common hallmark is an outward movement of TM6 (see figure 2). The activated receptor can then couple to different downstream effectors. Coupling to G proteins results in GDP/GTP exchange and dissociation of the  $G\alpha$  and  $G\beta\gamma$  subunits, which in turn regulate several downstream effectors (see figure 3). The activated receptor can be phosphorylated and engage  $\beta$ -arrestins, which can lead to desensitization, activation of downstream effectors, or internalization. The latter can result in either degradation or recycling to the plasma membrane.

### 1.1.3.3. G protein-independent signaling.

Upon activation by an agonist, GPCRs generally transmit a signal to G proteins and rapidly become phosphorylated (commonly at seryl/threonyl residues) by GRKs and/or other downstream-activated kinases, such as PKA and PKC (Komolov and Benovic, 2018). These phosphorylations on the intracellular side of the receptor were generally thought to prevent further activation of G proteins by the agonist-stimulated receptors and promote binding to  $\beta$ -arrestins, terminating G protein-dependent signaling. This process is known as receptor desensitization. Nevertheless, over the past years, it has become clear that the role of  $\beta$ -arrestins goes beyond “blocking” the activated GPCRs/G protein-mediated signaling, and increasing number of roles for these proteins have emerged. These molecules can serve as signal transducers on their own, initiating or modulating the activity of several downstream effector proteins, such as Src kinases and mitogen-activated protein kinases (MAPK), including extracellular-regulated kinases (ERKs), p38 MAPK, and C-Jun N-terminal kinase (JNK) 3 (Buchanan and DuBois, 2006; DeWire et al., 2007; Gurevich and Gurevich, 2019). Whether  $\beta$ -arrestin-mediated signaling is completely independent of G proteins is still under intensive research and recent findings showed that in total absence of G protein activity, arrestin-mediated signaling in response to GPCR activation cannot be detected (Alvarez-Curto et al., 2016; Grundmann et al., 2018).

$\beta$ -arrestins also function as adaptor proteins, recruiting different partners to GPCRs and specifically targeting them for dynamin-dependent endocytosis via clathrin-coated vesicles. Internalization can be followed by dephosphorylation and subsequent receptor recycling or degradation (**Figure 4**). Interestingly, increasing evidence indicates that once internalized, some GPCRs can still continue to signal from endosomes (Calebiro et al., 2009; Calebiro and Godbole, 2018).

#### **1.1.3.4. Kinetics of the early events in the GPCR signaling cascade.**

Förster resonance energy transfer (FRET)-based approaches are very useful to investigate the dynamics and kinetics of the initial steps of GPCR activation and signaling in intact cells (Lohse, Nuber and Hoffmann, 2012). This approach is described in detail in section 1.5.4. By means of using intramolecular receptor sensors, activation kinetics on the order of 40-100 ms have been established for the  $\alpha_{2A}$ -,  $\beta_1$ - and  $\beta_2$ -adrenergic receptors (AR), adenosine A<sub>2A</sub> receptor (A<sub>2A</sub>-R), B<sub>2</sub>-bradykinin receptors, and various muscarinic acetylcholine receptors (AChR) in response to small agonist molecules (Vilardaga et al., 2003; Hoffmann et al., 2005; Rochais et al., 2007; Jensen et al., 2009; Maier-Peuschel et al., 2010; Ziegler et al., 2011; Hlavackova et al., 2012). Remarkably faster kinetics have been observed for the rhodopsin receptor with activation kinetics of about 1-2 ms in response to light (Knierim et al., 2007). In contrast, the activation rate of the class B parathyroid hormone receptor (PTHr) was  $\approx 1$ s upon stimulation with the large agonist ligand PTH(1-34), which association proceeds via a two-step binding mechanism (Vilardaga et al., 2003; Castro et al., 2005). An interesting case is the activation of dimeric receptors, which can be measured by intermolecular FRET between the protomers. For instance, class C metabotropic glutamate receptor 1 (mGluR1) form obligatory dimers, which is essential for their functioning. In this case, it has been demonstrated that initial inter-subunit rearrangements occur within 1-2 ms after agonist exposure, whereas conformational changes within the TM domain (intra-subunit rearrangements) occur within  $\approx 20$  ms (Grushevskiy et al., 2019). Hence, this suggests that motions within a single GPCR protomer are slower than motions between protomers relative to each other. Nonetheless, how protomers within a dimer specifically influence each other, the activation of the receptor, or the activation of downstream signaling partners is still an open question. Studies on  $\alpha_{2A}$ -AR/ $\mu$ -opioid heterodimers as well as mGluR1 homodimers suggest that only one of the protomers is activated (Hlavackova et al., 2005; Vilardaga et al., 2008). However, it appears clear now that activation of both protomers is required for full activation (Kniazeff et al., 2004; Grushevskiy et al., 2019).

G protein engagement to the receptor can occur as fast as receptor activation when G protein expression levels are high and therefore not limiting, with time constants ranging from 40 ms to 1 s, depending on the ligand/receptor pair (Hein et al., 2005; Hein et al., 2006; Ferrandon et al., 2009). Slower activation kinetics have been observed for G protein activation, which involves the exchange

of GDP for GTP and rearrangement/dissociation of the  $G\alpha$  and  $G\beta\gamma$  subunits. For adenosine and adrenergic receptors as well as histamine H1 receptor, G protein activation kinetics were in the range of 0.5-1s (Adjobo-Hermans et al., 2011; van Unen et al., 2016), while the kinetics for the PTHR were  $\approx 2$ s (Ferrandon et al., 2009). This last step is thus significantly slower than the previous ones and represents the rate-limiting step.

The direct interaction of receptors with GRKs has been observed to occur rapidly after receptor activation and to achieve the maximum after a few seconds or minutes, depending on the pair studied (Hasbi et al., 2004; Jorgensen et al., 2007; Jorgensen et al., 2008). However, these studies have been performed using different experimental set-ups with bioluminescence resonance energy transfer (BRET) technique and cannot be directly compared to the kinetic data presented above. Using a FRET approach again,  $\beta$ -arrestin interaction and activation has been investigated using the  $\beta_2$ -AR. While,  $\beta$ -arrestin interaction with the receptor was immediate upon agonist stimulation and occurred with a time constant of  $\sim 1.3$ s, the conformational change that represents activation occurred with a delay from the time of the stimulation and with a time constant of  $\sim 2.2$ s (Nuber et al., 2016). This same study observed that  $\beta$ -arrestin remained active after dissociating from the receptor, which would leave it available for further  $\beta$ -arrestin-mediated signaling. Studies have shown that receptor/ $\beta$ -arrestin interaction is highly dependent on GRKs, and that phosphorylation mediated by this group of kinases is the rate-limiting step (Krasel et al., 2004).

Overall, several studies indicate that the entire GPCR signaling cascade can be activated within a few hundred milliseconds to seconds. For example, for rhodopsin, the downstream closure of the cGMP-gated cation channels is observed within 200 ms (Makino, Wen and Lem, 2003), whereas for  $\alpha_{2A}$ - and  $\alpha_{2C}$ -ARs, opening of GIRK channels occurs within 200-500 ms (Bünemann et al., 2001). In the case of PTHR, cAMP production is initiated and reaches its maximal level within  $\approx 10$  s (Ferrandon et al., 2009).

## 1.2. THE CHEMOKINE:CHEMOKINE RECEPTOR NETWORK.

The chemokine network is a complex group of pro-inflammatory cytokines that were first recognized by their ability to act as chemoattractants. Hence, they are referred to as “chemotactic cytokines”. They exert their various biological functions by interacting with the subfamily of GPCRs known as chemokine receptors. In humans, at least 45 chemokines have been described, constituting the largest family of cytokines, as well as 22 chemokine receptors, constituting the largest branch of the  $\gamma$  subfamily of class A GPCRs (Hughes and Nibbs, 2018). The large number of chemokines in comparison to chemokine receptors implies redundancy in their interactions, with multiple ligands binding to the same receptor and vice versa (bidirectional promiscuity). Yet, some aspects suggest that under physiological conditions the system might not be as redundant as initially considered. For instance, chemokines differ in the cells that produce them, the stimuli that induce their release, and their binding affinity, biological efficacies and potencies. Additionally, they can be modified in multiple ways in their target environment. All these are likely to decrease the level of redundancy.

Chemokines and their receptors are key players in cell migration, particularly of leukocytes, which is critical for the development of the immune system under both homeostatic and inflammatory conditions, as well as immune surveillance (Esche, Stellato and Beck, 2005). However, they also regulate a number of other processes, as shown in **figure 5** (López-Cotarelo et al., 2017; Hughes and Nibbs, 2018). In addition to some subsets of leukocytes, other cell types, including neurons, astrocytes, epithelial, mesenchymal, and endothelial cells can also express chemokine receptors and respond to chemokines (Bleul et al., 1997; Cartier et al., 2005; Beck et al., 2006). As a result of shaping major physiological processes, this network of proteins is involved in many pathologies and diseases. For example, dysregulation or abnormal function has been linked to autoimmune diseases, including multiple sclerosis (Szczuciński and Losy, 2007) and rheumatoid arthritis (Szekanecz et al., 2010), infectious diseases, such as malaria (Ioannidis, Nie and Hansen, 2014) and AIDS (Suresh and Wanchu, 2006), and more recently, cancer (Chow and Luster, 2014). Consequently, great efforts to develop drugs to modulate the function of chemokine receptors are being done and, there are several FDA-approved drugs that target chemokine receptors (Woollard and Kanmogne, 2015; Bilgin and de Greef, 2016; Makita and Tobinai, 2017).

Two of the most studied axes in this network involve the CXC chemokine receptor 4 (CXCR4) and atypical chemokine receptor 3 (ACKR3), which bind the same chemokine, the CXC ligand 12 (CXCL12). However, the interaction of this ligand with these two receptors leads to significantly different outcomes. These axes CXCL12/CXCR4 and CXCL12/ACKR3 are the focus of this work and are further described in section 1.3 and section 1.4, respectively.

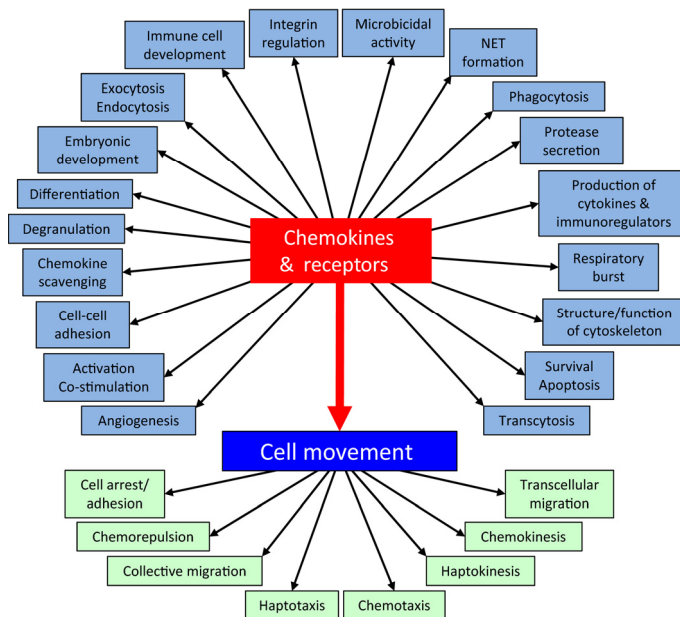


**Figure 5. Functions regulated by chemokines and chemokine receptors.** In blue, the processes reported to be regulated by this network of proteins. “Cell movement” in dark blue is the dominant process, with the different types of migratory behavior in green. Reproduced from Hughes and Nibbs (2018). (<https://febs.onlinelibrary.wiley.com/doi/full/10.1111/febs.14466>).

### 1.2.1. Chemokines.

Chemokines are proteins with a molecular weight usually between 7-12 kDa that present high structural homology. Their conserved topology consists of a disordered N-terminal tail, which plays a crucial role in the activation of chemokine receptors, followed by a more structured “globular core domain” that consists of an extended N-loop, three stranded anti-parallel  $\beta$ -sheets connected by loops (30s, 40s and 50s loops), and a  $\alpha$ -helix at the C-terminus (**Figure 6A**). Variation in the two conserved cysteines closest to the N-terminus of the mature proteins allows chemokines to be classified in four different subfamilies: XC, CC, CXC and CX<sub>3</sub>C, where X can be any amino acid. The XC chemokines lack two cysteines of the typical structure, containing a single one at the N-terminus; in CC chemokines the two cysteines at the N-terminus are directly juxtaposed, while CXC and CX<sub>3</sub>C chemokines have one and three amino acids between them, respectively (**Figure 6B**). These cysteine residues are structurally very important, stabilizing the conformation of the chemokine by forming disulfide bonds. All chemokines are produced with a signal peptide at the N-terminal end, which is removed before secretion. Besides, some present an extended C-terminus and can bind to the cell surface through a mucin-like domain, which can be cleaved later to release the proteins into the extracellular area (Hughes and Nibbs, 2018).

A systematic nomenclature to name the chemokines was introduced in 2000, which consists of the subfamily designation (XC, CC, CXC, CX<sub>3</sub>C), followed by “L” (ligand), and the number according to when the gene was first isolated (Murphy et al., 2000; Zlotnik and Yoshie, 2000). Most chemokines belong to the CC and CXC classes, while there are only two known XC chemokines and one known CX<sub>3</sub>C chemokine. The CXC family can be further subdivided into ELR+ and ELR-, depending on whether they contain the tripeptide ELR (Glu-Leu-Arg) motif at the N-terminus or not.

Chemokines can also be defined based on their functional properties. In a broad manner, they can be homeostatic or inflammatory. Homeostatic chemokines are constitutively expressed in certain tissues or organs and regulate the basal recruitment of cells involved in immune responses. Inflammatory chemokines are not abundantly expressed, but their expression is rapidly induced under certain circumstances, such as infection or tissue injury, which serves to recruit inflammatory leukocytes.

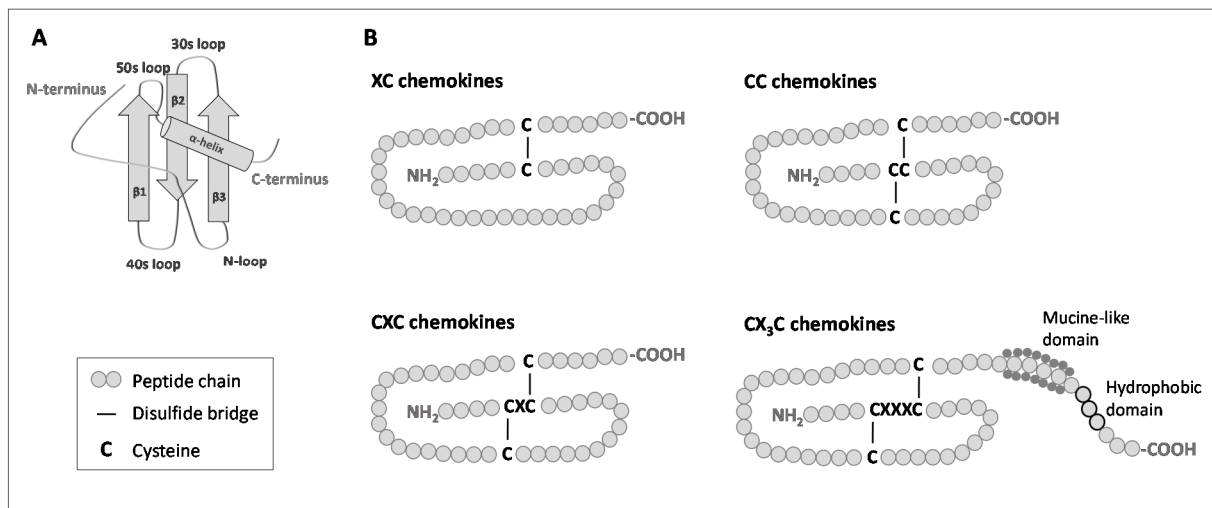


**Figure 6. Chemokines structure and classification. (A)** General conserved architecture of chemokines. **(B)** Classification of chemokines according to their cysteine motif, which is highlighted in black.

#### 1.2.1.1. CXCL12.

CXCL12, a homeostatic chemokine of about 8 kDa also known as stromal cell derived factor-1, presents the common architecture of CXC chemokines. Its N-terminus, particularly the residues Lys-1 and Pro-2 of the mature protein, play a crucial role in CXCR4 activation. The structural motif RFFESH near the N-terminus also plays a crucial role in directing the interaction with the receptor (**Figure 7**; Crump et al., 1997). CXCL12 is abundantly expressed in many tissues, including the brain, lung, thymus, heart, and the bone marrow (Lavi et al., 1998; Wang, Liu and Groopman, 1998; Wang, Park, and Groopman, 2000; Tham et al., 2001; Banisadr et al., 2003; Agarwal et al., 2016).

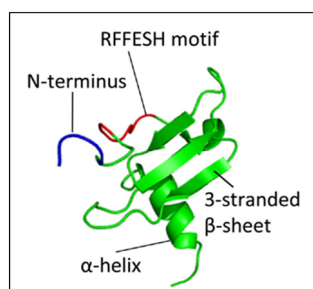


**Figure 7. Crystal structure of CXCL12.** Modified from Pawig et al. (2015). (<https://www.frontiersin.org/articles/10.3389/fimmu.2015.00429/full>).

The activity of CXCL12 is tightly regulated at multiple levels, which has been recently reviewed by Janssens, Struyf and Proost (2018). It is the only CXC chemokine which mRNA undergoes differential splicing, leading to the generation of six different splice variants in humans, named from  $\alpha$  to  $\phi$ . Each of them has a specific tissue distribution and *in vivo* activity. CXCL12 $\alpha$  is abundantly expressed and is the most studied form. The activity of CXCL12 is also regulated by post-translational modifications, including proteolytic removal of amino acids from the N- and C-terminus, citrullination of arginine residues, or nitration of tyrosine residues. These modifications generally inactivate or reduce the activity of the chemokine. Furthermore, CXCL12 can homo- and heterodimerize under physiological conditions. The equilibrium between monomeric and dimeric CXCL12 is potentially relevant since it has been shown that these two species exhibit different signaling through CXCR4 and ACKR3 (Drury et al., 2011; Ray et al., 2012a). In addition, CXCL12 can also form complexes with other chemokine and non-chemokine proteins, such as the nuclear protein high mobility group box 1 (HMGB1; Schiraldi et al., 2012), CCL5, CXCL4, and CXCL7 (Carlson et al., 2013). Its oligomeric state is modulated by pH, concentration, the presence of divalent cations as well as glycosaminoglycans (GAGs), which have recently emerged as important interaction partners for chemokines (Sadir et al., 2004; Crown et al., 2006; Poluri et al., 2013).

### 1.2.2. Chemokine receptors.

Chemokine receptors present the general common architecture of GPCRs. Their N-termini are generally acidic and often contain tyrosine residues that are post-translationally sulfated, which has been shown to modulate the affinity and potency of chemokine ligands and even play a role in selectivity (Ludeman and Stone, 2014). Their C-termini present numerous serine and threonine residues that are relevant for phosphorylation upon ligand binding to the receptor (Busillo et al., 2010; Mueller et al., 2013).

Chemokine receptors can be divided into two families: conventional chemokine receptors (cCKRs) and atypical chemokine receptors (ACKRs). A total of 22 chemokine receptors have been described to date in humans, from which 4 are ACKRs. Conventional receptors are classified according to the subfamily of chemokine they preferably bind and are named following the same principle as the chemokines, but replacing “L” by “R”, which denotes “receptor”. Most cCKRs belong to the CCR and CXCR classes, with 10 and 6 members, respectively, while there is only one CX<sub>3</sub>CR and one XCR (Hughes and Nibbs, 2018). Conventional receptors typically transduce their signals via G<sub>i</sub> proteins and  $\beta$ -arrestins, while the atypical receptors do not generally couple to G proteins and fail to induce typical transduction pathways activated by cCKRs.



### 1.2.3. Chemokine:chemokine receptor interaction.

In the mid-1990s, the interaction of chemokines with their receptors was described to proceed via a two-step/two-site mechanism. In this model, the globular core of the chemokine interacts with the N-terminus of the receptor, which is known as 'chemokine recognition site 1 (CRS1)'. Then, the flexible N-terminus of the chemokine interacts with the TM domain, which is known as 'chemokine recognition site 2 (CRS2)'. This model segregated the chemokine:receptor interactions functionally ('two-step') and spatially ('two-site'), with CRS1 defining specificity and affinity, and CRS2 mediating receptor activation (Montecarlo and Charo, 1996; Pakianathan et al., 1997). However, later functional and crystallographic studies challenged the structural and functional independence of these two sites and suggested that the model overlooks the complexity and diversity of chemokine:receptor interactions.

In 2015, the crystal structure of CXCR4 in combination with the chemokine antagonist vMIP-II was solved, as well as the structure of the human cytomegalovirus receptor US28 with the chemokine agonist CX<sub>3</sub>CL1 (Burg et al., 2015; Qin et al., 2015). Both structures confirmed the existence of CRS1 and CRS2 of the two-site model: the N-termini interact with the N-loop and 40s loop of the chemokines (CRS1) and the flexible N-termini of the chemokines reach into the TM pockets (CRS2). Interestingly, both structures showed an extensive and continuous interacting surface spanning from the proximal N-termini part until the upper part of the TM domain that did not present clear boundaries with CRS1 and CRS2. This intermediate region was thus named CRS1.5 and likely acts as a flexible pivot point to allow the rotation of the chemokine, providing some freedom in its positioning (Qin et al., 2015). This intermediate region has been also observed in the structure of CCR5 in complex with the chemokine antagonist [5P7]CCL5 (Zheng et al., 2017). Furthermore, experimental data and modeling studies on several chemokine:receptor pairs, including CXCL12:ACKR3, suggest an additional interaction epitope in which the distal N-terminus of the receptor interacts with the  $\beta_1$ -strand of the CXC chemokines (Katancik, Sharma and de Nardin, 2000; Gustavsson et al., 2017). This region was termed CRS0.5 and is probably difficult to observe in crystal structures due to difficulties to detect and solve the flexible N-termini of receptors.

Altogether, numerous studies reveal a complex model of chemokine:receptor interaction and activation with extensive interacting interfaces that seem to be physically and allosterically linked. This has led to propose the binding mechanism as a complex "multi-site model", in which functionally distinct outcomes upon chemokine binding may be generated by a "selection" of a unique subset of interactions, binding modes, and conformations (Kleist et al., 2016).

### 1.3. CXCR4.

CXCR4 is broadly expressed in cells of the immune system, including most leukocyte subsets, as well as in stem cells in both blood and the bone marrow (Förster et al., 1998; Ara et al., 2003). It is also highly expressed in cells of the CNS and endothelial cells (Hesselgesser et al., 1997; Gupta et al., 1998). The cognate ligand for this receptor is the chemokine CXCL12. CXCR4-expressing cells respond to and migrate along CXCL12 gradients, which modulates their directional migration. This axis is crucial during early embryonic development for the correct formation of vascular, nervous, hematopoietic, and cardiac systems (Miller, Banisadr and Bhattacharyya, 2008). It is equally vital in adults for homing of hematopoietic precursor and stem cells in the bone marrow and their mobilization into peripheral blood and tissues as well for mediating immune cell movement (Moll and Ransohoff, 2010; Guyon, 2014). The relevance of this axis is well reflected by the fact that knock-out mice of either CXCL12 or CXCR4 are lethal and die at late gestational stage with highly similar phenotypes, including abnormalities in B cell lymphopoiesis, bone marrow colonization, blood vessel formation, and defects in cardiovascular and neuronal development (Nagasawa et al., 1996; Ma et al., 1998; Tachibana et al., 1998; Zou et al., 1998).

CXCR4 acts as a co-receptor for HIV-1 entry into T cells and is involved in a large number of diseases, including autoimmune, neurodegenerative, and cardiovascular diseases (Feng, et al., 1996; Döring et al., 2014; Bonham et al., 2018). In addition, increasing evidence has shown that CXCR4 is also involved in tumor growth and metastasis in more than 23 types of cancers (Chatterjee, Azad and Nimmagadda, 2014). Therefore, the CXCL12/CXCR4 axis represents an important therapeutic target. In fact, CXCR4 is the target of the FDA-approved drug Mozobil™ (AMD3100, Genzyme, Cambridge, USA), a small antagonist molecule that was approved in 2008 for hematopoietic stem cell mobilization after failed attempts to use it as a HIV inhibitor (Uy, Rettig and Cashen, 2008). Besides, more drugs against this target are currently under development for treating other pathologies (Walenkamp et al., 2017).

#### 1.3.1. CXCR4-mediated signaling in response to CXCL12.

In response to CXCL12, CXCR4 generally leads to the activation of G proteins of the G<sub>i</sub> subfamily. Accordingly, most of the outcomes related to its function described to date have been shown to be sensitive to PTX treatment (Busillo and Benovic, 2007; Heuninck et al., 2019). Activation of G<sub>i</sub> proteins results in inhibition of AC, ultimately reducing cAMP levels in the cell and therefore the activity of cAMP-dependent kinases such as PKA. At some extent, it also induces activation of PLC-β through the Gβγ subunits, leading to Ca<sup>2+</sup> release, and activation of phosphatidylinositol 3-kinase (PI3K), leading to the activation of ERK and Akt pathways. These various signaling routes result in diverse biological outcomes, such as cell proliferation, migration, adhesion, and survival.

CXCR4 has been shown to couple to and activate the G protein subtypes  $G_{i1}$ ,  $G_{i2}$ ,  $G_{i3}$ , and  $G_{i0}$  in response to CXCL12 stimulation using BRET. In particular, CXCR4 was observed to couple more efficiently to  $G_{i1}$  and  $G_{i2}$  subtypes than to  $G_{i3}$  and  $G_{i0}$  (Kleemann et al., 2008; Quoyer et al., 2013). No activation of  $G_z$  has been observed (Armando et al., 2014). In some contexts, CXCR4 has also been reported to signal via  $G_{i3}$  and  $G_q$  proteins. On one hand, CXCL12/CXCR4-induced migration in Jurkat T cells was regulated by the dual activation of Rho via  $G_{i3}$  and Rac via  $G_i$  (Tan et al., 2006), and this axis was crucial for the metastatic spread of basal-like breast cancer cells (Yagi et al., 2011). In addition, the CXCL12-induced trafficking of CXCR4 into Rab11+ endosomes was also controlled through the Rho/ $G_{i3}$  axis (Kumar et al., 2011). On the other hand, CXCL12-driven dissemination and invasion of T cell hybridomas in mice required  $G_q$  proteins (Soede et al., 2001), and CXCL12/CXCR4-driven chemotaxis was dependent on  $G_q$  in dendritic cells and granulocytes (Shi et al., 2007).

Following activation by CXCL12, phosphorylation of CXCR4 results in the recruitment of  $\beta$ -arrestin-1 and -2, leading to internalization of the receptor, more markedly via  $\beta$ -arrestin-2 (Cheng et al., 2000). In accordance, attenuated desensitization and enhanced G protein coupling of CXCR4 was observed in lymphocytes isolated from  $\beta$ -arrestin-2 knock-out mice (Fong et al., 2002). In line with the ability of  $\beta$ -arrestins to promote signaling, both  $\beta$ -arrestins have been reported to significantly enhance CXCR4-mediated p42/44 MAPK activation in response to CXCL12, promoting proliferation and survival.  $\beta$ -arrestin-2 also regulates the chemotactic response of cells via the activation of p38 MAPK. These two effects of  $\beta$ -arrestin on the CXCR4 function appear to be mediated through distinct interaction sites on CXCR4, including the C-terminus and ICL-3 (Cheng et al., 2000; Lagane et al., 2008). CXCR4 can also associate transiently with the Janus kinases (JAK) 2/3, leading to activation and nuclear translocation of several signal transducer and activator of transcription (STAT) proteins (Vila-Coro et al., 1999). **Figure 8** shows a schematic summary of the CXCR4-mediated signaling upon CXCL12 binding.

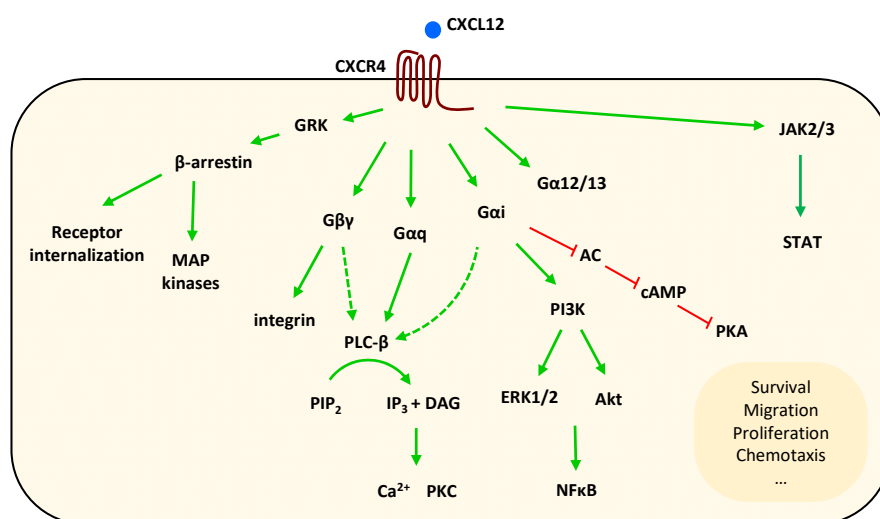


**Figure 8. CXCR4-mediated signaling in response to CXCL12.** Activation and inhibition of the primary pathways is depicted in green and red, respectively. Modified from Janssens et al. (2018).

### 1.3.2. Structure of CXCR4.

Three crystal structures have been reported for CXCR4, which is composed of 352 amino acids, in complex with different ligands: the small molecule IT1t, the cyclic peptide CVX15, and the viral CC chemokine vMIP-II (Wu et al., 2010; Qin et al., 2015).

These studies showed that the overall structure of CXCR4 resembles the common architecture of GPCRs with a seven transmembrane topology. In accordance with increasing biochemical and biophysical evidence that suggest that CXCR4 can form homo- and heterodimers (section 1.3.3), these crystal structures support the concept of CXCR4 dimerization. Importantly, several differences in comparison to other class A receptor structures could be observed. For instance, CXCR4 presents a larger ligand-binding pocket that is found closer to the extracellular surface. It is more solvent accessible and less protected by ECL-2, which might be due to the fact that it generally binds bigger ligands than other class A receptors. In addition, the N-terminus and the binding pocket are more acidic, which is consistent with the fact that the natural ligands are basic proteins. Many class A GPCRs contain a short 3-4 turn  $\alpha$ -helix at the C-terminus, named helix 8, with the characteristic motif F(R/K)xx(F/L)xxx(L/F). In contrast, CXCR4 only contains a partially conserved motif FKxxAxxxL that might be able to form a less stable helix (**Figure 9**). Also, it lacks a palmitoylation site right after this helix, which anchors other GPCRs to the lipid membrane, and the helix 7 is one turn shorter at the intracellular side (Arimont et al., 2017).

Highly conserved microswitches within GPCRs are known to control the G protein interface during inactive-to-active state transition. A thorough mutagenesis work by Wescott et al. (2016) identified several amino acids that are critical microswitch residues in CXCR4, including the tyrosine residue of the Y(x)<sub>5</sub>KL motif and the tyrosine residue of the NPxxY motif. Both structural motifs are critical determinants of GPCR activation, and homologous residues have been identified in other receptors. The DRY motif at the intracellular end of TM3 is highly conserved in many class A GPCRs. In most chemokine receptors, including CXCR4, this motif is “DRYLAIV”, in which the arginine residue is an important microswitch for the binding to G proteins.

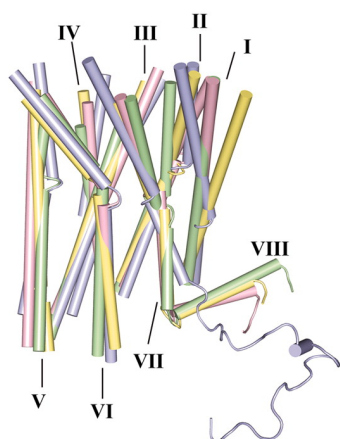


**Figure 9. CXCR4 structure.** Comparison of the CXCR4 structure (blue) with other GPCR structures:  $\beta_2$ -AR (yellow), A<sub>2A</sub>-AR (green) and rhodopsin (pink). Adapted from Wu et al., (2010) with permission via RightsLink.

### 1.3.3. Oligomerization of CXCR4.

Increasing number of studies suggest that oligomerization of GPCRs represents an important event in the activation process of the receptors and could open new avenues for drug targeting (Guidolin et al., 2019). Crystallization of CXCR4 in complex with various ligands revealed that CXCR4 forms homodimers (Wu et al., 2010; Qin et al., 2015). This is supported by biochemical and functional studies that showed that CXCR4 can form dimers even in the absence of ligand using a variety of techniques (Babcock, Farzan and Sodroski, 2003; Percherancier et al., 2005; Wang et al., 2006; Armando et al., 2014; Ge et al., 2017). Percherancier et al. (2005) demonstrated that CXCR4 forms homodimers and that addition of different ligands led to different changes in BRET without leading to dissociation, suggesting that they induce different conformational changes within the pre-formed complex. This is in line with the different crystal structures of CXCR4, in which slightly different dimer interfaces have been observed depending on the bound ligand: the dimer interface involved TM5/6 in the presence of IT1t, but also the intracellular tips of TM3/4 in the presence of CVX15 (Wu et al., 2010). In contrast, Lao et al., (2017) observed CXCR4 predominantly as a monomer at near-physiological expression levels in mammalian cells using single-cell microscopy.

CXCR4 has also been observed to oligomerize with several other chemokine receptors, including CCR2 (Sohy, Parmentier and Springael, 2007; Armando et al., 2014), CCR7 (Hayasaka et al., 2015), CCR5 (Hammad et al., 2010), CXCR3 (Watts et al., 2013), and ACKR3 (Hartmann et al., 2008; Levoye et al., 2009; Décaillot et al., 2011), as well as with other non-chemokine receptors, including  $\alpha_1$ -adrenergic (Tripathi et al., 2015; Gao et al., 2018) and  $\delta$ -opioid receptors (Pello et al., 2008). Although the fact that CXCR4 is able to form dimers or even higher-oligomeric structures has been well established, further studies are required to provide evidence of their functional importance in the activation transduction pathways and their relevance in the physiological context.

### 1.3.4. Stoichiometry of the CXCL12: CXCR4 complex.

As described previously (section 1.3.3), evidence from numerous studies showed that CXCR4 can form homodimers. Additionally, CXCL12 also exists in equilibrium as monomer and dimer (Ray et al., 2012a). This opens several possibilities regarding the stoichiometry for the chemokine:receptor complex, including the following: (i) 1:1 stoichiometry, with each receptor accommodating one monomeric ligand; (ii) 1:2 stoichiometry, with a single monomeric ligand binding simultaneously to each protomer of a dimer; (iii) a 2:1 stoichiometry, with a dimeric chemokine binding to one protomer; (iv) a 2:2 stoichiometry, with a dimeric chemokine binding to the receptor dimer.

By means of using functional complementation experiments, dimer dilution and cysteine trapping studies, Kufareva et al. (2014) showed that, despite the observed dimeric nature of CXCR4, this

receptor interacts with CXCL12 in a 1:1 stoichiometry. These results add to increasing evidence of monomers as fully competent signaling units (Whorton et al., 2007) yet does not dismiss the existence or potential role of dimers. This was further supported by the latest CXCR4 crystal structure in which CXCR4 interacted as a dimer with the chemokine vMIP-II in a 1:1 stoichiometry, with both subunits of the dimer occupied with one molecule of ligand (Qin et al., 2015). In contrast, a later study using protein-protein docking and molecular dynamics simulations proposed that in the 1:2 complex, the N-terminus of CXCL12 bound to one protomer established more steady contacts with critical residues in the TM domain of the other protomer, more efficiently favoring signaling than the 1:1 stoichiometry (Cutolo et al., 2017). Overall, the stoichiometry of chemokine:receptor interaction in functional signaling complexes is still under evaluation, and gathering more information on the relevance of receptor and chemokine dimerization seems to be crucial to elucidate this facet.

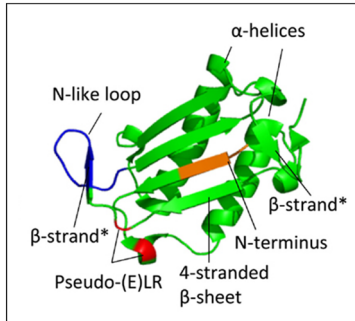
### **1.3.5. Other CXCR4 ligands.**

For a long time, CXCL12 was thought to be the sole ligand for CXCR4. However, over the years, other endogenous non-chemokine molecules have been described to be able to bind and signal through CXCR4, including extracellular ubiquitin, the viral glycoprotein gp120,  $\beta$ 3-defensin, macrophage migration inhibitory factor (MIF), and lactoferrin (Lf) (Pawig et al., 2015). The last two ligands have been investigated in this work.

#### **1.3.5.1. Macrophage migration inhibitory factor.**

Macrophage migration inhibitory factor, abbreviated MIF, is a 12.3 kDa inflammatory cytokine that plays a major role in acute and chronic inflammatory diseases, such as rheumatoid arthritis, septic shock, and atherogenesis (Morand, 2005; Schober, Bernhagen and Weber, 2008), as well as neurological diseases (Leyton-Jaimes, Kahn and Israelson, 2018) and numerous cancers (O'Reilly et al., 2016), therefore representing a potential therapeutic target. MIF belongs to the emerging group of proteins termed “chemokine-like function chemokines”. These are mediators with intracellular functions that, once secreted to the extracellular space, bind to and activate chemokine receptors. However, they cannot be classified into one of the well-established chemokine subfamilies due to the lack of canonical structural elements (**Figure 6**). In this case, MIF does not present an N-terminal cysteine motif but presents potent chemotactic properties and is known to interact with the chemokine receptors CXCR2, CXCR4, and ACKR3 (Bernhagen et al., 2007; Alampour-Rajabi et al., 2015). In addition, it also signals through CD74 and CD44 (Leng et al., 2003; Shi et al., 2006).

The crystal structure of MIF showed a homotrimer, with each monomer consisting of two antiparallel  $\alpha$ -helices and one four-stranded  $\beta$ -sheet (**Figure 10**; Sun et al., 1996). Several studies have revealed that it can exist in different conformations, including monomer, dimer, trimer or even higher-oligomeric structures, and that this is mainly concentration-dependent (Mischke et al., 1998; Philo,



Yang and LaBarre, 2004). However, which conformation is physiologically relevant under which conditions is still unclear. In contrast to CXCL12, MIF lacks the structural motif RFFESH at the N-terminus.

**Figure 10. MIF monomer crystal structure.** Modified from Pawig et al. (2015). (<https://www.frontiersin.org/articles/10.3389/fimmu.2015.00429/full>).

Using a broad spectrum of techniques, Rajasekaran et al. (2016) showed that MIF and CXCL12 present different mechanisms of CXCR4 binding and activation. They observed that MIF does not establish direct interactions with the TM cavity of the receptor, but rather induces a conformational change when binding to the N-terminus. In accordance with this idea, CXCL12 could only be displaced up to 50% by MIF in Jurkat T-cells (Bernhagen et al., 2007). Moreover, using a peptide array approach, binding assays and circular dichroism spectroscopy, the authors demonstrated that the N-terminus, ECL-1 and ECL-2 of CXCR4 are involved in the interaction with MIF, while ECL-3 is not. This same study also identified the MIF catalytic cavity as well as some residues in the second  $\alpha$ -helix and a loop close to the catalytic cavity as critical determinants for the binding to CXCR4 (Rajasekaran et al., 2016). Recently, the three-dimensional space formed by the continuous amino acids Arg-Leu-Arg from the second  $\alpha$ -helix was identified as a pseudo-(E)LR motif (as of typical of CXC chemokines) and to be crucial for the binding to the N-terminus of the receptor (CRS1). Alanine mutations of these residues completely abolished binding to CXCR4 and significantly reduced CXCR4-mediated signaling and chemotaxis (Lacy et al., 2018).

In contrast to CXCL12, it has been reported that MIF binding to CXCR4 does not result in  $\beta$ -arrestin activation in breast cancer cells or inhibition of HIV entry into T cells. However, it leads to G protein signaling in Chinese hamster ovary cells expressing CXCR3/CXCR4 receptors as well as in CXCR4-expressing *Saccharomyces cerevisiae* cells (Rajasekaran et al., 2016). Also, in monocytes and T cells, MIF triggered  $G_i$ - and integrin-dependent arrest and chemotaxis, as well as rapid integrin activation and  $Ca^{2+}$  fluxes. Importantly, using *in vitro* two- and three-dimensional assays, MIF was discovered to be the key director of mesenchymal stem cells (MSCs) recruitment to tumors, mainly through its functional interaction with CXCR4. Accordingly, knocking-down either CXCR4 or MIF totally abolished MSC homing to tumor cells in an *in vivo* metastasis model (Lourenco et al., 2015).

### 1.3.5.2. Lactoferrin.

Lactoferrin, a member of the transferrin family of approximately 80 kDa, is a natural iron-binding glycoprotein that is present in several human external secretions, such as saliva, tears, and milk. It plays an important role in host defense due its immune modulatory and anti-bacterial activities (Valenti and Antonini, 2005; Siqueiros-Cendón et al., 2014).

The structural organization of all transferrins is highly conserved in mammals. The amino acid chain of lactoferrin is folded into two globes, named N- and C-lobes, which are joint by a short  $\alpha$ -helix. They represent the N- and C-terminal halves of the protein, respectively. Each lobe is further divided into two domains, named N1 and N2 for the N-lobe and C1 and C2 for the C-lobe. In between each of these two domains, there is one iron-binding site. Lactoferrin can adopt two conformationally different states, depending on the presence or absence of iron molecules in the structure (**Figure 11**). On the iron-free state (apo-lactoferrin; apo-Lf), the conformation of lactoferrin is wide open. Upon binding of two atoms of iron, lactoferrin adopts its iron-bound state (holo-lactoferrin;  $\text{Fe}_2\text{-Lf}$ ), which causes the two domains of each globe to adopt a highly closed conformation around each of these atoms. This closed conformation is highly stable and rigid since the metal ions lock the domains together (Baker and Baker, 2005; Baker and Baker, 2012).

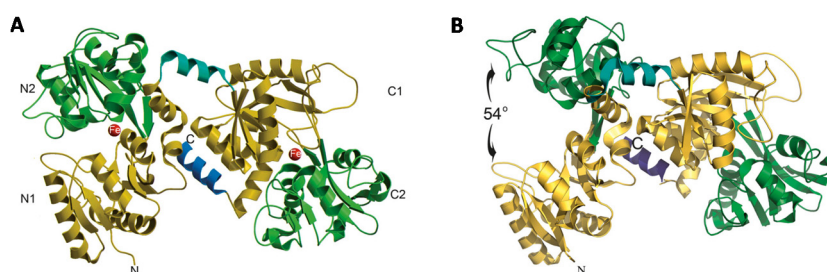


**Figure 11. Conformational states of lactoferrin. (A)** Iron-bound state. **(B)** Iron-free state. Iron is represented as red balls. Adapted from Baker and Baker (2012) with permission via RightsLink.

The antiviral activity of lactoferrin was first suggested due to the observed fluctuations in the concentration of this protein: it can be increased by 50 times under pathological conditions, such as autoimmune diseases or microbial infections (Lash et al., 1983; Nuijens et al., 1992). The first study reporting its antiviral activity showed that it was capable of blocking HIV-1 infection by variants of this virus that use CXCR4 as co-receptor for entry into host cells but had no effect on HIV-2 (Harmsen et al., 1995). A recent report provided some evidence of CXCR4 as a lactoferrin receptor (Takayama et al., 2016). The authors showed that bovine lactoferrin (bLf) specifically bound to CXCR4-expressing lipoparticles, and that this interaction was not inhibited by the presence of CXCL12, suggesting that these two ligands present different binding sites on the receptor. In this same study, they showed that stimulation of HaCaT keratinocytes and Caco-2 intestinal cells with bLf led to Akt phosphorylation, which was inhibited by pre-treatment of cells with AMD3100 or a CXCR4-neutralizing antibody.



In contrast, bLf-induced Akt activation in human dermal fibroblasts was not mediated by CXCR4, suggesting that a different receptor might be involved in this activation, and that therefore the role of CXCR4 in mediating the lactoferrin response might be cell-type specific. They also indicated that bLf triggered dimerization, tyrosine phosphorylation, ubiquitination, and internalization of CXCR4 in a similar way to CXCL12 in HaCaT keratinocytes. No information on the binding mechanism of lactoferrin to the receptor is available yet.

#### 1.4. ACKR3/CXCR7.

In contrast to conventional chemokine receptors, atypical chemokine receptors are generally unable to activate G proteins and induce the typical downstream cellular responses such as migration. As a consequence, they were initially excluded from the standard nomenclature system approved for chemokine receptors (Murphy et al., 2000) and it was not until recently that a consensus was reached to designate them as 'ACKR', an abbreviation of 'atypical chemokine receptor' (Bachelier et al., 2014). To date, the family of ACKRs comprises four members and two others are under evaluation (Leick et al., 2010; Chen et al., 2011). They are evolved from canonical chemokine receptors but differ in the amino acid composition of intracellular motifs relevant for signal transduction (Daiyasu, Nemoto and Toh, 2012). Historically, these receptors were initially defined as 'silent' and 'non-signaling' and thought to act exclusively as decoy or scavenging receptors, binding and internalizing their ligands, leading to the creation of ligand gradients that are crucial for cell migration. Nevertheless, it is clear now that at least some ACKRs can signal via G protein-independent signaling cascades of GPCRs.

Originally identified as an orphan receptor and named RDC1 (Libert et al., 1990), this 7TM protein was first suggested to be a chemokine receptor related to CXC receptors based on sequence homology and genomic location, and therefore named CXCR7 (Heesen et al., 1998). It was then de-orphanized as a receptor for CXCL11 and CXCL12 (Balabanian et al., 2005; Burns et al., 2006) and renamed ACKR3 due to the lack of signaling via G proteins. In this work, the ACKR3 designation is used.

In humans, ACKR3 is found in embryonic neuronal and heart tissue, in some leukocyte subsets, including B cells, and endothelial cells (Infantino, Moepps and Thelen, 2006; Wang et al., 2012). The importance of this receptor is well reflected by the fact that ACKR3 knock-out mice die peri- or postnatally due to abnormalities in the CNS and the cardiovascular system (Sierro et al., 2007; Gerrits et al., 2008). In addition, elevated levels of this receptor are found in many cancer types, including prostate, breast, and lung cancer, in which it plays an important role in tumor growth and metastasis (Miao et al., 2007; Wang et al., 2008).

### **1.4.1. Ligand binding to ACKR3.**

It is currently accepted that ACKR3 has two chemokine ligands: CXCL11, which also binds to CXCR3, and CXCL12, which also binds to CXCR4. Binding of CXCL12 to ACKR3 occurs with an affinity that is ten times higher than that for CXCR4 (Balabanian et al., 2005), and ACKR3 binds CXCL12 with 10- to 20-fold greater affinity than CXCL11 (Burns et al., 2006). In addition, it also binds vMIPII (Szpakowska et al., 2016), MIF (Alampour-Rajabi et al., 2015), adrenomedullin (Klein et al., 2014), and bovine adrenal medulla 22 (Ikeda et al., 2013; Szpakowska et al., 2018). Interestingly, two structurally unrelated CXCR4 antagonists, TC14012 and AMD3100, present agonistic properties on ACKR3, inducing the recruitment of  $\beta$ -arrestin to the receptor (Kalatskaya et al., 2009; Gravel et al., 2010). These findings suggest that CXCR4 drug candidates should also be routinely tested on ACKR3 to avoid unexpected outcomes.

Gustavsson et al. (2017) combined different approaches to map the interaction interfaces between ACKR3 and CXCL12 and the changes that the receptor undergoes upon activation. Their data are consistent with expectations from the CRS1/2 model but reveal a more extensive binding interface that covers virtually the entire surface of the chemokine, as described in section 1.2.3. Their data suggest a structural mechanism for agonist-induced activation of ACKR3 that is similar to canonical GPCRs, such as rhodopsin and  $\mu$ -opioid receptor. By means of using radiolytic footprinting, the authors observed that ACKR3 opens up in its active (CXCL12-bound) state to expose a binding site for intracellular partners, which is in line with the outward movement of TM6 observed in many other receptors upon activation. Considering its atypical nature, this indicates that the mechanistic details or conformational control of bias towards  $\beta$ -arrestin might be subtle.

### **1.4.2. ACKR3 function and signaling.**

#### **1.4.2.1. Scavenging function.**

One of the most established roles of ACKR3 is its decoy/scavenging function. This receptor continuously shuttles between the plasma membrane and intracellular compartments, removing chemokine ligands from the extracellular space and transporting them to lysosomes for degradation (Naumann et al., 2010). This constitutive endocytosis and recycling accounts for observations that the receptor predominantly localizes to intracellular vesicles. The scavenger activity of ACKR3 modulates CXCL12 levels, controlling the growth- and migration-promoting activities of CXCR4, and establishes chemokine gradients necessary for cell migration (Luker et al., 2012). This scavenging function is required, for instance, for the optimal migration of primordial germ cells during zebrafish development (Dambly-Chaudiere, Cubedo and Ghysen, 2007; Valentin, Haas and Gilmour, 2007; Boldajipour et al., 2008; Donà et al., 2013) and has been further demonstrated in mammalian models (Naumann et al., 2010) and several cancer cell lines (Luker et al., 2012).

Some reports have shown that the internalization of ACKR3 occurs via clathrin-mediated endocytosis and interaction with  $\beta$ -arrestins, more markedly  $\beta$ -arrestin-2 (Zabel et al., 2009; Luker et al., 2010; Saaber et al., 2019). The C-terminal tail of the receptor is critical for ACKR3 location and function. Its progressive truncation increases the location of the receptor in the plasma membrane and reduces internalization. Also, a similar phenotype is observed upon treatment with inhibitors of clathrin-mediated endocytosis (Ray et al., 2012b). In accordance, loss of functional  $\beta$ -arrestin-2 also reduced ACKR3-dependent uptake of CXCL12 from the extracellular space (Luker et al., 2009).

The migration of rat vascular smooth muscle cells (VSMCs) in response to CXCL11 and CXCL12 was shown to be mediated by ACKR3 in a  $\beta$ -arrestin-2-dependent manner (Rajagopal et al., 2010). In contrast, a recent report investigating interneurons migration showed that the main function of ACKR3 was the adjustment of CXCL12 levels by phosphorylation-dependent,  $\beta$ -arrestin-independent endocytosis, demonstrating that phosphorylation regulates this receptor independently of  $\beta$ -arrestin (Saaber et al., 2019).

#### **1.4.2.2. G protein-mediated signaling.**

Several studies have shown that ligand binding to ACKR3 does not induce activation of G proteins nor triggers the activation of their classical downstream signaling pathways (Sierra et al., 2007; Levoye et al., 2009; Rajagopal et al., 2010). In fact, although ACKR3 shares high structural homology with other chemokine receptors, it lacks the conserved DRYLAIV consensus sequence of these receptors and instead presents a DRYLSIT sequence (Ulvmar, Hub and Rot, 2011). Interestingly, replacing such a region of ACKR3 with that of CXCR4 did not result in a G protein-coupled ACKR3 chimera, suggesting that the altered DRYLAIV motif is not the only determinant for the lack of G protein-dependent signaling (F. Hoffmann et al., 2012). Despite these findings, its ability to interact with G proteins has been reported in two specific studies. In one study, the authors observed that ACKR3 constitutively interacted with G proteins although failed to activate them (Levoye et al., 2009). In another study, the authors reported  $G_{i/o}$ -mediated signaling through ACKR3 in human glioma cells and rodent astrocytes. In the latter, CXCL12 exposure led to G protein-mediated ERK and Akt activation (Ödemis et al., 2012).

#### **1.4.2.3. $\beta$ -arrestin-mediated signaling.**

Several studies have shown that ACKR3 functions as an atypical chemokine signaling receptor by activating ERK and Akt via  $\beta$ -arrestin-2 (Wang et al., 2008; Hattermann et al., 2010; Rajagopal et al., 2010), which makes ACKR3 the first identified GPCR biased for arrestin-dependent signaling. A schematic summary of the signaling mediated by ACKR3 upon CXCL12 binding is shown in **figure 12**.

Overall, although the functions of ACKR3 remain controversial and most of the activities related to this receptor have not been identified consistently across model systems, there is increasing evidence for a  $\beta$ -arrestin biased receptor in most cell types. Crystal structure of atypical chemokine receptors, including ACKR3, remains unresolved to date. This could help to further understand the structural determinants for the lack or impairment of G protein coupling and at the same time shed light on the determinants for receptor biased activity.

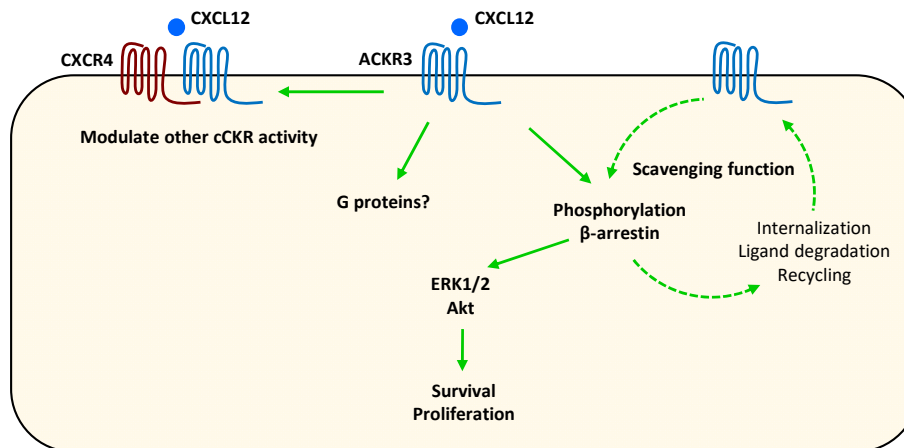


**Figure 12. ACKR3-mediated signaling in response to CXCL12.**

### 1.4.3. ACKR3 oligomerization.

Two studies have shown that ACKR3 is able to form homodimers. In transfected cells, a specific BRET signal was observed between ACKR3-RLuc and ACKR3-YFP, and addition of CXCL12 or AMD3100 further increased the observed BRET signal (Levoye et al., 2009; Kalatskaya et al., 2009).

Several studies have shown that ACKR3 can also modulate other cellular signaling pathways, potentially by forming higher-oligomeric complexes with other receptors. There is evidence for the existence of  $\alpha_1$ -AR:ACKR3: CXCR4 oligomers in VSMCs, in which activation of ACKR3 has a trans-inhibitory effect on the adrenergic receptor (Albee et al., 2017). Also, oligomers between ACKR3 and the epithelial growth factor receptor (EGFR) are known to form in a  $\beta$ -arrestin-2-dependent manner, and to be important for EGFR phosphorylation (Salazar et al., 2014). Last, the interaction of ACKR3 with CXCR4, often found co-expressed in many cell types, is one of the most studied. Several lines of evidence indicate that these two receptors form hetero-oligomers and that the presence of ACKR3 modifies the CXCR4 signaling properties, including its ability to mobilize intracellular  $\text{Ca}^{2+}$  (Sierro et al., 2007; Hartmann et al., 2008; Levoye et al., 2009; Décaillot et al., 2011). Depending on the context, ACKR3 has been reported to enhance CXCR4-mediated chemotaxis towards CXCL12 (Décaillot et al., 2011) or inhibit it (Levoye et al., 2009).

## 1.5. FLUORESCENCE-BASED IMAGING METHODS TO STUDY GPCRS.

Imaging methods based on the phenomenon of fluorescence are very commonly used to study different aspects of GPCRs, such as interactions between molecules, trafficking, location, conformational changes, or kinetics. Some of the most employed methods include protein fragment complementation (Waadt et al., 2014), FRET (Kauk and Hoffmann, 2018), fluorescence recovery after photobleaching (Veerapathiran and Wohland, 2018), fluorescence correlation spectroscopy (Briddon, Kilpatrick and Hill, 2018), as well as single molecule-based approaches (Sungkaworn et al., 2014). These methods require the proteins of interest to be tagged with fluorescent probes and, as a consequence, increasing number of strategies to label proteins with fluorescent tags have emerged.

### 1.5.1. Fluorescence.

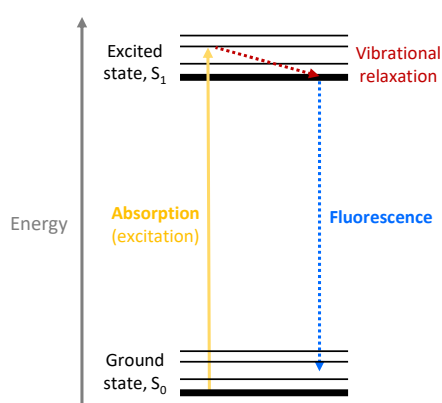


Figure 13. Jablonski Diagram.

The phenomenon of fluorescence can be explained with the Jablonski energy diagram (Figure 13). Upon absorption of a photon by a fluorophore, an electron transitions to an excited energy state. Within this state, the electron drops to the lowest energetic level via non-radiatively vibrational relaxation. Since the excited state is very unstable, the electron returns to ground state. Fluorescence occurs when the energy quantum of this difference is emitted via a photon.

### 1.5.2. Fluorescent labeling strategies.

Labeling molecules of interest in biological systems has become essential for intracellular molecular imaging. The most conventional method to label proteins is by genetically introducing intrinsically fluorescent proteins as fusion tags. The discovery of the green fluorescent protein (GFP), which was first isolated from the jellyfish *Aequorea victoria*, represented a technical revolution due to its autofluorescence and served as a basis for the development of more fluorescent proteins with different properties. GFP is a protein of 27 kDa that is made of an eleven-stranded  $\beta$ -barrel, threaded by a  $\alpha$ -helix, running up along the axis of the cylinder. On the  $\alpha$ -helix, there is the tri-peptide motif S65-Y66-G67 that spontaneously forms the fluorescent chromophore (Cody et al., 1993; Yang, Moss and Phillips, 1996; Figure 14A). Since its discovery, several modifications were introduced into the native GFP protein to facilitate its use in biological research, leading to improved folding, increased temperature and pH stability, monomeric configuration, and increased photostability. In addition, GFP has been further engineered to produce numerous variants with different properties varying in

brightness, chromophores, or spectral profiles (absorption and emission spectra), which has resulted in a large number of fluorescent probes that range in color from blue to yellow, covering all the visible spectrum (Aliye et al., 2015). For instance, additive mutations introduced into GFP yielded the fluorophores cyan fluorescent protein (CFP), enhanced CFP and mTurquoise, as well as yellow fluorescent protein (YFP), enhanced YFP and Venus. Some of them are used in this work. In addition, fluorescent proteins from other species have been identified and isolated, resulting in further expansion of the color palette to the red and far-red spectra.

Another method to label proteins of interest is by using self-labeling enzymes, such as Halo-tag, SNAP-tag, or CLIP-tag (Juillerat et al., 2003; Gautier et al., 2008; Los et al., 2008). These can covalently attach to themselves cell-permeable substrates that are modified to contain a fluorescent label or dye. By using this technology, fluorescence is only initiated upon addition of the substrate and a single construct can be labelled with different dye substrates at a time. Alternatively, a protein can also be targeted with specific reagents, such as fluorescently labeled antibodies and nanobodies, or synthetic ligands (Tian, Fürstenberg and Huber, 2017).

The main disadvantage of most labeling methods is the relatively big size of the tags, which is likely to affect the overall structure or function of the target protein. One of the smallest expression tags used on GPCRs is based on the biarsenical dye Fluorescein Arsenical Hairpin binder (FIAsH) and the red-shifted variant ReAsH (Resorufin Arsenical Hairpin binder). They are small (0.7 kDa), cell-permeable dyes that can covalently react with tetracysteine (TC) sequences that are genetically introduced into the protein of interest. The amino acid sequences of the TC motifs range from a short 6-amino acid version (CCPGCC) to longer and more specific versions. FIAsH is provided as non-fluorescent complex with ethanedithiol (EDT). Upon binding to the TC motif, it becomes fluorescent (**Figure 14B**), exhibiting comparable optical properties to YFP. Using this technology involves the introduction of a labelling protocol, which has been optimized over the years and provides reduced fluorescent background from non-specific binding (Hoffmann et al., 2010). In comparison to other labeling strategies, such as autofluorescent proteins, this technology is advantageous due to the very small TC sequence that is engineered into the receptor and the considerably smaller size of the probe (**Figure 14A**), which overall is likely to have a lower impact on the structure or function of the protein of interest. Also, labeling of the proteins is fast, stable for hours, and reversible by adding dithiols. There are other peptide-based tags that are conceptually similar to FIAsH/ReAsH, such as the rhodamine-based bisboronic acid probe that specifically binds to a tetraserine motif (Halo et al., 2009) and the tetranuclear Zinc(II) probe that specifically binds to a cysteine-containing oligoaspartate motif (Nonaka et al., 2007).

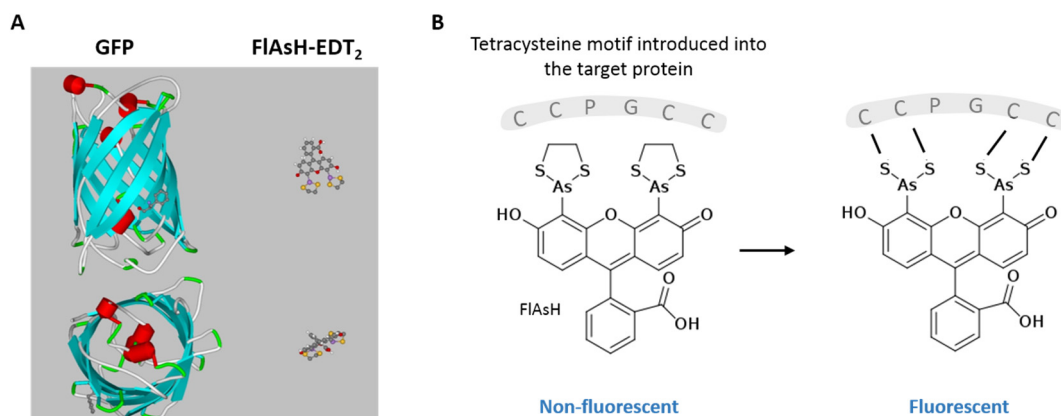


**Figure 14. GFP and FIAsh.** (A) GFP and FIAsh-EDT<sub>2</sub> structures and size comparison. Adapted from Hoffmann et al. (2005) (<https://www.nature.com/nmeth/>) with permission via RightsLink. (B) Binding of FIAsh to the TC motif CCPGCC. Modified from ThermoFisher Scientific.

### 1.5.3. Förster Resonance Energy Transfer.

The theory of FRET was described by Theodor Förster in 1948, and therefore the principle was named after him (Förster, 1948). FRET is the process by which energy is transferred non-radiatively from an excited donor fluorophore to an acceptor fluorophore through intermolecular long-range dipole-dipole coupling. In the Jablonski diagram (**Figure 13**), the energy that is released from the relaxation of one molecule (donor) is taken up by another molecule (acceptor), leading to the excitation of one of its electrons, and to the emission of a photon by the acceptor rather than the donor. Three factors are important to successfully implement FRET: (i) the donor emission spectrum must partially overlap with the excitation spectrum of the acceptor; (ii) the donor and acceptor fluorophores must be in close proximity, typically between 1-10 nm; (iii) the dipole moments of the donor and the acceptor must have a certain spatial orientation, with the highest energy transfer efficiency when the dipole moment orientation is parallel (**Figure 15**; Jares-Erijman and Jovin, 2003).

The existence of energy transfer in the system can be studied by quenching the acceptor molecule, which would lead to an increase in the donor's fluorescence. This concept is known as FRET efficiency or basal FRET ( $E_{\text{FRET}}$ ) and can be determined using the following formula:  $E_{\text{FRET}} = R_0^6 / (R_0^6 + r^6)$ .  $R_0$  or Förster radius is the distance at which the efficiency of energy transfer is 50% and depends on the spectral overlap of the fluorophore pair used, normally ranging from 4 to 7 nm. The  $r$  is the distance between the two fluorophores. As a consequence, exploring different positions or distances between the fluorescent probes is important for optimal results, and determining the FRET efficiency is one of the first steps in characterizing FRET-based systems. Nowadays, there are numerous combinations of fluorophores that can be used in FRET-based techniques. Some of the most frequently used combinations include CFP/YFP, mTurquoise/Venus, and CFP/FIAsh.

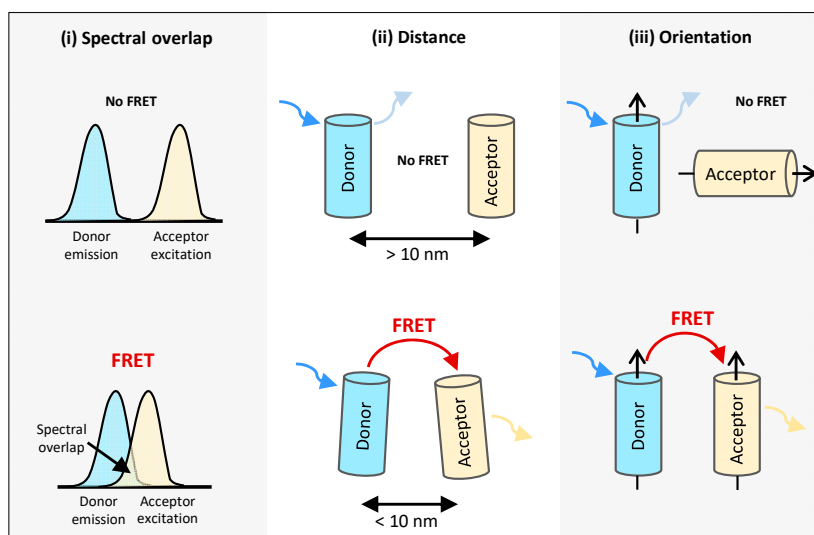


**Figure 15. Main requirements for FRET to occur between two fluorophores.**

Modified from Kochuveedu and Kim (2014).

The FRET detection methods used in this work are sensitized emission and acceptor bleaching. The donor and acceptor emissions as well as the FRET ratio are simultaneously collected over time by using specific filters. Sensitized emission measurements are useful for rapid dynamic experiments, while in acceptor bleaching, the emission of the donor is investigated prior to and following bleaching of the acceptor. There are two sources of non-FRET signal that need to be controlled and corrected in FRET measurements. One is the slight direct excitation of the acceptor upon external excitation of the donor fluorophore (known as cross-talk). The other is the fluorescence from the donor that leaks into the detection channel for the acceptor fluorescence (known as bleed-through) and is caused by the partial overlap of the emission spectral profiles of the fluorophores (Jares-Erijman and Jovin, 2003; Lohse et al., 2012).

#### 1.5.4. FRET to study kinetics of the early steps of the GPCR signaling cascade.

FRET presents high spatial and temporal resolution and can be used to directly investigate the spatiotemporal dynamics of GPCR-related processes in real time in intact cells (section 1.1.3.4; Vilardaga et al., 2010). Since the efficiency of FRET is dependent on the distance between the two fluorophores, this technique is widely used to study both intra- and intermolecular changes within a single protein or between proteins (**Figure 16A-B**; Kauk and Hoffmann, 2018). Several FRET-based approaches have been developed to individually record the initial steps of GPCR signaling, including ligand binding, receptor activation, coupling to and activation of G proteins and  $\beta$ -arrestins, oligomerization, etc.



For monitoring receptor conformational changes, intramolecular FRET-based receptor sensors can be developed by attaching two fluorophores to domains of the receptor known to be sensitive to conformational changes, most commonly the C-terminus and ICL-3, due to the fact that TM5-6 undergo the biggest conformational changes upon activation of the receptor (section 1.1.3.1). For instance, many GPCR sensors have been created by using CFP/YFP as FRET pairs. Alternatively, FIAsh can substitute the YFP as the acceptor fluorophore. Previous studies have shown that the insertion of CFP or YFP into the ICL-3 perturbed the function of some receptors, especially disturbing G protein coupling, whereas the insertion of the TC sequence did not due to its smaller size (Hoffmann et al., 2005). The first FRET-based sensor for a GPCR was developed for the PTHR over 15 years ago (Vilardaga et al., 2003) and since then sensors for more than 20 different receptors have been described (Stumpf and Hoffmann, 2016). In the field of chemokine receptors, no intramolecular receptor sensors have been described to date.

Measurements are performed under a fluorescence microscope and in single cells. Illumination (excitation) of the donor results in efficient transfer of energy to the acceptor, and both emission intensities emitted by the fluorophores as well as the FRET ratio ( $F_{\text{acceptor}}/F_{\text{donor}}$ ) are recorded over time. Binding of a ligand to the receptor would induce a conformational change that alters the distance and/or orientation between the fluorescent proteins, resulting in a change in FRET. This change can be used to determine the kinetics of the process, as described in **Figure 16C**.

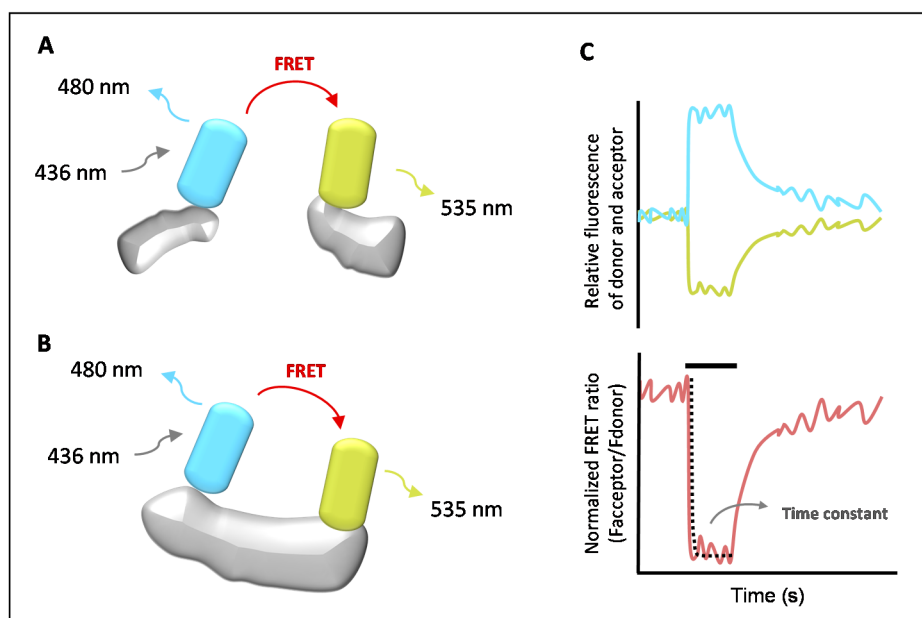


**Figure 16. FRET-based approach. (A, B)** Inter- (A) and intramolecular (B) FRET. Modified from Lohse et al. (2012). **(C)** FRET measurement via sensitized emission. Donor (cyan) and acceptor (yellow) emissions and the FRET ratio (red) are collected over time. A stimulus (black line) leads to a structural rearrangement, which is observed as a FRET change. An antiparallel movement in the donor and acceptor emissions is observed. Kinetics of the conformational change are determined by fitting a curve into the FRET signal.

The same principle is used to study conformational changes in other proteins, such as G proteins and  $\beta$ -arrestins, in which fluorophores are attached in different positions or subunits (Adjobo-Hermans et al., 2011; Nuber et al., 2016; Van Unen et al., 2016). For instance, for  $G_i$  and  $G_q$  proteins, one fluorophore is normally inserted into the  $G\alpha$  subunit while the other is fused to the C- or N-termini of the  $G\beta$  or  $G\gamma$  subunits (Bünemann et al., 2003; Adjobo-Hermans et al., 2011; van Unen et al., 2016). Intermolecular interactions in the GPCR signaling cascade have also been widely studied, including the interaction of receptors with ligands (Castro et al., 2005), G proteins (Hein et al., 2005; Ferrandon et al., 2009) and  $\beta$ -arrestins (Nuber et al., 2016), as well as receptor oligomerization (Vilardaga et al., 2008). In these cases, a fluorophore is attached to each of the interacting partners. By combining all these approaches, the activation of every step of the GPCR signaling cascade can be temporally resolved (**Figure 17**; Lohse et al., 2008; Vilardaga et al., 2009).

In this thesis, some of these approaches have been employed to elucidate different aspects of CXCR4 and ACKR3 activation and signaling.

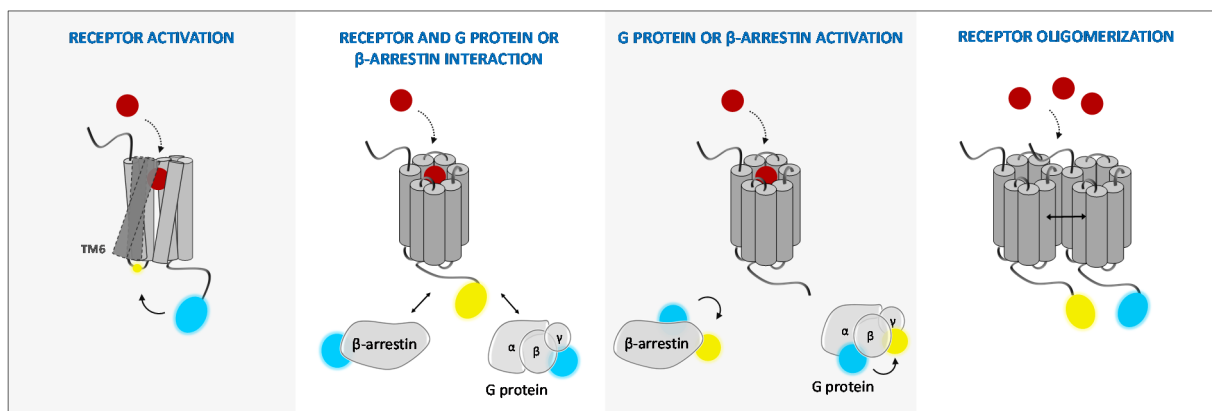


**Figure 17. FRET-based approaches to study the early steps of GPCR signaling.** Insertion of fluorescent proteins or tags into different positions within a protein or in different proteins allows to measure structural rearrangements or interactions. Arrows indicate structural rearrangements.

## 2. MOTIVATION AND OBJECTIVES

The chemokine receptors CXCR4 and ACKR3 are implicated in many pathological processes and are the targets of numerous drug discovery efforts. On one hand, several CXCR4 crystal structures have been resolved in combination with several antagonistic ligands, but the dynamic and kinetic properties of the ligand-induced activation of this receptor remain poorly understood. On the other hand, structural information of ACKR3 is still limited and due to its scavenging nature, a small number of read-outs are available to study its ligand-induced activation. Therefore, the main aims of this thesis work were:

(i) Investigate the signaling pattern of CXCR4 in response to different ligands. For that purpose, several FRET-based approaches will be established to individually study the early steps of the signaling cascade.

- Develop FRET-based CXCR4 sensors in order to study the ligand-induced activation of the receptor.
- Establish FRET-based strategies to investigate the interaction of CXCR4 with G proteins, structural rearrangements between CXCR4 protomers, and the activation of G proteins via this receptor.
- Analyze the dynamics and kinetics of each step of the transduction pathway of CXCR4 using the aforementioned settings in response to several ligands, including CXCL12, MIF, and lactoferrin.

(ii) Develop a tool that allows measuring the activation of ACKR3 in response to various ligands and investigate the ability of this receptor to activate G proteins.

- Develop a FRET-based ACKR3 sensor in order to study the ligand-induced activation of the receptor.
- Investigate the activation of ACKR3 in response to CXCL12 and other agonistic molecules using the receptor sensor.
- Investigate G protein activation via ACKR3 in response to CXCL12.

### 3. MATERIALS AND METHODS

#### 3.1. MATERIALS.

##### 3.1.1. DNA.

The following table presents all the DNA constructs used in this work.

All proteins are human-derived unless specified.

NAME	VECTOR	DESCRIPTION	SOURCE	ANTIBIOTIC RESISTANCE
pcDEF3	pcDEF3	Empty pcDEF3 plasmid	MJ Smit (VU, Amsterdam)	Ampicillin
pcDNA3	pcDNA3	Empty pcDNA3 plasmid	Invitrogen	Ampicillin
CXCR4	pcDEF3	CXCR4 protein	MJ Smit (VU, Amsterdam)	Ampicillin
3HA-CXCR4	pcDEF3	CXCR4 protein with three HA tags fused to the N-terminus	MJ Smit (VU, Amsterdam)	Ampicillin
3HA-CXCR4-CFP	pcDNA3	CXCR4 protein with three HA tags fused to the N-terminus and CFP fused to the C-terminus	This work	Ampicillin
CXCR4-YFP	pRK5	CXCR4 protein with YFP fused to the C-terminus	F Bachelierie (INSERM, Paris)	Ampicillin
3HA-CXCR4-FIAshH226	pcDNA3	CXCR4 protein with three HA tags fused to the N-terminus and the FIAsh-binding sequence inserted in ICL-3, between L226 and S227	This work	Ampicillin
3HA-CXCR4-FIAshH228	pcDNA3	CXCR4 protein with three HA tags fused to the N-terminus and the FIAsh-binding sequence inserted in ICL-3, between H228 and S229	This work	Ampicillin
3HA-CXCR4-FIAshH229	pcDNA3	CXCR4 protein with three HA tags fused to the N-terminus and the FIAsh-binding sequence inserted in ICL-3, between S229 and K230	This work	Ampicillin
3HA-CXCR4-FIAshH226-CFP	pcDNA3	CXCR4 protein with three HA tags fused to the N-terminus, CFP fused to the C-terminus and the FIAsh-binding sequence inserted in ICL-3, between L226 and S227	This work	Ampicillin
3HA-CXCR4-FIAshH228-CFP	pcDNA3	CXCR4 protein with three HA tags fused to the N-terminus, CFP fused to the C-terminus and the FIAsh-binding sequence inserted in ICL-3, between H228 and S229	This work	Ampicillin
3HA-CXCR4-FIAshH229-CFP	pcDNA3	CXCR4 protein with three HA tags fused to the N-terminus, CFP fused to the C-terminus and the FIAsh-binding sequence inserted in ICL-3, between S229 and K230	This work	Ampicillin
3HA- <sup>W94R,D97G</sup> CXCR4-CFP	pcDNA3	CXCR4 protein containing the two mutations W94R and D97G, and with three HA tags fused to the N-terminus and CFP fused to the C-terminus	This work	Ampicillin

(continued)

NAME	VECTOR	DESCRIPTION	SOURCE	ANTIBIOTIC RESISTANCE
3HA <sup>-W94R,D97G</sup> CXCR4-FIAsH228-CFP	pcDNA3	CXCR4 protein containing the two mutations W94R and D97G, with three HA tags fused to the N-terminus, CFP fused to the C-terminus and the FIAsH-binding sequence inserted in ICL-3, between H228 and S229	This work	Ampicillin
ACKR3	pcDEF3	ACKR3 protein	MJ Smit (VU, Amsterdam)	Ampicillin
HA-ACKR3	pcDEF3	ACKR3 protein with one HA tag fused to the N-terminus	MJ Smit (VU, Amsterdam)	Ampicillin
HA-ACKR3-CFP	pcDNA3	ACKR3 protein with one HA tag fused to the N-terminus and CFP fused to the C-terminus	This work	Ampicillin
HA-ACKR3-FIAsH	pcDNA3	ACKR3 protein with one HA tag fused to the N-terminus and the FIAsH-binding sequence inserted in ICL-3, between S242 and S243	This work	Ampicillin
HA-ACKR3-FIAsH-CFP	pcDNA3	ACKR3 protein with one HA tag fused to the N-terminus, CFP fused to the C-terminus and the FIAsH-binding sequence inserted in ICL-3, between S242 and S243	This work	Ampicillin
HA-ACKR3(1-321)-FIAsH-CFP	pcDNA3	ACKR3 protein with one HA tag fused to the N-terminus, CFP fused to the C-terminus at N321 and the FIAsH-binding sequence inserted in ICL-3, between S242 and S243. The last 41 aa of the C-terminus have been deleted	This work	Ampicillin
HA-ACKR3(1-346)-FIAsH-CFP	pcDNA3	ACKR3 protein with one HA tag fused to the N-terminus, CFP fused to the C-terminus at A346 and the FIAsH-binding sequence inserted in ICL-3, between S242 and S243. The last 16 aa of the C-terminus have been deleted	This work	Ampicillin
K44A dynamin (rat)	pCMV5	Dynamin 1a containing the mutation K44A	Sontag et al., 1994	Ampicillin
$\alpha_{2A}$ -AR (murine)	pcDNA3	$\alpha_{2A}$ -AR protein	Bünemann et al., 2003	Ampicillin
$\alpha_{2A}$ -AR-YFP (murine)	pcDNA3	$\alpha_{2A}$ -AR protein with YFP fused to the C-terminus	Hein et al., 2005	Ampicillin
G $\alpha_{i1}$ subunit (rat)	pcDNA3	G $\alpha_{i1}$ subunit (G protein)	Hein et al., 2005	Ampicillin
G $\beta_1$ subunit	pCMV	G $\beta_1$ subunit (G protein)	Hein et al., 2005	Ampicillin
G $\gamma_2$ subunit	-	G $\gamma_2$ subunit (G protein)	Hein et al., 2005	Kanamycin
G $\alpha_{i1}$ -CFP subunit (rat)	pcDNA3	G $\alpha_{i1}$ subunit with CFP inserted between positions 91 and 92 of the protein	Hein et al., 2005	Ampicillin
G $\gamma_2$ -CFP subunit	pcDNA3	G $\gamma_2$ subunit with CFP fused to the N-terminus	Hein et al., 2005	Ampicillin
G $_i$ (G $_{i1}$ , G $_{i2}$ , G $_{i3}$ ) trimer sensors	Clontech-style N1	pG $\beta_1$ -2A-cp173Venus-G $\gamma_2$ -IRES-G $\alpha_i$ -mTurquoise- $\Delta 9$	Van Unen et al., 2016	Kanamycin
G $_q$ trimer sensor	-	G $\alpha_q$ -mTq- $\Delta 6$ + G $\beta_1$ + cpVenus-G $\gamma_2$	Adjobo-Hermans et al., 2011	Kanamycin
CRE-Luc	pcDEF3	Firefly luciferase gene under the control of the cAMP response element CRE	MJ Smit (VU, Amsterdam)	-
M $_3$ -AChR	pcDNA3	M $_3$ -AChR protein	-	Ampicillin

## 3.1.2. Consumables.

CHEMICALS AND REAGENTS	SUPPLIER	IDENTIFIER
25k linear polyethylenimine (PEI)	Polysciences	23966-2
Agar	Applichem	A0949
Agarose	Applichem	A0949
Ampicillin	Sigma-Aldrich	A9518
ATP	Sigma-Aldrich	A3377
BAL (2,3-dimercapto-1-propanol)	Fluka / Sigma-Aldrich	38520 / 54046
Bromophenol blue	Applichem	A23310025
Bovine serum albumin (BSA) fraction V	Applichem	A1391
CaCl <sub>2</sub>	Merck	102382
Dimethyl sulfoxide (DMSO)	Sigma-Aldrich	D8418
DNA ladders (100 bp / 1 kbp)	New England Biolabs	N3231S / N3231L
Dithiothreitol (DTT)	-	-
D-luciferin	Duchefa	L9504
EDT (1,2-Ethanedithiol)	Sigma-Aldrich	02390
Ethanol 100%	Sigma-Aldrich	32205
Ethanol 70%	T.H. Geyer	2202
Ethylenediaminetetraacetic acid (EDTA)	Roth	X986.2
FIAsh	Dr. E. Heller	-
Forskolin	Cayman chemical LC Laboratories	11018 F-9929
Gel loading dye	This lab	-
Geneticin G-418 Sulphate	Gibco	11811-031
Glucose	PanReac AppliChem	A0883
Glycerol	Melford	G22020/G1345
Glycine	Roth	3790.2
HDGreen Plus DNA stain	Intas	ISII-HDGreen Plus
HEPES	Sigma-Aldrich	H3375
Immersion oil for microscopy	Applichem	A0699
Isopropanol	Sigma-Aldrich	33539 2.5L-M
Kanamycin	Roth	T832.3
KCl	Applichem	A2939
Liquid nitrogen	-	-
MgCl <sub>2</sub>	Applichem	1036
NaCl	Applichem	131659
NaOH	Applichem	A1551
Peptone	Applichem	A1553
Poly-D-Lysine	MP Biomedicals	150175
Scintillation fluid (MicroScint-O)	PerkinElmer	-
Sucrose	-	-
Terralin	Schulke	23184-A
Tris H <sub>3</sub> PO <sub>4</sub>	Melford	B2005/G25803
TritonX	Fluka	93426
Trypsin	-	-
Yeast extract	Applichem	A1552

BUFFER/SOLUTION, GEL	COMPOSITION
Binding buffer	50mM HEPES, 1mM CaCl <sub>2</sub> , 5mM MgCl <sub>2</sub> , 100mM NaCl, 1% BSA (pH 7.4)
Gel loading dye	0.1M EDTA, 50% glycerin, 0.1% bromophenol
Imaging Buffer	10mM HEPES, 140mM NaCl, 5.4mM KCl, 1mM MgCl <sub>2</sub> , 2mM CaCl <sub>2</sub> (pH 7.3)
KCM buffer 5X	500mM KCl, 150mM CaCl <sub>2</sub> , 250mM MgCl <sub>2</sub>
Labeling Buffer	10mM HEPES, 150mM NaCl, 25mM KCl, 2mM MgCl <sub>2</sub> , 4mM CaCl <sub>2</sub> , 10mM glucose (pH 7.3)
Luciferase Assay Reagent	45mM Tris H <sub>3</sub> PO <sub>4</sub> pH 7.8, 45% glycerol, 3% Triton X-100, 1mM DTT, 20mM MgCl <sub>2</sub> , 800μM D-luciferin, 80μM ATP
Membrane Buffer	15mM Tris pH 7.5, 0.3mM EDTA, 2mM MgCl <sub>2</sub> (pH 7.5)
NaCl transfection solution	150mM NaCl, filter sterilized
Tris-Sucrose Buffer	20mM Tris pH 7.4, 250mM sucrose (pH 7.4)
Wash buffer	Binding buffer supplemented with 0.5M NaCl

EXPENDABLE MATERIALS	SUPPLIER	IDENTIFIER
100 mm plates	Sarstedt	83.3902
150 mm plates	Sarstedt	83.3903
6-well plates	Sarstedt	83.3920
12-well plates	Sarstedt	83.3921
24-well plates	Sarstedt	83.3922
96-well plates, black, F-bottom	Brand	781968
96-well plates, clear, F-bottom	Sarstedt	83.3924
96-well plates, clear, U-bottom	Greiner Bio One	-
96-well plates, white, F-bottom	Greiner Bio One	-
Attofluor Cell chamber	Molecular Probes	-
Cryo-Tubes	Nunc/ThermoScientific	375418 / 368632
Falcon tubes 15 ml / 50 ml	Corning	352096 / 352070
Gloves - SensiCare Ice / Peha-soft nitrile	Medline / Hartmann	486802 / 942207
Hemocytometer (cell counting)	Hecht-assistent	-
Needle 23G	-	-
Parafilm M	Bemis	PM-996
PCR tubes (0.5 ml)	Eppendorf	-
Pipette Research Plus, 8-channel, variable, 1-10μl / 10-100μl / 30-300μl	Eppendorf	3125000010 / 3125000036 / 3125000052
Pipettes (P2.5, P10, P100, P1000)	Eppendorf	-
Pipettes, electronic, Xplorer plus, 8-channel, variable, 5-100μl	Eppendorf	4861 000.783
Pipettes tips	SurPhob biozym	VT0270/0230/0200/0240
Protein LoBind Tubes 1.5 ml	Eppendorf	022431081
Round glass coverslips 24mm	Hartenstein	0111640
Safe-Lock Tubes 1.5 ml	Eppendorf	0030120.086
Syringe filtration unit Filtropur S0.2	Sarstedt	83.1826.001
Teflon glass homogenizer	-	-
UniFilter 96-well plate GF/C plates	PerkinElmer	-
WillCo-dish® 40mm glass bottom dishes	WillCo Wells	GWST-5040/1.5-0.5

REAGENTS FOR EUKARYOTIC CELL CULTURE	SUPPLIER	IDENTIFIER
Dulbecco's Modified Eagle Medium (DMEM)	Gibco	21969035
Dulbecco's Phosphate Buffered Saline (DPBS)	Gibco	14190094
Fetal Calf Serum (FCS)	Biochrom	S0115
L-Glutamine	PanBiotech	P04-80100
NucleoBond Xtra Midi Kit	Macherey-Nagel	740410.50
Penicillin-Streptomycin	Gibco	15140-122
Trypsin/EDTA	PanBiotech	P10-023100

COMMERCIAL KITS	SUPPLIER	IDENTIFIER
BCA Protein Assay Kit	Thermo Scientific	-
DNA Gel Extraction Kit	Millipore	LSKGEL050
Effectene Transfection Reagent	Qiagen	301427
Modified TAE Buffer (50x)	Millipore	CS201628

ENZYMES AND RELATED REAGENTS	SUPPLIER
Nucleotides	New England Biolabs
Pfu buffer	Promega
Pfu polymerase	Promega
Restriction enzymes	New England Biolabs
Restriction enzyme buffers	New England Biolabs
Taq polymerase	New England Biolabs
Taq polymerase buffer	New England Biolabs
T4 DNA Ligase	New England Biolabs
T4 DNA Ligase buffer	New England Biolabs

### 3.1.3. Ligands.

NAME	SOURCE	IDENTIFIER
<sup>125</sup> I-CXCL12	PerkinElmer	NEX346005UC
Acetylcholine	-	-
CXCL12	Peprtech	300-28A
GD301	VU, Griffin Discoveries	-
IT1t	Tocris	4596
Lactoferrin (low iron content)	Sigma	L0520
Lactoferrin (high iron content)	Sigma	3770
MIF	Peprtech	300-69
Norepinephrine	Sigma	A9512
VUF11072	VU, Griffin Discoveries	-
VUF11074	VU, Griffin Discoveries	-

All vials were shortly centrifuged prior to opening. CXCL12 was reconstituted in imaging buffer containing 0.1% BSA (1 mg in 1 ml; final concentration: 125  $\mu$ M) and stored at -20°C. MIF was reconstituted in imaging buffer containing 0.1% BSA (1 mg in 400  $\mu$ l; final concentration: 167  $\mu$ M) and stored at -20°C. IT1t was reconstituted in water (10 mg in 205  $\mu$ l; final concentration: 100 mM) and stored at 4°C. Lactoferrin (low iron content) was reconstituted in water (5 mg in 500  $\mu$ l; final



concentration: 120  $\mu$ M) and stored at 4°C. Lactoferrin (high iron content) was reconstituted in DPBS (5 mg in 500  $\mu$ l; final concentration: 120  $\mu$ M) and stored at 4°C. Norepinephrine was reconstituted in imaging buffer and stored at -20°C. GD301, VUF11072, and VUF11074 were reconstituted in DMSO and stored at -20°C. Acetylcholine was freshly prepared in imaging buffer right before the measurements due to its instability in solution. After reconstitution, working aliquots containing small amounts of ligand were prepared and stored at the indicated temperature. Low-binding peptide vials were used for peptidic ligands in order to reduce their binding to the surface. All ligands were further diluted in imaging buffer containing 0.1% BSA for the measurements.

### 3.1.4. Cell lines.

#### 3.1.4.1. Eukaryotic cell lines.

Name	Source
Human Embryonic Kidney cells 293 (HEK293)	C Hoffmann (U. Würzburg, Würzburg)
HEK293 T	MJ Smit (VU, Amsterdam)

#### 3.1.4.2. Prokaryotic cell lines.

Name	Source
<i>Escherichia coli</i> ( <i>E. coli</i> ) DH5 $\alpha$	Invitrogen

### 3.1.5. Media for cell culture.

#### 3.1.5.1. Eukaryotic cell culture.

DMEM+++: Dulbecco's Modified Eagle Medium supplemented with 4.5 g/l glucose containing 10% (v/v) FCS, 100 U/ml penicillin and 100  $\mu$ g/ml streptomycin, and 2 mM L-glutamine. It was used to culture HEK293 and HEK293T cells.

Freezing DMEM+++: DMEM+++ containing 5% DMSO and extra 5% FCS. It was used to freeze cells.

#### 3.1.5.2. Prokaryotic cell culture.

Lysogeny Broth (LB) medium: 1.6% peptone, 1% yeast extract, and 0.5% NaCl.

LB medium supplemented with ampicillin (final concentration 0.1 mg/ml).

LB medium supplemented with kanamycin (final concentration was 0.04 mg/ml).

LB medium supplemented with 1% agar. It was used to prepare LB agar plates for bacteria growth. The antibiotic, either ampicillin or kanamycin, was added before the preparation of the plates.

### 3.1.6. Primers for cloning.

All oligonucleotides were synthesized by Eurofins (Eurofins Genomics).

A list of primers used in this work for construct cloning is shown below. 'Rev' and 'fwd' stand for reverse and forward primers, respectively.

Number	Sequence (5' to 3')
#1 (fwd)	CTTAAGCTTGGTACCACC
#2 (rev)	AAAATCTAGAGCTGGAGTGAAAACCTGA
#3 (rev)	ACAGCAGCCCCGGGCAACACAGCTTGGAGATGATAAT
#4 (fwd)	TGTTGCCCGGGCTGCTGTTCACTCCAAGGGCCAC
#5 (rev)	ACAGCAGCCCCGGGCAACAGTGTGACAGCTTGGAGAT
#6 (fwd)	TGTTGCCCGGGCTGCTGTTCCAAGGGCCACCAGAAG
#7 (fwd)	CTGGTCATGGGTTACCAGAAG
#8 (rev)	ACAGCAGCCCCGGGCAACAGGAGTGTGACAGCTTGGAGAT
#9 (rev)	GCGCTTCTGGTGGCCCTTACAGCAGCCCCGGGCAACAGGA
#10 (rev)	ATGACTGTGGGAGGGCCTTGCCTTCTGGTGGCCCTT
#11 (rev)	TTTTGCGGCCGCTTAGCTGGAGTGAAAACCTGA
#12 (fwd)	AAAAAAGCTTATGGGCTACCCGTACGAC
#13 (rev)	AAAATCTAGATTTGGTGTCTGCTCCAA
#14 (fwd)	TGTTGCCCGGGCTGCTGTAGTGACCAGGAGAAGCAC
#15 (rev)	ACAGCAGCCCCGGGCAACAGGACGCCGAGATGGCTCT
#16 (rev)	TTTGCGGCCGCTTATTTGGTGTCTGCTCCAA
#17 (rev)	AAAATCTAGAGTTGCGATTGATGAAGCTG
#18 (rev)	AAAATCTAGAGGCATCGATGAGCTTGGT
#19 (rev)	AAAATCTAGAGTTGCGATTGATGAAGCTG
#20 (rev)	TGCCACGGCACCAACTGCACGGAAGGGAAGCGTGATGAC
#21 (rev)	TGCCTTGCATAGGAAGTTCCCAAAGTACCAGTTTGCCACGGCACCAACTGCAC

### 3.1.7. Software.

SOFTWARE	SUPPLIER	VERSION
OriginPro	OriginLab	2016
GraphPad	GraphPad Prism	7
ClustalX2	ClustalX	2
Clampex / Clampfit	Molecular Devices	9 / 10.7
Gen5 Data Analysis	BioTek	-
Serial cloner	Serial Basics	2.6.1
Image J	Image J	v1.51 k
Leica AF	Leica Microsystems	-
Adobe Reader / Acrobat	Adobe	2015
Microsoft Office	Microsoft	2013
Inkscape	Inkscape	0.92.3

## 3.2. METHODS.

### 3.2.1. Development of the CXCR4 constructs.

In order to create the 3HA-CXCR4-CFP construct, CFP (BD Bioscience Clontech) was fused to the C-terminal end of CXCR4. For that, the entire coding sequence of the receptor was amplified with the forward primer **#1** and the reverse primer **#2** on the 3HA-CXCR4 construct. This introduced the *HindIII* and *XbaI* restriction sites on the 5' and 3' ends of the coding sequence of the 3HA-CXCR4, respectively. Then, this PCR product and a pcDNA3 vector containing the CFP protein were cut with the *HindIII* and *XbaI* restriction enzymes and subsequently ligated. This resulted in 3HA-CXCR4 tagged with CFP after the position S352 in pcDNA3. The C-terminal stop codon of the receptor and the start codon for methionine of the fluorescent protein were deleted.

To create the three different receptor sensors, additional modifications were made to the ICL-3 of the receptor in the 3HA-CXCR4-CFP construct. The nucleotide sequence TGTTGCCCGGGCTGCTGT, coding for the amino acid motif CCPGCC (one letter amino acid code) that specifically binds FIAsh, was introduced in three different positions within this loop.

(i) To create the 3HA-CXCR4-FIAsh226-CFP construct, the FIAsh-binding sequence was introduced between amino acids L226 and S227 of the receptor coding sequence using site-directed mutagenesis by PCR overlap extension. For that, the forward primer **#1** and the reverse primer **#2**, containing the restriction sites, were used as flanking primers; the reverse primer **#3** and the forward primer **#4**, which contain an extra tail with the FIAsh-binding sequence, were used as internal primers. Two initial PCRs were performed using the primers **#1+#3** and **#2+#4**. The two resulting products were mixed and used for PCR using the primers **#1+#2**. The final PCR product and the 3HA-CXCR4-CFP vector were digested with *HindIII* and *XbaI* and ligated, which resulted in the creation of the 3HA-CXCR4-FIAsh226-CFP construct in pcDNA3.

(ii) To create the 3HA-CXCR4-FIAsh228-CFP construct, the FIAsh-binding sequence was introduced between amino acids H228 and S229 of the receptor coding sequence. The same protocol as above was used but using the reverse primer **#5** and the forward primer **#6** as internal primers.

(iii) To create the 3HA-CXCR4-FIAsh229-CFP construct, the FIAsh-binding sequence was introduced between amino acids S229 and K230 of the receptor coding sequence. Three consecutive PCRs were performed using the forward primer **#7** (which includes the *BstEII* restriction site) and three reverse primers **#8**, **#9** and **#10** (the latter contains the *PshAI* restriction site). In brief, a first PCR was performed using **#7+#8**. The product was used to perform a second PCR using **#7+#9**. This product was used to perform a final PCR using **#7+#10**. The final product and the 3HA-CXCR4-CFP vector were digested with

*BstEII* and *PshAI* and subsequently ligated. This resulted in the successful creation of the 3HA-CXCR4-FIAsH229-CFP construct in pcDNA3.

The constructs 3HA-CXCR4-FIAsH226, 3HA-CXCR4-FIAsH228 and 3HA-CXCR4-FIAsH229 were created by performing PCR on each of the sensors using the forward primer **#1** and the reverse primer **#11**, which contains the restriction site for *NotI*. The final product of each of the PCRs and the respective sensor constructs were digested with *HindIII* and *NotI* and subsequently ligated. This resulted in the creation of the three different constructs which contain the FIAsH-binding motif at the indicated different positions in the ICL-3 but lack the CFP at the C-terminus.

The two mutations W94R (TGG changed to CGT) and D97G (GAT changed to GGT) were introduced into the CXCR4 sequence in the constructs 3HA-CXCR4-CFP and 3HA-CXCR4-FIAsH228-CFP. For that, a PCR was performed on the 3HA-CXCR4-CFP plasmid using the forward primer **#1** and the reverse primer **#20**, which contains the point mutations. The resulting product was used to perform a subsequent PCR using the forward primer **#1** and the reverse primer **#21**, which contains the restriction site for *EcoNI*. This PCR product and the 3HA-CXCR4-CFP or the 3HA-CXCR4-FIAsH228-CFP vector were digested with *HindIII* and *EcoNI* and ligated, which resulted in the creation of the constructs 3HA-W94R,D97GCXCR4-CFP and 3HA-W94R,D97GCXCR4-FIAsH228-CFP, respectively.

### 3.2.2. Development of the ACKR3 constructs.

In order to create the HA-ACKR3-CFP construct, CFP was fused to the C-terminal end of ACKR3. First, the entire coding sequence of the receptor was amplified with the forward primer **#12** and the reverse primer **#13** on the HA-ACKR3 construct. This introduced the *HindIII* and *XbaI* restriction sites on the 5' and 3' ends of the coding sequence of the HA-ACKR3, respectively. Then, this PCR product and a pcDNA3 vector containing the CFP protein were cut with the *HindIII* and *XbaI* restriction enzymes and subsequently ligated. This resulted in HA-ACKR3 tagged with CFP after the position K362 in pcDNA3. The C-terminal stop codon of the receptor and the start codon for methionine of the fluorescent protein were deleted.

To create the HA-ACKR3-FIAsH-CFP construct, an additional modification was made to the predicted ICL-3 of the receptor. The nucleotide sequence TGTTGCCCGGGCTGCTGT, coding for the amino acid motif CCPGCC, was introduced between S242 and S243 using site-directed mutagenesis by PCR overlap extension. For that, the forward primer **#12** and the reverse primer **#13**, containing the restriction sites, were used as flanking primers; the forward primer **#14** and the reverse primer **#15**, which contain an extra tail with the FIAsH-binding sequence, were used as internal primers. Two initial PCRs were performed using the primers **#12+#15** and **#13+#14**. The two resulting products were mixed and used for PCR using the primers **#12+#13**. The final PCR product and the HA-ACKR3-CFP vector were digested

with *HindIII* and *XbaI* and ligated, which resulted in the creation of the HA-ACKR3-FIAsH-CFP construct in pcDNA3.

The construct HA-ACKR3-FIAsH was created by performing PCR on the HA-ACKR3-FIAsH-CFP construct using the forward primer **#12** and the reverse primer **#16**. The latter contains the restriction site for *NotI*. The final product and the HA-ACKR3-FIAsH-CFP construct were digested with *HindIII* and *NotI* and subsequently ligated. This resulted in the creation of the HA-ACKR3 containing the FIAsH-binding motif in the ICL-3 but lacking the CFP at the C-terminus.

In order to create the HA-ACKR3(1-321)-FIAsH-CFP construct, the C-terminus of the ACKR3 protein was truncated after position N321. For that, the entire coding sequence of the receptor was amplified with the forward primer **#12** and the reverse primer **#17** on the HA-ACKR3-FIAsH-CFP construct. This introduced the *HindIII* and *XbaI* restriction sites on the 5' and the truncated 3' end of the coding sequence, respectively. Then, this PCR product and the HA-ACKR3-FIAsH-CFP were cut with the *HindIII* and *XbaI* restriction enzymes and subsequently ligated. This resulted in the creation of the HA-ACKR3(1-321)-FIAsH-CFP construct, in which the last 41 amino acids of the C-terminus of the receptor have been deleted. To create the HA-ACKR3(1-346)-FIAsH-CFP construct, the C-terminus of the ACKR3 protein was truncated after position A346 (the last 16 amino acids of the C-terminus of the receptor are deleted) following the same protocol as before but using the reverse primer **#18**.

The construct HA-ACKR3(1-321)-CFP was created by performing PCR on the HA-ACKR3-CFP construct using the forward primer **#12** and the reverse primer **#19**. The latter contains the restriction site for *XbaI*. The final product and the HA-ACKR3-CFP construct were digested with *HindIII* and *XbaI* and subsequently ligated. This resulted in the creation of the HA-ACKR3(1-321) containing CFP after N321 but lacking the FIAsH-binding motif.

### 3.2.3. PCR protocol.

PCR technique was used to amplify DNA fragments of interest.

Reaction mixture:

Component (concentration)	Quantity ( $\mu$ l)
DNA template (10 ng/ $\mu$ l)	10
dNTPs (10 mM)	2
Forward primer (20 pM/ $\mu$ l)	2.5
Reverse primer (20 pM/ $\mu$ l)	2.5
Pfu polymerase buffer (10x)	10
Pfu polymerase	1
H <sub>2</sub> O	72

Thermocycling conditions:

Step	Temperature	Time
Initial denaturation	94°C	3 min
Annealing (30 cycles)	94°C	30 s
	55°C	1 min
	72°C	2 min
Final extension	72°C	5 min
Hold	4°	Hold

After PCR of the samples, 5  $\mu$ l of loading dye were added to each PCR tube and the DNA separated using 1% agarose gel electrophoresis containing 0.01% HDGreen Plus DNA stain at 100V. DNA bands were observed using a UV trans-illuminator.

### 3.2.4. Restriction enzyme digestion.

Digestion of PCR products was performed by incubating the DNA with the enzymes of choice, according to the following general reaction.

Reaction mixture:

Component (concentration)	Quantity ( $\mu$ l)
DNA (1 $\mu$ g/ $\mu$ l)	1-4
Restriction enzyme	1
Restriction enzyme buffer	5
H <sub>2</sub> O	Up to 50 $\mu$ l

In case of a double digestion, the protocol was adjusted following the manufacturer's instructions. The temperature was chosen depending on the enzyme of choice.

After digestion, 5  $\mu$ l of loading dye were added to the samples and the DNA separated using 1% agarose gel electrophoresis containing 0.01% HDGreen Plus DNA stain at 100V. The desired DNA bands were extracted from the gel, purified and used for ligation.

### 3.2.5. Ligations.

Ligations were performed by incubating the following reaction mixture at 16°C ON. Generally, the insert:vector ratio was 3:1 or 5:1.

Components
Vector (20 ng)
Insert (3x or 5x)
2 µl 10x T4 DNA ligase buffer
1 µl T4 DNA ligase buffer
H <sub>2</sub> O up to 20 µl

A control reaction without the DNA insert was prepared in parallel to account for religation of the vector.

### 3.2.6. DNA plasmid amplification and purification.

#### 3.2.6.1. Transformation of chemically competent *E. coli* cells.

Chemically competent *E. coli* cells were used to amplify the DNA of interest. The bacterial cells were slowly thawed on ice. For amplification of plasmids, 0.5 µg of DNA were used. For amplification of ligation products, all the volume of the ligation reaction was used. DNA were mixed with 100 µl of 1x KCM buffer in a 1.5 ml eppendorf tube and incubated on ice for 10 min. Then, 100 µl of competent cells were added to each tube and the cell/DNA mixture incubated on ice for 20 min, followed by incubation at room temperature (RT) for additional 10 min. 1 ml of LB medium was added per tube and cells grown in a shaking incubator (400 rpm) for 1h at 37°C. Later, generally, 100 µl were plated onto LB agar plates containing the appropriate antibiotic. Plates were incubated at 37°C overnight (ON), for approximately 16h, until isolated colonies were visible. Then, an individual colony was picked and used to inoculate culture for further plasmid extraction. In brief, the colony was picked with the help of a tip, put into a flask with 200 ml LB containing the appropriate antibiotic and grown ON in a shaking incubator at 180 rpm and 37°C. After, bacterial cells were harvested by centrifugation at 5000 rpm for 20 min at 4°C. The supernatant was eliminated and the pellet was used for further plasmid extraction.

### 3.2.6.2. Extraction and purification of DNA plasmids.

In order to extract plasmid DNA from *E. coli*, NucleoBond® Xtra Midi from Macherey-Nagel was used following the manufacturer's instructions. In brief, the cell pellet was homogeneously resuspended in 8 ml of buffer RES+RNase A and lysed by adding 8 ml of buffer LYS and incubating for 5 min at RT. After lysis, 8 ml of buffer NEU were added to the mix and the tube inverted three times. This led to precipitation and formation of a fluffy white material containing the genomic DNA. The lysate was then loaded on column filters that had been previously equilibrated by washing with 12 ml of buffer EQU. After loading of the lysate, the column filter was washed a second time with 5 ml of buffer EQU and then the filter was discarded. Another washing step was performed by carefully adding 8 ml of buffer WASH directly onto the column. Finally, the DNA was eluted by adding 5 ml of buffer ELU. For precipitation, the DNA was mixed with 3.5 ml of isopropanol, shortly vortexed, and centrifuged at 5000 rpm for 30 min at 4°C. The supernatant was discarded, and the pellet was washed by adding 2 ml of 70% ethanol and centrifuging at 5000 rpm for 10 min. The supernatant was discarded, and the dried pellet resuspended in the proper amount of H<sub>2</sub>O. Plasmids were generally stored at -20°C.

### 3.2.6.3. Determination of the DNA plasmid concentration.

The concentration of the DNA samples was determined using a UV-Vis spectrophotometer NanoDrop One (Thermo Scientific), following the manufacturer's guidelines. This machine provides the DNA concentration of the samples based on absorbance at 260 nm. In short, after performing the appropriate blank, 1 µl of sample was pipetted directly onto the bottom lens and measured. The DNA concentration was then adjusted with H<sub>2</sub>O to reach a final concentration of 1 µg/µl.

### 3.2.7. Eukaryotic cell culture.

#### 3.2.7.1. Maintenance routine.

HEK293 and HEK293T cells were cultured using DMEM+++ and kept in a humidified 7% CO<sub>2</sub> atmosphere at 37°C. Cells were split every two or three days when they reached ~80% confluency and discarded after 25 passages. For routine maintenance, cells in a 100 mm dish were rinsed with 2 ml DPBS and, after, detached by rinsing with 1 ml trypsin-EDTA. Then, cells were resuspended in 5 ml of media and the appropriate volume was then transferred to a new plate containing fresh media. Cells were handled in a laminar air flow hood under sterile conditions. Cell lines were tested for mycoplasma contamination every two weeks, approximately, following the protocol described in section 3.2.7.2.



### 3.2.7.2. Mycoplasma contamination test.

Cells were routinely tested for mycoplasma contamination by PCR using a primer set specific for the highly conserved 16S rRNA coding region in the mycoplasma genome. To do this, 100  $\mu$ l of supernatant of cell media were collected and heated at 95°C during 5 min, and later centrifuged during 1 min at 13000 rpm. Then, 2  $\mu$ l of the supernatant were used as template for the PCR. A positive and a negative control for mycoplasma contamination of supernatant cell media were tested in parallel. The PCR reaction mixture and conditions are shown below.

Reaction mixture:

Component (concentration)	Quantity ( $\mu$ l)
DNA template (10 ng/ $\mu$ l)	10
dNTPs (2 mM)	2.5
MgCl <sub>2</sub> (50 mM)	1
GPO primer (50 pM/ $\mu$ l)	0.25
MGSO primer (50 pM/ $\mu$ l)	0.25
Taq polymerase buffer (10x)	2.5
Taq polymerase	0.2
H <sub>2</sub> O	25

Thermocycling conditions:

Step	Temperature	Time
Initial denaturation	95°C	5 min
Annealing (30 cycles)	95°C	20 s
	60°C	30 s
	72°C	1 min
Final extension	72°C	5 min
Hold	4°	Hold

Primer sequences:

Name	Sequence (5' to 3')
GPO primer	ACTCCTACGGGAGGCAGCAGT
MGSO primer	TGCACCATCTGTCACTCTGTTAACCTC

After PCR of the samples, 5  $\mu$ l of loading dye were added to each PCR tube and the DNA separated using 1% agarose gel electrophoresis containing 0.01% HDGreen Plus DNA stain at 100V. A mycoplasma-positive sample would show a distinct band at 720 base pairs, which should be absent in the mycoplasma-free sample.

### 3.2.7.3. Freezing cells.

Cells of interest were grown in a 150 mm dish using DMEM+++. When cells reached 80% confluency, the media was aspirated, and cells were washed with 4 ml DPBS. Next, cells were detached by rinsing with 2 ml trypsin and resuspended in 10 ml of cold freezing DMEM+++ freshly prepared. Then, 1 ml of the cell suspension was dispensed into cryogenic storage vials that were immediately placed at -20°C for approximately 4h until frozen. Finally, the vials were transferred to -80°C for extended storage.

#### **3.2.7.4. Thawing frozen cells.**

Cells were removed from -80°C and immediately placed into a 37°C water bath to quickly thaw them. Then, the vial was wiped with 70% ethanol and transferred into the laminar flow hood. The cell suspension was transferred into a 100 mm dish containing 15 ml of DMEM+++. After approximately 4h, when cells were attached to the bottom of the dish, the freezing media was replaced by fresh media to avoid the toxic effects of DMSO on the cells.

#### **3.2.8. FIAsh labeling of living cells.**

FIAsh labeling was performed using the procedure previously described (Hoffmann et al., 2010). In short, cells transfected with the proper constructs and grown on 24 mm glass coverslips or 40 mm WillCo dishes were washed twice with 2 ml of labeling buffer (freshly supplemented with glucose) to remove all trace of media. After, cells were incubated with 1 ml of labeling buffer containing 1 µM FIAsh and 12.5 µM EDT for 1h at 37°C. Cells were rinsed twice with 2 ml of labeling buffer and incubated for 10 min at 37°C in labeling buffer containing 250 µM EDT to reduce non-specific FIAsh labeling. Finally, cells were washed twice again with 2 ml of labeling buffer and kept in media at 37°C until measurement.

#### **3.2.9. Confocal microscopy.**

Confocal microscopy was used to investigate the expression and localization of the different constructs developed. HEK293 cells were seeded on individual 24 mm glass coverslips, which had been pre-incubated with ploy-D-lysine (1 mg/ml) for 30 min and washed once with DPBS, placed in wells of a 6-well plate. For CXCR4-related work, cells were transfected 6h after seeding the cells with 0.5 µg of 3HA-CXCR4-CFP, 3HA-CXCR4-FIAsh226-CFP, 3HA-CXCR4-FIAsh228-CFP or 3HA-CXCR4-FIAsh229-CFP, per well. For ACKR3-related work, cells were transfected 24h after seeding the cells with 0.5 µg of HA-ACKR3(1-346)-FIAsh-CFP, HA-ACKR3(1-321)-FIAsh-CFP or HA-ACKR3-FIAsh-CFP, or 0.5 µg of HA-ACKR3-FIAsh-CFP and 1 µg K44A dynamin, per well. Effectene transfection reagent was used following the manufacturer's instructions. Prior to transfection, the media was replaced with fresh media.

Measurements were performed 48h after seeding the cells using a Leica TCS SP8 system with a 63× water objective (numerical aperture, 1.4). The day of the measurement, the coverslips with the cells were mounted on an Attofluor holder and kept in 600 µl of imaging buffer. CFP was excited with a diode laser line at 442 nm and the emission fluorescence intensity was generally detected from 450 to 600 nm. Images were generally acquired at 1024 ×1024 pixel format, line average 3, and 400 Hz.

When required, line profile analyses on cells expressing the construct of interest were performed using the Leica AF software (Leica Microsystems). For that, a line was drawn across the cell, from side to side, avoiding the nucleus. The CFP fluorescence detected along the line drawn across the cell was represented.

### **3.2.10. FRET measurements in single cells.**

#### **3.2.10.1. Microscopic set-up for FRET experiments.**

For FRET measurements, an inverted microscope (Zeiss Axiovert 200) equipped with an oil immersion 63x objective lens and a dual-emission photometric system from Till Photonics was used. Cells of interest were excited at a frequency of 10 Hz with 40 ms illumination out of a total time of 100 ms with light from a polychrome IV (Till Photonics). Upon excitation at 436 nm ( $436 \pm 10$  nm with a dichroic long-pass beam splitter DCLP 460 nm), the emission of the donor (CFP or mTurquoise2;  $480 \pm 20$  nm), the emission of the acceptor (YFP, Venus or FIAsh;  $535 \pm 15$  nm) and the FRET ratio ( $F_{\text{acceptor}}/F_{\text{donor}}$ ) were monitored simultaneously over time using a dual emission photometric system from TILL photonics (beam splitter DCLP 505 nm). Fluorescence signals were digitized using an analogue-digital converter (Axon Digidata 1440A, Axon Instruments) and stored with the Clampex 9.0 software.

#### **3.2.10.2. Determination of the FRET efficiency.**

Determination of FRET efficiency was performed as previously described (Jost et al., 2008). HEK293 cells were seeded on individual 24 mm glass coverslips as described for confocal microscopy in section 3.2.9. To study intramolecular FRET in the CXCR4 sensors, cells were transfected 6h later with 0.5  $\mu\text{g}$  of 3HA-CXCR4-FIAsh226-CFP, 3HA-CXCR4-FIAsh228-CFP or 3HA-CXCR4-FIAsh229-CFP, per well. For the ACKR3 sensors, cells were transfected 24h later with 0.5  $\mu\text{g}$  of HA-ACKR3(1-321)-FIAsh-CFP, or 0.5  $\mu\text{g}$  HA-ACKR3-FIAsh-CFP and 1  $\mu\text{g}$  K44A dynamin, per well. To study intermolecular FRET, the appropriate control constructs were employed. On one hand, cells were transfected with 0.3  $\mu\text{g}$  of 3HA-CXCR4-CFP and 0.3  $\mu\text{g}$  of 3HA-CXCR4-FIAsh226, 3HA-CXCR4-FIAsh228 or 3HA-CXCR4-FIAsh229, per well. On the other hand, 0.3  $\mu\text{g}$  of HA-ACKR3(1-321)-CFP and 0.3  $\mu\text{g}$  of HA-ACKR3-FIAsh, or 0.3  $\mu\text{g}$  of HA-ACKR3-CFP and 0.3  $\mu\text{g}$  of HA-ACKR3-FIAsh and 1.2  $\mu\text{g}$  of K44A dynamin were transfected, per well. Prior to transfection with Effectene transfection reagent, the media of the cells was replaced with fresh media.

The measurements were performed 48h after seeding the cells using the microscopic FRET set-up described in section 3.2.10.1. Prior to the measurement, cells were FIAsh-labeled as described in section 3.2.8. Then, the coverslips were mounted on the Attofluor holder and kept in 999  $\mu\text{l}$  of imaging buffer. After approximately 30s of recording, 1  $\mu\text{l}$  of British Anti-Lewisite (BAL; 2-3-dimercapto-1-

propanol) was added to the cells to yield a final concentration of 5 mM. High concentrations of BAL displace FIAsh from its binding site in the ICL-3 of the receptor. The FRET efficiency was calculated by analyzing the increase in the CFP emission due to dequenching using the formula shown below.

$$\text{FRET efficiency} = \frac{\text{FCFP}_{\text{max}} - \text{FCFP}_{\text{min}}}{\text{FCFP}_{\text{max}}}$$

Data was processed and analyzed using Clampfit and GraphPad Prism. Data is shown as a dot plot with mean  $\pm$  SEM, in which each dot represents an individual cell/measurement. When required, statistical significance was assessed using unpaired t-test or one-way ANOVA followed by Tukey's test. Details on the statistical analysis and the number of independent measurements performed is indicated in the figure legends.

### 3.2.10.3. Biopen<sup>®</sup> microchannel pipette.

The Biopen<sup>®</sup> microchannel pipette (Fluicell, Gothenburg, Sweden) was used to deliver the different solutions onto cells (Ainla et al., 2010; Ainla et al., 2012). This device allows drug delivery onto single cells with sub-second exchange time in a precise and localized manner, leaving the surrounding cells and environment intact. An internal recirculation system constantly collects the solutions applied into the external environment back into the pipette, and thus, makes it possible to measure many cells in a single plate. Additionally, this system only requires  $\approx$ 30  $\mu$ l of the solution of interest.

### 3.2.10.4. Kinetic measurements.

For kinetic experiments using FRET, HEK293 cells were seeded on 40 mm WillCo dishes which had been previously coated with poly-D-lysine for 30 minutes and washed once with DPBS. Regarding CXCR4-related work, cells were transfected 6h later with the appropriate construct(s). For measuring receptor activation, 0.7  $\mu$ g of receptor sensor (3HA-CXCR4-FIAsh226-CFP, 3HA-CXCR4-FIAsh228-CFP, 3HA-CXCR4-FIAsh229-CFP, or 3HA-<sup>W94R,D97G</sup>CXCR4-FIAsh228-CFP) were transfected per dish, and cells were FIAsh-labeled before the measurement (section 3.2.8). For receptor/G protein interaction studies, 0.6  $\mu$ g of CXCR4-YFP, 0.7  $\mu$ g of G $\alpha_{i1}$  subunit, 0.3  $\mu$ g of G $\beta_1$  subunit, and 0.2  $\mu$ g of G $\gamma_2$ -CFP subunit were transfected per dish. When indicated, 0.7  $\mu$ g of G $\alpha_{i1}$ -CFP subunit and 0.2  $\mu$ g of G $\gamma_2$  subunit were transfected instead. For measuring G protein activation, 0.4  $\mu$ g of untagged CXCR4 or  $\alpha_{2A}$ -AR and 0.75  $\mu$ g of G protein sensor (G $_{i1}$ , G $_{i2}$  or G $_{i3}$ ) were transfected per dish. For dimerization studies, 0.5  $\mu$ g of CXCR4-YFP and 0.5  $\mu$ g of 3HA-CXCR4-CFP or 3HA-<sup>W94R,D97G</sup>CXCR4-CFP were transfected per dish. Regarding ACKR3-related work, cells were transfected 24h after seeding them. For measuring receptor activation, 0.5  $\mu$ g of HA-ACKR3(1-321)-FIAsh-CFP sensor or 0.5  $\mu$ g of HA-ACKR3-FIAsh-CFP sensor with

or without 1  $\mu\text{g}$  K44A dynamin were transfected per dish. Prior to transfection with Effectene reagent, the media of the cells was replaced with fresh media.

FRET measurements were performed 48h after seeding the cells using the microscopic FRET set-up described in section 3.2.10.1. When required, cells were FIAsh-labeled as described in section 3.2.8. During the experiment, cells were kept in 5 ml of imaging buffer and superfused with the buffer or buffer supplemented with the appropriate ligand using the Biopen<sup>®</sup> microfluidic pipette described in section 3.2.10.3. All the solutions contained 0.1% BSA.

The emission of the acceptor upon excitation at 490 nm was determined for each individual experiment to correct for its excitation upon external excitation of the donor (*cross-talk*). Additionally, the emission of the acceptor was corrected for bleed-through (spillover of the donor emission into the acceptor channel). The corrected FRET signal was then normalized and corrected for photo-bleaching. The data was processed using Clampfit and OriginPro.

For determining the activation kinetics (on-rate) of each process, the FRET change of individual experiments was fitted to a one component exponential decay function using the Clampfit software. For determining the deactivation kinetics (off-rate), the return of the FRET signal to baseline was also fitted to a one component exponential decay function. This fitting provides a time constant called tau ( $\tau$ ), which equals to  $t_{1/2}$  values divided by  $\ln 2$ . For each case,  $\tau$  values of pooled data are shown as a dot plot with median and the interquartile range (IQR), in which each dot represents an individual cell/measurement. When required, statistical significance was tested using Mann-Whitney or Kruskal-Wallis test using GraphPad Prism. Details on the statistical analysis and the number of independent measurements performed is indicated in the figure legends.

### **3.2.10.5. Acceptor photobleaching in receptor/G protein interaction studies.**

Acceptor photobleaching experiments were performed on HEK293 cells seeded on individual 24 mm glass coverslips as described for confocal microscopy in section 3.2.9. After 6h of seeding, cells were transfected with 0.6  $\mu\text{g}$  of CXCR4-YFP or  $\alpha_{2A}$ -AR-YFP, 0.7  $\mu\text{g}$  of  $G\alpha_{i1}$  subunit, 0.3  $\mu\text{g}$  of  $G\beta_1$  subunit, and 0.2  $\mu\text{g}$  of  $G\gamma_2$ -CFP subunit, per dish, using Effectene reagent. Cells were kept in 600  $\mu\text{l}$  of imaging buffer during the experiment. When indicated, cells expressing CXCR4-YFP,  $G\alpha_{i1}$ ,  $G\beta_1$  and  $G\gamma_2$ -CFP were incubated with media containing 10  $\mu\text{M}$  IT1t for 4h prior to the measurement and kept in imaging buffer containing 10  $\mu\text{M}$  IT1t during the experiments.

For the measurements, the FRET microscopic set-up described in section 3.2.10.1 was used. The CFP and YFP emission intensities were recorded for 30-40s with 20 ms illumination out of a total time of 100 ms. Next, the YFP was photobleached by illuminating at 490 nm with 90 ms illumination out of a

total time of 100 ms during 9 min. Then, the CFP and YFP emission intensities were recorded again for an additional 30-40s with 20 ms illumination out of a total time of 100 ms. The change in the CFP fluorescence ( $\Delta\text{FCFP}$ ) was calculated using the formula shown below, which takes into account fluorescence values before ( $\text{FCFP}_{\text{before}}$ ) and after ( $\text{FCFP}_{\text{after}}$ ) the photobleaching process.

$$\Delta\text{FCFP} = \frac{\text{FCFP}_{\text{after}} - \text{FCFP}_{\text{before}}}{\text{FCFP}_{\text{after}}}$$

Data was processed and analyzed using Clampfit and GraphPad Prism. Data is shown as a box plot, in which the whiskers represent maximum and minimum values. The differences between the different groups/conditions were assessed using the unpaired t-test. Details on the statistical analysis and the number of independent measurements performed is indicated in the figure legends.

### 3.2.11. Concentration-response curves in 96-well plates.

#### 3.2.11.1. Microplate reader.

The microplate reader Synergy™ Neo2 Multi-Mode from BioTEK was employed. During the measurements, cells were excited at 420/50 nm (Biotek CFP-YFP Filter; 1035013) and emission was monitored at 485/20 nm and 540/25 nm (Biotek CFP-YFP Filter; 1035043).

#### 3.2.11.2. Experimental procedure.

HEK293T cells were placed in 100 mm plates and grown until they reached 60% confluency, approximately. To measure G protein activation, 3  $\mu\text{g}$  of G protein sensor ( $G_{i1}$ ,  $G_{i2}$ ,  $G_{i3}$  or  $G_q$ ) and 1.5  $\mu\text{g}$  of receptor construct (CXCR4, 3HA-CXCR4-FIAsh226, 3HA-CXCR4-FIAsh228, 3HA-CXCR4-FIAsh229, ACKR3 or  $M_3$ -AChR) were transfected per dish. When needed, a control with cells transfected with empty plasmid instead of receptor was performed. 24h after transfection, the media of the cells was aspirated, cells were washed with 2 ml of DPBS and rinsed with 1 ml of trypsin to facilitate detachment. After, cells were resuspended in 10 ml of media and pipetted up and down several times to ensure homogenization of the cell suspension, and cell density was determined by using the Neubauer chamber. Cells were seeded at a density of 30000 cells/well in 96-well plates (black, F-bottom). The wells of the plates had been previously coated with 90  $\mu\text{l}$  poly-D-lysine for 30 minutes, the poly-D-lysine aspirated, and the wells washed once with 200  $\mu\text{l}$  of DPBS. Cells were incubated ON. 48h after transfection, the media was replaced with 90  $\mu\text{l}$ /well of imaging buffer containing 0.1% BSA, and cells incubated for 30 min at 37°C. Then, the fluorescence was read to determine the basal FRET ratio (pre-read signal). Following the pre-read measurement, 10  $\mu\text{l}$  of either imaging buffer or appropriate concentration of ligand was added to the wells for a total assay volume of 100  $\mu\text{l}$  using an electronic

multichannel pipette. The ligand concentrations are indicated in the corresponding figures. All the solutions contained 0.1% BSA. The plate was shaken shortly to ensure mix, and fluorescence was read again for additional 20 min to determine the post-read signal. The data point acquisition time was 39s. A scheme reporting the work flow for generating concentration-response curves in 96-well plates using a FRET microplate reader is shown below (**Figure 18**).

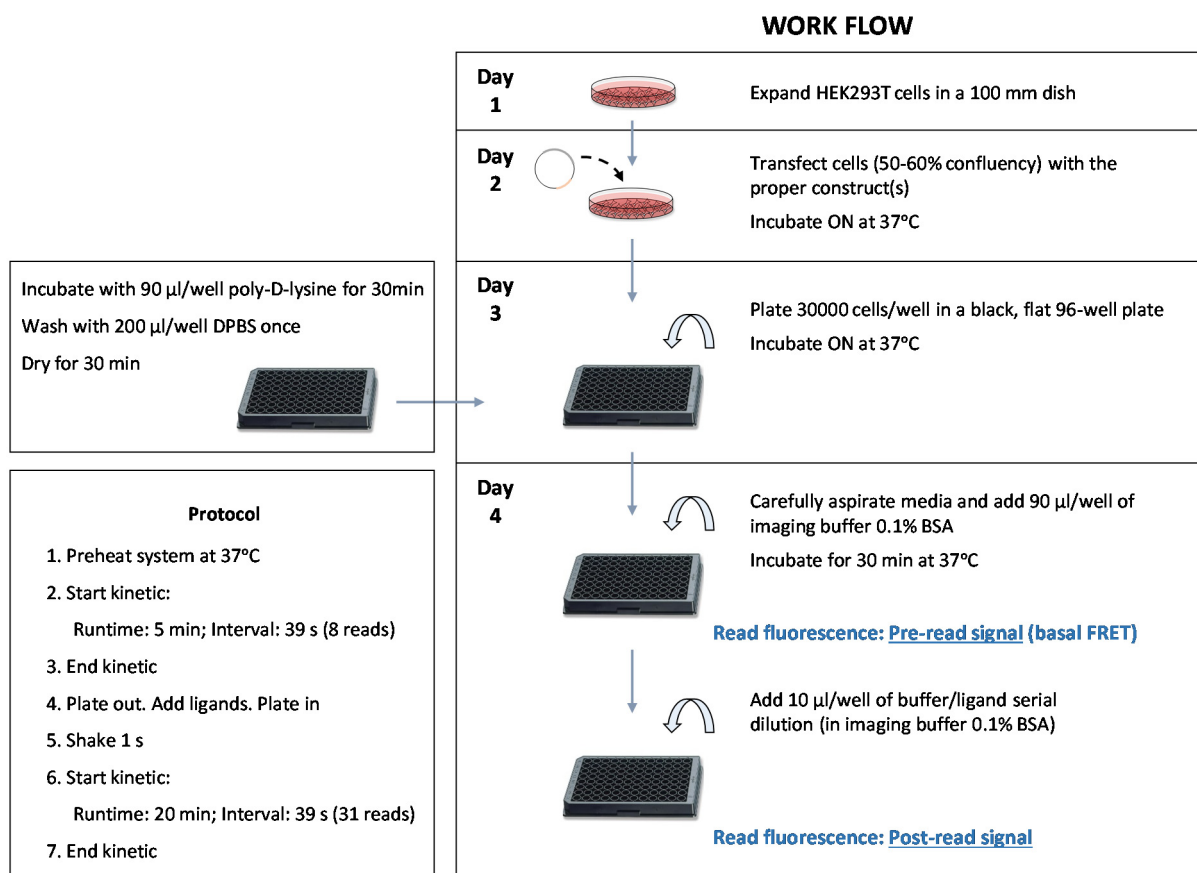


**Figure 18.** Procedure to perform concentration-response curves in 96-well plate assay format.

### 3.2.11.3. Data analysis.

The software Gen5™ Data Analysis was employed to design and perform the experiments. The protocol employed for the measurements is described in **figure 18**. Once a measurement was finished, the data was exported from the software as an excel file, which provides three tables: basal 420/50, 485/20; basal 420/50, 540/25; and the FRET ratio. The latter was used for further analysis.

First, in order to determine the FRET change produced by each concentration of ligand, the averages of the FRET values determined before ( $F_{\text{before}}$ ) and after ( $F_{\text{after}}$ ) ligand addition were calculated. The FRET change was then calculated as the ratio  $F_{\text{after}}/F_{\text{before}}$ , which is referred to as  $F_{\text{ligand}}$ . Following, each FRET change was corrected for the signal obtained in vehicle-treated cells ( $F_{\text{buffer}}$ , no ligand). For that, the FRET change produced by each concentration of ligand tested was divided by the one obtained in vehicle-treated cells:  $F_{\text{ligand}}/F_{\text{buffer}}$ .

To determine the  $EC_{50}$  values of the concentration-response curves, the data were fitted to a three-parameter sigmoidal model using GraphPad. Data show an individual experiment with mean  $\pm$  SEM. For each condition tested, at least three independent experiments were performed in quadruplicate. The mean of the  $EC_{50}$  values and the asymmetric 95% confidence interval (CI) are reported in the text. Statistical tests applied to assess differences between  $EC_{50}$  values as well as the number of independent experiments performed are indicated in the figure legends.

### 3.2.12. G protein activity in 96-well plates.

To investigate agonist-independent G protein activity via CXCR4, HEK293T cells were transfected with CXCR4 and the FRET-based  $G_{i2}$  sensor and placed in a 96-well plate at a density of 15000 cells/well (black, F-bottom) following the same procedure as described in section 3.2.11.2. 48h after transfection, the media was carefully aspirated. Cells were then treated with (i) 100  $\mu$ l of buffer for 4h; (ii) 100  $\mu$ l of buffer supplemented with 100  $\mu$ M IT1t for 4h; or (iii) 90  $\mu$ l of buffer during 4h followed by addition of 10  $\mu$ l of 1 $\mu$ M CXCL12 2min before the measurement (final agonist concentration: 100 nM). All solutions were prepared with imaging buffer containing 0.1% BSA. Then, the fluorescence was read for 10 minutes with data point acquisition time of 39s (**Figure 19**).

The microplate reader Synergy™ Neo2 Multi-Mode with the software Gen5™ were employed for the measurements (section 3.2.11.1). In order to determine the FRET under each condition, the averages of the FRET values recorded over time were calculated. Then, data were normalized to “(i) buffer treatment”, which was set to 100. Data is shown as a bar graph with SEM. Three independent repeats were performed in quadruplicate. Statistical significance was tested using unpaired t-test.



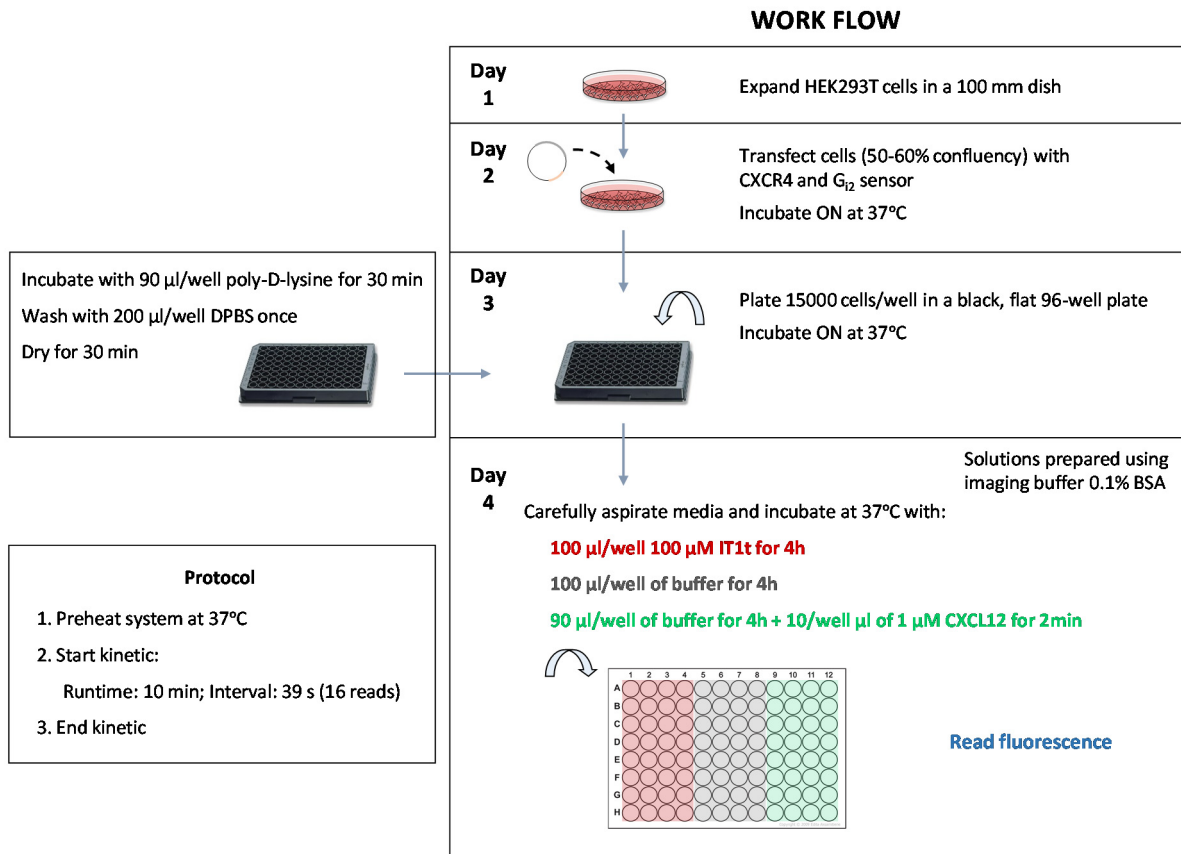


**Figure 19. Procedure to measure G protein activity in 96-well plate assay format.**

### 3.2.13. Membrane preparation.

HEK293T cell membranes were prepared at the Vrije University. 1.5 million HEK293T cells were seeded in a 100 mm dish. After 24h, the culture media was replaced with 8 ml of fresh media and cells transfected. For transfection, 5 µg of DNA (250 ng of plasmid of interest (ACKR3, HA-ACKR3, HA-ACKR3-CFP or HA-ACKR3-FIAsH-CFP) and 4.75 µg of empty pcDEF3 plasmid) were combined with 30 µl of PEI (25 kDa linear) in a total volume of 500 µl 150 mM NaCl solution. The mix was vortexed and incubated for 20 minutes at RT. Subsequently, the DNA/PEI mix was added to the cells. Two days after transfection, cells were washed with 5 ml ice-cold PBS, then resuspended in 5 ml ice-cold DPBS and centrifuged at 1500g for 10 min at 4°C. The supernatant was discarded. The pellet was resuspended in 2.5 ml cold PBS, centrifuged again under the same conditions and the pellet resuspended in 0.5 ml of membrane buffer. Cells were homogenized by 10 strokes at 1100–1200 rpm using a teflon-glass homogenizer and rotor. Then, the membranes were subjected to two freeze-thaw cycles using liquid nitrogen and centrifuged at 40000g for 25 min at 4°C. The supernatant was discarded, and the pellet was washed with cold Tris-sucrose buffer. Finally, the pellet was resuspended in cold Tris-sucrose buffer, frozen in liquid nitrogen and stored at -80°C until further use in binding assays. Protein concentration was determined using a BCA protein assay kit.

### 3.2.14. Radioligand competition binding assays.

The binding assays were performed at the Vrije University. Membranes prepared as in section 3.2.13 were thawed, homogenized using a syringe and a 23G needle (10x), and diluted in binding buffer to the desired concentration. Then, 50  $\mu$ l (1  $\mu$ g/well) of membranes were added per well in a 96-well plate (clear, U-bottom) and incubated with 25  $\mu$ l of increasing concentrations of unlabeled CXCL12 (concentrations are indicated in the corresponding figures). Next, 25  $\mu$ l/well of 50 pM  $^{125}$ I-CXCL12 were added and the plate was incubated for 2 h at 25°C with gentle agitation. The incubations were terminated by rapid filtration through UniFilter 96-well GF/C plates presoaked with 0.5% PEI using ice-cold wash buffer to separate free from bound radioligand. The filter plates were then dried at 52°C, and 25  $\mu$ l/well scintillation fluid were added. Bound radioactivity was quantified using a MicroBeta scintillation counter (PerkinElmer).

To determine the EC<sub>50</sub> values of the concentration-response curves, the data were fitted to a three-parameter sigmoidal model using GraphPad. Data show an individual experiment with mean  $\pm$  SEM. The mean of the EC<sub>50</sub> values obtained and the asymmetric 95% confidence interval (CI) are reported in the text. Statistical significance was tested using one-way ANOVA followed by Tukey's test.

### 3.2.15. Luciferase reporter assay.

The luciferase reporter assays to characterize the activity of the cAMP/PKA signaling pathway triggered by different CXCR4 constructs were performed at the Vrije University. For transfection, 2  $\mu$ g of DNA were combined with 12  $\mu$ g of PEI (25 kDa linear) in a total volume of 250  $\mu$ l 150 mM NaCl and incubated at RT for 20 minutes. The construct of interest (CXCR4, 3HA-CXCR4, 3HA-CXCR4-CFP or 3HA-CXCR4-FIAsh228-CFP) and the pcDEF3-CRE-Luc construct (Watts et al., 2013) were transfected in a 1:6 ratio (DNA/PEI). Next, 1 million resuspended HEK293T cells were added to the DNA/PEI mix, and 80  $\mu$ l/well were seeded on a 96-well plate (white, F-bottom) at a density of 32000 cells/well. Analysis was done 24h after seeding the cells using Mithras LB940 (Berthold Technologies). The day of the measurement, cells were incubated in media alone or media supplemented with 1  $\mu$ M forskolin and increasing concentrations of CXCL12 (indicated in the figure), and incubated for 6 hours at 37°C. Following, media was aspirated, and 25  $\mu$ l/well of luciferase assay reagent added and incubated for 20 minutes in the dark. Then, the plate luminescence was measured and quantified.

The data from concentration-response curves were fitted to a three-parameter sigmoidal model using GraphPad. Data shows an individual experiment with mean  $\pm$  SEM. For each construct tested, four independent experiments were conducted in quadruplicate. The mean of the EC<sub>50</sub> values obtained and the asymmetric 95% CI are reported in the text.

## 4. RESULTS

### 4.1. CXCR4.

In the past few years, the crystal structure of CXCR4 has been solved in combination with different molecules, which provided more detailed information on how the interaction of chemokine receptors with chemokines occur. Nevertheless, the kinetic and dynamic details of the activation mechanism of this receptor upon ligand binding remain unknown. This section is focused on the study of the early signaling steps of CXCR4 activation in response to CXCL12 binding, an important axis in many physiological and pathological processes. For this purpose, FRET-based methods were employed to study the following events: receptor activation, interaction of the receptor with the G protein, G protein activation, and rearrangements between receptor protomers. In addition, the activation of CXCR4 in response to MIF and lactoferrin, two ligands recently described to bind this receptor, was investigated.

#### 4.1.1. Design of FRET-based CXCR4 sensors.

FRET-based sensors for CXCR4 were generated to study the conformational changes that this receptor undergoes during ligand-induced activation. It is well known that the TM region of GPCRs as well as the intracellular loops undergo significant movements when the receptor is activated. Specifically, there is a conserved shift of TM6 away from the TM bundle (section 1.1.3.1). This information has been used in several occasions to develop FRET-based sensors for several receptors (Stumpf and Hoffmann, 2016), in which FRET-compatible fluorescent probes are attached into domains of the receptor known to be conformationally sensitive, such as the intracellular loops or the C-terminus (section 1.5.4).

The structural information published in recent years on CXCR4 was used as a basis for the development of FRET-based sensors for this receptor. CFP was fused to the end of the C-terminus and the short FIAsh-binding sequence CCPGCC (one letter amino acid code) was introduced at three different positions within the ICL-3 of the receptor. Therefore, a total of three different sensors were generated, which were named according to the position of the FIAsh-binding sequence in the loop: 3HA-CXCR4-FIAsh226-CFP (between L226 and S227), 3HA-CXCR4-FIAsh228-CFP (between H228 and S229), and 3HA-CXCR4-FIAsh229-CFP (between S229 and K230). In addition, all the constructs contained three consecutive HA tags fused to the N-terminal end of the receptor. **Figure 20** schematically shows the insertion sites.

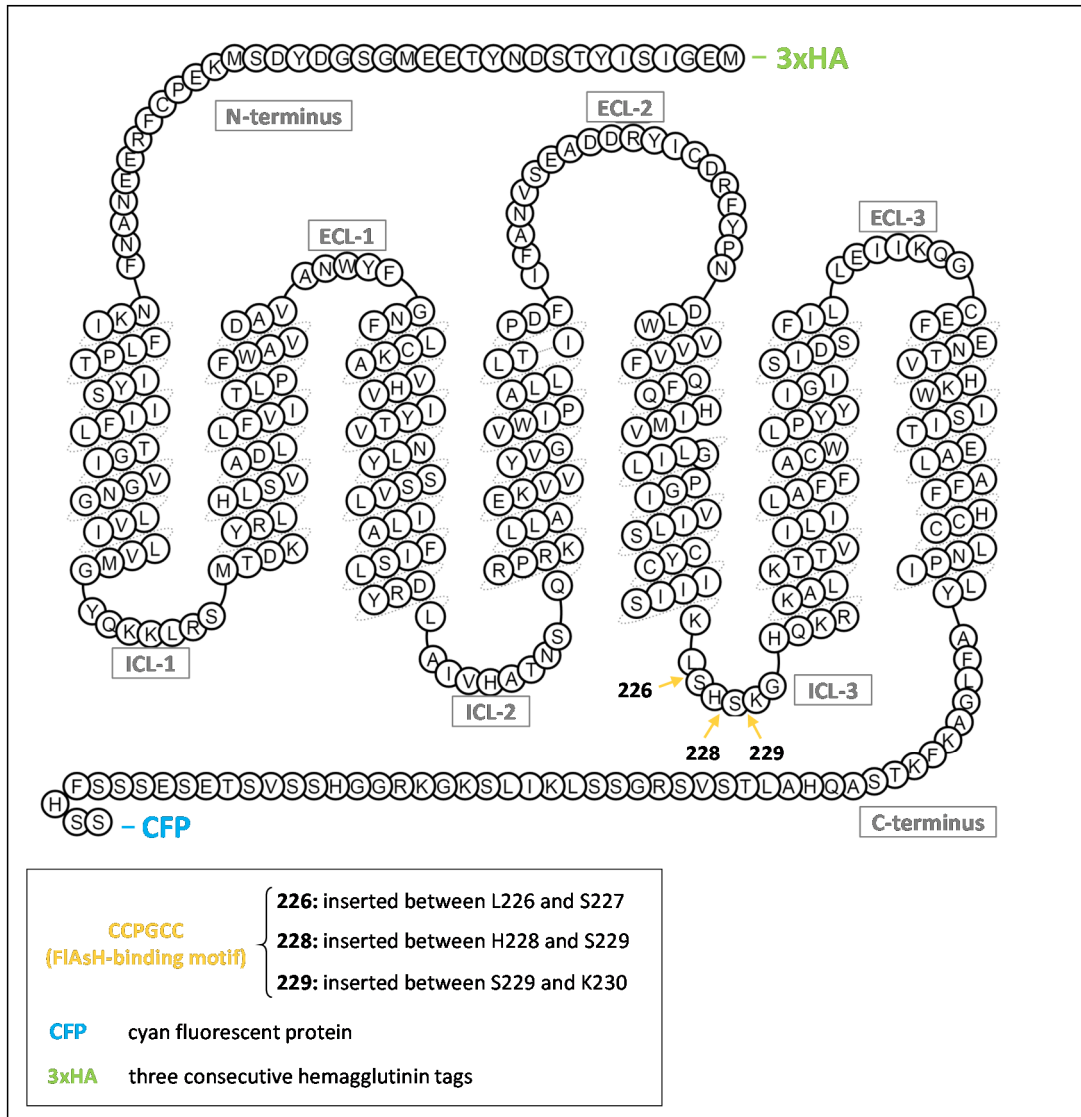


**Figure 20.** Protein sequence of the human CXCR4 depicting the insertion positions of the tags and fluorophores used. Source: GPCR database (GPCRdb).

#### 4.1.2. Characterization of the FRET-based CXCR4 sensors.

The first step after the development of the sensors was the characterization of the constructs properties to confirm the existence of FRET in the system and to verify that the functions of the receptor remain unaltered. For that purpose, the expression and cellular localization of the sensors, the FRET efficiency, as well as downstream signaling properties were investigated.

##### 4.1.2.1. Expression and localization.

The expression and localization of the CXCR4 constructs was assessed by fluorescence confocal microscopy in HEK293 cells transiently expressing each of the sensors. The images obtained after excitation of CFP at 442 nm show that the construct 3HA-CXCR4-CFP, which contains the CFP at the C-terminus, as well as all the receptor sensors, which additionally contain the FIAsh-binding motif at different positions within the ICL-3 (3HA-CXCR4-FIAshH226-CFP, 3HA-CXCR4-FIAshH228-CFP and 3HA-CXCR4-FIAshH229-CFP), localize to the plasma membrane (**Figure 21A-D**). This indicates that neither the fusion of CFP nor the insertion of the FIAsh-binding sequence affect the overall structure of the receptor or trafficking to the plasma membrane.

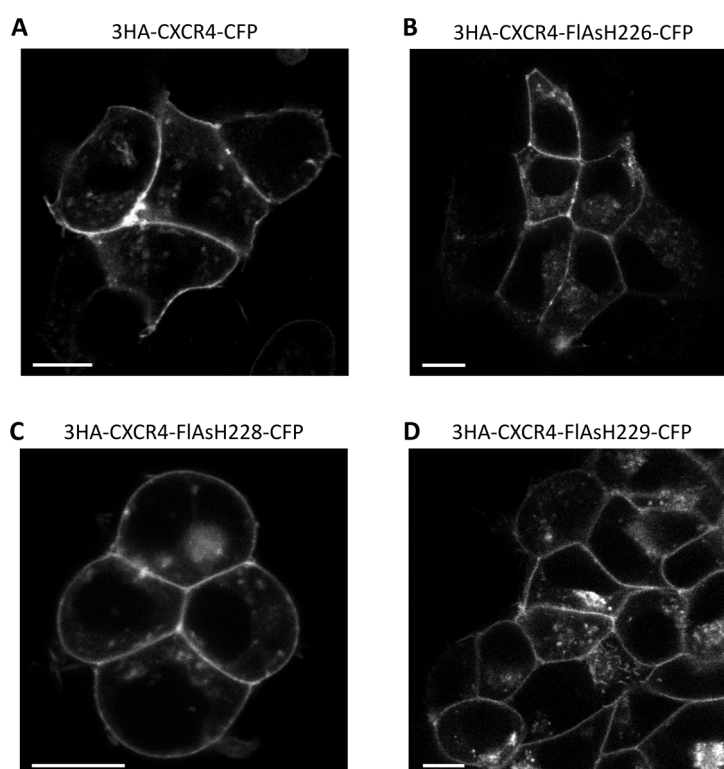


**Figure 21. The CXCR4 constructs are expressed in the plasma membrane of HEK293 cells.** Confocal images of cells transiently overexpressing 3HA-CXCR4-CFP (A), 3HA-CXCR4-FIAshH226-CFP (B), 3HA-CXCR4-FIAshH228-CFP (C), or 3HA-CXCR4-FIAshH229-CFP (D). Panels show CFP emission upon excitation at 442 nm. Scale bars represent 10  $\mu$ m.

#### 4.1.2.2. FRET efficiency.

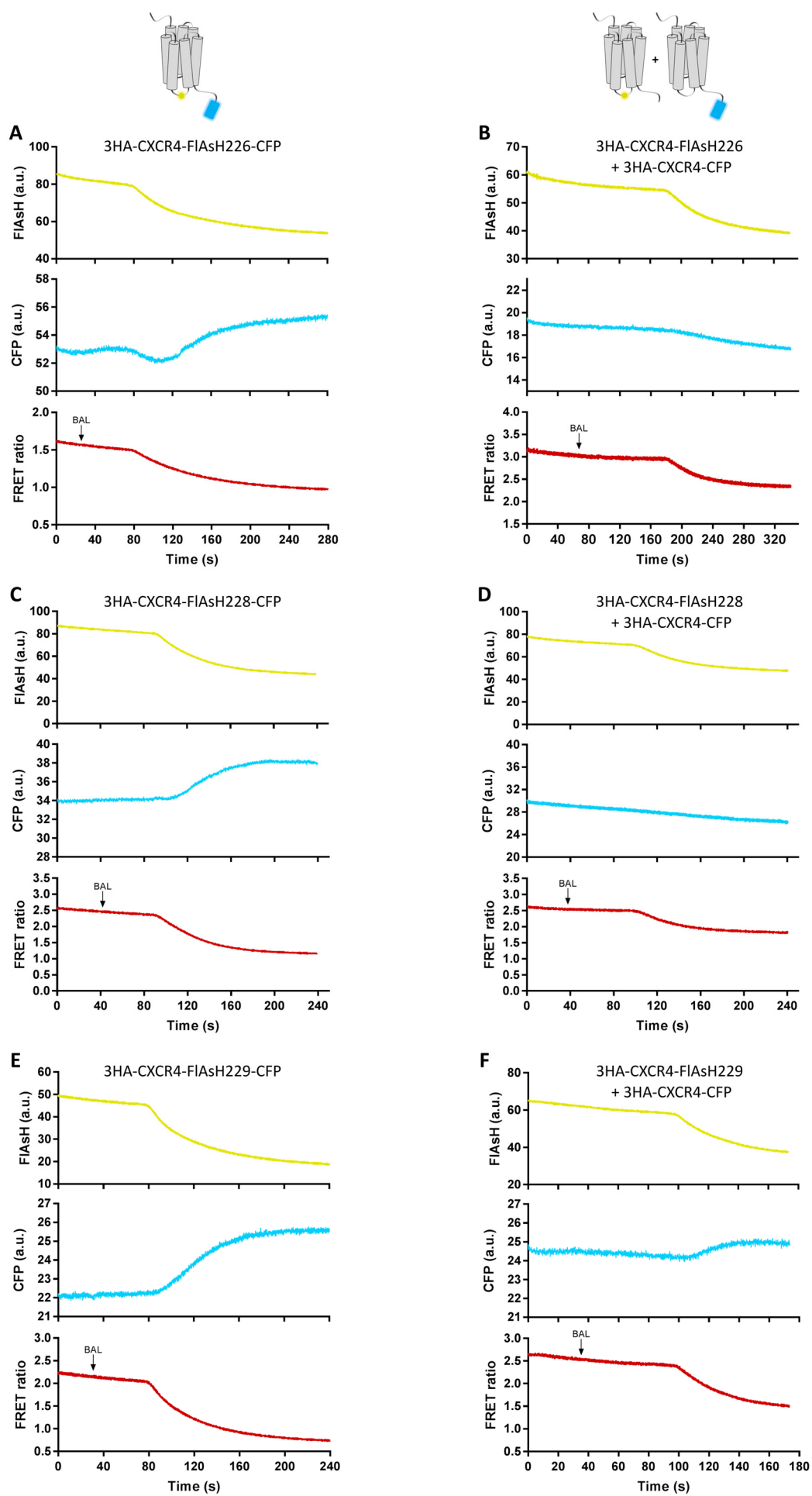
The existence of basal intramolecular FRET was investigated by means of acceptor bleaching experiments using BAL in HEK293 cells expressing each of the sensors (3HA-CXCR4-FIAsH226-CFP, 3HA-CXCR4-FIAsH228-CFP or 3HA-CXCR4-FIAsH229-CFP) and FIAsH-labeled prior to the measurement. This compound presents high affinity for arsenicals and, at high concentrations, displaces FIAsH from its binding site inserted into the receptor's ICL-3. Addition of 5 mM BAL produced a loss in the FIAsH fluorescence and an increase in the CFP fluorescence, indicating the existence of basal FRET in all three sensors (**Figure 22A, C and E**). The FRET efficiency was calculated based on the increase in the CFP emission, and was determined to be  $5.0 \pm 0.8 \%$ ,  $12.0 \pm 0.7 \%$ , and  $16.5 \pm 1.0 \%$  (mean  $\pm$  SEM) for 3HA-CXCR4-FIAsH226-CFP, 3HA-CXCR4-FIAsH228-CFP, and 3HA-CXCR4-FIAsH229-CFP, respectively (**Figure 22G; Table 4**).

The same procedure was followed to investigate the existence of intermolecular FRET, which is FRET between fluorophores found in different receptors. In this case, cells co-expressing individually CFP- and FIAsH-labeled receptors were analyzed. No basal FRET was detected when the constructs 3HA-CXCR4-FIAsH226 or 3HA-CXCR4-FIAsH228 were co-expressed with 3HA-CXCR4-CFP (**Figure 22B, D and H; Table 4**). Considering that CXCR4 has been described to form homodimers (section 1.3.3), the lack of basal intermolecular FRET excludes the possibility that the observed FRET signal is influenced by neighboring receptors or protomers within dimers. A small signal of  $3.8 \pm 0.6 \%$  was observed when 3HA-CXCR4-FIAsH229 was co-expressed with 3HA-CXCR4-CFP (**Figure 22F and H; Table 4**).

**Table 4. Intra- and intermolecular FRET efficiency values of the CXCR4 constructs.**

Values are given in percentage as mean  $\pm$  SEM.

Sensor	Intramolecular FRET (%)	Intermolecular FRET (%)
3HA-CXCR4-FIAsH226-CFP	$5.0 \pm 0.8$	0
3HA-CXCR4-FIAsH228-CFP	$12.0 \pm 0.7$	0
3HA-CXCR4-FIAsH229-CFP	$16.5 \pm 1.0$	$3.8 \pm 0.6$



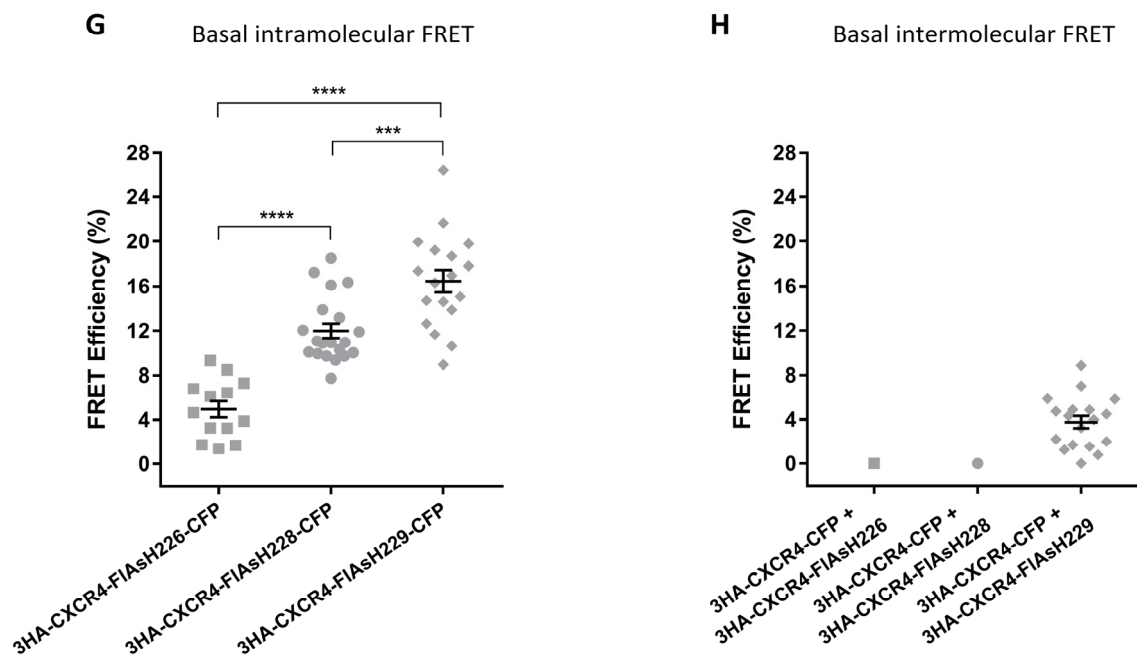


**Figure 22. The CXCR4 sensors exhibit basal intramolecular FRET.** Basal FRET was determined based on the changes detected in the CFP fluorescence after addition of BAL. **(A-F)** Representative traces of FRET efficiency measurements. Intramolecular FRET of the 3HA-CXCR4-FIAsH226-CFP (A), 3HA-CXCR4-FIAsH228-CFP (C), and 3HA-CXCR4-FIAsH229-CFP (E) sensors. Intermolecular FRET when 3HA-CXCR4-CFP was co-expressed with 3HA-CXCR4-FIAsH226 (B), 3HA-CXCR4-FIAsH228 (D), or 3HA-CXCR4-FIAsH229 (F). **(G)** Intramolecular FRET efficiency values. Data show mean  $\pm$  SEM of  $n=13-20$  cells measured on at least three independent experimental days. Statistical significance was tested using one-way ANOVA followed by Tukey's test. \*\*\* $p \leq 0.001$ . \*\*\*\* $p \leq 0.0001$ . **(H)** Intermolecular FRET efficiency values. Data show mean  $\pm$  SEM of  $n=11-18$  cells measured on two independent experimental days.



#### 4.1.2.3. Downstream signaling properties.

The CXCR4 sensors contain the FIAsh-binding motif CPGGCC inserted in different positions within ICL-3, a loop generally known to be important for G protein coupling (Oldham and Hamm, 2008). Therefore, their ability to induce G protein activation upon CXCL12 stimulation was tested by means of using a FRET-based sensor for the  $G_{i1}$  protein (van Unen et al., 2016). This sensor, composed of the  $G\alpha_{i1}$  subunit fused to mTurquoise2, the  $G\beta_1$  subunit, and the  $G\gamma_2$  subunit fused to Venus, monitors the activation of  $G_{i1}$  proteins as a decrease in FRET between the fluorophores. For the measurements, HEK293 cells co-transfected with the  $G_{i1}$  sensor and CXCR4 or CXCR4 containing the FIAsh-binding motif in ICL-3 (3HA-CXCR4-FIAshH226, 3HA-CXCR4-FIAshH228, or 3HA-CXCR4-FIAshH229) were stimulated with increasing concentrations of CXCL12 to obtain a concentration-response curve. The data show that the constructs containing the FIAsh-binding sequence preserve the ability to activate  $G_{i1}$ , although with slight lower potency than the wt receptor. Importantly, the maximal activity elicited by these constructs is comparable to the wt receptor (**Figure 23A; Table 5**).

**Table 5.  $EC_{50}$  values for G protein activation mediated by different CXCR4 constructs in response to increasing concentrations of CXCL12.** Mean and 95% confidence interval are shown.

Construct	$EC_{50}$ [95% CI], nM
CXCR4	3.4 [2.3-4.9]
3HA-CXCR4-FIAshH226	18.1 [5.3-62.2]
3HA-CXCR4-FIAshH228	15.5 [9.3-25.9]
3HA-CXCR4-FIAshH229	17.1 [4.9-59.3]

The 3HA-CXCR4-FIAshH228-CFP construct was employed to test the functionality of the sensor, i.e. in the presence of both the FIAsh-binding sequence and the CFP. The ability of CXCL12 to inhibit FSK-induced cAMP accumulation in HEK293T cells expressing the sensor, in comparison to cells expressing 3HA-CXCR4-CFP, 3HA-CXCR4 or the wt receptor, was tested. All the constructs mediate the inhibition of cAMP production in response to CXCL12 stimulation, although the construct 3HA-CXCR4-FIAshH228-CFP exhibits slight lower potency than the wt receptor. Moreover, the introduction of the HA tags at the N-terminus does not have a significant effect on the receptor's ability to signal, and the fusion of CFP at the C-terminus contributes to a lower potency of these constructs in downstream signaling. Most importantly, the maximal activity elicited by the sensor is comparable to the wt receptor (**Figure 23B; Table 6**).

**Table 6. EC<sub>50</sub> values for FSK-induced cAMP inhibition mediated by different CXCR4 constructs in response to increasing concentrations of CXCL12.** Mean and 95% confidence interval are shown.

Construct	EC <sub>50</sub> [95% CI], nM
CXCR4	2.2 [0.6-8.0]
3HA-CXCR4	4.7 [1.2-18.1]
3HA-CXCR4-CFP	10.6 [1.9-57.9]
3HA-CXCR4-FIAsh228-CFP	19.0 [3.5-102.7]

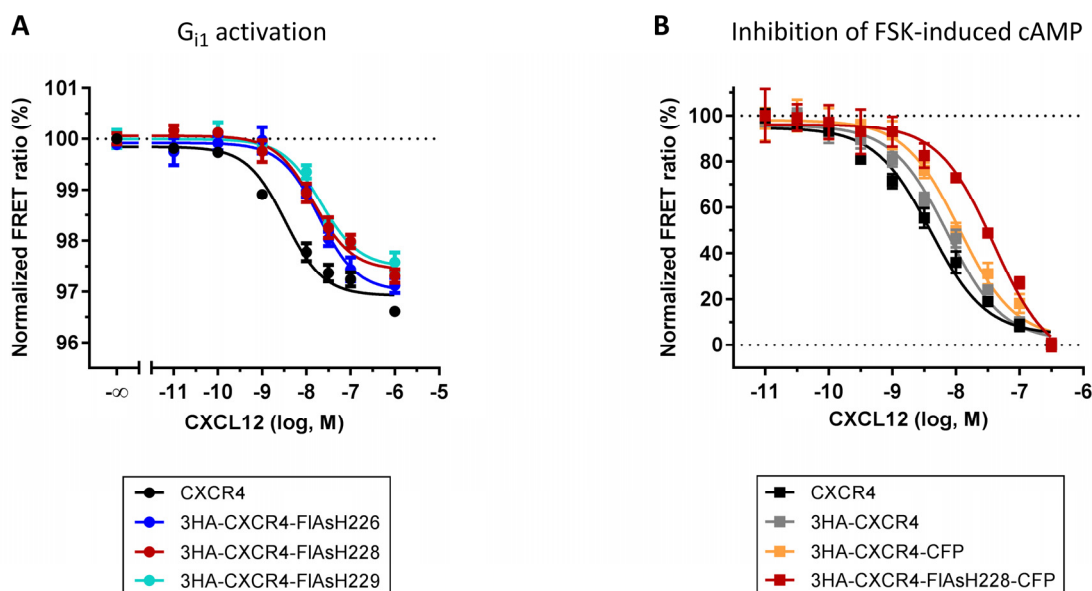


**Figure 23. The CXCR4 constructs preserve the ability to signal via G<sub>i</sub> proteins. (A)** G protein activation by CXCR4, 3HA-CXCR4-FIAsh226, 3HA-CXCR4-FIAsh228, or 3HA-CXCR4-FIAsh229 in response to increasing concentrations of CXCL12 was assessed by using the FRET-based G<sub>i1</sub> sensor. Three independent experiments were conducted in quadruplicate. An individual experiment is shown with mean ± SEM. In this particular case, the EC<sub>50</sub> values for each of the constructs, in order, were 3.3, 14.7, 19.3, and 21.4 nM. **(B)** G<sub>αi</sub> activity in response to CXCL12 was measured as inhibition of FSK-induced cAMP production in cells expressing CXCR4, 3HA-CXCR4, 3HA-CXCR4-CFP, or 3HA-CXCR4-FIAsh228-CFP. Four independent experiments were conducted in triplicate. An individual experiment is shown with mean ± SEM. In this particular case, the EC<sub>50</sub> values for each of the constructs, in order, were 4.0, 7.3, 11.3, and 39.0 nM. All data were fitted using a three-parameter sigmoidal model.

#### 4.1.3. Activation of CXCR4 in response to CXCL12.

The CXCR4 sensors were used to investigate the conformational changes that the receptor undergoes upon CXCL12 binding (**Figure 24A**). HEK293 cells transiently expressing each of the constructs were FIAsh-labeled prior to the measurement. Then, single HEK293 cells were superfused with buffer, followed by a saturating concentration of CXCL12 and buffer again. The concentration of ligand must be saturating in order to determine the maximal (fastest) kinetics as well as to ensure that diffusion of the molecules to the receptors is not time-limiting. The BioPen<sup>®</sup> microfluidic system, which permits to deliver the solutions to one or few cells without affecting the surrounding cells, was employed for the measurements (Ainla et al., 2010; Ainla et al., 2012; Wright et al., 2018).

All three CXCR4 sensors reported conformational changes in response to ligand binding. Upon stimulation with 30  $\mu$ M CXCL12, a fast increase in the FIAsh emission and a simultaneous decrease in the CFP emission were detected, leading to an increase in the FRET signal (**Figure 24B-D**). The amplitude of the FRET change detected upon activation was different in each of the sensors:  $2.1 \pm 0.2$  % (mean  $\pm$  SEM) for 3HA-CXCR4-FIAsh226-CFP,  $2.9 \pm 0.2$  % for 3HA-CXCR4-FIAsh228-CFP, and  $1.7 \pm 0.2$  % for 3HA-CXCR4-FIAsh229-CFP (**Figure 24F; Table 7**). Therefore, 3HA-CXCR4-FIAsh228-CFP produced the highest FRET change. Since the CFP is found in the same position in every sensor, the differences in the amplitude are probably due to the different positions in which the FIAsh-binding motif has been introduced in ICL-3.

In a similar manner as it has been previously done for other GPCRs, these rapid FRET measurements were used to determine the activation and deactivation kinetics of the receptor (Hoffmann et al., 2005). For this purpose, a one component exponential decay function was fitted into the FRET signal, which provides the time constant  $\tau$  (**Figure 24E**). Activation of the receptor (on-rate) upon CXCL12 binding occurred with  $\tau = 600$  (360-820) ms (median and interquartile range, IQR) using the 3HA-CXCR4-FIAsh226-CFP sensor,  $\tau = 590$  (440-710) ms using the 3HA-CXCR4-FIAsh228-CFP sensor, and  $\tau = 530$  (400-660) ms using the 3HA-CXCR4-FIAsh229-CFP sensor (**Figure 24G**). After activation of the receptor, rapid superfusion of the cells with buffer produced ligand withdrawal and returned the FRET signal to baseline, allowing to determine the off-kinetics of the receptor (off-rate). Deactivation of CXCR4 after wash-out of cells with buffer occurred with  $\tau = 20.7$  (11.6-27.1) s using the 3HA-CXCR4-FIAsh228-CFP sensor (**Figure 24H**). Data have been summarized in **table 7**.

**Table 7. Summary of the parameters determined using the FRET-based CXCR4 sensors.**

Construct	Signal amplitude (%) Mean $\pm$ SEM	On-rate ( $\tau$ , ms) Median (IQR)	Off-rate ( $\tau$ , s) Median (IQR)
3HA-CXCR4-FIAsh226-CFP	$2.1 \pm 0.2$	600 (360-820)	-
3HA-CXCR4-FIAsh228-CFP	$2.9 \pm 0.2$	590 (440-710)	20.7 (11.6-27.1)
3HA-CXCR4-FIAsh229-CFP	$1.7 \pm 0.2$	530 (400-660)	-

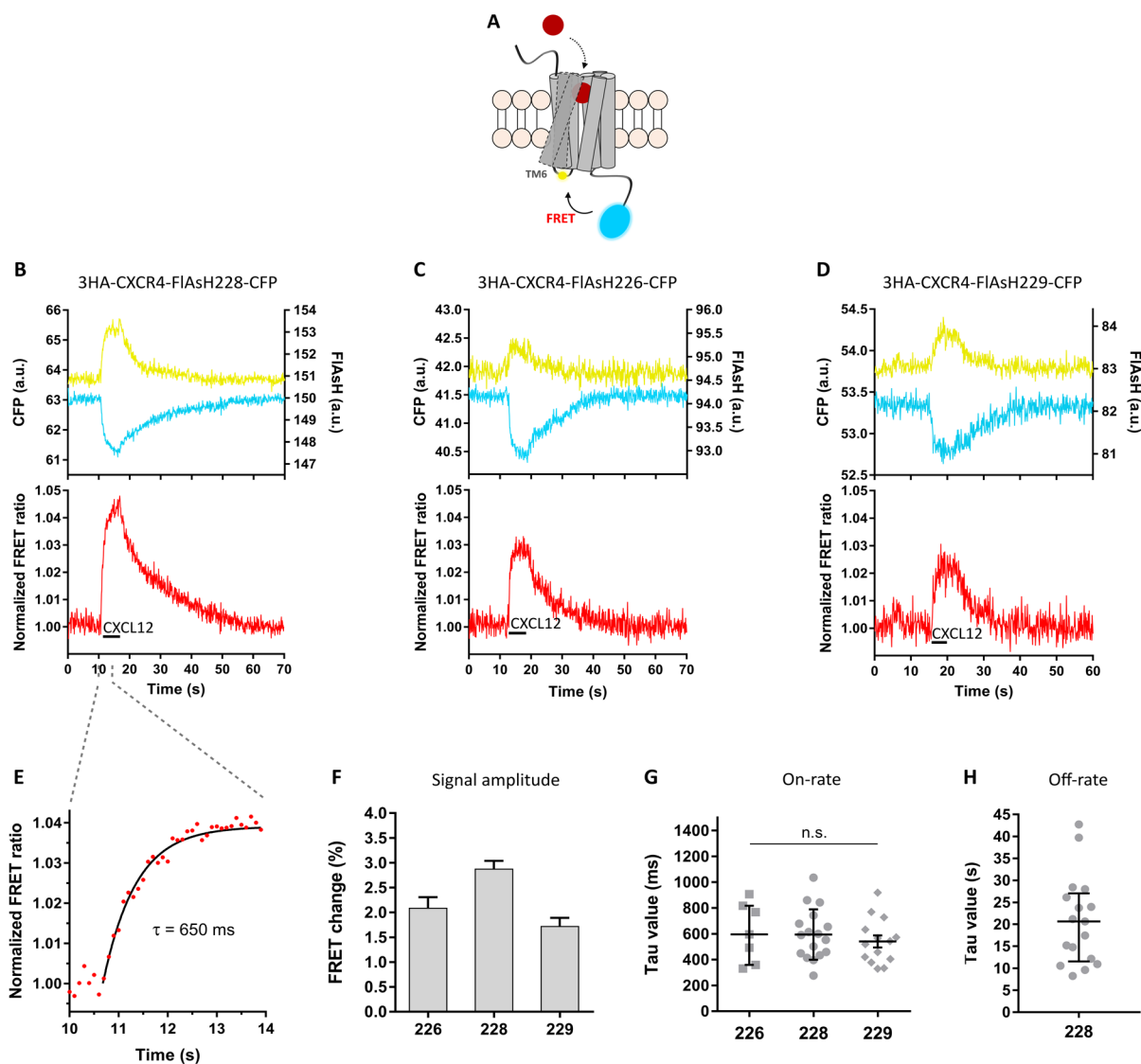


**Figure 24. The FRET-based CXCR4 sensors report the dynamics and kinetics of receptor activation and deactivation.** **(A)** FRET-based receptor sensor. Ligand-induced structural rearrangements are monitored as changes in FRET. **(B-D)** Representative traces of the FRET response from a single HEK293 cell transiently overexpressing the 3HA-CXCR4-FIAsH228-CFP (B), 3HA-CXCR4-FIAsH226-CFP (C), or 3HA-CXCR4-FIAsH229-CFP (D) sensor and stimulated with 30  $\mu$ M CXCL12. Corrected and normalized FRET ratios are shown in the lower panels. Corrected FIAsh (yellow) and CFP (cyan) emission intensities are shown in the upper panels. **(E)** Kinetic analysis of receptor activation using the 3HA-CXCR4-FIAsH228-CFP sensor. The FRET change was fitted to a one component exponential decay function to obtain the time constant  $\tau$ . **(F)** FRET amplitude detected in each of the sensors upon CXCL12 stimulation. Mean  $\pm$  SEM is shown. **(G)** On-kinetics of CXCR4 upon CXCL12 binding as determined using the three sensors. Data show median and IQR. Statistical significance was tested using Kruskal-Wallis test (n.s.=non-significant). **(H)** Off-kinetics of CXCR4 as determined using the 3HA-CXCR4-FIAsH228-CFP sensor upon wash-out of the ligand with buffer. Data show median and IQR. In F-H, n=7 cells for 3HA-CXCR4-FIAsH226-CFP, n=17 cells for 3HA-CXCR4-FIAsH228-CFP, and n=14 cells for 3HA-CXCR4-FIAsH229-CFP, measured at least on three independent experimental days. 226, 228, and 229 refer to 3HA-CXCR4-FIAsH226-CFP, 3HA-CXCR4-FIAsH228-CFP, and 3HA-CXCR4-FIAsH229-CFP, respectively.

#### 4.1.4. Interaction of CXCR4 with G<sub>i</sub> proteins.

Generally, the next step in the signaling cascade after receptor activation is the interaction of the receptor with G proteins. In particular, CXCR4 couples primarily to G proteins of the G<sub>i</sub> family, thus the speed of coupling of the receptor with G<sub>i1</sub> was investigated. For that, HEK293 cells were transfected with CXCR4-YFP and the individual G protein subunits G $\alpha_{i1}$ /G $\beta_1$ /G $\gamma_2$ -CFP. Single cells were then stimulated with a saturating concentration of CXCL12 (30  $\mu$ M) using the BioPen<sup>®</sup>. In parallel, the interaction of  $\alpha_{2A}$ -AR-YFP with the G protein in response to norepinephrine (100  $\mu$ M) was also analyzed under the same conditions. **Figure 25A** schematically shows the setting of the experiment. Regarding  $\alpha_{2A}$ -AR, a rapid increase in the FRET ratio was observed upon stimulation with norepinephrine (**Figure 25C**), as previously described for this and other GPCRs in response to agonist stimulation (Hein et al., 2005; Hein et al., 2006; Ferrandon et al., 2009; C. Hoffmann et al., 2012). In contrast, stimulation of CXCR4 with CXCL12 (30  $\mu$ M) resulted in a decrease in the FRET signal with an amplitude of  $3.3 \pm 0.3$  % (**Figure 25D and G**), and this interaction occurred with a time constant  $\tau = 960$  (870-980) ms (**Figure 25F**). To further investigate this effect, the interaction of CXCR4-YFP with the G protein CFP-labeled at the G $\alpha_{i1}$  subunit was investigated (**Figure 25B**). Again, stimulation of the cells with CXCL12 led to a decrease in FRET, although the amplitude of the FRET signal was smaller than when the G protein was labeled at the G $\gamma_2$  subunit ( $2.6 \pm 0.2$  %; **Figure 25E and G**). In this setting, the receptor/G protein interaction occurred at a speed of  $\tau = 1030$  (750-1320) ms (**Figure 25F**), which is similar to the kinetics determined when the G protein was CFP-labeled at the G $\gamma_2$  subunit.

As described in section 1.1.3.2, whether receptors are pre-associated with G proteins or only associate upon agonist exposure is still a matter of debate, and so far, it seems to be dependent on the receptor/G protein pair. To further investigate the coupling of CXCR4 with the G<sub>i1</sub> protein in the absence of agonist, acceptor photobleaching experiments were performed on HEK293 cells expressing CXCR4-YFP and the G protein subunits G $\alpha_{i1}$ /G $\beta_1$ /G $\gamma_2$ -CFP (**Figure 26A**). The  $\alpha_{2A}$ -AR-YFP construct was tested in parallel under the same conditions. Theoretically, an increase in the CFP fluorescence ( $F_{\text{CFP}}$ ) after YFP bleaching would indicate the existence of basal FRET and suggest close proximity between the receptor and the G protein. After YFP photobleaching, no considerable change in  $F_{\text{CFP}}$  was detected with the  $\alpha_{2A}$ -AR ( $\Delta F_{\text{CFP}} = 0.1 \pm 0.4$  % (mean  $\pm$  SEM; **Figure 26B-C**), in agreement with published data (Hein et al., 2005). In contrast, a significant increase in  $F_{\text{CFP}}$  was detected with CXCR4 ( $\Delta F_{\text{CFP}} = 2.1 \pm 0.3$  %; **Figure 26B and D**), indicating the existence of basal energy transfer prior to the photobleaching process. To further investigate this effect, cells were treated with 10  $\mu$ M IT1t prior to and during the measurement. In this case, no increase in  $F_{\text{CFP}}$  upon YFP bleaching was observed ( $\Delta F_{\text{CFP}} = 0.3 \pm 0.3$  %; **Figure 26B and E**). Altogether, these findings indicate that, in contrast to  $\alpha_{2A}$ -AR, CXCR4 and G<sub>i</sub> proteins remain within FRET distance, which might reflect a potential interaction between these two partners in the absence of agonist.

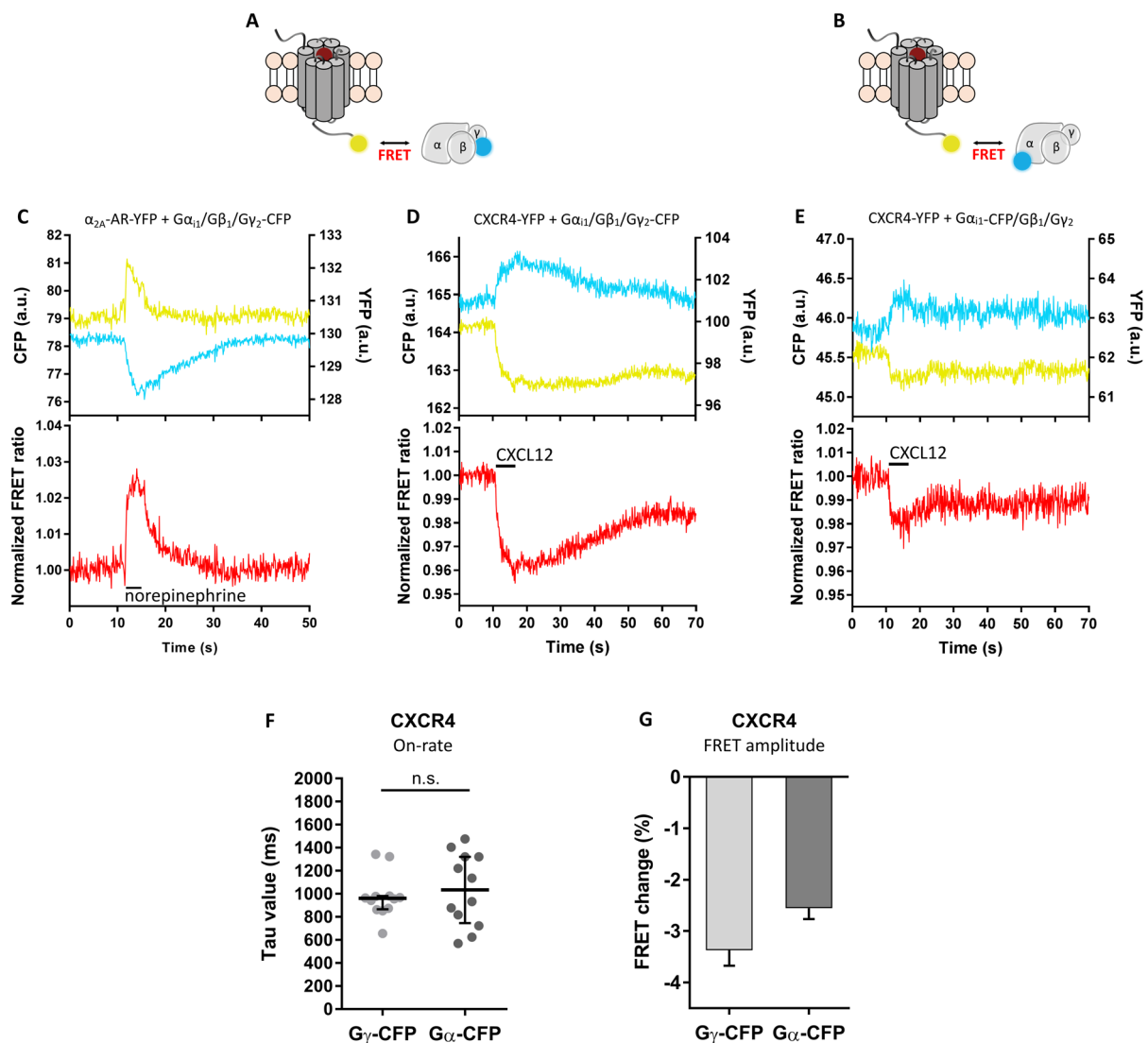


**Figure 25. CXCL12 binding to CXCR4 induces rearrangements between the receptor and the G<sub>11</sub> protein. (A, B)** Schematic depicting the setting employed to investigate the kinetics of receptor/G protein interaction. HEK293 cells transiently expressing CXCR4-YFP or  $\alpha_{2A}$ -AR-YFP and the G protein subunits G $\alpha_{i1}$ /G $\beta_1$ /G $\gamma_2$ -CFP (A) or G $\alpha_{i1}$ -CFP/G $\beta_1$ /G $\gamma_2$  (B) were stimulated with their respective agonists. Upon activation, rearrangements between the receptor and the G protein lead to a change in FRET. **(C-E)** Representative traces of the FRET response from a single cell expressing  $\alpha_{2A}$ -AR-YFP + G $\alpha_{i1}$ /G $\beta_1$ /G $\gamma_2$ -CFP (C), CXCR4-YFP + G $\alpha_{i1}$ /G $\beta_1$ /G $\gamma_2$ -CFP (D), or CXCR4-YFP + G $\alpha_{i1}$ -CFP/G $\beta_1$ /G $\gamma_2$  (E), and stimulated with 100  $\mu$ M norepinephrine or 30  $\mu$ M CXCL12. Upper panels show corrected YFP (yellow) and CFP (cyan) emission intensities. Lower panels show corrected and normalized FRET ratio. **(F)** On-kinetics of CXCR4/G protein interaction in response to CXCL12. The scatter plots show median and IQR. Statistical significance was tested using Mann-Whitney test (n.s.=non-significant). **(G)** FRET amplitude detected in each of the settings with CXCR4 upon CXCL12 stimulation. In F-G, n=12 cells for each setting from at least three independent experiments.

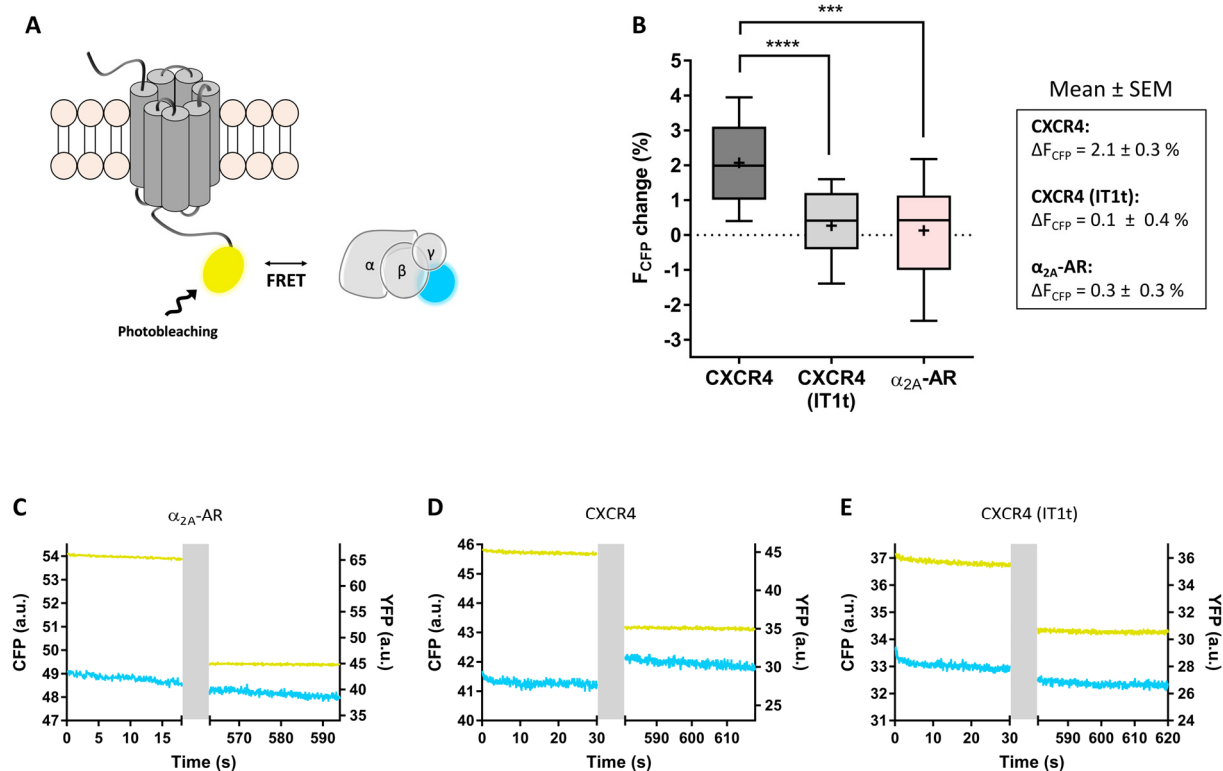


**Figure 26. CXCR4 and  $G_{i1}$  proteins remain within FRET distance in the absence of agonist. (A)** Schematic depicting the setting employed to investigate the interaction of CXCR4 or  $\alpha_{2A}$ -AR with the  $G_{i1}$  protein by means of acceptor photobleaching. The CFP and YFP emission intensities were analyzed prior to and after YFP photobleaching in cells expressing  $G_{\alpha_{i1}}/G_{\beta_1}/G_{\gamma_2}$ -CFP and either  $\alpha_{2A}$ -AR-YFP or CXCR4-YFP. The latter receptor was also measured when cells were treated with 10  $\mu$ M IT1t. If there is basal FRET between the fluorophores, CFP is dequenched upon YFP photobleaching. **(B)** The change in the CFP fluorescence ( $\Delta F_{CFP}$ ) was determined by considering the data points right before and after bleaching the YFP. The whiskers of the box plots represent minimum and maximum values. N=19, 13, and 12 cells for CXCR4, CXCR4 (IT1t), and  $\alpha_{2A}$ -AR, respectively. Measurements were performed on three independent experimental days. Statistical significance was tested using an unpaired t-test. \*\*\* $p \leq 0.001$ . \*\*\*\* $p \leq 0.0001$ . **(C-E)** Representative CFP (cyan) and YFP (yellow) traces from individual cells under the different conditions tested. The photobleaching period is indicated in grey.

#### 4.1.5. G protein activation mediated by CXCR4 in response to CXCL12.

In order to investigate G protein activation, previously published FRET-based sensors for  $G_{i1}$ ,  $G_{i2}$ ,  $G_{i3}$ , and  $G_q$  proteins were employed (Adjobo-Hermans et al., 2011; van Unen et al., 2016). These sensors are composed of the  $G\alpha$  subunit labeled with mTurquoise, the  $G\beta_1$  subunit, and the  $G\gamma_2$  subunit labeled with Venus, all three encoded in a single plasmid. The receptor-mediated activation of G proteins in response to agonist binding is monitored as a decrease in FRET between the fluorophores due to conformational changes within the protein upon activation (**Figure 27A**).

To analyze the kinetics of G protein activation, HEK293 cells transfected with CXCR4 or  $\alpha_{2A}$ -AR and the  $G_{i1}$ ,  $G_{i2}$ , or  $G_{i3}$  sensor were stimulated with a saturating concentration of agonist (30  $\mu$ M CXCL12 or 100  $\mu$ M norepinephrine) using the BioPen<sup>®</sup>. For the  $\alpha_{2A}$ -AR, a pronounced decrease in the FRET ratio with all three  $G_i$  sensors was observed upon stimulation with norepinephrine (**Figure 27B-D**). The activation kinetics for all the  $G_i$  subtypes were very similar and in the range of  $\approx$ 650 ms (**Figure 27H; Table 8**). Interestingly, for CXCR4, a pronounced decrease in the FRET ratio with all three  $G_i$  sensors was also observed upon stimulation with CXCL12 (**Figure 27E-G**), but the kinetics of G protein activation were significantly slower and in the range of  $\approx$ 4 s (**Figure 27H; Table 8**). Also, no significant difference in the kinetics between the  $G_i$  subtypes was detected. After ligand exposure, cells were continuously washed with buffer in order to remove the ligands. In the case of the  $\alpha_{2A}$ -AR, washing resulted in the FRET signal returning rapidly to baseline, which suggests that the G proteins rapidly adopt once again the inactive conformation (**Figure 27B-D**). However, activation of CXCR4 by CXCL12 induced a prolonged  $G_i$  activation, reflected by slower G protein off-kinetics that could not be resolved in the time frame of the experiments (**Figure 27E-G**). These observations illustrate how different the underlying activation mechanisms of these two receptors are, even though they both belong to class A GPCRs.

In order to test the effect of different concentrations of CXCL12 on G protein activation, further experiments were performed in a 96-well plate assay format. A concentration-dependent activation of  $G_{i1}$ ,  $G_{i2}$ , and  $G_{i3}$  mediated by CXCR4 was observed (**Figure 27I**). The  $EC_{50}$  values for G protein activation are displayed in **table 8** and are in good agreement with the potency of CXCL12 on CXCR4 described in other systems (Gupta et al., 2001; Rosenkilde et al., 2004; Kleemann et al., 2008; Levoye et al., 2009). The data showed that CXCL12 activates the isoforms  $G_{i1}$  and  $G_{i2}$  with higher potency than  $G_{i3}$ , which is in agreement with published data (Kleemann et al., 2008). No activation of G proteins was observed in cells expressing the G protein sensors but not CXCR4, indicating that under this condition the CXCL12-induced changes are below the detection threshold. Although  $G_q$  signaling by this axis has been reported previously (Soede et al., 2001; Shi et al., 2007), no  $G_q$  activation by CXCR4 in response to CXCL12 could be detected using the  $G_q$  sensor. As a positive control, the activation of  $G_q$  by the  $M_3$ -AChR in response to ACh was tested in parallel (**Figure 27J**).



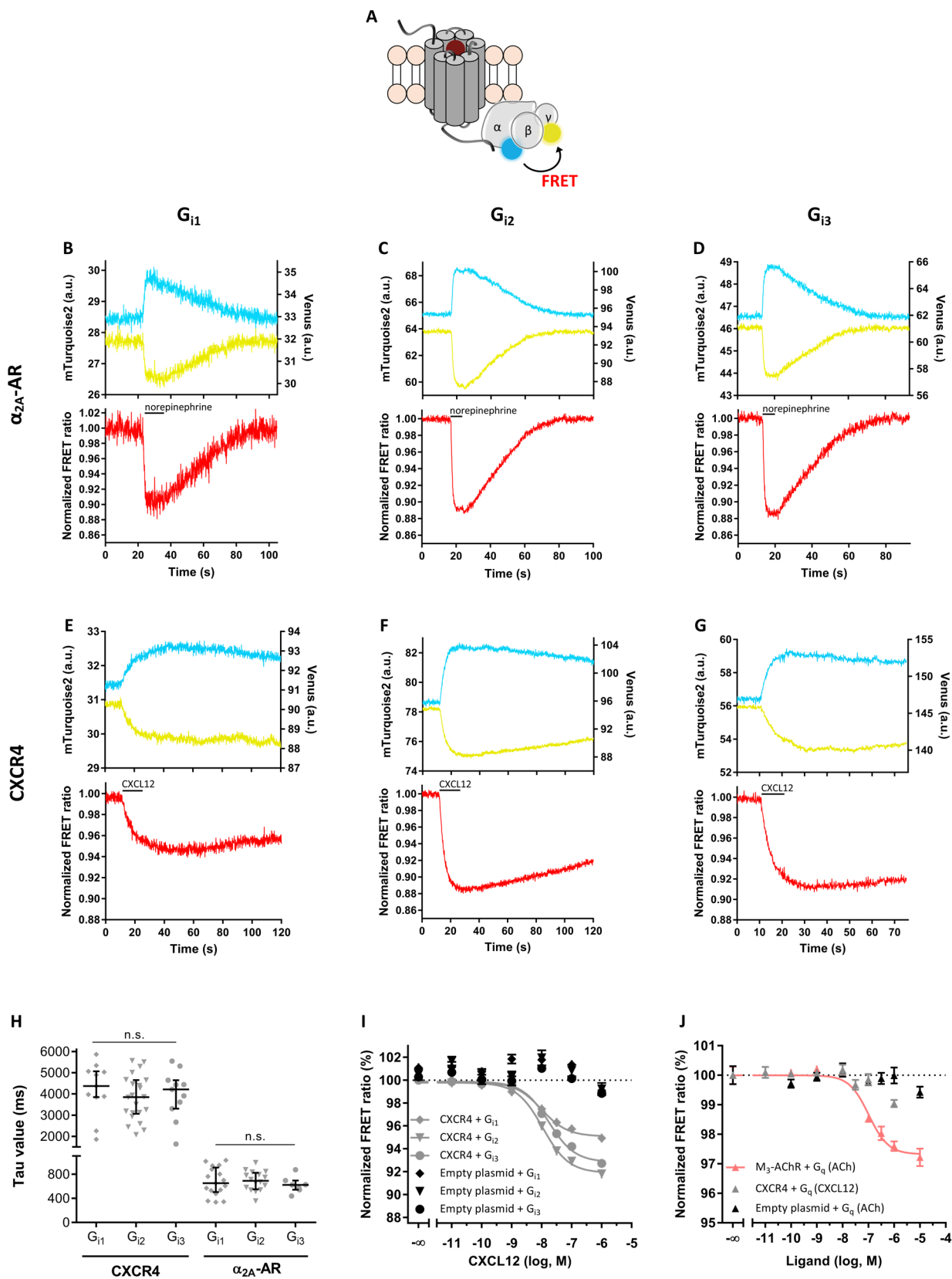


**Figure 27. CXCR4 activates  $G_{i1}$ ,  $G_{i2}$ , and  $G_{i3}$ , but not  $G_q$ , in response to CXCL12.** (A) Schematic depicting the setting employed to investigate G protein activation. Cells were transfected with the receptor and one of the FRET-based G protein sensors, which provide a read-out for G protein activation by the loss of FRET between the  $G\gamma$ - and  $G\alpha$ -labeled subunits. (B-G) Representative traces of the FRET response from a single HEK293 cell expressing  $\alpha_{2A}$ -AR +  $G_{i1}$  (B),  $\alpha_{2A}$ -AR +  $G_{i2}$  (C),  $\alpha_{2A}$ -AR +  $G_{i3}$  (D), CXCR4 +  $G_{i1}$  (E), CXCR4 +  $G_{i2}$  (F) or CXCR4 +  $G_{i3}$  (G), and stimulated with 30  $\mu$ M CXCL12 or 100  $\mu$ M norepinephrine. Upper panels show corrected Venus (yellow) and mTurquoise2 (cyan) emission intensities. Lower panels show normalized and corrected FRET ratios. (H) Kinetics of the activation of the different  $G_i$  protein subtypes by CXCR4 or  $\alpha_{2A}$ -AR in response to 30  $\mu$ M CXCL12 and 100  $\mu$ M norepinephrine, respectively. Median and IQR are shown. Statistical significance was tested using Kruskal-Wallis test (n.s.=non-significant). For CXCR4, n=11, 22, and 11 cells for  $G_{i1}$ ,  $G_{i2}$  and  $G_{i3}$ , respectively, measured on at least three independent experimental days. For  $\alpha_{2A}$ -AR, n=17, 16, and 7 cells for  $G_{i1}$ ,  $G_{i2}$  and  $G_{i3}$ , respectively, measured on at least two independent experimental days. (I) Concentration-response curves for  $G_{i1}$ ,  $G_{i2}$ , and  $G_{i3}$  activation mediated by CXCR4 in response to increasing concentrations of CXCL12. Negative control was performed by co-transfecting empty plasmid instead of receptor. An individual experiment is shown with mean  $\pm$  SEM. N=5 independent experiments conducted in quadruplicate. In this particular case, the  $EC_{50}$  values for G protein activation were 9.8, 10.8, and 17.1 nM for  $G_{i1}$ ,  $G_{i2}$ , and  $G_{i3}$ , respectively. (J) Concentration-response curves for  $G_q$  activation by  $M_3$ -AChR or CXCR4 in response to increasing concentrations of ACh or CXCL12, respectively. Negative control was performed by co-transfecting empty plasmid instead of receptor. An individual experiment is shown with mean  $\pm$  SEM. In this particular case, the  $EC_{50}$  for  $G_q$  activation by ACh/ $M_3$ -AChR was 0.1  $\mu$ M. N=3 independent experiments conducted in quadruplicate. All data were fitted using a three-parameter sigmoidal model.

**Table 8. Summary of the parameters determined for G protein activation mediated by the axis CXCL12/CXCR4, norepinephrine/ $\alpha_{2A}$ -AR, and ACh/ $M_3$ -AChR.** Statistical significance between the  $EC_{50}$  values was tested using one-way ANOVA followed by Tukey's test.

Axis	G protein subtype	On-rate ( $\tau$ , ms) Median (IQR)	$EC_{50}$ [95% CI]
CXCL12/CXCR4	$G_{i1}$	4380 (3850-5070)	6.7 [2.9-15.4] nM } n.s. ] 9.9 [4.8-20.2] nM } * ] 18.6 [8.4-40.9] nM } * ]
	$G_{i2}$	3850 (3070-4660)	
	$G_{i3}$	4220 (3310-4650)	
	$G_q$	-	Not detected
Norepinephrine/ $\alpha_{2A}$ -AR	$G_{i1}$	650 (500-910)	-
	$G_{i2}$	690 (550-820)	-
	$G_{i3}$	620 (540-700)	-
ACh/ $M_3$ -AChR	$G_q$	-	0.2 [0.1-1.5] $\mu$ M

n.s.=non-significant; \* $p \leq 0.05$

Previous data in section 4.1.4 suggest a potential interaction between the receptor and  $G_i$  proteins in the absence of agonist. Therefore, the effects of CXCL12 and IT1t on the  $G_{i2}$  sensor were investigated in HEK293T cells expressing CXCR4. For that purpose, the FRET signal in cells treated with buffer, 100  $\mu$ M IT1t, or 100 nM CXCL12 was analyzed. The data showed that, in comparison to buffer treatment, cells treated with CXCL12 presented a significant lower FRET signal, whereas cells treated with IT1t presented a significant higher FRET signal (**Figure 28**). This suggests that the receptor activates G proteins in the absence of agonist exposure, i.e. exhibits some degree of agonist-independent constitutive activity, and that this can be blocked by treating the cells with IT1t, hence suggesting that this ligand acts as inverse agonist on this receptor.

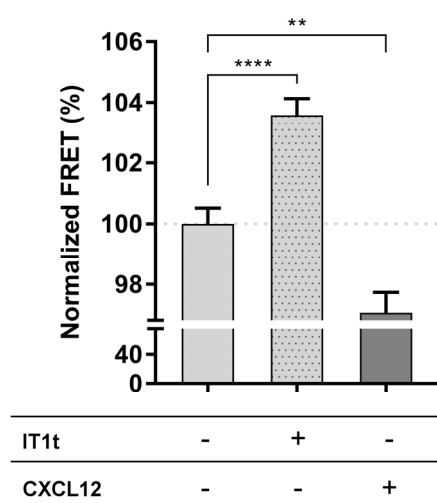


**Figure 28. CXCR4 activates  $G_{i2}$  proteins in the absence of agonist.** The FRET signal of cells expressing CXCR4 and the  $G_{i2}$  sensor was measured under different conditions: buffer treatment, 100  $\mu$ M IT1t treatment, or 100 nM CXCL12 treatment. Three independent experiments were performed. An individual experiment, in which the data sets have been normalized to the buffer, is shown with mean  $\pm$  SEM. In this particular experiment,  $n = 30, 30,$  and  $15$  wells (15000 cells/well) of a 96-well plate for the treatment with buffer, IT1t, and CXCL12, respectively. Statistical significance was tested using an unpaired t-test.  $**p \leq 0.01$ .  $****p \leq 0.0001$ .

#### 4.1.6. Structural rearrangements between CXCR4 protomers in response to CXCL12.

Using a range of techniques, it has been previously shown that CXCR4 forms homodimers even in the absence of ligand binding (section 1.3.3; Vila-Coro et al., 1999; Babcock et al., 2003; Percherancier et al., 2005; Wang et al., 2006; Levoye et al., 2009). In addition, the crystal structure of CXCR4 is also consistent with the existence of CXCR4 dimers (Wu et al., 2010). Nevertheless, the relevance that these have during the activation course of the signaling cascade and the kinetics of this process are still unknown. Moreover, given the characteristic behavior of CXCR4 observed at the level of G protein activation, a close look at the structural rearrangements that occur between CXCR4 protomers might provide an interesting insight into the activation mechanism of this receptor in response to CXCL12.

For that purpose, HEK293 cells expressing 3HA-CXCR4-CFP and CXCR4-YFP were stimulated with CXCL12 (30  $\mu$ M) using the BioPen® (**Figure 29A**). Ligand binding produced a large increase in the FRET signal with an amplitude of  $7.5 \pm 0.5$  % and a time constant  $\tau = 1660$  (1370-2010) ms (**Figure 29B-C**).

This indicates that this rearrangement occurs faster than the activation of G proteins and suggests that homodimers might play a role in the activation mechanism of CXCR4. Wash-out of the cells with buffer returned the FRET signal to baseline and allowed to determine the off-kinetics of this process to be  $\tau = 34.1$  (21.3-36.1) s (**Figure 29D**).

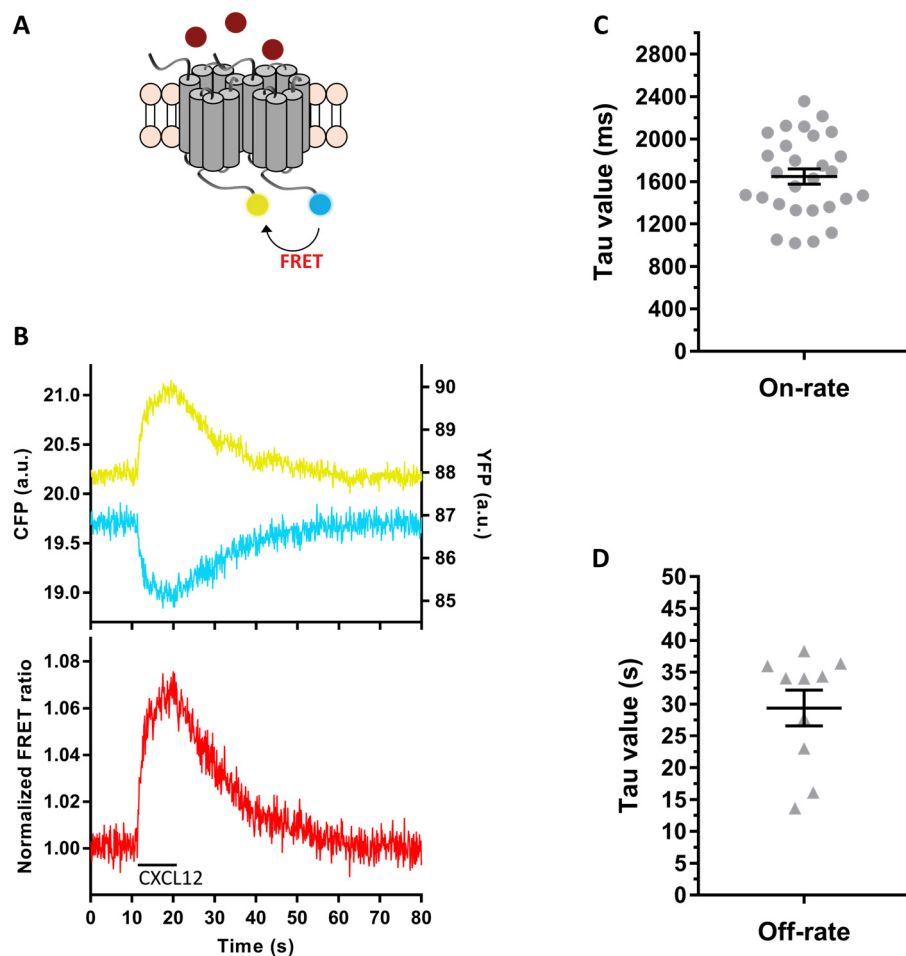


**Figure 29. CXCL12 induces rearrangements between CXCR4 protomers. (A)** Cells expressing 3HA-CXCR4-CFP and CXCR4-YFP were stimulated with CXCL12. Upon activation, rearrangements between labeled CXCR4 protomers leads to a change in FRET. **(B)** Representative traces of the FRET response from a single HEK293 cell stimulated with 30  $\mu$ M CXCL12. Corrected YFP (yellow) and CFP (cyan) emission intensities are shown in the upper panel. Corrected and normalized FRET ratio is shown in the lower panel. **(C, D)** On-kinetics upon CXCL12 binding (C) and off-kinetics upon ligand wash-out with buffer. Median and IQR are shown. N=28 cells for the on-rate and 10 cells for the off-rate, measured at least in three independent experimental days.

#### 4.1.7. Investigating the stoichiometry of CXCR4 in complex with CXCL12.

Although the structural basis of CXCR4: CXCL12 interaction has been examined before, discrepancies still exist regarding this topic. The dimeric behavior of CXCR4 observed in a large number of studies leads to several possibilities for chemokine: receptor complex stoichiometry (section 1.3.4). Here, whether the two CXCR4 protomers from a dimer or only one are required for efficiently activating the receptor in response to CXCL12 was investigated. For this purpose, two mutations were introduced into one of the protomers to attempt to abolish its ability to bind the ligand and to activate the receptor. Among all the candidates, the two mutations W94R and D97G have been described to fully impair signaling in response to CXCL12 (the ligand-induced  $\text{Ca}^{2+}$  flux is reduced by more than 75% by each individual mutation), while each mutant receptor is still correctly folded and trafficked to the plasma membrane (Wescott et al., 2016). Therefore, the combination of these two mutations, both residues found at the top of TM2, represent potential good candidates (**Figure 30A**).

The two mutations were introduced into the 3HA-CXCR4-CFP construct, referred to as 3HA-<sup>W94R,D97G</sup>CXCR4-CFP. The rearrangement between protomers was then analyzed in cells expressing CXCR4-YFP and 3HA-<sup>W94R,D97G</sup>CXCR4-CFP, and compared to the rearrangements observed in the absence of mutations. Upon 30  $\mu\text{M}$  CXCL12 stimulation, rearrangements occurred with  $\tau = 1650$  (1510-1910) ms, which is not significantly different to the kinetics observed in the absence of the mutations (**Figure 30B**). To directly assess if the introduction of these two mutations abolishes the activation of the receptor, they were introduced into the 3HA-CXCR4-FIAsH228-CFP sensor (3HA-<sup>W94R,D97G</sup>CXCR4-FIAsH228-CFP). Stimulation with 30  $\mu\text{M}$  CXCL12 led to activation of the receptor with  $\tau = 590$  (400-1020) ms, which is comparable to the on-kinetics established with the 3HA-CXCR4-FIAsH228-CFP sensor (**Figure 30C**). This suggests that these two mutations alone are not sufficient to impair the binding of the ligand and the activation of the receptor. Therefore, no information on the stoichiometry of CXCR4 in complex to CXCL12 could be deduced from these measurements.

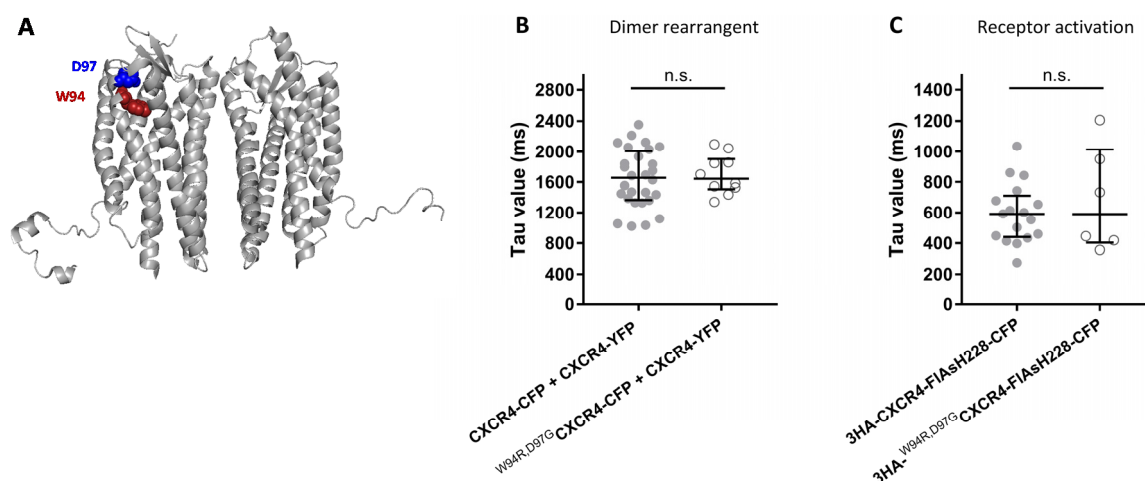


**Figure 30. The two mutations W94 and D97 do not impair the activation of CXCR4 or the rearrangement between protomers upon CXCL12 binding.** (A) The mutated residues W94 and D97 are found on the top of TM2. The receptor is shown as a dimer (PDB code 3ODU; Wu et al., 2010). (B) On-kinetics upon stimulation with 30  $\mu$ M CXCL12 measured on cells expressing CXCR4-YFP and 3HA-CXCR4-CFP (data from figure 29C) or 3HA-W<sup>94R,D97G</sup>CXCR4-CFP (n=10 cells). (C) On-kinetics of receptor activation upon stimulation with 30  $\mu$ M CXCL12 measured on cells expressing the 3HA-CXCR4-FIAsH228-CFP sensor (data from figure 24G) or the 3HA-W<sup>94R,D97G</sup>CXCR4-FIAsH228-CFP sensor (n=6 cells). Statistical significance was tested using Mann-Whitney test (n.s.=non-significant). Data show median and IQR.

#### 4.1.8. Characterization of other CXCR4 ligands.

For a long time, CXCL12 was thought to be the sole ligand for CXCR4. However, over the past few years, other endogenous molecules have been also proposed to bind, activate and signal through this receptor, including MIF (section 1.3.5.1) and lactoferrin (section 1.3.5.2). Therefore, the tools and settings that have been earlier established in this thesis to study the CXCL12/CXCR4 axis were employed to investigate the activation of CXCR4 in response to these ligands.

##### 4.1.8.1. Macrophage migration inhibitory factor.

In order to characterize the MIF/CXCR4 axis in single-cell experiments, cells were stimulated with 100  $\mu$ M MIF, followed by a short wash-out with buffer and subsequent stimulation with 30  $\mu$ M CXCL12. Firstly, in order to investigate receptor activation, HEK293 cells transiently expressing the 3HA-CXCR4-FIAsH228-CFP sensor and FIAsH-labeled prior to the measurement were employed. In contrast to CXCL12, which produced an increase in the FRET signal, MIF stimulation led to a fast decrease in the FRET signal with  $\tau = 270$  (250-440) ms (**Figure 31A-B**). Opposite signals suggest different conformational changes in CXCR4 upon binding of these two ligands and likely reflects the different pharmacological properties of these two proteins on CXCR4. The MIF-induced FRET signal rapidly returned to baseline upon washing of the cells with buffer, indicating that MIF can be easily removed from the receptor and thus suggesting a low binding affinity. Subsequent stimulation with CXCL12 produced responses that were undistinguishable from those observed when cells were directly stimulated with this ligand, indicating that prior stimulation with MIF does not affect the response of the cells to CXCL12 (**Figure 32A**). Secondly, the interaction between CXCR4 and the G<sub>i</sub> protein was studied in cells expressing CXCR4-YFP and the G protein CFP-labeled at G $\gamma$ <sub>2</sub>. Stimulation with MIF led to an increase in the FRET signal that occurred with  $\tau = 380$  (300-560) ms (**Figure 31C-D**). Therefore, MIF stimulation again produced a FRET signal that is opposite to that of CXCL12, suggesting that these

two ligands lead to different coupling or rearrangements between the  $G_i$  protein and the receptor. This further supports the notion that CXCR4 adopts distinct conformations when bound to CXCL12 and MIF. Again, washing of the cells with buffer rapidly returned the FRET signal to baseline and cells could be subsequently stimulated with CXCL12, exhibiting a response that was very similar to the one observed when stimulating the cells with this ligand for the first time (**Figure 32B**). Thirdly, the rearrangement between CXCR4 protomers was investigated in cells expressing 3HA-CXCR4-CFP and CXCR4-YFP. In this case, addition of MIF produced a decrease in the FRET signal with  $\tau = 870$  (580-930) ms (**Figure 31E-F**). The MIF-induced signal is opposite to CXCL12, indicating once again different conformational changes in the receptor induced by these two ligands. Upon wash-out with buffer, the response induced by MIF rapidly returned to baseline and did not affect the response observed upon subsequent stimulation of the cells with CXCL12 (**Figure 32C**). Fourthly, G protein activation was examined in cells expressing CXCR4 and the  $G_{i2}$  sensor. Addition of MIF did not produce any change in FRET, indicating that there is no G protein activation by CXCR4 in response to this ligand (**Figure 31G**). Therefore, in contrast to what is described in the literature, no  $G_i$  protein signaling could be detected under these conditions. As a positive control, subsequent stimulation of the same cell with CXCL12 led to the activation of the G proteins. A summary of the on-kinetics of the processes analyzed can be found in **table 9**. **Figure 31K** shows the on-kinetics determined for CXCR4 in response to MIF in comparison to CXCL12.

The activation of G proteins was then tested in response to increasing concentrations of MIF in a 96-well plate assay format using the FRET-based  $G_i$  sensors. A concentration-dependent activation of  $G_{i1}$ ,  $G_{i2}$ , and  $G_{i3}$  was observed, suggesting that stimulation of the cells with MIF leads to the activation of G proteins. However, this response was similarly observed in cells that had not been transfected with the receptor (**Figure 31H-J**), thus suggesting that it is not mediated by CXCR4. Instead, a different receptor endogenously present in HEK293T cells might be responsible for the MIF-mediated G protein activation. Thus, these data are in agreement with the single-cell experiments, in which CXCR4-mediated G protein activation could not be detected in response to MIF.

**Table 9. Summary of the on-kinetics determined for each of the processes studied for the axis MIF/CXCR4.**

<b>PROCESS</b> Setting/constructs employed	<b>On-rate (<math>\tau</math>, ms)</b> Median (IQR)
<b>Receptor activation</b> 3HA-CXCR4-FIAsh228-CFP sensor	270 (250-440)
<b>Receptor/<math>G_i</math> protein interaction</b> CXCR4-YFP + $G_{\alpha_{i1}}/G_{\beta_1}/G_{\gamma_2}$ -CFP	380 (300-560)
<b>Protomers rearrangement</b> 3HA-CXCR4-CFP + CXCR4-YFP	870 (580-930)
<b><math>G_i</math> protein activation</b> CXCR4 + $G_{i2}$ sensor	Not detected

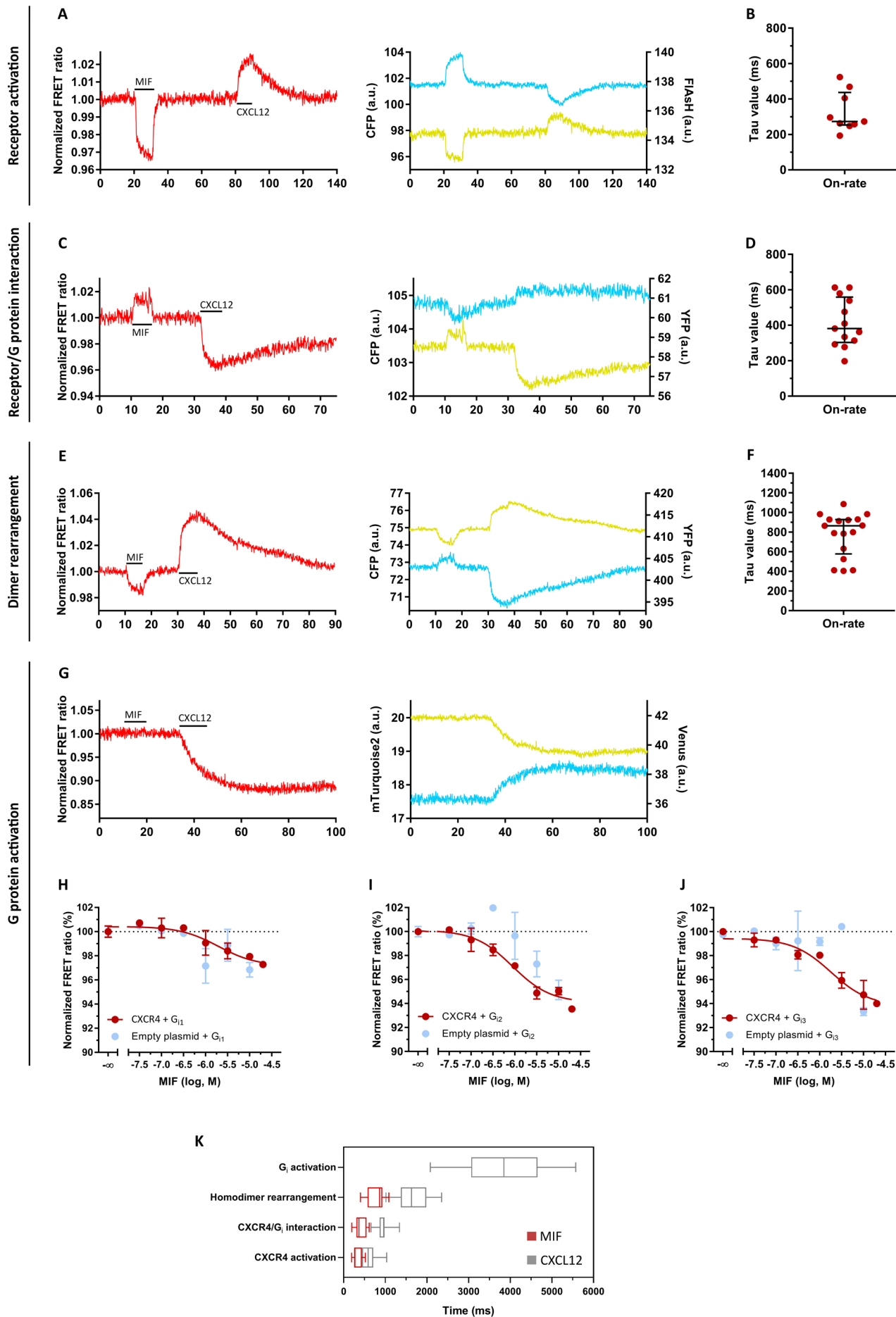




**Figure 31. MIF binding induces structural rearrangements in CXCR4 but does not lead to  $G_i$  protein activation via this receptor.** (A, C, E, G) Representative traces of the FRET response from a single HEK293 cell expressing the indicated construct(s) and stimulated with 100  $\mu$ M MIF, followed by a short wash-out with buffer and stimulation with 30  $\mu$ M CXCL12. (A) 3HA-CXCR4-FIAsH228-CFP sensor; (C) CXCR4-YFP,  $G\alpha_{i1}$ ,  $G\beta_1$ , and  $G\gamma_2$ -CFP; (E) 3HA-CXCR4-CFP and CXCR4-YFP; (G) CXCR4 and  $G_{i2}$  sensor. The normalized and corrected FRET ratios are shown in the left panels. The corrected emission intensities of the acceptor and donor fluorophores are shown in the right panels. (B, D, F) Kinetics of CXCR4 activation,  $n=9$  cells (B), CXCR4/ $G_i$  protein interaction,  $n=13$  cells (D), and dimer rearrangement,  $n=17$  cells (F) in response to 100  $\mu$ M MIF stimulation. Measurements were performed in at least two independent experimental days. Data show median and IQR. (H-J) Concentration-response curves for  $G_{i1}$ ,  $G_{i2}$ , and  $G_{i3}$  in response to increasing concentrations of MIF, in the presence or absence of CXCR4. Individual experiments are shown with mean  $\pm$  SEM. (K) Comparison of CXCR4 on-kinetics in response to CXCL12 and MIF. Data from receptor activation belongs to figure 24G and 31B. Data from receptor/ $G$  protein interaction belongs to figure 25F ( $G\gamma$ -labeled) and 31D. Data from protomers rearrangement belongs to figure 29C and 31F. Data from  $G$  protein activation belongs to figure 27H ( $G_{i2}$  sensor).

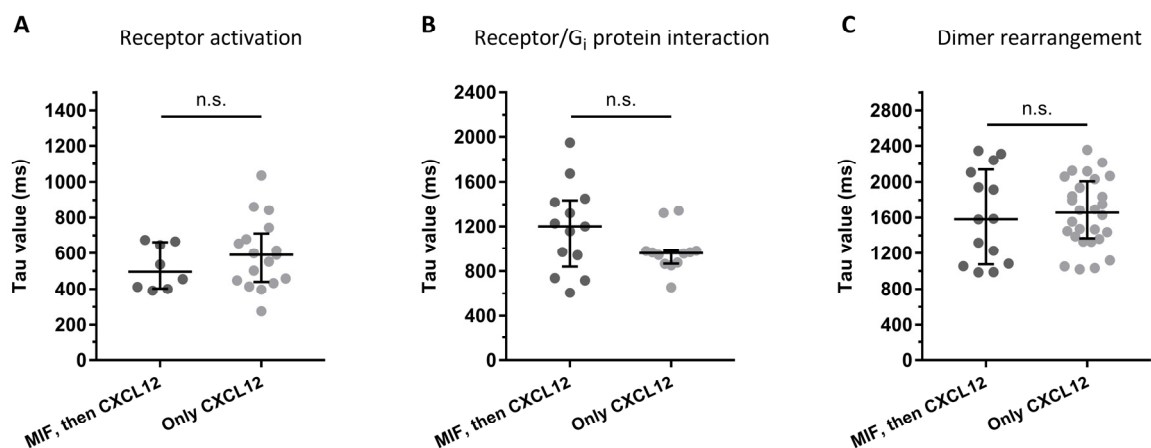


**Figure 32. The kinetics of CXCR4 activation, CXCR4/ $G_i$  interaction, and CXCR4 dimer rearrangement in response to CXCL12 are not affected by prior stimulation of the cells with MIF.** Kinetics of receptor activation (A), receptor/ $G$  protein interaction (B), and dimer rearrangement (C) in response to 30  $\mu$ M CXCL12 with or without prior stimulation with 100  $\mu$ M MIF. Median and IQR are shown. Data for single CXCL12 stimulation have been taken from figures 24G (3HA-CXCR4-FIAsH228-CFP), 25F ( $G\gamma_2$ -CFP), and 29C. For CXCL12 response after MIF stimulation,  $n=8$  cells for receptor activation measured on two independent experimental days, 13 cells for receptor/ $G$  protein interaction measured on four independent experimental days, and 14 cells for dimer rearrangement measured on three independent experimental days. Statistical significance was tested using Mann-Whitney test (n.s.=non-significant).

#### 4.1.8.2. Lactoferrin.

Lactoferrin is an iron-binding protein that has been recently described to bind and signal through CXCR4 (Takayama et al., 2016). Its saturation state can significantly change under specific circumstances and alter its properties (Gibbons, Kanwar and Kanwar, 2015). Therefore, it was tested in two different states: iron-free (apo-Lf) and iron-bound lactoferrin (Fe<sub>2</sub>-Lf).

Cells transiently expressing the 3HA-CXCR4-FIAsh228-CFP sensor were employed to study receptor activation in single cells. During the measurement, cells were stimulated with 60 μM apo-Lf or Fe<sub>2</sub>-Lf, followed by a short wash-out with buffer and subsequent stimulation with 30 μM CXCL12. Upon stimulation with either form of lactoferrin, no structural rearrangements in the receptor were detected. However, receptor activation upon subsequent stimulation of the cell with CXCL12 was observed, proving that the cell is able to respond (**Figure 33A-B**). These results suggest that either these molecules do not bind to the receptor under these experimental conditions, or that the conformational change induced is not detected using this sensor.

Following, the FRET-based G<sub>i</sub> sensors were used to investigate the activation of G proteins in response to both forms of lactoferrin in a 96-well plate assay format. For the measurements, HEK293T cells expressing CXCR4 and the G<sub>i1</sub>, G<sub>i2</sub>, or G<sub>i3</sub> sensor were stimulated with increasing concentrations of apo-Lf or Fe<sub>2</sub>-Lf. While no activation of G proteins could be detected in response to apo-Lf, Fe<sub>2</sub>-Lf led to the activation of the G<sub>i2</sub> and G<sub>i3</sub> protein subtypes, but not G<sub>i1</sub> (**Figure 33C-E**). Due to experimental limitations, it was not possible to test higher concentrations of the ligands, and therefore the EC<sub>50</sub> can only be estimated to be in the low micro molar range. As control, G protein activation in response to CXCL12 was tested in parallel. To facilitate examination, the average of the FRET change detected for each G protein subtype at the highest concentration of lactoferrin tested (10 μM) is shown in **figure 33I**. It can be observed that CXCR4 mediates the activation of G<sub>i2</sub> and G<sub>i3</sub> in response to Fe<sub>2</sub>-Lf, while the FRET change detected for G<sub>i1</sub> in response to Fe<sub>2</sub>-Lf is comparable to the one detected in the absence of receptor or when cells were stimulated with apo-Lf.

Interestingly, in comparison to CXCL12, the activation of G<sub>i2</sub> and G<sub>i3</sub> induced by Fe<sub>2</sub>-Lf is more transient: whereas the signal observed upon CXCL12 stimulation is notably constant for at least 20 min, the Fe<sub>2</sub>-Lf-mediated signal shows a maximum right after the addition of the ligand and slowly decreases over time (**Figure 33G-H, pink lines**). This is in line with observations in section 4.1.5, in which CXCL12 induced a prolonged G protein activation even after removal of the ligand with buffer. The signal detected for G<sub>i1</sub> activation by Fe<sub>2</sub>-Lf was very similar to the one produced by the addition of buffer or apo-Lf (**Figure 33F**).

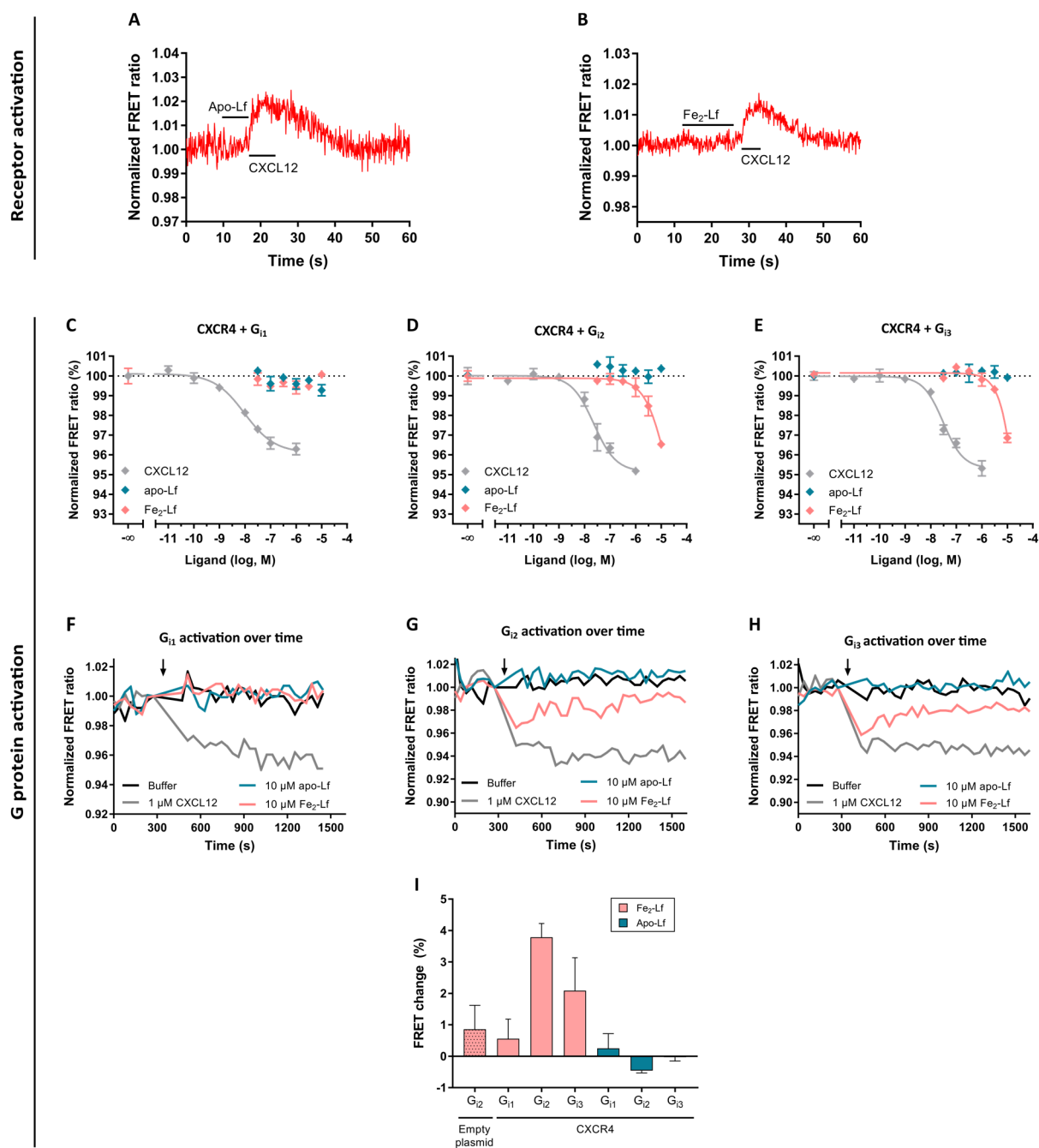


**Figure 33. Fe<sub>2</sub>-Lf induces G<sub>12</sub> and G<sub>13</sub> but not G<sub>11</sub> activation via CXCR4, while apo-Lf does not lead to activation of any G<sub>i</sub> protein subtype. (A)** Representative FRET traces from a single HEK293 cell expressing the 3HA-CXCR4-FIAsH228-CFP sensor and stimulated with 60 μM apo-Lf (A) or Fe<sub>2</sub>-Lf (B), followed by a short wash-out with buffer and stimulation with 30 μM CXCL12. Normalized and corrected FRET ratios are shown. **(C-E)** G<sub>11</sub>, G<sub>12</sub>, and G<sub>13</sub> activation by CXCR4 in response to increasing concentrations of apo-Lf, Fe<sub>2</sub>-Lf, or CXCL12. An individual experiment is shown with mean ± SEM. For Fe<sub>2</sub>-Lf, n (independent experiments conducted in triplicate) = 2 for G<sub>11</sub> and G<sub>13</sub>, and 4 for G<sub>12</sub>. For apo-Lf, n=2. In this particular case, the EC<sub>50</sub> values for G protein activation in response to CXCL12 were 9.5 nM for G<sub>11</sub>, 23.0 nM for G<sub>12</sub>, and 30.8 nM for G<sub>13</sub>. Data were fitted using a three-parameter sigmoidal model. **(F-H)** G<sub>i</sub> activation over time. FRET signals before and after buffer/ligand addition, which is indicated with an arrow, are shown. **(I)** Average of the amplitude of the FRET change detected for G protein activation in the presence or absence of CXCR4 upon stimulation with 10 μM apo-Lf or Fe<sub>2</sub>-Lf.

#### 4.2. ACKR3.

In contrast to conventional chemokine receptors, atypical chemokine receptors are generally unable to signal through G proteins or lead to the more typical downstream responses, such as  $\text{Ca}^{2+}$  mobilization or downregulation of cAMP production. Instead, chemokine binding generally leads to  $\beta$ -arrestin recruitment and internalization of the chemokine:receptor complex, which results in the formation of chemokine gradients in the extracellular side. As a consequence, fewer number of read-outs are available to study the direct activation of these receptors in response to newly developed ligands, which might have therapeutic potential. This section describes the development and characterization of a FRET-based ACKR3 sensor that has been used to study the activation of the receptor in response to different ligands, including CXCL12.

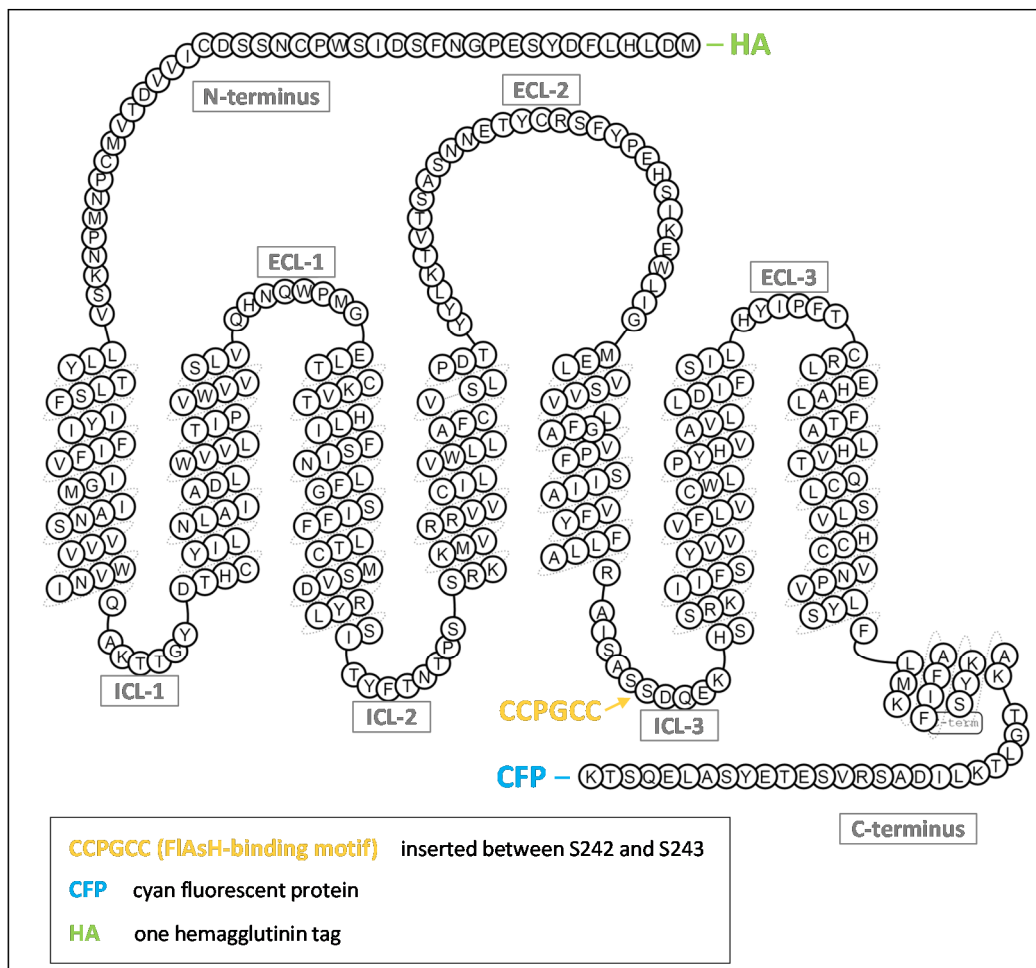


**Figure 34. Protein sequence of the human ACKR3 depicting the insertion positions of the tags and fluorophores used.** Source: GPCRdb.

#### 4.2.1. Design of FRET-based ACKR3 sensors.

Similar to the strategy followed with CXCR4 in section 4.1.1, a FRET-based sensor for ACKR3 was developed in order to be able to study the ligand-induced activation of the receptor. Despite the increasing number of released GPCR crystal structures, limited structural data for ACKR3 is available. Therefore, the FRET-based sensor was created based on the predicted structure and protein sequence of the receptor. The CFP was fused to the end of the C-terminus and the FIAsh-binding sequence CCPGCC was inserted in the predicted ICL-3, between S242 and S243 (**Figure 34**). In addition, one HA tag was fused to the N-terminus. The ACKR3 sensor is referred to as HA-ACKR3-FIAsh-CFP.

#### 4.2.2. Characterization of the FRET-based ACKR3 sensor.

##### 4.2.2.1. Expression and localization.

ACKR3 predominantly localizes in intracellular compartments in basal conditions in most cell types, as previously reported in numerous occasions (section 1.4.2; Boldajipour et al., 2008; Luker et al., 2010; Shimizu et al., 2011; Ray et al., 2012b). As expected, confocal images of HEK293 cells transfected with the HA-ACKR3-FIAsh-CFP sensor showed that it is mostly found in intracellular compartments (**Figure 35A**). When developing receptor sensors, it is important that they are expressed in the plasma membrane and thus accessible from the extracellular side. Therefore, two different strategies were followed to limit the expression of the receptor to the plasma membrane, as already described in the literature (Ray et al., 2012b). On one hand, the sensor was co-transfected with K44A dynamin, which blocks receptor endocytosis in cells. This strategy significantly increased the localization of the sensor to the plasma membrane (**Figure 35B**). On the other hand, the C-terminus of the receptor was truncated at two positions: after A346 (deleting 16 amino acids) or after N321 (deleting 41 amino acids). These constructs were named HA-ACKR3(1-346)-FIAsh-CFP and HA-ACKR3(1-321)-FIAsh-CFP, respectively. HEK293 cells transfected with these sensors showed that progressive truncation of the C-terminus led to a redistribution of the truncated constructs to the plasma membrane, although to a lesser extent than what is described in Ray et al. (2012b). The HA-ACKR3(1-346)-FIAsh-CFP sensor was still mostly localized in intracellular compartments while the HA-ACKR3(1-321)-FIAsh-CFP sensor was partially redistributed and could be observed in both intracellular compartments and the cell membrane (**Figure 35C-D**).

In order to confirm these qualitative observations, line profile analyses of fluorescence intensity across cells were performed. In accordance, HA-ACKR3-FIAsh-CFP and HA-ACKR3(1-346)-FIAsh-CFP showed several peaks of fluorescence all across the line section, especially in the middle, which corresponds to

the fluorescent receptor found mostly in intracellular compartments (**Figure 35E and G**). In contrast, HA-ACKR3(1-321)-FIAsH-CFP and HA-ACKR3-FIAsH-CFP co-expressed with K44A dynamin displayed lesser fluorescent peaks in the region corresponding to the intracellular space and more pronounced peaks at the plasma membrane (**Figure 35F and H**).

#### 4.2.2.2. FRET efficiency.

As concluded in section 4.2.2.1, the best strategy to increase the presence of the sensor in the plasma membrane is by co-expressing HA-ACKR3-FIAsH-CFP with K44A dynamin or by truncating the C-terminal tail of the sensor by 41 amino acids (HA-ACKR3(1-321)-FIAsH-CFP). Therefore, these two constructs were characterized based on their FRET efficiency by means of bleaching experiments using BAL. HEK293 cells were transfected with the HA-ACKR3-FIAsH-CFP sensor and K44A dynamin, or with the HA-ACKR3(1-321)-FIAsH-CFP sensor, and labeled with FIAsH prior to the measurements. Addition of BAL led to an increase in the CFP fluorescence in both cases, proving the existence of basal intramolecular FRET (**Figure 36A and C**). The FRET efficiency was determined to be  $4.3 \pm 0.5$  % for HA-ACKR3-FIAsH-CFP and  $7.2 \pm 1.0$  % for HA-ACKR3(1-321)-FIAsH-CFP (**Figure 36E; Table 10**). No basal intermolecular FRET was detected when HA-ACKR3-FIAsH was co-expressed with HA-ACKR3-CFP or HA-ACKR3(1-321)-CFP, indicating that the FRET signals detected come from individual receptors rather than adjacent receptors or from protomers within dimers (**Figure 36B and D**).

**Table 10. Intra- and intermolecular FRET efficiency values of the ACKR3 constructs.**

Values are given in percentage as mean  $\pm$  SEM.

Sensor	Intramolecular FRET (%)	Intermolecular FRET (%)
HA-ACKR3-FIAsH-CFP	$4.3 \pm 0.5$	0
HA-ACKR3(1-321)-FIAsH-CFP	$7.2 \pm 1.0$	0

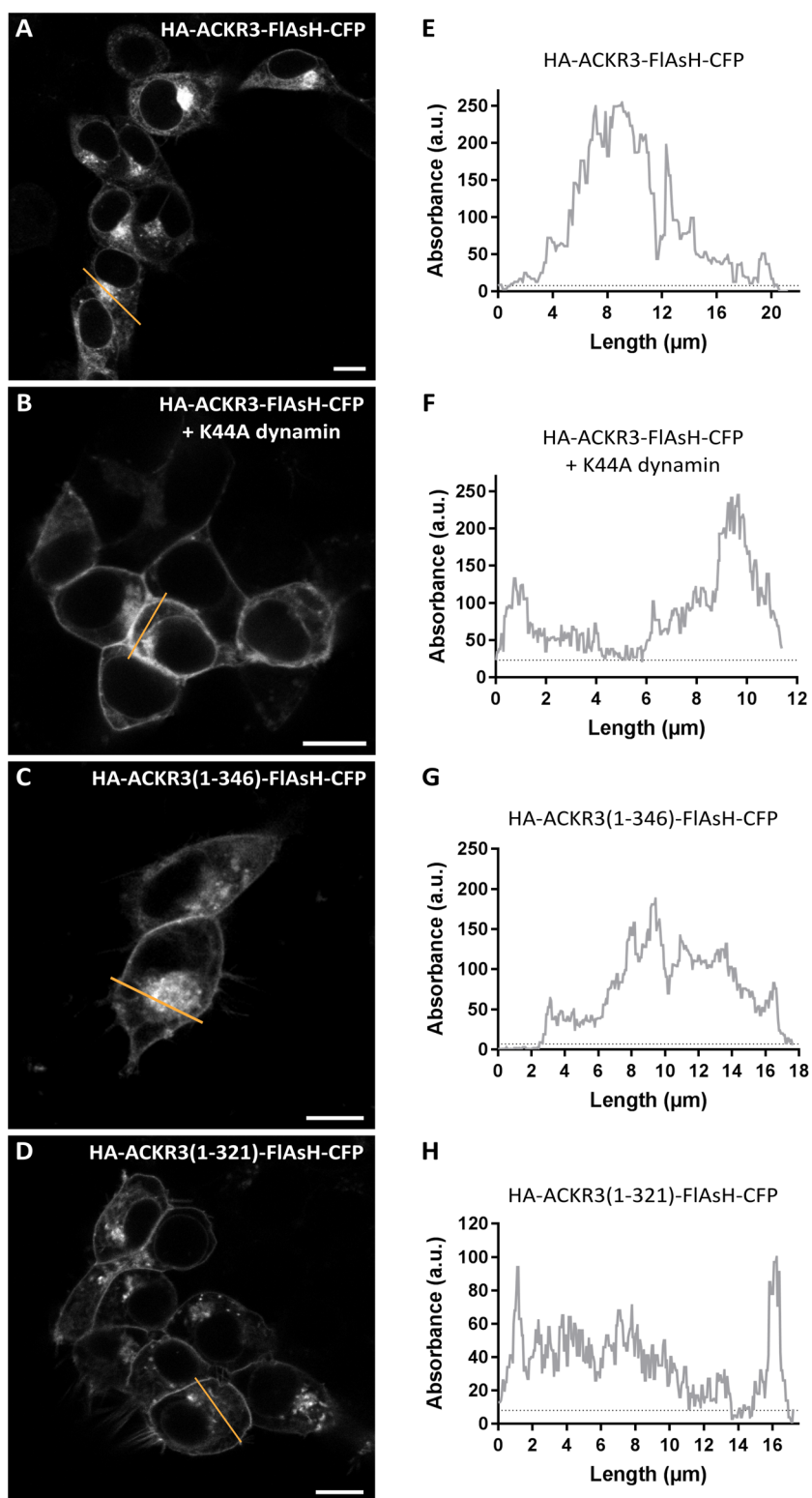
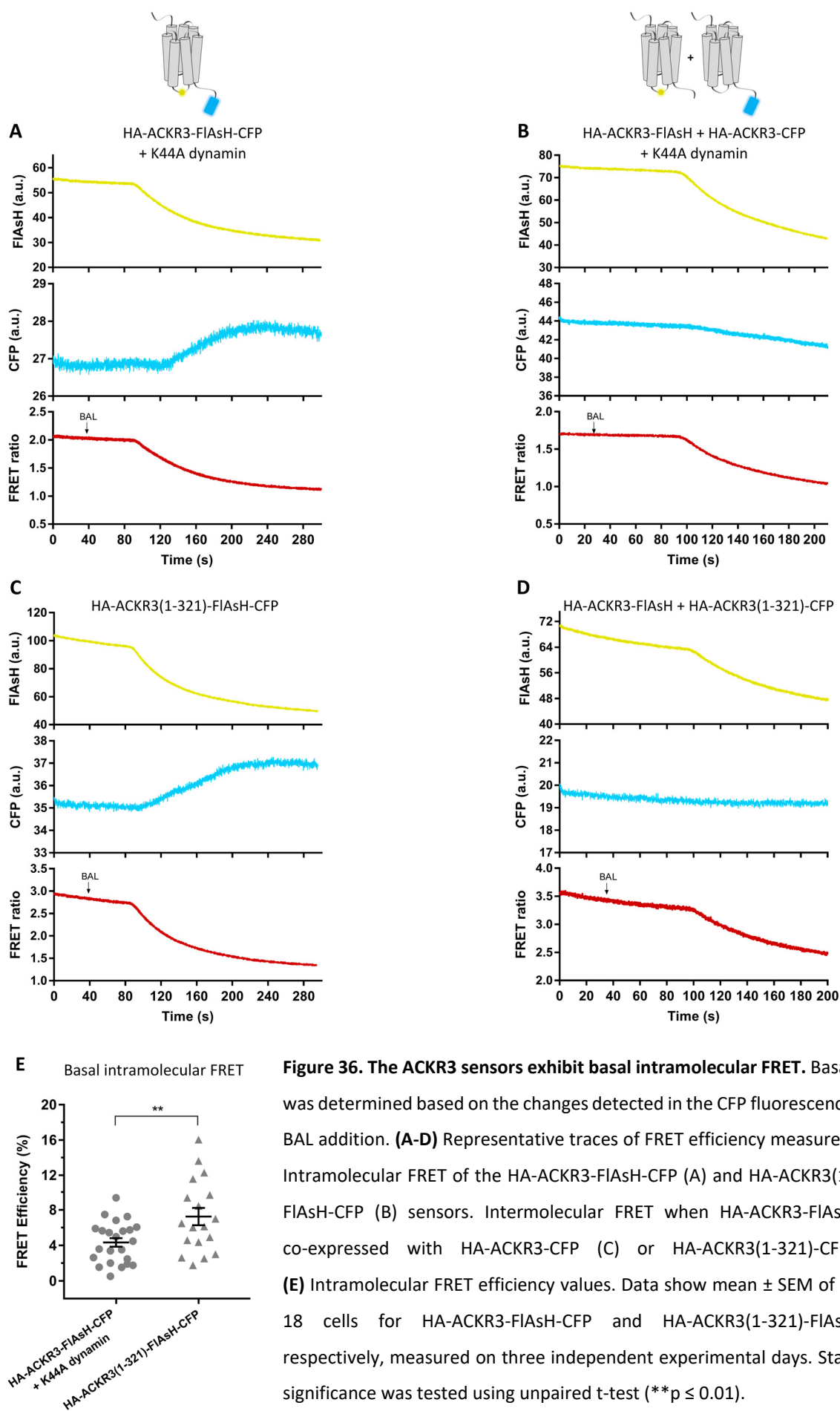


**Figure 35. Expression and localization of the different ACKR3 constructs analyzed by confocal microscopy.** (A-D) Representative confocal images of HEK293 cells transiently expressing the HA-ACKR3-FIAsH-CFP sensor (A), the HA-ACKR3-FIAsH-CFP sensor and K44A dynamin (B), the HA-ACKR3(1-346)-FIAsH-CFP sensor (C) or the HA-ACKR3(1-321)-FIAsH-CFP sensor (D). Images show CFP emission upon excitation at 442 nm. Scale bars denote 10 μm. (E-H) Line profile analyses of fluorescence intensity and distribution profiles across individual cells (excluding the nucleus) expressing the indicated constructs. The graphics show the fluorescence corresponding to the region drawn by the orange lines shown in A-D.





#### 4.2.2.3. Ligand binding.

Competition binding experiments were performed in order to assess the ligand binding properties of the different ACKR3 constructs in comparison to the wt receptor. For this purpose, increasing concentrations of unlabeled CXCL12 were used to displace  $^{125}\text{I}$ -CXCL12 in total membranes of HEK293T cells transfected with ACKR3, HA-ACKR3, HA-ACKR3-CFP or HA-ACKR3-FIAsH-CFP. The results showed that the constructs containing the different tags display binding affinities for CXCL12 that are very similar to the wt receptor (**Figure 37 and Table 11**). Therefore, the fusion of the HA tag, the introduction of the FIAsH-binding motif, and/or the fusion of the CFP do not alter the ability of the receptor to bind CXCL12.

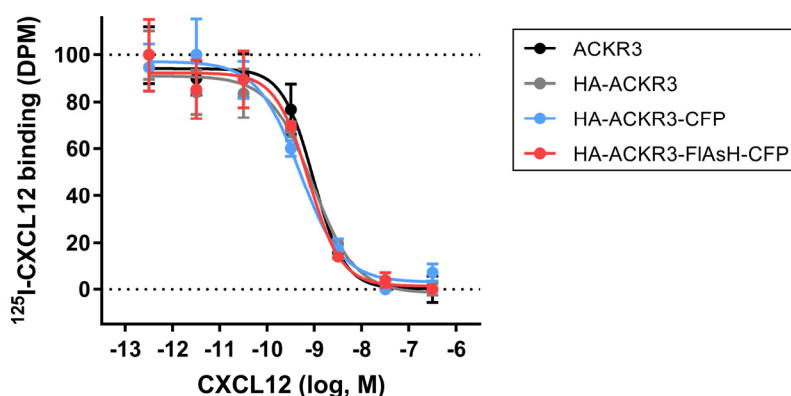


**Figure 37. Addition of the HA tag, the FIAsH-binding motif, and/or CFP into ACKR3 do not affect its ability to bind CXCL12.** Experiments were performed in total membranes of HEK293T cells transfected with ACKR3, HA-ACKR3, HA-ACKR3-CFP, or HA-ACKR3-FIAsH-CFP.  $^{125}\text{I}$ -CXCL12 radioligand was displaced with increasing concentrations of unlabeled CXCL12. Three independent experiments were conducted in triplicate. An individual experiment is shown with mean  $\pm$  SEM. Data was fitted to a three-parameter sigmoidal model. In this particular case,  $\text{IC}_{50}$  values were 1.0, 0.9, 0.5, and 0.8 nM for ACKR3, HA-ACKR3, HA-ACKR3-CFP, and HA-ACKR3-FIAsH-CFP, respectively.

**Table 11.  $\text{IC}_{50}$  values resulting from the competitive binding assays performed with the different ACKR3 constructs.** Statistical significance was tested using one-way ANOVA.

Construct	$\text{IC}_{50}$ [95% CI], nM
ACKR3	0.7 [0.3-1.4]
HA-ACKR3	0.6 [0.3-1.3]
HA-ACKR3-CFP	0.5 [0.1-4.3]
HA-ACKR3-FIAsH-CFP	0.4 [0.1-1.5]

n.s.

n.s.=non-significant.

#### 4.2.3. Activation of ACKR3 in response to CXCL12.

The activation of ACKR3 in response to CXCL12 was investigated using the two following sensors: HA-ACKR3(1-321)-FIAsH-CFP and HA-ACKR3-FIAsH-CFP, the latter in the presence and absence of K44A dynamin. To do that, single HEK293 cells transiently expressing the construct(s) of interest were stimulated with a saturating concentration of CXCL12 using the BioPen<sup>®</sup>. Stimulation of cells expressing the HA-ACKR3-FIAsH-CFP sensor and K44A dynamin with 30  $\mu$ M CXCL12 led to a fast decrease in the FRET signal with a time constant  $\tau = 1170$  (810-1390) ms. This signal is derived from the antiparallel movement in the FIAsH and CFP fluorescence intensities and presented an amplitude of  $2.6 \pm 0.1$  % (**Figure 38B and D**). In contrast, no CXCL12-induced conformational changes in the receptor were detected with the HA-ACKR3(1-321)-FIAsH-CFP sensor or when the HA-ACKR3-FIAsH-CFP sensor was transfected alone (**Figure 38A and C**).

#### 4.2.4. Activation of ACKR3 in response to other ligands.

The HA-ACKR3-FIAsH-CFP sensor in combination with K44A dynamin was used to characterize the activation of the receptor in response to several ligands, following the same protocol as in section 4.2.3. These ligands were provided by the group of Dr. R. Leurs (Vrije University, Amsterdam), which developed a set of proteins with agonistic properties that target ACKR3. A total of three different ligands, named GD301, VUF11072, and VUF11074, were tested.

For all the ligands, a decrease in the FRET signal from the sensor was detected upon 50  $\mu$ M ligand stimulation. The FRET changes detected were similar in regard to the signal amplitude, which was determined to be  $2.4 \pm 1.1\%$  for GD301,  $2.6 \pm 0.3$  % for VUF11072, and  $2.4 \pm 0.2$  % for VUF11074 (**Figure 39A-C**). ACKR3 activation occurred with  $\tau = 1970$  (1830-2100) ms in response to GD301, while slower kinetics were determined for VUF11072 and VUF11074 ( $\tau = 3010$  (2750-3100) ms and  $\tau = 3080$  (2710-3650) ms, respectively (**Figure 39D**). Overall, in comparison to CXCL12, these three ligands induced activation of ACKR3 with slower kinetics, but led to FRET changes with similar amplitudes, suggesting that they induce similar conformational rearrangements in the receptor upon binding.

On the basis of these results, the HA-ACKR3-FIAsH-CFP sensor, which displays comparable functional properties to the wt receptor, used together with K44A dynamin, represents a valuable tool to study the ligand-induced activation of the receptor.

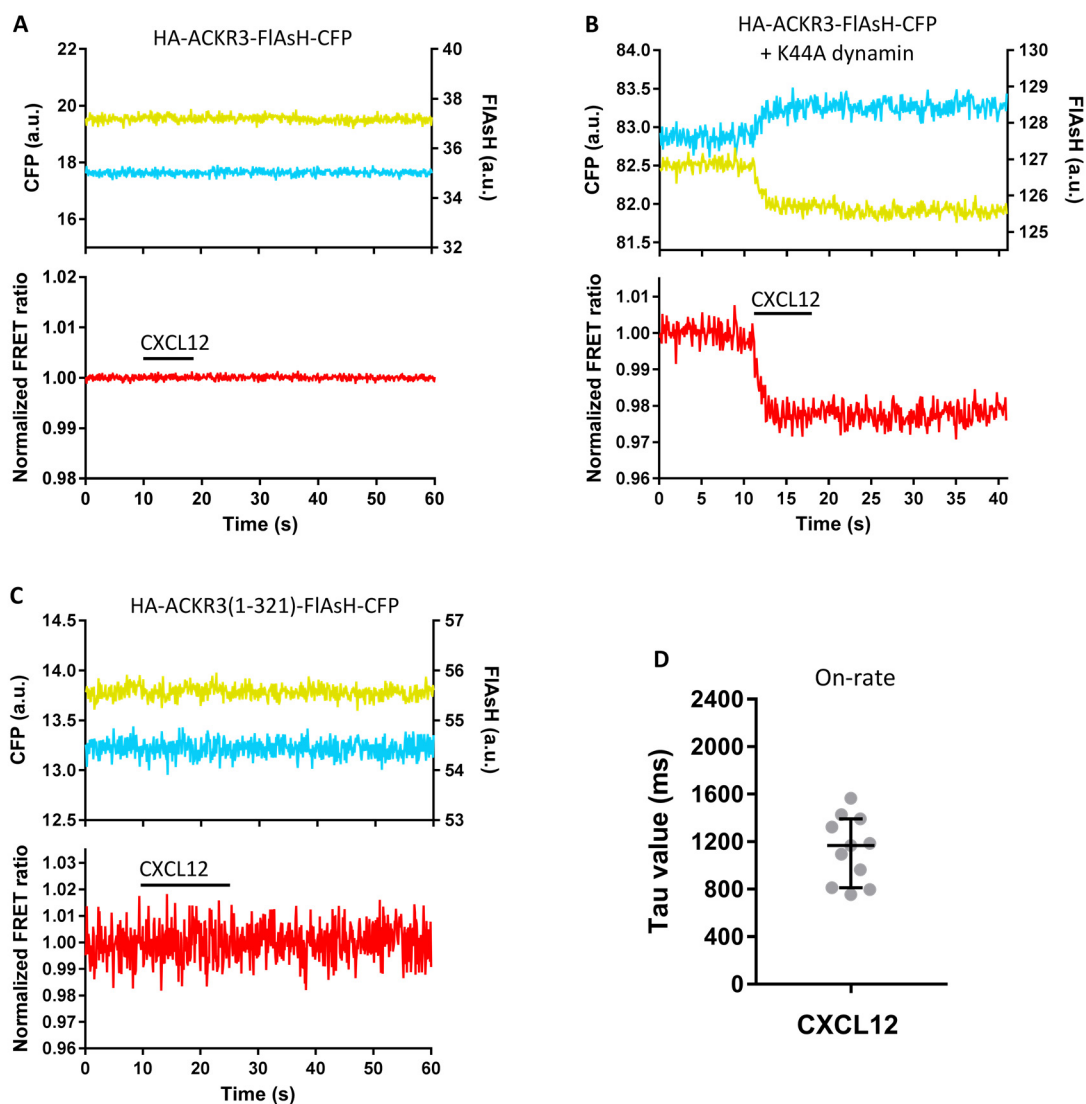


**Figure 38. The FRET-based ACKR3 sensor combined with K44A dynamin reports the CXCL12-induced conformational changes in the receptor. (A-C)** Representative traces of the FRET response from a single HEK293 cell expressing the construct(s) HA-ACKR3-FIAsH-CFP (A), HA-ACKR3-FIAsH-CFP and K44A dynamin (B), or HA-ACKR3(1-321)-FIAsH-CFP (C), and stimulated with 30  $\mu$ M CXCL12 for the indicated period of time. Upper panels show the corrected FIAsH (yellow) and CFP (cyan) emission intensities. Lower panels show corrected and normalized FRET ratio. **(D)** On-kinetics of ACKR3 upon stimulation with CXCL12 as determined using the HA-ACKR3-FIAsH-CFP sensor and K44A dynamin. Data show median and IQR of 11 cells measured in four independent experimental days.

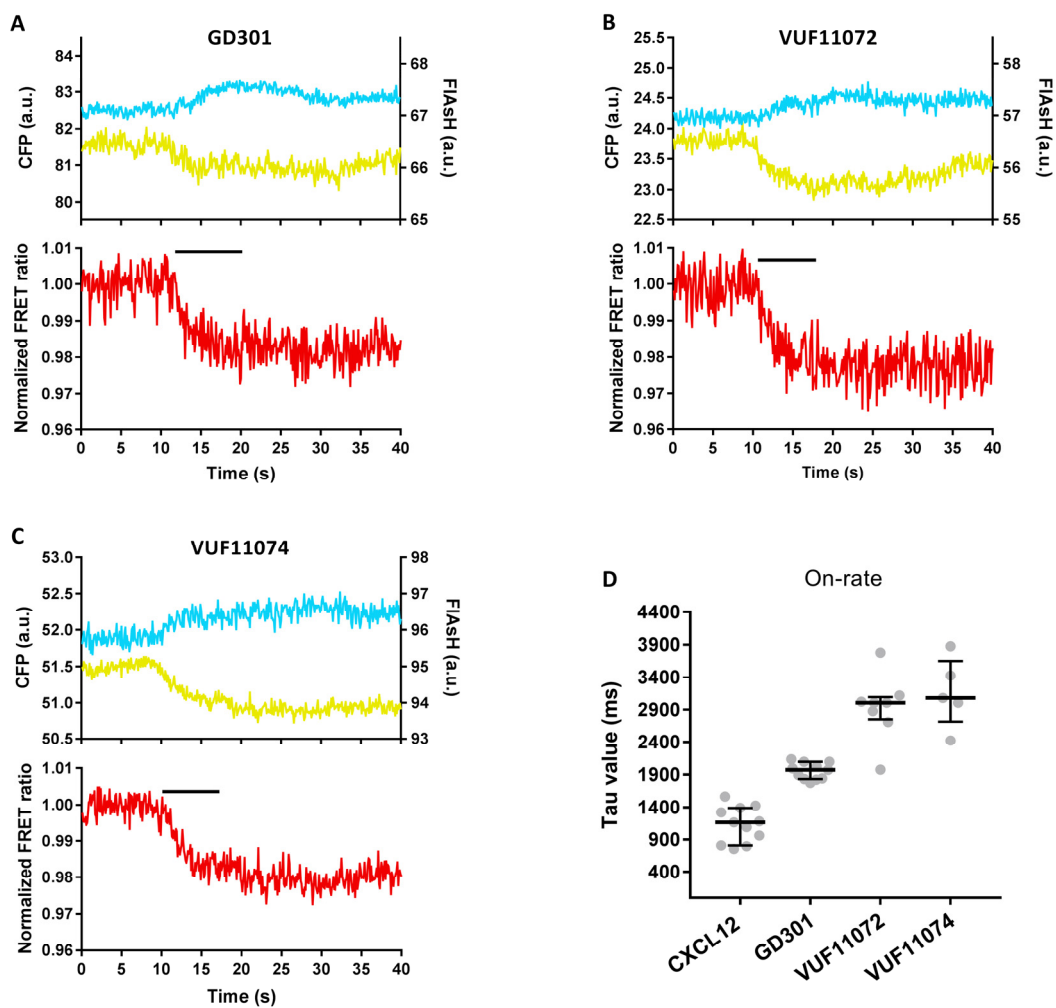


**Figure 39. The FRET-based ACKR3 sensor combined with K44A dynamin is a valid tool to investigate the dynamics and kinetics of receptor activation in response to different ligands. (A-C)** Representative traces of the FRET response from a single HEK293 cell expressing the HA-ACKR3-FIAsh-CFP sensor and K44A dynamin and stimulated with 50  $\mu$ M of GD301 (A), VUF11072 (B) or VUF11074 (C). Upper panels show normalized FIAsh (yellow) and CFP (cyan) emission intensities. Lower panels show corrected and normalized FRET ratio. **(D)** On-kinetics of ACKR3 upon stimulation with the different ligands. Data of CXCL12 is from figure 38D. Data show median and IQR of 11, 8, and 5 cells for GD301, VUF11072, and VUF11074, respectively, measured in at least three independent experimental days.

#### 4.2.5. G protein activation mediated by ACKR3 in response to CXCL12.

A large number of studies have shown that ACKR3 does not generally activate G proteins in response to CXCL12, but rather behaves as a scavenger or  $\beta$ -arrestin-biased receptor (section 1.4.2). This, combined with the fact that ACKR3 is largely found in intracellular compartments in most cell types, opens the possibility that the preferential localization of ACKR3 within the cell might contribute to its inability to activate G proteins. In order to test this possibility, HEK293T cells were transfected with ACKR3 and one of the G protein sensors ( $G_{i1}$ ,  $G_{i2}$ , or  $G_{i3}$ ) in the presence or absence of K44A dynamin. Then, cells were stimulated with increasing concentrations of CXCL12 in a 96-well plate assay format. As expected, no activation of G proteins by ACKR3 in response to CXCL12 could be detected in the absence of K44A dynamin (**Figure 40A**). In addition, further expression of the mutant dynamin did not lead to CXCL12-induced G protein activation by ACKR3 either (**Figure 40B**), suggesting that other factors might be responsible for the lack of G protein activation via this receptor.

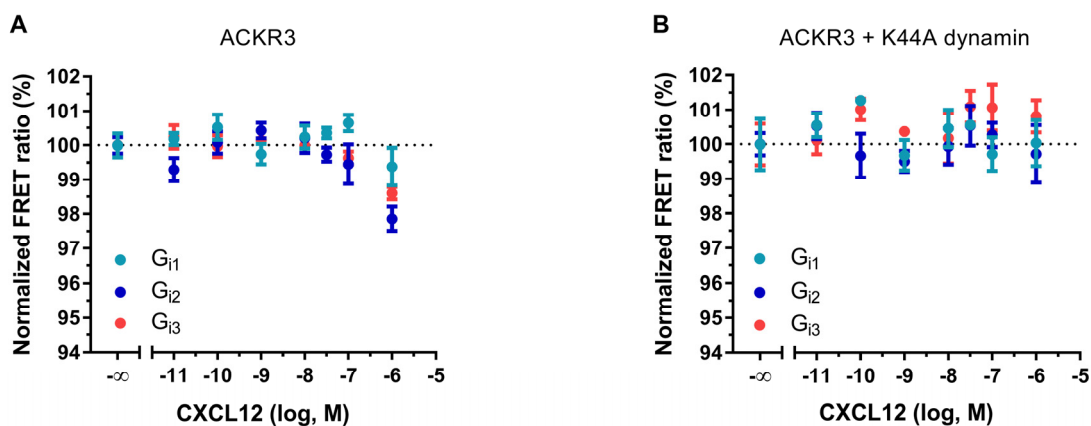


**Figure 40. Re-localization of ACKR3 to the plasma membrane by using K44A dynamin is not sufficient to activate  $G_i$  proteins.**  $G_{i1}$ ,  $G_{i2}$ , and  $G_{i3}$  protein activation mediated by ACKR3 in response to CXCL12 was measured in a 96-well plate assay format. Experiments were performed in HEK293T cells transfected with the constructs: (A) ACKR3 and G protein sensor ( $G_{i1}$ ,  $G_{i2}$ , or  $G_{i3}$ ); (B) ACKR3, K44A dynamin, and G protein sensor ( $G_{i1}$ ,  $G_{i2}$ , or  $G_{i3}$ ). An individual experiment is shown with mean  $\pm$  SEM. N=2 independent experiments.

## 5. DISCUSSION

Since their discovery, GPCRs are the most studied family of proteins in terms of their implication in physiological and pathological processes. Among the family of GPCRs, chemokine receptors represent important therapeutic targets due to their involvement in important physiological processes and thus are the center of exhaustive research. On one hand, the biomedical importance of CXCR4 and its ligands has been well established, and understanding how signaling proceeds via this receptor and the underlying mechanism of its signaling pathway might open new avenues to therapeutically target it. On the other hand, the non-classical ACKR3 is involved in several pathologies and its function as signaling receptor is still under debate. Due to the lack of signaling in most cellular systems, investigating the direct activation of this receptor has been challenging.

The aim of this work was to temporally elucidate the activation mechanisms of the two chemokine receptors CXCR4 and ACKR3 in response to various ligands, especially CXCL12, and to understand the dynamic movements involved in these processes with the help of FRET-based approaches.

### 5.1. The FRET-based CXCR4 sensors report ligand-induced conformational changes in the receptor and reveal slower kinetics of CXCR4 activation in comparison to other well-known class A GPCRs.

The crystal structure of CXCR4 in complex with different ligands has provided great insights into the binding mode of these molecules to the chemokine receptor. However, the dynamics and kinetics of receptor activation cannot be resolved in these studies, especially since these structures have been resolved solely in complex with antagonists (Wu et al., 2010; Qin et al., 2015). Therefore, in this project, FRET-based CXCR4 sensors were created in order to monitor the conformational changes that the receptor undergoes upon activation. For that purpose, CFP was fused to the end of the C-terminus, and the FIAsh-binding motif was inserted in three different positions within the ICL-3 in order to optimize the positions of the fluorophores (**Figure 20**). Characterization of the sensors revealed that all three constructs were expressed on the plasma membrane of HEK293 cells, preserved the ability to signal via  $G_i$  proteins, and exhibited basal intramolecular FRET (**Figures 21-23**), thus representing good candidates for studying receptor activation.

Based on this validation, the sensors were further employed to investigate the conformational changes that CXCR4 undergoes upon CXCL12 engagement in single-cell experiments. Binding of CXCL12 to the receptor resulted in a simultaneous anti-parallel movement in the CFP and FIAsh emissions, which translated into an increase in the FRET signal. This presumably results from a movement of the ICL-3

domain relative to the C-terminus. The three CXCR4 FRET sensors exhibited activation kinetics in the range of  $\tau \approx 600$  ms upon binding to the peptide ligand CXCL12 (**Figure 24**).

Using these type of sensors, the activation of other GPCRs, such as  $\alpha_{2A}$ -AR,  $\beta_1$ -AR,  $\beta_2$ -AR,  $A_{2A}$ -R, mGluR and some muscarinic receptors, has been investigated and ranges between  $\approx 30$ -100 ms in response to small agonist molecules (Vilardaga et al., 2003; Hoffmann et al., 2005; Rochais et al., 2007; Reiner et al., 2010; Ziegler et al., 2011; Grushevskiy et al., 2019). This speed of receptor activation is considerably faster than that recorded for CXCR4 in this work or that determined for the PTHR, a class B GPCR, in response to the peptide hormone PTH(1-34) ( $\tau \approx 1$  s; Vilardaga et al., 2003; **Figure 41**). These differences in the activation kinetics might be due to the distinct nature of the receptors or depend on the type of ligand (e.g. small molecules *versus* peptides) and their binding mode to the receptor. In this case, the binding of CXCL12 to CXCR4 proceeds via a two-step mechanism and involves extensive interactions between the two proteins, as described in section 1.2.3 (Kleist et al., 2016). This might be reflected into slower activation kinetics in comparison to small molecules. Likewise, the association of PTH(1-34) and PTHR also proceeds via a two-step binding process (Castro et al., 2005). It can be hypothesized that those ligands and receptors which association involves a “multi-step” binding mechanism would exhibit slower on-rates.

The kinetics of CXCR4 deactivation upon ligand wash-out are significantly slower ( $\tau \approx 20$  s) than those reported for other class A GPCRs binding small agonist molecules. For instance, deactivation time constants for the  $\alpha_{2A}$ -AR and  $\beta_1$ -AR upon wash-out of norepinephrine is in the range of  $\tau \approx 2$ -3 s (Vilardaga, 2011a). These kinetic differences might be due to the different structure and size of the ligands, their binding affinity to the receptor and/or the ability of the receptor to switch back to an inactive state. In this case, CXCL12 is a peptide, significantly bigger than norepinephrine and presents a high binding affinity for CXCR4.

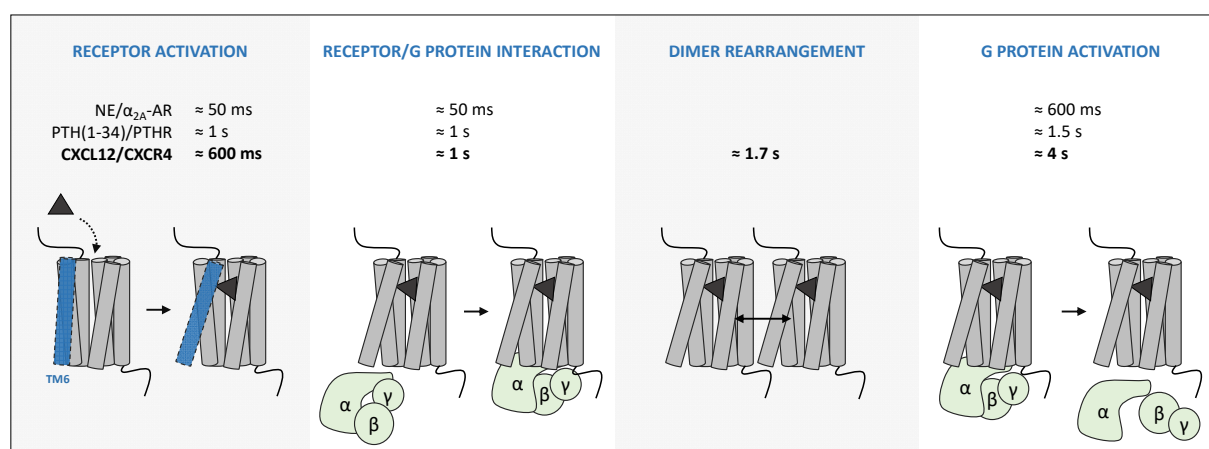


**Figure 41. Kinetics of the early reactions in the signaling cascade of GPCRs.** The time constants of receptor activation, receptor/G protein interaction, dimer rearrangement and G protein activation are shown for three different axes: NE/ $\alpha_{2A}$ -AR/ $G_i$ , PTH/PTH/ $G_s$ , and CXCL12/CXCR4/ $G_i$ . NE stands for norepinephrine.

## 5.2. CXCR4 exhibits a complex activation mechanism in response to CXCL12 as revealed by analysis of its early signaling steps.

By combining several FRET-based approaches, the early steps of the transduction pathway of CXCR4 in response to CXCL12 were temporally resolved. Upon binding to CXCL12, structural rearrangements within the TM domain associated to receptor activation ( $\tau \approx 600\text{ms}$ ) are followed by rearrangements between CXCR4 and the  $G_i$  protein in the intracellular side ( $\tau \approx 1\text{s}$ ). During the activation time course, structural rearrangements between CXCR4 protomers within dimers occur with  $\tau \approx 1.7\text{s}$  while  $G_i$  protein activation finally occurs in  $\tau \approx 4\text{s}$  (**Figure 41**). These data indicate that rearrangements between receptor protomers precede G protein activation and suggest that CXCR4 homodimers might play a role in the activation mechanism of this receptor. In contrast to this sequence of events, several reports have demonstrated that rearrangements between mGluR1 protomers are faster than intramolecular rearrangements within the TM domain of single protomers (Hlavackova et al., 2012; Grushevskiy et al., 2019). This distinct behavior might be related to the different nature of the receptors and might be a characteristic feature of class C GPCRs, for which dimerization is obligatory for function (Kniazeff et al., 2011; Zhang, Liu and Jiang, 2014).

Using FRET, the mode of coupling or interaction between labeled-GPCRs and labeled-G proteins can be analyzed. Generally, an increase in the FRET signal upon agonist binding to the receptor is interpreted as recruitment of the G protein to the activated receptor, while a decrease in the FRET signal is interpreted as dissociation. In this project, a decrease in FRET between CXCR4-YFP and the CFP-labeled G protein was observed upon stimulation of the cells with CXCL12 (**Figure 25**). This data is in contrast to other studies that have also investigated the mode of coupling of several GPCRs with different G proteins. For instance, Andressen et al. (2018) investigated the coupling mode of two serotonin receptors with  $G_s$  proteins. They showed that 5-HT<sub>7</sub> pre-associates with  $G_s$ , and that agonist-stimulation leads to a fast increase in the FRET signal between 5-HT<sub>7</sub>-YFP and  $G\alpha_s$ -CFP, whereas to a slow decrease in the FRET signal between 5-HT<sub>7</sub>-YFP and  $G\gamma_2$ -CFP. This indicated that agonist stimulation of the receptor leads to a conformational change within the pre-assembled complex that involves a rapid movement of  $G\alpha$  relative to the receptor, followed by slower dissociation of  $G\beta\gamma$  from both 5-HT<sub>7</sub> and  $G\alpha$ . This model for the interaction between 5-HT<sub>7</sub> and the  $G_s$  protein is in contrast to the collision coupling model observed for 5-HT<sub>4</sub> and the  $\beta_1$ -AR in this same study (Andressen et al., 2018). In another study, Hein et al. (2005) showed that  $\alpha_{2A}$ -ARs and  $G_i$  proteins interact by collision coupling. They observed an agonist-induced increase in the FRET signal between  $\alpha_{2A}$ -AR-YFP and CFP-labeled  $G_i$ , regardless of the position of the fluorescent tag in the G protein (at  $G\alpha_{i1}$  or  $G\gamma_2$  subunit). The rearrangements measured in both settings occurred with comparable kinetics, suggesting that the heterotrimeric G protein is recruited to the receptor altogether. In this thesis, a fast decrease in the



FRET signal between CXCR4-YFP and labeled- $G_i$  proteins was observed, regardless of the position of the tag in the G protein (at  $G\alpha_{i1}$  or  $G\gamma_2$  subunit) and these rearrangements occurred with very similar kinetics. The CXCL12-induced decrease in the FRET signal might indicate that CXCR4 is pre-associated with G proteins before agonist binding. Another possibility is that the constitutive activity of CXCR4, which is discussed in more detail in section 5.5, is responsible for the agonist-induced reduction in FRET. Altogether, these diverse data indicate that receptor/G protein coupling is complex and differs among GPCRs. Nevertheless, it is important to keep in mind that the fluorescent proteins have been tagged at different positions in the different studies mentioned.

Another interesting observation are the high off-kinetics observed for G protein activation, which reflect a prolonged  $G_i$  protein activation induced by the CXCL12/CXCR4 axis. The CXCL12-induced FRET signals measured with the receptor sensors return to baseline upon washing with buffer, indicating that the agonist is removed from the receptor (**Figure 24**). Likewise, FRET signals measured between protomers of dimers also return to baseline upon washing with buffer (**Figure 29**). However, the CXCL12-induced FRET signals measured for receptor/G protein interaction and G protein activation only partially return to baseline and the off-kinetics cannot be determined within the time frame of the experiments (**Figures 25 and 27**), in contrast to the norepinephrine-induced FRET signals using  $\alpha_{2A}$ -AR. An explanation might be that the labeled-G protein subunits associate with unlabeled (wt) G protein subunits endogenously present in HEK293 cells, therefore preventing the return of the FRET signal to baseline. Nonetheless, these observations reveal a different activation mechanism for CXCR4 in comparison to other classical GPCRs.

### 5.3. MIF induces distinct structural rearrangements than CXCL12 in CXCR4 and does not activate $G_i$ proteins via this receptor.

By employing different FRET-based approaches in single cells, the early steps of the transduction pathway of CXCR4 in response to MIF have been temporally resolved. Upon MIF binding, structural rearrangements within the TM domain ( $\tau \approx 300$  ms) are followed by rearrangements between CXCR4 and the  $G_i$  protein in the intracellular side ( $\tau \approx 400$  ms) and by rearrangements between CXCR4 protomers within dimers ( $\tau \approx 700$  ms) (**Table 9; Figure 31**). Similar to the activation of CXCR4 by CXCL12, these kinetic data also indicate that structural rearrangements within the TM domain of the receptor precede rearrangements between CXCR4 protomers, in contrast to the temporal events described for mGluR1 (Grushevskyi et al., 2019). This suggests that the sequence of events that occur via CXCR4 upon ligand binding might be conserved and further suggests that rearrangements within homodimers play a role in signal transduction via this receptor.

The data in this thesis show that binding of CXCL12 and MIF induce distinct structural rearrangements at each step of the signaling cascade of CXCR4. Each of these can be distinguished dynamically and kinetically, with MIF triggering opposite signals to CXCL12 and inducing faster rearrangements (**Figure 31**). These observations support the notion of different binding modes and/or mechanisms of action of these two ligands on CXCR4. It is known that binding of CXCL12 to CXCR4 proceeds via a two-step mechanism, which involves interactions between the CXCR4 N-terminus and the globular core of the chemokine, and the N-terminus of the chemokine with the TM binding pocket of the receptor (section 1.2.3; Wu et al., 2010; Qin et al., 2015; Kufareva, Salanga and Handel, 2015). In contrast, different residues from the N-terminus of the receptor are involved in the interaction with MIF, which also does not establish direct interactions with the TM binding pocket (section 1.3.5.1; Rajasekaran et al., 2016). In fact, the structure of MIF shows that its N-terminus is buried into its catalytic pocket and thus unavailable for interactions with the TM cavity of the receptor.

In contrast to the literature, CXCR4 did not mediate the activation of  $G_i$  proteins in response to MIF binding in single-cell experiments (**Figure 31G**; Rajasekaran et al., 2016). However, MIF-induced activation of  $G_{i1}$ ,  $G_{i2}$  and  $G_{i3}$  was detected in 96-well plate assays. This response was also observed in cells that had not been transfected with the receptor and thus is likely not mediated by CXCR4 (**Figure 31H-J**). According to the literature, there are two other MIF-binding receptors: ACKR3 and CXCR2 (Bernhagen et al., 2007; Alampour-Rajabi et al., 2015). ACKR3 is generally described to not bind to or signal via G proteins. Hence, the activation of G proteins that is detected in these experimental conditions could be mediated by CXCR2.

Overall, the data in this thesis indicate that MIF regulates the activity of CXCR4 distinctly to CXCL12 and that these two ligands present important different pharmacological properties. The fact that MIF induces opposite signals to CXCL12 at each step of the signaling cascade could suggest that it acts as an inverse agonist on CXCR4. However, further studies will be needed to test this possibility.

#### **5.4. Iron-bound lactoferrin, but not iron-free lactoferrin, leads to the activation of $G_{i2}$ and $G_{i3}$ proteins but not $G_{i1}$ via CXCR4.**

Lactoferrin is an iron-binding glycoprotein of the immune system that is therapeutically relevant due to its antibacterial, antifungal and antiviral activities (Van der Strate et al., 2001; Jenssen and Hancock, 2009; Fernandes and Carter, 2017), but also because it has been recently described to be a CXCR4 ligand (Takayama et al., 2016). Considering that the arrangement of this protein differs depending on whether it is bound to iron ( $Fe_2$ -Lf) or not (apo-Lf) (**Figure 11**; section 1.3.5.2), the effects of both configurations were characterized on CXCR4 activation and CXCR4-mediated G protein activation.

CXCR4-mediated  $G_i$  protein signaling in response to lactoferrin was investigated using the FRET-based sensors for  $G_{i1}$ ,  $G_{i2}$ , and  $G_{i3}$  in 96-well plate assays. The data revealed that stimulation of CXCR4-expressing cells with  $Fe_2$ -Lf leads to the activation of  $G_{i2}$  and  $G_{i3}$  but not  $G_{i1}$ . In contrast, no activation of  $G_i$  proteins by CXCR4 was observed in response to apo-Lf (**Figure 33C-I**). It is known that the conformation of lactoferrin is remarkably different depending on the presence or absence of iron atoms in its structure (section 1.3.5.2). The data in this thesis suggest that iron-bound lactoferrin might be the most relevant form in the axis lactoferrin:CXCR4. Considering these data, one should take into account which state applies when performing or interpreting functional studies, since the data suggest that the properties of the molecule will be drastically different. Interestingly, in contrast to CXCL12,  $Fe_2$ -Lf produced a FRET signal that slowly returned to baseline within the time frame of the experiment, indicating that the induction of G protein activation by this ligand is transient. This might be an intrinsic characteristic of the signaling induced by this ligand or might as well be due to conversion of  $Fe_2$ -Lf to apo-Lf over the time course of the measurement.

Another interesting observation is that CXCR4 activates the G protein subtypes  $G_{i2}$  and  $G_{i3}$  but not  $G_{i1}$  upon binding to  $Fe_2$ -Lf, while it is able to activate the three  $G_i$  subtypes in response to CXCL12 binding. These observations support the idea that, within a given GPCR, ligands can discriminate between  $G_i$  family members, as described previously for other GPCRs (Busnelli et al., 2012). A detailed analysis of the differences and similarities in the binding modes and interactions of CXCL12 *versus*  $Fe_2$ -Lf with CXCR4 could help to understand the basis of selectivity and contribute to the development of drugs with selectivity towards specific pathways.

Using the FRET-based CXCR4 sensor, no structural changes in the receptor were detected in response to any form of lactoferrin (**Figure 33A-B**). Considering that CXCR4-mediated G protein signaling in response to  $Fe_2$ -Lf was observed, one can hypothesize that  $Fe_2$ -Lf binds to CXCR4 but induces different rearrangements in the receptor to those induced by CXCL12, probably small rearrangements, which are not detected using this sensor. Overall, and in agreement with Takayama et al. (2016), the data in this thesis supports the idea of CXCR4 as a lactoferrin receptor.

#### 5.5. CXCR4 exhibits some degree of ligand-independent constitutive activity.

Increasing number of reports show that many GPCRs display constitutive activity, which means that they spontaneously transition between inactive and active-like conformations, leading to the activation of G proteins or other alternative signaling pathways independent of ligand activation. In this work, the interaction of CXCR4 with  $G_i$  proteins as well as  $G_i$  protein activation via this receptor in the absence of agonist were analyzed. On one hand, photobleaching experiments showed that there was basal energy transfer between labeled-CXCR4 and labeled- $G_i$  proteins in the absence of ligand

(**Figure 26**). This indicates close proximity between these two partners and suggests a potential interaction previous to agonist stimulation. This observation would be in agreement with a previous study by Levoye et al. (2009) in which a constitutive interaction between CXCR4 and  $G_{i1}$  proteins was observed using BRET. On the other hand, by means of using a FRET-based  $G_i$  sensor, activation of  $G_i$  proteins by CXCR4 was observed in the absence of agonist (**Figure 28**). These findings suggest that CXCR4 exhibits some degree of constitutive activity, which not only involves a potential basal interaction with  $G_i$  proteins, but also their activation. Interestingly, in both experimental conditions, the FRET signals observed could be prevented by incubation of the cells with IT1t, suggesting that this ligand acts as an inverse agonist on CXCR4.

The existence of constitutive activity on CXCR4 has been suggested in previous studies. Mishra et al. (2016) observed a ligand-independent internalization of the receptor, which could be blocked by treating the cells with AMD3100 or NUCC-390 (CXCR4 antagonists). In line, a recent study has correlated the level of constitutive internalization of GPCRs with constitutive activity (Hendrik Schmidt et al., 2019). Also, Mona et al. (2016) described that IT1t and a series of CXCR4 ligands had inverse agonism activity on the receptor, observing a slight reduction of the basal activity of CXCR4 in  $G_i$ - and  $\beta$ -arrestin-based assays upon treatment with these molecules. It is not surprising that AMD3100 and IT1t, two well recognized CXCR4 neutral antagonists until now, act as inverse agonists in these studies as well as the latter in this work. In fact, it has been described that 85% of compounds initially classified as neutral antagonists turn out to be inverse agonists when tested on constitutively active mutant receptors or on wt receptors with constitutive activity (Kenakin, 2004).

On the basis of observations in this thesis, the existence or the degree of constitutive activity of CXCR4 needs to be further validated in more physiological systems and *in vivo*. It is an important feature to take into account for drug development since it can be reduced with inverse agonists but not neutral antagonists. Consequently, there can be significant differences in the outcome between these two types of ligands depending on whether the receptor exhibits constitutive activity or not. For instance, a large number of studies have reported that CXCR4 is overexpressed or upregulated in many different types of cancer, such as prostate, breast, ovarian, lung, kidney and brain (Müller et al., 2001; Balkwill, 2004; Darash-Yahana et al., 2004; Chatterjee et al., 2014), and elevated CXCR4 expression is associated with poor prognosis in some cancers (Zhao et al., 2015). Under normal (healthy) physiological conditions, the degree of constitutive activity might be difficult to detect because the fraction of receptors in active-like conformations is probably below the detection threshold. However, when the receptor is overexpressed in *in vitro* systems or, importantly, under certain pathological contexts, the degree of spontaneous activity might be detectable and therapeutically relevant. Therefore, a more detailed understanding of the biology of CXCR4 in this respect could provide new opportunities for improved design of targeting drugs.

### 5.6. The HA-ACKR3-FIAsH-CFP sensor in combination with K44A dynamin is a powerful tool to investigate the ligand-induced activation of the receptor.

Due to the lack of activation of classical pathways via ACKR3, only a small number of read-outs are available to study its activation. Therefore, one of the aims in this project was to develop a functional FRET-based ACKR3 sensor to be able to monitor ligand-induced structural rearrangements in this receptor. For this purpose, CFP was fused to the end of the C-terminus and the FIAsH-binding motif was inserted into the ICL-3 (**Figure 34**). The sensor HA-ACKR3-FIAsH-CFP exhibited basal intramolecular FRET and unaltered ligand binding properties (**Figures 36 and 37**) but was mainly expressed in intracellular compartments of HEK293 cells (**Figure 35A**), which is consistent with its atypical nature and scavenging function (section 1.4.2; Boldajipour et al., 2008; Luker et al., 2010; Shimizu et al., 2011; Ray et al., 2012b; Torossian et al., 2014). Stimulation of cells expressing the HA-ACKR3-FIAsH-CFP sensor with CXCL12 did not result in a change in FRET in the system (**Figure 38A**). This is probably due to the fact that the sensor is predominantly found in intracellular compartments and thus it has limited access to the ligand that is applied on the extracellular side. In fact, most molecules that bind to GPCRs, such as drugs or endogenous ligands, do not have the ability to cross the cell membrane. Therefore, in order to develop a functional ACKR3 sensor, different strategies had to be implemented to increase the presence of the ACKR3 sensor in the plasma membrane.

On one hand, the C-terminus of the receptor sensor was truncated at two different positions, deleting the last 16 (HA-ACKR3(1-346)-FIAsH-CFP) or 41 amino acids (HA-ACKR3(1-321)-FIAsH-CFP). These truncations have been previously demonstrated to redistribute ACKR3 to the cell membrane due to the role of the C-terminus in receptor trafficking and stability (Ray et al., 2012b). These truncations eliminate residues that are important for phosphorylation by GRKs and subsequent  $\beta$ -arrestin binding and internalization. Nevertheless, in this study, the HA-ACKR3(1-346)-FIAsH-CFP construct still localized mostly to intracellular compartments and the HA-ACKR3(1-321)-FIAsH-CFP construct only partially redistributed to the plasma membrane (**Figure 35C-D**). Although the HA-ACKR3(1-321)-FIAsH-CFP construct was found in the cell membrane in sufficient amounts to perform single-cell FRET experiments, no conformational changes were detected upon exposure to CXCL12 (**Figure 38C**). According to the literature, the truncation of the C-terminal tail of the receptor does not impair CXCL12 binding (Ray et al., 2012b). However, it is possible that the C-terminal truncation affects the activation of the receptor. An alternative explanation is that shortening the C-terminal tail of the receptor alters the distance and orientation of the fluorophores in a way that may not be optimal for detecting FRET changes upon activation (as reflected by the increase in FRET efficiency; **Table 10**).

On the other hand, the functions of dynamin, a molecule essential for endocytosis of receptors, was blocked by transfecting the cells with K44A dynamin. This is a dominant negative mutant of dynamin

that is defective in GTP binding and hydrolysis and therefore blocks receptor endocytosis in cells (Sontag et al., 1994). Co-transfection of the HA-ACKR3-FIAsH-CFP construct with K44A dynamin significantly increased the presence of the sensor in the plasma membrane (**Figure 35B**). In this case, stimulation of cells with several agonists, including CXCL12, led to changes in FRET in the sensor, reporting conformational changes in the receptor upon activation within seconds (**Figure 38B and D; Figure 39**). While all the ligands tested produced FRET changes with similar amplitudes in the sensor, the activation kinetics were different for each ligand: CXCL12 produced the fastest activation, followed by GD301, VUF11072 and VUF11074.

Previous studies have shown that ligands with different pharmacological properties can be distinguished using FRET-based receptor sensors. Generally, partial agonists are found to induce smaller and slower FRET changes than full agonists (Nikolaev et al., 2006; Zürn et al., 2009; Vilardaga, 2011b). CXCL12 induced changes in the sensor that were two- to three-fold faster than the changes induced by the other ligands, but all of them produced responses with very similar amplitudes, suggesting that they all induce very similar conformational rearrangements in the receptor. Considering CXCL12 as the full agonist reference compound, an explanation for these observations might be that the other ligands are also full agonists (stabilizing the same or similar receptor conformation) but present different ways of getting into the binding pocket of the receptor than CXCL12.

### 5.7. Re-localization of ACKR3 to the plasma membrane by using K44A dynamin is not sufficient to activate G proteins.

Whether the preferential localization of ACKR3 within the cell contributes to the inability of this receptor to activate G proteins was investigated in section 4.2.5. The data showed that re-locating ACKR3 to the plasma membrane is not sufficient to gain the ability to signal via G<sub>i</sub> proteins upon CXCL12 exposure. This was demonstrated in HEK293 cells expressing the ACKR3 receptor, a FRET-based G protein sensor, and K44A dynamin (**Figure 40**). The latter blocks internalization in the cell and significantly increased the presence of ACKR3 in the cell surface. However, this did not result in CXCL12-induced G protein activation. In addition to the preferential location within the cell, other determinants might contribute to the inability of ACKR3, and in general of ACKRs, to promote G protein-dependent signaling. For instance, structural determinants or the presence/absence of other interacting partners that modulate the activity of this receptor might play a role.

### 5.8. The Biopen® microfluidic system is suitable for kinetic studies.

In this work, the BioPen® microfluidic device has been used to deliver the solutions onto one or few cells. In contrast to the more traditional multi-syringe perfusion system, the Biopen® permits to maintain a localized solution delivery with high precision and avoids contamination of the environment immediately surrounding the targeted cells. Besides, this system was chosen for this work due to the small volume of solutions needed for operation, which significantly reduces the use of expensive reagents, such as the ligands CXCL12 and MIF. Since it is the first time that this system has been used for analyzing the kinetics of GPCR processes, the kinetics of  $G_i$  activation by the  $\alpha_{2A}$ -AR in response to norepinephrine were tested in parallel using the Biopen® (**Figure 27**). This process has been previously investigated using the multi-syringe perfusion system in our lab (Hein et al., 2005; van Unen et al., 2016). The results from this thesis using the Biopen® are in good agreement with the earlier published observations using the multi-syringe perfusion system and thus prove that the BioPen® is suitable for kinetic analyses with sub-second resolution.

### 5.9. Conclusions and future directions.

The CXCR4 and ACKR3 sensors developed in this work have allowed to monitor and analyze the conformational changes that these two receptors undergo upon binding of various ligands. Chemokine receptors are well recognized therapeutic targets and drugs targeting these proteins are in continuous development. Hence, these sensors represent valuable tools to further investigate the activation of these receptors in response to newly developed drugs, facilitating their primary pharmacological characterization. Furthermore, they set the basis for the development of sensors for other chemokine receptors. Specially, the strategies employed with the ACKR3 sensor could be extended to other atypical chemokine receptors, which are challenging to study due to their constant shuttle between the cell membrane and intracellular compartments. In this respect, the use of phosphorylation-deficient mutants or a  $\beta$ -arrestin knock-out cell line could also be a valuable tool, potentially facilitating the expression of these type of receptors on the plasma membrane of cells (Saaber et al., 2019). Furthermore, it would be very useful to use these sensors as a basis for developing analogue CXCR4 and ACKR3 BRET sensors, more suitable for high-throughput screening.

The combination of several FRET-based approaches has allowed the temporal resolution of the signaling pattern of CXCR4. The data in this project show a complex activation mechanism of CXCR4 and provide a more detailed understanding on how signaling proceeds via this receptor and how different ligands distinctly modulate its activation. It would be interesting to further investigate the dynamic and kinetic interaction of CXCR4 with different GRKs and  $\beta$ -arrestins as well as  $\beta$ -arrestin

activation via this receptor upon binding to CXCL12 and MIF. This would provide a more detailed insight into the signaling cascades triggered by this receptor and further identify similarities and differences between these two axes, hence opening new opportunities to distinctly and specifically target each of them. An additional interesting point would be to further confirm the level of CXCR4 constitutive activity in relevant biological systems, such as cancer cell lines. This would help in the development of specific targeting drugs for CXCR4 (antagonists *versus* inverse agonists).



## 6. ANNEXES

### 6.1. ABBREVIATIONS.

<b>Abbreviation</b>	<b>Full name</b>
AC	Adenylyl cyclase
ACh	Acetylcholine
ACKR	Atypical chemokine receptor
AIDS	Acquired immune deficiency syndrome
ATP	Adenosine triphosphate
A <sub>2A</sub> -R	Adenosine A <sub>2A</sub> receptor
bLf	Bovine lactoferrin
BRET	Bioluminescence resonance energy transfer
BSA	Bovine serum albumin
Ca <sup>2+</sup>	Calcium
cAMP	Cyclic adenosine monophosphate
cCKR	Conventional chemokine receptor
CCL	C C ligand
CCR	CC receptor
CD	Cluster of differentiation
CFP	Cyan fluorescent protein
CNS	Central nervous system
CRS	Chemokine recognition site
CXCL	C X C ligand
CXCR	C X C receptor
CX <sub>3</sub> CL	C X <sub>3</sub> C ligand
DAG	Diacylglycerol
PBS	Phosphate-buffered saline
ECL	Extracellular loop
EDT	1,2-Ethanedithiol
EGFR	Epithelial growth factor receptor
ERK	Extracellular signal-regulated kinases
FCS	Fetal calf serum
FDA	Food and drugs administration
FIAsH	Fluorescein arsenical hairpin
FRET	Förster resonance energy transfer
GAG	Glycosaminoglycan
GDP	Guanosine diphosphate
GFP	Green fluorescence protein
GIRK	G protein-coupled, inwardly-rectifying potassium channels
G protein	Guanine nucleotide binding protein
GPCR	G protein-coupled receptor
gp120	Glycoprotein 120
GRK	G protein-coupled receptor kinases
GTP	Guanosine triphosphate

<b>Abbreviation</b>	<b>Full name</b>	<i>(continued)</i>
HA	Hemagglutinin	
HEK293	Human embryonic kidney cells 293	
HIV	Human immunodeficiency virus	
HMGB1	High mobility group box 1	
ICL	Intracellular loop	
IP <sub>3</sub>	Inositol triphosphate	
JAK	Janus kinase	
JNK	C-Jun N-terminal kinase	
Lf	Lactoferrin	
LB	Lysogeny broth	
mGluR1	Metabotropic glutamate receptor 1	
MIF	Macrophage migration inhibitory factor	
mRNA	Messenger ribonucleic acid	
MAPK	Mitogen activated protein kinases	
MSC	Mesenchymal stem cell	
M <sub>1</sub> -AChR	Muscarinic acetylcholine receptor 1	
M <sub>3</sub> -AChR	Muscarinic acetylcholine receptor 3	
M <sub>5</sub> -AChR	Muscarinic acetylcholine receptor 5	
ON	Overnight	
PCR	Polymerase chain reaction	
P <sub>i</sub>	Inorganic phosphate	
PIP <sub>2</sub>	Phosphatidylinositol 4,5-bisphosphate	
PI3K	Phosphatidylinositol 3-kinase	
PKA	Protein kinase A	
PKC	Protein kinase C	
PLC	Phospholipase C	
PTH	Parathyroid hormone	
PTHR	Parathyroid hormone receptor type 1	
PTX	Pertussis toxin	
ReAsH	Resorufin arsenical hairpin	
RLuc	Renilla luciferase	
RT	Room temperature	
STAT	Signal transducer and activator of transcription	
TC	Tetracysteine	
TM	Transmembrane	
vMIP-II	Viral macrophage inflammatory protein II	
VSMC	Vascular smooth muscle cell	
WT	Wild-type	
YFP	Yellow fluorescent protein	
α <sub>1</sub> -AR	α <sub>1</sub> -adrenergic receptor	
α <sub>2A</sub> -AR	α <sub>2A</sub> -adrenergic receptor	
β <sub>1</sub> -AR	β <sub>1</sub> -adrenergic receptor	
β <sub>2</sub> -AR	β <sub>2</sub> -adrenergic receptor	
5-HT	5-hydroxytryptamine receptor (serotonin receptors)	



**pcDNA3-3HA-CXCR4-FIAsH226**

aagcttGGTACCACCATG**TACCCATACGATGTTCCAGATTACGCTTACCCATACGATGTTCCAGATTACGCTTACCCATACGATGTTCCAGATTACGCTGAT**GAGGGGATCAGTATATACTTACAGATAACTACACCGAGGAAATGGGCTCAGGGGACTATGACTCCATGAAGGAACCCTGTTCCGTGAAGAAAATGCTAATTTCAATAAAAATCTTCTGCCACCATCTACTCCATCATCTTCTAACTGGCATTGTGGGCAATGGATTGGTCATCCTGGTCATGGGTTACCAGAAGAACTGAGAAGCATGACGGACAAGTACAGGCTGCACCTGTCAGTGGCCGACCTCCTCTTTGTCATCACGCTCCCTTCTGGGCAGTTGATGCCGTGGCAAACCTGGTACTTTGGAACTTCTATGCAAGGCAGTCCATGTCATCTACACAGTCAACCTCTACAGCAGTGCCTCATCTGGCCTTCATCAGTCTGGACCGCTACCTGGCCATCGTCCACGCCACCAACAGTCAGAGGCCAAGGAAGCTGTTGGCTGAAAAGGTGGTCTATGTTGGCGTCTGGATCCCTGCCCTCTGCTGACTATTCCGACTTCATCTTTGCCAACGTCAGTGAGGCAGATGACAGATATATCTGTGACCGCTTCTACCCAATGACTTGTGGGTGGTTGTGTTCCAGTTTCAGCACATCATGGTTGGCCTTATCCTGCCTGGTATTGTCATCCTGTCTGCTATTGCATTATCATCTCCAAGCTGT**GTTGCCCGGGCTGCTGT**TCACACTCCAAGGGCCACCAGAAGCGCAAGGCCCTCAAGACCACAGTCATCCTCATCTGGCTTCTTCGCCTGTTGGCTGCCTTACTACATTGGGATCAGCATCGACTCCTTCATCTCCTGGAAATCATCAAGCAAGGGTGTGAGTTTGAGAACACTGTGCACAAGTGGATTTCCATCACCAGGCCCTAGCTTTCTTCCACTGTTGTCTGAACCCATCTCTATGCTTTCCTTGGAGCCAAATTTAAAACCTCTGCCAGCACGCACTACCTCTGTGAGCAGAGGGTCCAGCCTCAAGATCCTCTCAAAGGAAAGCGAGGTGGACATTCATCTGTTTCCACTGAGTCTGAGTCTTCAAGTTTTCACTCCAGCT**TAAgcgccgct**

**pcDNA3-3HA-CXCR4-FIAsH228**

aagcttGGTACCACCATG**TACCCATACGATGTTCCAGATTACGCTTACCCATACGATGTTCCAGATTACGCTTACCCATACGATGTTCCAGATTACGCTGAT**GAGGGGATCAGTATATACTTACAGATAACTACACCGAGGAAATGGGCTCAGGGGACTATGACTCCATGAAGGAACCCTGTTCCGTGAAGAAAATGCTAATTTCAATAAAAATCTTCTGCCACCATCTACTCCATCATCTTCTAACTGGCATTGTGGGCAATGGATTGGTCATCCTGGTCATGGGTTACCAGAAGAACTGAGAAGCATGACGGACAAGTACAGGCTGCACCTGTCAGTGGCCGACCTCCTCTTTGTCATCACGCTCCCTTCTGGGCAGTTGATGCCGTGGCAAACCTGGTACTTTGGAACTTCTATGCAAGGCAGTCCATGTCATCTACACAGTCAACCTCTACAGCAGTGCCTCATCTGGCCTTCATCAGTCTGGACCGCTACCTGGCCATCGTCCACGCCACCAACAGTCAGAGGCCAAGGAAGCTGTTGGCTGAAAAGGTGGTCTATGTTGGCGTCTGGATCCCTGCCCTCTGCTGACTATTCCGACTTCATCTTTGCCAACGTCAGTGAGGCAGATGACAGATATATCTGTGACCGCTTCTACCCAATGACTTGTGGGTGGTTGTGTTCCAGTTTCAGCACATCATGGTTGGCCTTATCCTGCCTGGTATTGTCATCCTGTCTGCTATTGCATTATCATCTCCAAGCTGTACACT**GTTGCCCGGGCTGCTGT**TCCAAGGGCCACCAGAAGCGCAAGGCCCTCAAGACCACAGTCATCCTCATCTGGCTTCTTCGCCTGTTGGCTGCCTTACTACATTGGGATCAGCATCGACTCCTTCATCTCCTGGAAATCATCAAGCAAGGGTGTGAGTTTGAGAACACTGTGCACAAGTGGATTTCCATCACCAGGCCCTAGCTTTCTTCCACTGTTGTCTGAACCCATCTCTATGCTTTCCTTGGAGCCAAATTTAAAACCTCTGCCAGCACGCACTACCTCTGTGAGCAGAGGGTCCAGCCTCAAGATCCTCTCAAAGGAAAGCGAGGTGGACATTCATCTGTTTCCACTGAGTCTGAGTCTTCAAGTTTTCACTCCAGCT**TAAgcgccgct**

**pcDNA3-3HA-CXCR4-FIAsH229**

aagcttGGTACCACCATG**TACCCATACGATGTTCCAGATTACGCTTACCCATACGATGTTCCAGATTACGCTTACCCATACGATGTTCCAGATTACGCTGAT**GAGGGGATCAGTATATACTTACAGATAACTACACCGAGGAAATGGGCTCAGGGGACTATGACTCCATGAAGGAACCCTGTTCCGTGAAGAAAATGCTAATTTCAATAAAAATCTTCTGCCACCATCTACTCCATCATCTTCTAACTGGCATTGTGGGCAATGGATTGGTCATCCTGGTCATGGGTTACCAGAAGAACTGAGAAGCATGACGGACAAGTACAGGCTGCACCTGTCAGTGGCCGACCTCCTCTTTGTCATCACGCTCCCTTCTGGGCAGTTGATGCCGTGGCAAACCTGGTACTTTGGAACTTCTATGCAAGGCAGTCCATGTCATCTACACAGTCAACCTCTACAGCAGTGCCTCATCTGGCCTTCATCAGTCTGGACCGCTACCTGGCCATCGTCCACGCCACCAACAGTCAGAGGCCAAGGAAGCTGTTGGCTGAAAAGGTGGTCTATGTTGGCGTCTGGATCCCTGCCCTCTGCTGACTATTCCGACTTCATCTTTGCCAACGTCAGTGAGGCAGATGACAGATATATCTGTGACCGCTTCTACCCAATGACTTGTGGGTGGTTGTGTTCCAGTTTCAGCACATCATGGTTGGCCTTATCCTGCCTGGTATTGTCATCCTGTCTGCTATTGCATTATCATCTCCAAGCTGTACACTCCT**GTTGCCCGGGCTGCTGT**AAGGGCCACCAGAAGCGCAAGGCCCTCAAGACCACAGTCATCCTCATCTGGCTTCTTCGCCTGTTGGCTGCCTTACTACATTGGGATCAGCATCGACTCCTTCATCTCCTGGAAATCATCAAGCAAGGGTGTGAGTTTGAGAACACTGTGCACAAGTGGATTTCCATCACCAGGCCCTAGCTTTCTTCCACTGTTGTCTGAACCCATCTCTATGCTTTCCTTGGAGCCAAATTTAAAACCTCTGCCAGCACGCACTACCTCTGTGAGCAGAGGGTCCAGCCTCAAGATCCTCTCAAAGGAAAGCGAGGTGGACATTCATCTGTTTCCACTGAGTCTGAGTCTTCAAGTTTTCACTCCAGCT**TAAgcgccgct**

**pcDNA3-3HA-CXCR4-FIAsh226-CFP**

[aagcttGGTACCACC](#)[ATG](#)[TACCCATACGATGTTCCAGATTACGCTTACCCATACGATGTTCCAGATTACGCTTACCCATACGAT](#)  
[GTTCCAGATTACGCTGAT](#)GAGGGGATCAGTATATACTTACAGATAACTACACCCGAGGAAATGGGCTCAGGGGACTATGA  
 CTCCATGAAGGAACCCTGTTCCGTGAAGAAAATGCTAATTTCAATAAAAATCTTCTGCCACCATCTACTCCATCATCTTCT  
 TAACTGGCATTGTGGGCAATGGATTGGTCATCCTGGTCATGGGTTACCAGAAGAACTGAGAAGCATGACGGACAAGTAC  
 AGGCTGCACCTGTCAAGTGGCCGACCTCCTTTGTATCACGCTCCCTTCTGGGCGATTGATGCCGTGGCAAACCTGGTACT  
 TTGGGAACTTCTATGCAAGGCAGTCCATGTATCTACACAGTCAACCTCTACAGCAGTGTCTCATCTGGCCTTCATCAG  
 TCTGGACCGCTACCTGGCCATCGTCCACGCCACCAACAGTCAGAGGCCAAGGAAGCTGTTGGCTGAAAAGGTGGTCTATG  
 TTGGCGTCTGGATCCCTGCCCTCTGCTGACTATTCCGACTTCATCTTTGCCAACGTCAGTGAGGCAGATGACAGATATAT  
 CTGTGACCGCTTCTACCCCAATGACTTGTGGGTGGTTGTGTTCCAGTTTCAGCACATCATGGTTGGCCTTATCCTGCCTGGT  
 ATTGTCATCCTGTCTGCTATTGCATTATCATCTCCAAGCTG[TGTGCCCCGGGCTGCTGT](#)TCACTCCAAGGGCCACCAGA  
 AGCGCAAGGCCCTCAAGACCACAGTCATCCTCATCTGGCTTCTTCGCTGTTGGCTGCCTTACTACATTGGGATCAGCAT  
 CGACTCCTTCATCTCCTGAAAATCATCAAGCAAGGGTGTGAGTTTGAGAACACTGTGCACAAGTGGATTTCCATCACCGA  
 GGCCCTAGCTTTCTTCCACTGTTGTCTGAACCCCATCTCTATGCTTTCCTTGGAGCCAAATTTAAAACCTCTGCCAGCACG  
 CACTACCTCTGTGAGCAGAGGGTCCAGCCTCAAGATCCTCTCAAAGGAAAGCGAGGTGGACATTCTGTTTCCACTG  
 AGTCTGAGTCTTCAAGTTTTCACTCCAGC[tctaga](#)[GTGAGCAAGGGCGAGGAGCTGTTACCCGGGGTGGTCCCCATCCTGGT](#)  
[CGAGCTGGACGGCGACGTAACCGGCCACAg](#)[GTTACGCGTGTCCGGCGAGGGCGAGGGCGATGCCACCTACGGCAAGCTG](#)  
[ACCCTGAAGTTCATCTGCACCACCGGCAAGCTGCCGTGCCCTGGCCACCTCGTGACCACCTGACCTGGGGCGTGCAG](#)  
[TGTTTCAGCCGCTACCCCGACCACATGAAGCAGCACGACTTCTTCAAGTCCGCCATGCCCGAAGGCTACGTCCAGGAGCGT](#)  
[ACCATCTTCTTCAAGGACGACGGCAACTACAAGACCCGCGCGAGGTGAAGTTCGAGGGCGACACCCTGGTGAACCGCAT](#)  
[CGAGCTGAAGGGCATCGACTTCAAGGAGGACGGCAACATCCTGGGGCACAAGCTGGAGTACAACATACATCAGCCACAAC](#)  
[GTCTATATCACCGCCGACAAGCAGAAGAACGGCATCAAGGCCc](#)[ACTTCAAGATCCGCCACAACATCGAGGACGGCAGCGT](#)  
[GCAGCTCGCCGACCACTACCAGCAGAACACCCCATCGGCGACGGCCCCGTGCTGCTGCCGACAACCACTACCTGAGCA](#)  
[CCCAGTCCGCCCTGAGCAAAGACCCCAACGAGAAGCGCGATCACATGGTCTGCTGGAGTTCGTGACCGCCGCGGGGATC](#)  
[ACTCTGGCATGGACGAGCTGTACAAG](#)[TAA](#)[g](#)[c](#)[g](#)[g](#)[c](#)[c](#)[g](#)[c](#)

**pcDNA3-3HA-CXCR4-FIAsh228-CFP**

[aagcttGGTACCACC](#)[ATG](#)[TACCCATACGATGTTCCAGATTACGCTTACCCATACGATGTTCCAGATTACGCTTACCCATACGAT](#)  
[GTTCCAGATTACGCTGAT](#)GAGGGGATCAGTATATACTTACAGATAACTACACCCGAGGAAATGGGCTCAGGGGACTATGA  
 CTCCATGAAGGAACCCTGTTCCGTGAAGAAAATGCTAATTTCAATAAAAATCTTCTGCCACCATCTACTCCATCATCTTCT  
 TAACTGGCATTGTGGGCAATGGATTGGTCATCCTGGTCATGGGTTACCAGAAGAACTGAGAAGCATGACGGACAAGTAC  
 AGGCTGCACCTGTCAAGTGGCCGACCTCCTTTGTATCACGCTCCCTTCTGGGCGATTGATGCCGTGGCAAACCTGGTACT  
 TTGGGAACTTCTATGCAAGGCAGTCCATGTATCTACACAGTCAACCTCTACAGCAGTGTCTCATCTGGCCTTCATCAG  
 TCTGGACCGCTACCTGGCCATCGTCCACGCCACCAACAGTCAGAGGCCAAGGAAGCTGTTGGCTGAAAAGGTGGTCTATG  
 TTGGCGTCTGGATCCCTGCCCTCTGCTGACTATTCCGACTTCATCTTTGCCAACGTCAGTGAGGCAGATGACAGATATAT  
 CTGTGACCGCTTCTACCCCAATGACTTGTGGGTGGTTGTGTTCCAGTTTCAGCACATCATGGTTGGCCTTATCCTGCCTGGT  
 ATTGTCATCCTGTCTGCTATTGCATTATCATCTCCAAGCTGTACACAT[GTTGCCCCGGGCTGCTGT](#)TCCAAGGGCCACCAGA  
 AGCGCAAGGCCCTCAAGACCACAGTCATCCTCATCTGGCTTCTTCGCTGTTGGCTGCCTTACTACATTGGGATCAGCAT  
 CGACTCCTTCATCTCCTGAAAATCATCAAGCAAGGGTGTGAGTTTGAGAACACTGTGCACAAGTGGATTTCCATCACCGA  
 GGCCCTAGCTTTCTTCCACTGTTGTCTGAACCCCATCTCTATGCTTTCCTTGGAGCCAAATTTAAAACCTCTGCCAGCACG  
 CACTACCTCTGTGAGCAGAGGGTCCAGCCTCAAGATCCTCTCAAAGGAAAGCGAGGTGGACATTCTGTTTCCACTG  
 AGTCTGAGTCTTCAAGTTTTCACTCCAGC[tctaga](#)[GTGAGCAAGGGCGAGGAGCTGTTACCCGGGGTGGTCCCCATCCTGGT](#)  
[CGAGCTGGACGGCGACGTAACCGGCCACAg](#)[GTTACGCGTGTCCGGCGAGGGCGAGGGCGATGCCACCTACGGCAAGCTG](#)  
[ACCCTGAAGTTCATCTGCACCACCGGCAAGCTGCCGTGCCCTGGCCACCTCGTGACCACCTGACCTGGGGCGTGCAG](#)  
[TGTTTCAGCCGCTACCCCGACCACATGAAGCAGCACGACTTCTTCAAGTCCGCCATGCCCGAAGGCTACGTCCAGGAGCGT](#)  
[ACCATCTTCTTCAAGGACGACGGCAACTACAAGACCCGCGCGAGGTGAAGTTCGAGGGCGACACCCTGGTGAACCGCAT](#)  
[CGAGCTGAAGGGCATCGACTTCAAGGAGGACGGCAACATCCTGGGGCACAAGCTGGAGTACAACATACATCAGCCACAAC](#)  
[GTCTATATCACCGCCGACAAGCAGAAGAACGGCATCAAGGCCc](#)[ACTTCAAGATCCGCCACAACATCGAGGACGGCAGCGT](#)  
[GCAGCTCGCCGACCACTACCAGCAGAACACCCCATCGGCGACGGCCCCGTGCTGCTGCCGACAACCACTACCTGAGCA](#)  
[CCCAGTCCGCCCTGAGCAAAGACCCCAACGAGAAGCGCGATCACATGGTCTGCTGGAGTTCGTGACCGCCGCGGGGATC](#)  
[ACTCTGGCATGGACGAGCTGTACAAG](#)[TAA](#)[g](#)[c](#)[g](#)[g](#)[c](#)[c](#)[g](#)[c](#)

**pcDNA3-3HA-CXCR4-FIAsh229-CFP**

[aagcttGGTACCACC](#)[ATG](#)[TACCCATACGATGTTCCAGATTACGCTTACCCATACGATGTTCCAGATTACGCTTACCCATACGAT](#)  
[GTTCCAGATTACGCTGAT](#)GAGGGGATCAGTATATACTTACAGATAACTACACCCGAGGAAATGGGCTCAGGGGACTATGA  
 CTCCATGAAGGAACCCTGTTCCGTGAAGAAAATGCTAATTTCAATAAAAATCTTCTGCCACCATCTACTCCATCATCTTCT  
 TAACTGGCATTGTGGGCAATGGATTGGTCATCCTGGTCATGGGTTACCAGAAGAACTGAGAAGCATGACGGACAAGTAC  
 AGGCTGCACCTGTCAAGTGGCCGACCTCCTTTGTATCACGCTCCCTTCTGGGCGATTGATGCCGTGGCAAACCTGGTACT  
 TTGGGAACTTCTATGCAAGGCAGTCCATGTATCTACACAGTCAACCTCTACAGCAGTGTCTCATCTGGCCTTCATCAG  
 TCTGGACCGCTACCTGGCCATCGTCCACGCCACCAACAGTCAGAGGCCAAGGAAGCTGTTGGCTGAAAAGGTGGTCTATG  
 TTGGCGTCTGGATCCCTGCCCTCTGCTGACTATTCCGACTTCATCTTTGCCAACGTCAGTGAGGCAGATGACAGATATAT  
 CTGTGACCGCTTCTACCCAATGACTTGTGGGTGGTTGTGTTCCAGTTTCAGCACATCATGGTTGGCCTTATCCTGCCTGGT  
 ATTGTCATCCTGTCTGCTATTGCATTATCATCTCCAAGCTGTCACACTCCTGTTGCCCCGGGCTGCTGTAAAGGGCCACCAGA  
 AGCGCAAGGCCCTCAAGACCACAGTCATCCTCATCTGGCTTCTTTCGCTGTTGGCTGCCTTACTACATTGGGATCAGCAT  
 CGACTCCTTCATCTCCTGAAAATCATCAAGCAAGGGTGTGAGTTTGAGAACACTGTGCACAAGTGGATTTCCATCACCGA  
 GGCCCTAGCTTTCTTCCACTGTTGTCTGAACCCCATCTCTATGCTTTCCTTGGAGCCAAATTTAAAACCTCTGCCAGCACG  
 CACTACCTCTGTGAGCAGAGGGTCCAGCCTCAAGATCCTCTCAAAGGAAAGCGAGGTGGACATTCATCTGTTTCCACTG  
 AGTCTGAGTCTTCAAGTTTTCACTCCAGCtctagaGTGAGCAAGGGCGAGGAGCTGTTACCCGGGGTGGTGCCATCCTGGT  
 CGAGCTGGACGGCGACGTAACCGCCACAgGTTACGCGTGTCCGGCGAGGGCGAGGGCGATGCCACCTACGGCAAGCTG  
 ACCCTGAAGTTCATCTGCACCACCGGCAAGCTGCCGTGCCCTGGCCACCCTCGTGACCACCCTGACCTGGGGCGTGCAG  
 TGCTTACGCCGCTACCCGACCACATGAAGCAGCACGACTTCTTCAAGTCCGCCATGCCGAAGGCTACGTCCAGGAGCGT  
 ACCATCTTCTCAAGGACGACGGCAACTACAAGACCCGCGCGAGGTGAAGTTCGAGGGCGACACCCTGGTGAACCGCAT  
 CGAGCTGAAGGGCATCGACTTCAAGGAGGACGGCAACATCCTGGGGCACAAGCTGGAGTACAACATACATCAGCCACAAC  
 GTCTATATCACCGCCGACAAGCAGAAGAACGGCATCAAGGCCcACTTCAAGATCCGCCACAACATCGAGGACGGCAGCGT  
 GCAGCTCGCCGACCACTACCAGCAGAACACCCCATCGGCGACGGCCCCGTGCTGCTGCCGACAACCACTACCTGAGCA  
 CCCAGTCCGCCCTGAGCAAAGACCCCAACGAGAAGCGCGATCACATGGTCTGCTGGAGTTCGTGACCGCCGCGGGGATC  
 ACTCTCGGCATGGACGAGCTGTACAAGTAAgcggccgc

**pcDNA3-3HA-W94R,D97G-CXCR4-CFP**

[aagcttGGTACCACC](#)[ATG](#)[TACCCATACGATGTTCCAGATTACGCTTACCCATACGATGTTCCAGATTACGCTTACCCATACGAT](#)  
[GTTCCAGATTACGCTGAT](#)GAGGGGATCAGTATATACTTACAGATAACTACACCCGAGGAAATGGGCTCAGGGGACTATGA  
 CTCCATGAAGGAACCCTGTTCCGTGAAGAAAATGCTAATTTCAATAAAAATCTTCTGCCACCATCTACTCCATCATCTTCT  
 TAACTGGCATTGTGGGCAATGGATTGGTCATCCTGGTCATGGGTTACCAGAAGAACTGAGAAGCATGACGGACAAGTAC  
 AGGCTGCACCTGTCAAGTGGCCGACCTCCTTTGTATCACGCTCCCTTCTGGGCGATTGATGCCGTGGCAAACCTGGTACT  
 TTGGGAACTTCTATGCAAGGCAGTCCATGTATCTACACAGTCAACCTCTACAGCAGTGTCTCATCTGGCCTTCATCAG  
 TCTGGACCGCTACCTGGCCATCGTCCACGCCACCAACAGTCAGAGGCCAAGGAAGCTGTTGGCTGAAAAGGTGGTCTATG  
 TTGGCGTCTGGATCCCTGCCCTCTGCTGACTATTCCGACTTCATCTTTGCCAACGTCAGTGAGGCAGATGACAGATATAT  
 CTGTGACCGCTTCTACCCAATGACTTGTGGGTGGTTGTGTTCCAGTTTCAGCACATCATGGTTGGCCTTATCCTGCCTGGT  
 ATTGTCATCCTGTCTGCTATTGCATTATCATCTCCAAGCTGTCACACTCCAAGGGCCACCAGAAGCGCAAGGCCCTCAAGA  
 CCACAGTCATCCTCATCTGGCTTCTTTCGCTGTTGGCTGCCTTACTACATTGGGATCAGCATCGACTCCTTCATCCTCCTG  
 GAAATCATCAAGCAAGGGTGTGAGTTTGAGAACACTGTGCACAAGTGGATTTCCATCACCAGGGCCCTAGCTTTCTTCCAC  
 TGTGTCTGAACCCATCCTCTATGCTTTCCTTGGAGCCAAATTTAAAACCTCTGCCAGCACGCACTCACCTCTGTGAGCA  
 GAGGGTCCAGCCTCAAGATCCTCTCAAAGGAAAGCGAGGTGGACATTCATCTGTTTCCACTGAGTCTGAGTCTTCAAGTT  
 TCACTCCAGCtctagaGTGAGCAAGGGCGAGGAGCTGTTACCCGGGGTGGTGCCATCCTGGTGCAGCTGGACGGCGACG  
 TAAACGGCCACAgGTTACGCGTGTCCGGCGAGGGCGAGGGCGATGCCACCTACGGCAAGCTGACCCTGAAGTTCATCTGC  
 ACCACGGCAAGCTGCCCTGCCCTGGCCACCCTCGTGACCACCCTGACCTGGGGCGTGCAGTGTTCAGCCGCTACCCC  
 GACCACATGAAGCAGCACGACTTCTTCAAGTCCGCCATGCCGAAGGCTACGTCCAGGAGCGtACCATCTTCTTCAAGGAC  
 GACGGCAACTACAAGACCCGCGCGGAGGTGAAGTTCGAGGGCGACACCCTGGTGAACCGCATCGAGCTGAAGGGCATCG  
 ACTTCAAGGAGGACGGCAACATCCTGGGGCACAAGCTGGAGTACAACATACATCAGCCACAACGTCTATATCACCGCCGAC  
 AAGCAGAAGAAGGCATCAAGGCCcACTTCAAGATCCGCCACAACATCGAGGACGGCAGCGTGCAGCTCGCCGACCACTA  
 CCAGCAGAACACCCCATCGGCGACGGCCCCGTGCTGCTGCCGACAACCACTACCTGAGCACCCAGTCCGCCCTGAGCA  
 AAGACCCCAACGAGAAGCGCGATCACATGGTCTGCTGGAGTTCGTGACCGCCGCGGGGATCACTCTCGGCATGGACGA  
 GCTGTACAAGTAAgcggccgc

**pcDNA3-3HA-W94R,D97G-CXCR4-FIAsH228-CFP**

[aagctt](#)**GGTACCACC****ATG****FACCCATACGATGTTCCAGATTACGCTTACCCATACGATGTTCCAGATTACGCTTACCCATACGAT**  
**GTTCCAGATTACGCTGAT**GAGGGGATCAGTATATACTTACAGATAACTACACCCGAGGAAATGGGCTCAGGGGACTATGA  
 CTCCATGAAGGAACCCTGTTCCGTGAAGAAAATGCTAATTTCAATAAAAATCTTCTGCCACCATCTACTCCATCATCTTCT  
 TAACTGGCATTGTGGGCAATGGATTGGTCATCCTGGTCATGGGTTACCAGAAGAACTGAGAAGCATGACGGACAAGTAC  
 AGGCTGCACCTGTCAGTGGCCGACCTCCTTTGTCATCACGCTCCCTT**TGG**G**CAGTTG**A**TGCCGTGGCAA**ACTGGTACT  
 TTGGAACTTCTATGCAAGGCAGTCCATGTCTACACAGTCAACCTCTACAGCAGTGTCTCATCTGGCCTTCATCAG  
 TCTGGACCGCTACCTGGCCATCGTCCACGCCACCAACAGTCAGAGGCCAAGGAAGCTGTTGGCTGAAAAGGTGGTCTATG  
 TTGGCGTCTGGATCCCTGCCCTCTGCTGACTATTCCCGACTTCATCTTTGCCAACGTCAGTGAGGCAGATGACAGATATAT  
 CTGTGACCGCTTCTACCCCAATGACTTGTGGGTGGTTGTGTTCCAGTTTCAGCACATCATGGTTGGCCTTATCCTGCCTGGT  
 ATTGTCATCCTGTCTGCTATTGCATTATCATCTCCAAGCTGTACAC**TGTTGCCGGGCTGCTGT**TCCAAGGGCCACCAGA  
 AGCGCAAGGCCCTCAAGACCACAGTCATCTCATCTGGCTTCTTCGCTGTTGGCTGCCTTACTACATTGGGATCAGCAT  
 CGACTCCTTCATCTCCTGAAAATCATCAAGCAAGGGTGTGAGTTTGAGAACACTGTGCACAAGTGGATTTCCATCACCGA  
 GGCCCTAGCTTTCTTCCACTGTTGTCTGAACCCCATCTCTATGCTTTCCTTGGAGCCAAATTTAAACCTCTGCCAGCACG  
 CACTACCTCTGTGAGCAGAGGGTCCAGCCTCAAGATCCTCTCAAAGGAAAGCGAGGTGGACATTATCTGTTTCCACTG  
 AGTCTGAGTCTTCAAGTTTTCACTCCAG**Cttaga****GTGAGCAAGGGCGAGGAGCTGTTACCGGGTGGTCCCCATCTGGT**  
**CGAGCTGGACGGCGACGTAACCGCCACAgGTT**CAGCGTGTCCGGCGAGGGCGAGGGCGATGCCACCTACGGCAAGCTG  
**ACCCTGAAGTTCATCTGCACCACCGCAAGCTGCCGTGCCCTGGCCACCTCGTGACCACCTGACCTGGGGCGTGCAG**  
**TGTTCAAGCCGCTACCCGACCACATGAAGCAGCACGACTTCTTCAAGTCCGCCATGCCGAAGGCTACGTCCAGGAGCGT**  
**ACCATCTTCTCAAGGACGACGGCAACTACAAGACCCGCGCGAGGTGAAGTTCGAGGGCGACACCCTGGTGAACCGCAT**  
**CGAGCTGAAGGGCATCGACTTCAAGGAGGACGGCAACATCCTGGGGCACAAGCTGGAGTACAACATACATCAGCCACAAC**  
**GTCTATATACCCGCCGACAAGCAGAAGAACGGCATCAAGGCCcACTTCAAGATCCGCCACAACATCGAGGACGGCAGCGT**  
**GCAGCTGCCGACCCTACCAGCAGAACCCCCATCGGCGACGGCCCCGTGCTGCTGCCGACAACCCTACCTGAGCA**  
**CCCAGTCCGCCCTGAGCAAAGACCCCAACGAGAAGCGCGATCACATGGTCTGCTGGAGTTCGTGACCGCCGCGGGATC**  
**ACTCTCGGCATGGACGAGCTGTACAAGTAA****gcggccgc**

**pcDNA3-HA-ACKR3-CFP**

[aagctt](#)**ATGGGCTACCCGTACGAGTCCAGACTACCG**GATCTGCATCTCTTCTGACTACTCAGAGCCAGGGAACCTCTCGG  
 ACATCAGCTGGCCATGCAACAGCAGCGACTGCATCGTGGTGGACACGGTATGATGTGCCAACATGCCCAACAAAAGCGTC  
 CTGCTCTACACGCTCTCCTTCATTTACATTTTCATTTTCGTCATCGGCATGATTGCCAACTCCGTGGTGGTCTGGGTGAATAT  
 CCAGGCCAAGACCACAGGCTATGACACGCACTGCTACATCTTGAACCTGGCCATTGCCGACCTGTGGGTGTCCTCACCAT  
 CCCAGTCTGGGTGGTCACTCGTGCAGCACAACAGTGGCCCATGGGCGAGCTCACGTGCAAAGTACACACCTCATCTT  
 CTCCATCAACCTCTTGGCAGCATTTTCTTCTCACGTGCATGAGCGTGGACCGTACCTCTCCATCACCTACTTACCAACA  
 CCCCAGCAGCAGGAAGAAGATGGTACGCCGTGTCGTCTGCATCCTGGTGTGGCTGCTGGCCTTCTGCGTGTCTGCGCTG  
 ACACCTACTACCTGAAGACCGTACAGTCTGCGTCCAACAATGAGACCTACTGCCGGTCTTCTACCCGAGCACAGCATCA  
 AGGAGTGGCTGATCGGCATGGAGCTGGTCTCCGTTGCTTGGGCTTTGCCGTTCCCTTCTCCATTATCGCTGTCTTCTACTT  
 CCTGCTGGCCAGAGCCATCTCGGCGTCCAGTGACCAGGAGAAGCACAGCAGCCGGAAGATCATCTTCTCCTACGTGGTGG  
 TCTTCTTGTCTGCTGGCTGCCCTACCAGTGGCGGTGCTGCTGGACATCTTCTCCATCCTGCACTACATCCCTTTACCTGC  
 CGGCTGGAGCACGCCCTCTTACGGCCCTGCATGTACACAGTGCCTGTCGCTGGTGCAGTGTGCTCAACCCTGTCTCT  
 ACAGTTCATCAATCGCAACTACAGGTACGAGCTGATGAAGGCCCTTCTTCAAGTACTCGGCCAAAACAGGGCTCACCA  
 AGTCTATCGATGCCTCCAGAGTCTCAGAGACGGAGTACTCTGCCTTGGAGCAGAGCACAAA**tctaga****GTGAGCAAGGGCG**  
**AGGAGCTGTTACCGGGTGGTGCCATCCTGGTTCGAGCTGGACGGCGACGTAACCGCCACAGGTTACGCGTGTCCGG**  
**CGAGGGCGAGGGCGATGCCACCTACGGCAAGCTGACCTGAAGTTCATCTGCACCACCGCAAGCTGCCGTGCCCTGGC**  
**CCACCCTCGTGACCACCTGACCTGGGGCGTGCAGTCTTACGCCCTACCCGACCACATGAAGCAGCACGACTTCTTCA**  
**AGTCCGCCATGCCGAAGGCTACGTCCAGGAGCGtACCATCTTCTTCAAGGACGACGGCAACTACAAGACCCGCGCCGAG**  
**GTGAAGTTCGAGGGCGACACCCTGGTGAACCGCATCGAGCTGAAGGGCATCGACTTCAAGGAGGACGGCAACATCCTGG**  
**GGCACAAGCTGGAGTACAACATACATCAGCCACAACGTCTATATACCCGCCGACAAGCAGAAGAACGGCATCAAGGCCcAC**  
**TTCAAGATCCGCCACAACATCGAGGACGGCAGCGTGCAGCTCGCCGACCCTACCAGCAGAACCCCCATCGGCGACGG**  
**CCCCGTGCTGCTGCCGACAACCCTACCTGAGCACCCAGTCCGCCCTGAGCAAAGACCCCAACGAGAAGCGCGATCACA**  
**TGGTCTGCTGGAGTTCGTGACCGCCGCGGGATCACTCTCGGCATGGACGAGCTGTACAAGTAA****gcggccgc**

**pcDNA3-HA-ACKR3-FIAsH**

[aagctt](#)**ATGGGCTACCCGTACGACGTCCAGACTACGCC**GATCTGCATCTCTTCGACTACTCAGAGCCAGGGAAGTTCTCGG  
 ACATCAGCTGGCCATGCAACAGCAGCGACTGCATCGTGGTGGACACGGTGATGTGTCCCAACATGCCCAACAAAAGCGTC  
 CTGCTCTACACGCTCTCCTTCATTTACATTTTCATTTTCGTCATCGGCATGATTGCCAACTCCGTGGTGGTCTGGGTGAATAT  
 CCAGGCCAAGACCACAGGCTATGACACGCACTGCTACATCTTGAACCTGGCCATTGCCGACCTGTGGGTTGCCTACCAT  
 CCCAGTCTGGGTGGTCACTCTCGTGCAGACAACCAGTGGCCCATGGGCGAGCTCACGTGCAAAGTACACACCTCATCTT  
 CTCCATCAACCTCTTCGGCAGCATTTCCTCCTCACGTGCATGAGCGTGGACCGTACCTCTCCATCACCTACTTCACCAACA  
 CCCCAGCAGCAGGAAGAAGATGGTACGCCGTGTCGTCTGCATCCTGGTGTGGCTGCTGGCCTTCTGCGTGTCTCTGCCTG  
 ACACCTACTACCTGAAGACCGTCACGTCTGCGTCCAACAATGAGACCTACTGCCGGTCTTCTACCCCGAGCACAGCATCA  
 AGGAGTGGCTGATCGGCATGGAGCTGGTCTCCGTTGCTTGGGCTTTGCCGTTCCCTTCTCCATTATCGCTGTCTTCTACTT  
 CCTGCTGGCCAGAGCCATCTCGGCGTCC**TGTTGCCGGGCTGCTGT**AGTGACCAGGAGAAGCACAGCAGCCGGAAGATCA  
 TCTTCTCCTACGTGGTGGTCTTCCTTGTCTGCTGGCTGCCCTACCACGTGGCGGTGCTGCTGGACATCTTCTCCATCCTGCAC  
 TACATCCCTTTCACCTGCCGGCTGGAGCACGCCCTTTCACGGCCCTGCATGTCACACAGTGCCTGTCGCTGGTGCCTGCT  
 GCGTCAACCCTGTCCTCTACAGCTTCAATCGCAACTACAGGTACGAGCTGATGAAGGCCTTCATCTTCAAGTACTCGGC  
 CAAAACAGGGCTACCAAGCTCATCGATGCCTCCAGAGTCTCAGAGACGGAGTACTCTGCCTTGGAGCAGAGCACCAAA**T**  
**AAgCGGCCgc**

**pcDNA3-HA-ACKR3-FIAsH-CFP**

[aagctt](#)**ATGGGCTACCCGTACGACGTCCAGACTACGCC**GATCTGCATCTCTTCGACTACTCAGAGCCAGGGAAGTTCTCGG  
 ACATCAGCTGGCCATGCAACAGCAGCGACTGCATCGTGGTGGACACGGTGATGTGTCCCAACATGCCCAACAAAAGCGTC  
 CTGCTCTACACGCTCTCCTTCATTTACATTTTCATTTTCGTCATCGGCATGATTGCCAACTCCGTGGTGGTCTGGGTGAATAT  
 CCAGGCCAAGACCACAGGCTATGACACGCACTGCTACATCTTGAACCTGGCCATTGCCGACCTGTGGGTTGCCTACCAT  
 CCCAGTCTGGGTGGTCACTCTCGTGCAGACAACCAGTGGCCCATGGGCGAGCTCACGTGCAAAGTACACACCTCATCTT  
 CTCCATCAACCTCTTCGGCAGCATTTCCTCCTCACGTGCATGAGCGTGGACCGTACCTCTCCATCACCTACTTCACCAACA  
 CCCCAGCAGCAGGAAGAAGATGGTACGCCGTGTCGTCTGCATCCTGGTGTGGCTGCTGGCCTTCTGCGTGTCTCTGCCTG  
 ACACCTACTACCTGAAGACCGTCACGTCTGCGTCCAACAATGAGACCTACTGCCGGTCTTCTACCCCGAGCACAGCATCA  
 AGGAGTGGCTGATCGGCATGGAGCTGGTCTCCGTTGCTTGGGCTTTGCCGTTCCCTTCTCCATTATCGCTGTCTTCTACTT  
 CCTGCTGGCCAGAGCCATCTCGGCGTCC**TGTTGCCGGGCTGCTGT**AGTGACCAGGAGAAGCACAGCAGCCGGAAGATCA  
 TCTTCTCCTACGTGGTGGTCTTCCTTGTCTGCTGGCTGCCCTACCACGTGGCGGTGCTGCTGGACATCTTCTCCATCCTGCAC  
 TACATCCCTTTCACCTGCCGGCTGGAGCACGCCCTTTCACGGCCCTGCATGTCACACAGTGCCTGTCGCTGGTGCCTGCT  
 GCGTCAACCCTGTCCTCTACAGCTTCAATCGCAACTACAGGTACGAGCTGATGAAGGCCTTCATCTTCAAGTACTCGGC  
 CAAAACAGGGCTACCAAGCTCATCGATGCCTCCAGAGTCTCAGAGACGGAGTACTCTGCCTTGGAGCAGAGCACCAAA**tc**  
**taga****GTGAGCAAGGGCGAGGAGCTGTTACCGGGTGGTGCCATCCTGGTCGAGCTGGACGGCGACGTAACGGCCAC**  
**AGGTTACAGCGTGTCGGCGAGGGCGAGGGCGATGCCACCTACGGCAAGCTGACCCTGAAGTTCATCTGCACCACCGGCA**  
**AGCTGCCGTGCCCTGGCCACCCTCGTACCACCCTGACCTGGGGCGTGCAGTGCTTCAGCCGCTACCCCGACCACATGA**  
**AGCAGCACGACTTCTTCAAGTCCGCCATGCCGAAGGCTACGTCCAGGAGCGtACCATCTTCTTCAAGGACGACGGCAACT**  
**ACAAGACCCGCGCCGAGGTGAAGTTCGAGGGCGACACCCTGGTGAACCGCATCGAGCTGAAGGGCATCGACTTCAAGGA**  
**GGACGGCAACATCCTGGGGCACAAGCTGGAGTACAACATACATCAGCCACAACGTCTATATCACCCGCCGACAAGCAGAAGA**  
**ACGGCATCAAGGCCcACTTCAAGATCCGCCACAACATCGAGGACGGCAGCGTGCAGCTCGCCGACCACTACCAGCAGAAC**  
**ACCCCATCGGGCAGCGCCCGTGTCTGCTGCCGACAACCACTACCTGAGCACCCAGTCCGCCCTGAGCAAAGACCCCAAC**  
**GAGAAGCGGATCACATGGTCTGCTGGAGTTCGTGACCGCCCGGGATCACTCTCGGCATGGACGAGCTGACAAG**TA****  
**AgCGGCCgc**



**pcDNA3-HA-ACKR3(1-321)-FIAsH-CFP**

[aagctt](#)**ATGGGCTACCCGTACGACGTCCAGACTACGCC**GATCTGCATCTCTTCGACTACTCAGAGCCAGGGAAGCTCTCGG  
 ACATCAGCTGGCCATGCAACAGCAGCGACTGCATCGTGGTGGACACGGTATGTGTCCCAACATGCCCAACAAAAGCGTC  
 CTGCTCTACACGCTCTCCTTCATTTACATTTTCATTTTCGTCATCGGCATGATTGCCAACTCCGTGGTGGTCTGGGTGAATAT  
 CCAGGCCAAGACCACAGGCTATGACACGCACTGCTACATCTTGAACCTGGCCATTGCCGACCTGTGGGTTGCCTCACCAT  
 CCCAGTCTGGGTGGTCACTCTCGTGCAGCACAACCAGTGGCCATGGGCGAGCTCACGTGCAAAGTACACACCTCATCTT  
 CTCCATCAACCTCTTCGGCAGCATTTTCTTCTCACGTGCATGAGCGTGGACCGCTACCTCTCCATCACCTACTTCACCAACA  
 CCCCCAGCAGCAGGAAGAAGATGGTACGCCGTGTCGTCTGCATCCTGGTGTGGCTGCTGGCCTTCTGCGTGTCTTGCTG  
 ACACCTACTACCTGAAGACCGTACGTCTGCGTCCAACAATGAGACCTACTGCCGGTCTTCTACCCCGAGCACAGCATCA  
 AGGAGTGGCTGATCGGCATGGAGCTGGTCTCCGTTGCTTGGGCTTTGCCGTTCCCTTCTCCATTATCGCTGTCTTCTACTT  
 CCTGCTGGCCAGAGCCATCTCGGCGTCC**TGTTGCCGGGCTGCTGT**AGTGACCAGGAGAAGCACAGCAGCCGGAAGATCA  
 TCTTCTCCTACGTGGTGGTCTTCTTGTCTGCTGGCTGCCCTACCACGTGGCGGTGCTGCTGGACATCTTCTCCATCCTGCAC  
 TACATCCCTTTCACCTGCCGGCTGGAGCACGCCCTTTCACGGCCCTGCATGTCACACAGTGCCTGTCGCTGGTGCAGTGT  
 GCGTCAACCCTGTCCTCTACAGCTTCAATCGCAACT**tctaga****GTGAGCAAGGGCGAGGAGCTGTTACCGGGGTGGTGCC**  
**CATCTGGTTCGAGCTGGACGGCGACGTAACGGCCACAGGTT**CAGCGTGTCCGGCGAGGGCGAGGGCGATGCCACCTAC  
**GGCAAGCTGACCTGAAGTTCATCTGCACCACCGCAAGCTGCCCGTGCCTGGCCACCCTCGTGACCACCTGACCTGG**  
**GGCGTGCAGTGCTTCAGCCGCTACCCCGACCACATGAAGCAGCAGACTTCTTCAAGTCCGCCATGCCGAAGGCTACGTC**  
**CAGGAGCGtACCATCTTCTTCAAGGACGACGGCAACTACAAGACCCGCGCCGAGGTGAAGTTCGAGGGCGACACCCTGGT**  
**GAACCGCATCGAGCTGAAGGGCATCGACTTCAAGGAGGACGGCAACATCCTGGGGCACAAGCTGGAGTACAACCTACATC**  
**AGCCACAACGTCTATATCACCGCCGACAAGCAGAAGAACGGCATCAAGGCCcACTTCAAGATCCGCCACAACATCGAGGA**  
**CGGCAGCGTGCAGCTCGCCGACCACTACCAGCAGAACACCCCCATCGGCGACGGCCCCGTGCTGCTGCCCGACAACCACT**  
**ACCTGAGCACCCAGTCCGCCCTGAGCAAAGACCCCAACGAGAAGCGCGATCACATGGTCTGCTGGAGTTCGTGACCGCC**  
**GCCGGGATCACTCTCGGCATGGACGAGCTGTACAAG****TAAg**cgggccgc

**pcDNA3-HA-ACKR3(1-346)-FIAsH-CFP**

[aagctt](#)**ATGGGCTACCCGTACGACGTCCAGACTACGCC**GATCTGCATCTCTTCGACTACTCAGAGCCAGGGAAGCTCTCGG  
 ACATCAGCTGGCCATGCAACAGCAGCGACTGCATCGTGGTGGACACGGTATGTGTCCCAACATGCCCAACAAAAGCGTC  
 CTGCTCTACACGCTCTCCTTCATTTACATTTTCATTTTCGTCATCGGCATGATTGCCAACTCCGTGGTGGTCTGGGTGAATAT  
 CCAGGCCAAGACCACAGGCTATGACACGCACTGCTACATCTTGAACCTGGCCATTGCCGACCTGTGGGTTGCCTCACCAT  
 CCCAGTCTGGGTGGTCACTCTCGTGCAGCACAACCAGTGGCCATGGGCGAGCTCACGTGCAAAGTACACACCTCATCTT  
 CTCCATCAACCTCTTCGGCAGCATTTTCTTCTCACGTGCATGAGCGTGGACCGCTACCTCTCCATCACCTACTTCACCAACA  
 CCCCCAGCAGCAGGAAGAAGATGGTACGCCGTGTCGTCTGCATCCTGGTGTGGCTGCTGGCCTTCTGCGTGTCTTGCTG  
 ACACCTACTACCTGAAGACCGTACGTCTGCGTCCAACAATGAGACCTACTGCCGGTCTTCTACCCCGAGCACAGCATCA  
 AGGAGTGGCTGATCGGCATGGAGCTGGTCTCCGTTGCTTGGGCTTTGCCGTTCCCTTCTCCATTATCGCTGTCTTCTACTT  
 CCTGCTGGCCAGAGCCATCTCGGCGTCC**TGTTGCCGGGCTGCTGT**AGTGACCAGGAGAAGCACAGCAGCCGGAAGATCA  
 TCTTCTCCTACGTGGTGGTCTTCTTGTCTGCTGGCTGCCCTACCACGTGGCGGTGCTGCTGGACATCTTCTCCATCCTGCAC  
 TACATCCCTTTCACCTGCCGGCTGGAGCACGCCCTTTCACGGCCCTGCATGTCACACAGTGCCTGTCGCTGGTGCAGTGT  
 GCGTCAACCCTGTCCTCTACAGCTTCAATCGCAACTACAGGTACGAGCTGATGAAGGCCTTCATCTTCAAGTACTCGGC  
 CAAAACAGGGCTCACCAAGCTCATCGATGC**tctaga****GTGAGCAAGGGCGAGGAGCTGTTACCGGGGTGGTGCCCATCCT**  
**GGTTCGAGCTGGACGGCGACGTAACGGCCACAgTTCAGCGTGTCCGGCGAGGGCGAGGGCGATGCCACCTACGGCAA**  
**GCTGACCCTGAAGTTCATCTGCACCACCGCAAGCTGCCCGTGCCTGGCCACCCTCGTGACCACCTGACCTGGGGCGT**  
**GCAGTGCTTCAGCCGCTACCCCGACCACATGAAGCAGCAGACTTCTTCAAGTCCGCCATGCCGAAGGCTACGTCCAGGA**  
**GCGtACCATCTTCTTCAAGGACGACGGCAACTACAAGACCCGCGCCGAGGTGAAGTTCGAGGGCGACACCCTGGTGAACC**  
**GCATCGAGCTGAAGGGCATCGACTTCAAGGAGGACGGCAACATCCTGGGGCACAAGCTGGAGTACAACCTACATCAGCCA**  
**CAACGTCTATATCACCGCCGACAAGCAGAAGAACGGCATCAAGGCCcACTTCAAGATCCGCCACAACATCGAGGACGGCA**  
**GCGTGCAGCTCGCCGACCACTACCAGCAGAACACCCCCATCGGCGACGGCCCCGTGCTGCTGCCCGACAACCACTACCTG**  
**AGCACCCAGTCCGCCCTGAGCAAAGACCCCAACGAGAAGCGCGATCACATGGTCTGCTGGAGTTCGTGACCGCCGCCG**  
**GATCACTCTCGGCATGGACGAGCTGTACAAG****TAAg**cgggccgc

## 7. REFERENCES

- Adjobo-Hermans, M.J.W., Goedhart, J., van Weeren, L., Nijmeijer, S., Manders, E.M.M., Offermanns, S., & Gadella Jr, T.W.J. (2011). Real-time visualization of heterotrimeric G protein Gq activation in living cells. *BMC Biology*, 9, 32.
- Agarwal, P., Li, H., Paterson, A.J., He, J., Nagasawa, T., & Bhatia, R. (2016). Role of CXCL12-Expressing Bone Marrow Populations in Leukemic Stem Cell Regulation. *Blood*, 128, 26.
- Ainla, A., Jansson, E.T., Stepanyants, N., Orwar, O., & Jesorka, A. (2010). A microfluidic pipette for single-cell pharmacology. *Anal. Chem*, 82, 4529–4536.
- Ainla, A., Jeffries, G.D., Brune, R., Orwar, O., & Jesorka, A. (2012). A multifunctional pipette. *Lab Chip*, 12, 1255–1261.
- Alampour-Rajabi, S., El Bounkari, O., Rot, A., Müller-Newen, G., Bachelerie, F., Gawaz, M., ... Bernhagen, J. (2015). MIF interacts with CXCR7 to promote receptor internalization, ERK1/2 and ZAP-70 signaling, and lymphocyte chemotaxis. *FASEB J*, 29(11), 4497–511.
- Albee, L.J., Eby, J.M., Tripathi, A., LaPorte, H.M., Gao, X., Volkman, B.F., ... Majetschak, M. (2017). Alpha1-Adrenergic Receptors Function Within Hetero-Oligomeric Complexes With Atypical Chemokine Receptor 3 and Chemokine (C-X-C motif) Receptor 4 in Vascular Smooth Muscle Cells. *J Am Heart Assoc*, 6(8), 1–17.
- Aliye, N., Fabbretti, A., Lupidi, G., Tsekoa, T., & Spurio, R. (2015). Engineering color variants of green fluorescent protein (GFP) for thermostability, pH-sensitivity, and improved folding kinetics. *Appl Microbiol Biotechnol*, 99(3), 1205–16.
- Alvarez-Curto, E., Inoue, A., Jenkins, L., Raihan, S. Z., Prihandoko, R., Tobin, A. B., & Milligan, G. (2016). Targeted Elimination of G Proteins and Arrestins Defines Their Specific Contributions to Both Intensity and Duration of G Protein-coupled Receptor Signaling. *The Journal of biological chemistry*, 291(53), 27147–27159.
- Andressen, K.W., Ulsund, A.H., Krobert, K.A., Lohse, M.J., Bünemann, M., & Levy, F.O. (2018). Related GPCRs couple differently to Gs: preassociation between G protein and 5-HT7 serotonin receptor reveals movement of Gas upon receptor activation. *FASEB J*, 32(2), 1059-1069.
- Ara, T., Tokoyoda, K., Sugiyama, T., Egawa, T., Kawabata, K., & Nagasawa, T. (2003). Long-term hematopoietic stem cells require stromal cell-derived factor-1 for colonizing bone marrow during ontogeny. *Immunity*, 19, 257–267.
- Arimont, M., Sun, S. L., Leurs, R., Smit, M., de Esch, I., & de Graaf, C. (2017). Structural Analysis of Chemokine Receptor-Ligand Interactions. *Journal of medicinal chemistry*, 60(12), 4735–4779.
- Armando, S., Quoyer, J., Lukashova, V., Maiga, A., Percherancier, Y., Heveker, N., ... Bouvier, M. (2014). The chemokine CXC4 and CC2 receptors form homo- and hetero-oligomers that can engage their signaling G-protein effectors and beta-arrestin. *FASEB J*, 28(10), 4509–4523.
- Attwood, T.K., & Findlay, J.B.C. (1994). Fingerprinting G-protein-coupled receptors. *Protein Engineering*, 7, 195–203.
- Babcock, G.J., Farzan, M., & Sodroski, J. (2003). Ligand-independent dimerization of CXCR4, a principal HIV-1 coreceptor. *J Biol Chem*, 278(5), 3378–85.
- Bachelerie, F., Ben-Baruch, A., Burkhardt, A.M., Combadiere, C., Farber, J.M., Graham, G.J., ... Zlotnik, A. (2014). International Union of Basic and Clinical Pharmacology. [corrected]. LXXXIX. Update on the extended family of chemokine receptors and introducing a new nomenclature for atypical chemokine receptors. *Pharmacological reviews*, 66(1), 1–79.

- Baker, E.N., & Baker, H.M. (2005). Molecular structure, binding properties and dynamics of lactoferrin. *Cell Mol Life Sci*, 62, 2531–2539.
- Baker, H.M., & Baker, E.N. (2012). A structural perspective on lactoferrin function. *Biochem. Cell Biol*, 90, 320–328.
- Balabanian, K., Lagane, B., Infantino, S., Chow, K.Y., Harriague, J., Moepps, B., ... Bachelier, F. (2005). The chemokine SDF-1/CXCL12 binds to and signals through the orphan receptor RDC1 in T lymphocytes. *J Biol Chem*, 280, 35760–35766.
- Balkwill, F. (2004). The significance of cancer cell expression of the chemokine receptor CXCR4. *Semin Cancer Biol*, 14, 171–9.
- Ballesteros, J.A., Shi, L. & Javitch, J.A. (2001). Structural mimicry in G protein-coupled receptors: implications of the high-resolution structure of rhodopsin for structure-function analysis of rhodopsin-like receptors. *Mol. Pharmacol*, 60, 1–19.
- Banisadr, G., Skrzydelski, D., Kitabgi, P., Rostene, W., & Parsadaniantz, S.M. (2003). Highly regionalized distribution of stromal cell-derived factor-1/CXCL12 in adult rat brain: constitutive expression in cholinergic, dopaminergic and vasopressinergic neurons. *European Journal of Neuroscience*, 18, 1593–1606.
- Beck, G.C., Rafat, N., Brinkkoetter, P., Hanusch, C., Schulte, J., Haak, M., ... Yard, B.A. (2006). Heterogeneity in lipopolysaccharide responsiveness of endothelial cells identified by gene expression profiling: role of transcription factors. *Clin Exp Immunol*, 143(3), 523–33.
- Bernhagen, J., Krohn, R., Lue, H., Gregory, J.L., Zernecke, A., Koenen, R.R., ... Weber, C. (2007). MIF is a noncognate ligand of CXC chemokine receptors in inflammatory and atherogenic cell recruitment. *Nat Med*, 13(5), 587–96.
- Bilgin, Y.M., & de Greef, G.E. (2016). Plerixafor for stem cell mobilization: the current status. *Curr Opin Hematol*, 23, 67–71.
- Bleul, C.C., Wu, L., Hoxie, J.A., Springer, T.A., & Mackay, C.R. (1997). The HIV co-receptors CXCR4 and CCR5 are differentially expressed and regulated on human T lymphocytes. *Proc Natl Acad Sci USA*, 94(5), 1925–30.
- Boldajipour, B., Mahabaleshwar, H., Kardash, E., Reichman-Fried, M., Blaser, H., Minina, S., ... Raz, E. (2008). Control of chemokine-guided cell migration by ligand sequestration. *Cell*, 132(3), 463–473.
- Bonham, L. W., Karch, C. M., Fan, C. C., Tan, C., Geier, E. G., Wang, Y., ... International Genomics of Alzheimer's Project (IGAP) (2018). CXCR4 involvement in neurodegenerative diseases. *Translational psychiatry*, 8(1), 73.
- Bridson, S.J., Kilpatrick, L.E., & Hill, S.J. (2018). Studying GPCR Pharmacology in Membrane Microdomains: Fluorescence Correlation Spectroscopy Comes of Age. *Trends Pharmacol Sci*, 39(2), 158–174.
- Buchanan, F.G., & DuBois, R.N. (2006). Emerging roles of beta-arrestins. *Cell Cycle*, 5(18), 2060-3.
- Bünemann, M., Bücheler, M.M., Philipp, M., Lohse, M.J., & Hein, L. (2001). Activation and deactivation kinetics of alpha 2A- and alpha 2C-adrenergic receptor-activated G protein-activated inwardly rectifying K<sup>+</sup> channel currents. *J Biol Chem*, 276(50), 47512–7.
- Bünemann, M., Frank, M., & Lohse, M.J. (2003). Gi protein activation in intact cells involves subunit rearrangement rather than dissociation. *PNAS*, 100(26), 16077–16082.
- Burg, J.S., Ingram, J.R., Venkatakrishnan, A. J., Jude, K.M., Dukkipati, A., Feinberg, E.N., ... Garcia, K.C. (2015). Structural biology. Structural basis for chemokine recognition and activation of a viral G protein-coupled receptor. *Science*, 347(6226), 1113–7.

- Burns, J.M., Summers, B.C., Wang, Y., Melikian, A., Berahovich, R., Miao, Z., ... Schall, T.J. (2006). A novel chemokine receptor for SDF-1 and I-TAC involved in cell survival, cell adhesion, and tumor development. *The Journal of experimental medicine*, 203(9), 2201–2213.
- Busillo, J.M., & Benovic, J.L. (2007). Regulation of CXCR4 signaling. *Biochim Biophys Acta*, 1768(4), 952–963.
- Busillo, J.M., Armando, S., Sengupta, R., Meucci, O., Bouvier, M., & Benovic, J.L. (2010). Site-specific phosphorylation of CXCR4 is dynamically regulated by multiple kinases and results in differential modulation of CXCR4 signaling. *The Journal of biological chemistry*, 285(10), 7805–17.
- Busnelli, M., Saulière, A., Manning, M., Bouvier, M., Galés, C., & Chini, B. (2012). Functional selective oxytocin-derived agonists discriminate between individual G protein family subtypes. *The Journal of biological chemistry*, 287(6), 3617–3629.
- Calebiro, D., Nikolaev, V.O., Gagliani, M.C., de Filippis, T., Dees, C., Tacchetti, C., ... Lohse, M.J. (2009). Persistent cAMP-signals triggered by internalized G-protein-coupled receptors. *PLoS Biol*, 7(8), e1000172.
- Calebiro, D., & Godbole, A. (2018). Internalization of G-protein-coupled receptors: Implication in receptor function, physiology and diseases. *Best Pract Res Clin Endocrinol Metab*, 32(2), 83–91.
- Carlson, J., Baxter, S.A., Dréau, D., & Nesmelova, I.V. (2013). The heterodimerization of platelet-derived chemokines. *Biochim Biophys Acta*, 1834(1), 158–68.
- Cartier, L., Hartley, O., Dubois-Dauphin, M., & Krause, K.H. (2005). Chemokine receptors in the central nervous system: role in brain inflammation and neurodegenerative diseases. *Brain Res Brain Res Rev*, 48(1), 16–42.
- Castro, M., Nikolaev, V.O., Palm, D., Lohse, M.J., & Vilardaga, J.P. (2005). Turn-on switch in parathyroid hormone receptor by a two-step parathyroid hormone binding mechanism. *Proc Natl Acad Sci USA*, 102, 16084–16089.
- Chatterjee, S., Behnam Azad, B., & Nimmagadda, S. (2014). The intricate role of CXCR4 in cancer. *Advances in cancer research*, 124, 31–82.
- Chen, J., Yao, Y., Gong, C., Yu, F., Su, S., Chen, J., ... Song, E. (2011). CCL18 from tumor-associated macrophages promotes breast cancer metastasis via PITPNM3. *Cancer cell*, 19(4), 541–555.
- Cheng, Z.J., Zhao, J., Sun, Y., Hu, W., Wu, Y.L., Cen, B., ... Pei, G. (2000). Beta-arrestin differentially regulates the chemokine receptor CXCR4-mediated signaling and receptor internalization, and this implicates multiple interaction sites between beta-arrestin and CXCR4. *J Biol Chem*, 275(4), 7.
- Chow, M.T., & Luster, A.D. (2014). Chemokines in cancer. *Cancer Immunol Res*, 2(12), 1125–31.
- Cody, C.W., Prasher, D.C., Westler, W.M., Prendergast, F.G., & Ward, W.W. (1993). Chemical structure of the hexapeptide chromophore of the Aequorea green-fluorescent protein. *Biochemistry*, 32(5), 1212–1218.
- Crown, S.E., Yu, Y., Sweeney, M.D., Leary, J.A., & Handel, T.M. (2006). Heterodimerization of CCR2 chemokines and regulation by glycosaminoglycan binding. *J Biol Chem*, 281(35), 25438–46.
- Crump, M.P., Gong, J.H., Loetscher, P., Rajarathnam, K., Amara, A., Arenzana-Seisdedos, F., ... Clark-Lewis, I. (1997). Solution structure and basis for functional activity of stromal cell-derived factor-1; dissociation of CXCR4 activation from binding and inhibition of HIV-1. *The EMBO journal*, 16(23), 6996–7007.
- Cutolo, P., Basdevant, N., Bernadat, G., Bachelier, F., & Ha-Duong, T. (2017). Interaction of chemokine receptor CXCR4 in monomeric and dimeric state with its endogenous ligand CXCL12: coarse-grained simulations identify differences. *J Biomol Struct Dyn*, 35(2), 399–412.

- Daiyasu, H., Nemoto, W., & Toh, H. (2012). Evolutionary Analysis of Functional Divergence among Chemokine Receptors, Decoy Receptors, and Viral Receptors. *Frontiers in microbiology*, 3, 264.
- Dambly-Chaudiere, C., Cubedo, N., & Ghysen, A. (2007). Control of cell migration in the development of the posterior lateral line: Antagonistic interactions between the chemokine receptors CXCR4 and CXCR7/RDC1. *BMC Developmental Biology*, 7, 23.
- Darash-Yahana, M., Pikarsky, E., Abramovitch, R., Zeira, E., Pal, B., Karplus, ... Peled, A. (2004). Role of high expression levels of CXCR4 in tumor growth, vascularization, and metastasis. *FASEB J*, 18, 1240–2.
- Décaillot, F.M., Kazmi, M.A., Lin, Y., Ray-Saha, S., Sakmar, T.P., & Sachdev, P. (2011). CXCR7/CXCR4 heterodimer constitutively recruits beta-arrestin to enhance cell migration. *The Journal of biological chemistry*, 286(37), 32188–97.
- DeWire, S.M., Ahn, S., Lefkowitz, R.J., & Shenoy, S.K. (2007). Beta-arrestins and cell signaling. *Annu Rev Physiol*, 69, 483–510.
- Donà, E., Barry, J.D., Valentin, G., Quirin, C., Khmelinskii, A., Kunze, A., ... Gilmour, D. (2013). Directional tissue migration through a self-generated chemokine gradient. *Nature*, 503, 285–289.
- Döring, Y., Pawig, L., Weber, C., & Noels, H. (2014). The CXCL12/CXCR4 chemokine ligand/receptor axis in cardiovascular disease. *Frontiers in physiology*, 5, 212.
- Downes, G.B., & Gautam, N. (1999). The G protein subunit gene families. *Genomics*, 62(3), 544–52.
- Drury, L.J., Ziarek, J.J., Gravel, S., Veldkamp, C.T., Takekoshi, T., Hwang, S.T., ... Dwinell, M.B. (2011). Monomeric and dimeric CXCL12 inhibit metastasis through distinct CXCR4 interactions and signaling pathways. *Proc Natl Acad Sci USA*, 108(43), 17655–60.
- El Moustaine, D., Granier, S., Doumazane, E., Scholler, P., Rahmeh, R., Bron, P., & Pin, J.P. (2012). Distinct roles of metabotropic glutamate receptor dimerization in agonist activation and G-protein coupling. *Proc Natl Acad Sci USA*, 109(40), 16342–16347.
- Esche, C., Stellato, C., & Beck, L.A. (2005). Chemokines: key players in innate and adaptive immunity. *J Invest Dermatol*, 125(4), 615–28.
- Feng, Y., Broder, C.C., Kennedy, P.E., & Berger, E.A. (1996). HIV-1 entry cofactor: functional cDNA cloning of a seven-transmembrane, G protein-coupled receptor. *Science*, 272(5263), 872–7.
- Fernandes, K.E., & Carter, D.A. (2017). The Antifungal Activity of Lactoferrin and Its Derived Peptides: Mechanisms of Action and Synergy with Drugs against Fungal Pathogens. *Frontiers in microbiology*, 8, 2.
- Ferrandon, S., Feinstein, T.N., Castro, M., Wang, B., Bouley, R., Potts, J.T., ... Vilardaga, J.P. (2009). Sustained cyclic AMP production by parathyroid hormone receptor endocytosis. *Nat Chem Biol*, 5(10), 734–42.
- Fong, A.M., Premont, R.T., Richardson, R.M., Yu, Y.R., Lefkowitz, R.J., & Patel, D.D. (2002). Defective lymphocyte chemotaxis in beta-arrestin2- and GRK6-deficient mice. *Proc Natl Acad Sci USA*, 99(11), 7478–83.
- Förster, R., Kremmer, E., Schubel, A., Breitfeld, D., Kleinschmidt, A., Nerl, C., ... Lipp, M. (1998). Intracellular and surface expression of the HIV-1 coreceptor CXCR4/fusin on various leukocyte subsets: rapid internalization and recycling upon activation. *J. Immunol*, 160, 1522–1531.
- Förster, T. (1948). Zwischenmolekulare Energiewanderung Und Fluoreszenz. *Annalen Der Physik*. 2, 55–75.
- Fredriksson, R., Lagerström, M.C., Lundin, L.G., & Schiöth, H.B. (2003). The G-protein-coupled receptors in the human genome form five main families: phylogenetic analysis, paralogon groups, and fingerprints. *Mol. Pharmacol*, 63, 1256–1272.

- Fukami, M., Suzuki, E., Igarashi, M., Miyado, M., & Ogata, T. (2018). Gain-of-function mutations in G-protein-coupled receptor genes associated with human endocrine disorders. *Clin Endocrinol*, 88(3), 351–359.
- Galés, C., Van Durm, J.J., Schaak, S., Pontier, S., Percherancier, Y., Audet, M., ... Bouvier, M. (2006). Probing the activation-promoted structural rearrangements in preassembled receptor-G protein complexes. *Nat Struct Mol Biol*, 13(9), 778–86.
- Gao, X., Abdelkarim, H., Albee, L. J., Volkman, B. F., Gaponenko, V., & Majetschak, M. (2018). Partial agonist activity of  $\alpha$ 1-adrenergic receptor antagonists for chemokine (C-X-C motif) receptor 4 and atypical chemokine receptor 3. *PloS one*, 13(9), e0204041.
- Gautier, A., Juillerat, A., Heinis, C., Correa, I.R.J., Kindermann, M., Beaufils, F., & Johnsson, K. (2008). An Engineered Protein Tag for Multiprotein Labeling in Living Cells. *Chem. Biol*, 15, 128–136.
- Ge, B., Lao, J., Li, J., Chen, Y., Song, Y., & Huang, F. (2017). Single-molecule imaging reveals dimerization/oligomerization of CXCR4 on plasma membrane closely related to its function. *Scientific reports*, 7(1), 16873.
- Gerrits, H., van Ingen Schenau, D.S., Bakker, N.E., van Disseldorp, A.J., Strik, A., Hermens, L.S., ... Gossen, J.A. (2008). Early postnatal lethality and cardiovascular defects in CXCR7-deficient mice. *Genesis*, 46(5), 235–45.
- Gibbons, J.A., Kanwar, J.R. & Kanwar, K.K. (2015). Iron-free and iron-saturated bovine lactoferrin inhibit survivin expression and differentially modulate apoptosis in breast cancer. *BMC Cancer*, 15.
- Glukhova, A., Draper-Joyce, C.J., Sunahara, R.K., Christopoulos, A., Wootten, D., & Sexton, P.M. (2018). Rules of engagement: GPCRs and G proteins. *ACS Pharmacology & Translational Science*, 1(2), 73–83.
- Gravel, S., Malouf, C., Boulais, P.E., Berchiche, Y. A., Oishi, S., Fujii, N., & Heveker, N. (2010). The peptidomimetic CXCR4 antagonist TC14012 recruits beta-arrestin to CXCR7: roles of receptor domains. *The Journal of biological chemistry*, 285(49), 37939–37943.
- Grundmann, M., Merten, N., Malfacini, D., Inoue, A., Preis, P., Simon, K., ... Kostenis, E. (2018). Lack of beta-arrestin signaling in the absence of active G proteins. *Nature communications*, 9(1), 341.
- Grushevskiy, E.O., Kukaj, T., Schmauder, R., Bock, A., Zabel, U., Schwabe, T., ... Lohse, M.J. (2019). Stepwise activation of a class C GPCR begins with millisecond dimer rearrangement. *Proc Natl Acad Sci USA*, 116, 10150–10155.
- Guidolin, D., Marcoli, M., Tortorella, C., Maura, G., & Agnati, L.F. (2019). Receptor-Receptor Interactions as a Widespread Phenomenon: Novel Targets for Drug Development?. *Frontiers in endocrinology*, 10, 53.
- Gupta, S.K., Lysko, P.G., Pillarisetti, K., Ohlstein, E., & Stadel, J.M. (1998). Chemokine receptors in human endothelial cells. Functional expression of CXCR4 and its transcriptional regulation by inflammatory cytokines. *J Biol Chem*, 273(7), 4282–7.
- Gupta, S.K., Pillarisetti, K., Thomas, R.A., & Aiyar, N. (2001). Pharmacological evidence for complex and multiple site interaction of CXCR4 with SDF-1 $\alpha$ : implications for development of selective CXCR4 antagonists. *Immunol Lett*, 78, 29–34.
- Gurevich, V.V., & Gurevich, E.V. (2019). GPCR Signaling Regulation: The Role of GRKs and Arrestins. *Frontiers in pharmacology*, 10, 125.
- Gustavsson, M., Wang, L., van Gils, N., Stephens, B. S., Zhang, P., Schall, T.J., ... Handel, T.M. (2017). Structural basis of ligand interaction with atypical chemokine receptor 3. *Nature communications*, 8, 14135.
- Guyon A. (2014). CXCL12 chemokine and its receptors as major players in the interactions between immune and nervous systems. *Frontiers in cellular neuroscience*, 8, 65.

- Halo, T.L., Appelbaum, J., Hobert, E.M., Balkin, D.M., & Schepartz, A. (2009). Selective Recognition of Protein Tetraserine Motifs with a Cell-Permeable, Pro-Fluorescent Bis-Boronic Acid. *J. Am. Chem. Soc*, 131, 438–439.
- Hammad, M.M., Kuang, Y.Q., Yan, R., Allen, H., & Dupré, D.J. (2010). Na<sup>+</sup>/H<sup>+</sup> exchanger regulatory factor-1 is involved in chemokine receptor homodimer CCR5 internalization and signal transduction but does not affect CXCR4 homodimer or CXCR4-CCR5 heterodimer. *The Journal of biological chemistry*, 285(45), 34653–64.
- Harmsen, M.C., Swart, P.J., de Béthune, M.P., Pauwels, R., De Clercq, E., The, T.H., & Meijer, D.K. (1995). Antiviral effects of plasma and milk proteins: lactoferrin shows potent activity against both human immunodeficiency virus and human cytomegalovirus replication in vitro. *J Infect Dis*, 172(2), 380–8.
- Hartmann, T.N., Grabovsky, V., Pasvolsky, R., Shulman, Z., Buss, E.C., Spiegel, A., ... Alon, R. (2008). A crosstalk between intracellular CXCR7 and CXCR4 involved in rapid CXCL12-triggered integrin activation but not in chemokine-triggered motility of human T lymphocytes and CD34<sup>+</sup> cells. *J Leukoc Biol*, 84(4), 1130–1140.
- Hasbi, A., Devost, D., Laporte, S.A., & Zingg, H.H. (2004). Real-time detection of interactions between the human oxytocin receptor and G protein-coupled receptor kinase-2. *Mol Endocrinol*, 18, 1277–1286.
- Hattermann, K., Held-Feindt, J., Lucius, R., Muerkoster, S.S., Penfold, M.E., Schall, T.J., & Mentlein, R. (2010). The Chemokine Receptor CXCR7 Is Highly Expressed in Human Glioma Cells and Mediates Antiapoptotic Effects. *Cancer Res*, 70(8), 3299–3308.
- Hauser, A.S., Chavali, S., Masuho, I., Jahn, L.J., Martemyanov, K.A., Gloriam, D.E., & Babu, M.M. (2018). Pharmacogenomics of GPCR Drug Targets. *Cell*, 172(1-2), 41–54.
- Hayasaka, H., Kobayashi, D., Yoshimura, H., Nakayama, E. E., Shioda, T., & Miyasaka, M. (2015). The HIV-1 Gp120/CXCR4 axis promotes CCR7 ligand-dependent CD4 T cell migration: CCR7 homo- and CCR7/CXCR4 hetero-oligomer formation as a possible mechanism for up-regulation of functional CCR7. *PLoS one*, 10(2), e0117454.
- Heesen, M., Berman, M.A., Charest, A., Housman, D., Gerard, C., & Dorf, M.E. (1998). Cloning and chromosomal mapping of an orphan chemokine receptor: mouse RDC1. *Immunogenetics*, 47(5), 364–70.
- Hein, P., Frank, M., Hoffmann, C., Lohse, M.J., & Bünemann, M. (2005). Dynamics of receptor/G protein coupling in living cells. *The EMBO journal*, 24(23), 4106–14.
- Hein, P., Rochais, F., Hoffmann, C., Dorsch, S., Nikolaev, V.O., Engelhardt, S., ... Bünemann, M. (2006). Gs activation is time-limiting in initiating receptor-mediated signaling. *J Biol Chem*, 281, 33345–33351.
- Hein, P., & Bünemann, M. (2009). Coupling mode of receptors and G proteins. *Naunyn Schmiedebergs Arch Pharmacol*, 379(5), 435–443.
- Hendrik Schmidt, J., Perslev, M., Bukowski, L., Stoklund, M., Herborg, F., Herlo, R., & Lindegaard Madsen, K. (2019). Constitutive internalization across therapeutically relevant GPCRs correlates with constitutive activity. *Basic Clin Pharmacol Toxicol*.
- Hesselgesser, J., Halks-Miller, M., DelVecchio, V., Peiper, S.C., Hoxie, J., Kolson, D.L., ... Horuk, R. (1997). CD4-independent association between HIV-1 gp120 and CXCR4: functional chemokine receptors are expressed in human neurons. *Curr Biol*, 7(2), 112–21.
- Heuninck, J., Perpiñá Viciano, C., İşbilir, A., Caspar, B., Capoferri, D., Briddon, S.J., Durroux, T., Hill, S.J., Lohse, M.J., Milligan, et al. (2019). Context-dependent signalling of CXC chemokine receptor 4 (CXCR4) and atypical chemokine receptor 3 (ACKR3). *Mol Pharmacol*, 96.

- Hlavackova, V., Goudet, C., Kniazeff, J., Zikova, A., Maurel, D., Vol, C., ... Blahos, J. (2005). Evidence for a single heptahelical domain being turned on upon activation of a dimeric GPCR. *The EMBO journal*, 24(3), 499–509.
- Hlavackova, V., Zabel, U., Frankova, D., Bätz, J., Hoffmann, C., Prezeau, L., ... Lohse, M.J. (2012). Sequential inter- and intrasubunit rearrangements during activation of dimeric metabotropic glutamate receptor 1. *Sci Signal*, 5(237), ra59.
- Hoffmann, C., Gaietta, G., Bünemann, M., Adams, S.R., Oberdorff-Maass, S., Behr, B., ... Lohse, M.J. (2005). A FIAsh-based FRET approach to determine G protein-coupled receptor activation in living cells. *Nat Methods*, 2(3), 171–176.
- Hoffmann, C., Gaietta, G., Zürn, A., Adams, S.R., Terrillon, S., Ellisman, M.H., ... Lohse, M.J. (2010). Fluorescent labeling of tetracysteine-tagged proteins in intact cells. *Nat Protoc*, 5, 1666–1677.
- Hoffmann, C., Nuber, S., Zabel, U., Ziegler, N., Winkler, C., Hein, P., ... Lohse, M.J. (2012) Comparison of the activation kinetics of the M3 Acetylcholine receptor and a constitutively active mutant receptor in living cells. *Molecular Pharmacology*, 82, 236–245.
- Hoffmann, F., Müller, W., Schütz, D., Penfold, M.E., Wong, Y.H., Schulz, S., & Stumm, R. (2012). Rapid uptake and degradation of CXCL12 depend on CXCR7 carboxyl-terminal serine/threonine residues. *The Journal of biological chemistry*, 287(34), 28362–77.
- Hughes, C.E., & Nibbs, R.J.B. (2018). A guide to chemokines and their receptors. *FEBS J*, 285, 2944-2971.
- Ikeda, Y., Kumagai, H., Skach, A., Sato, M., & Yanagisawa, M. (2013). Modulation of circadian glucocorticoid oscillation via adrenal opioid-CXCR7 signaling alters emotional behavior. *Cell*, 155(6), 1323–1336.
- Infantino, S., Moepps, B., & Thelen, M. (2006). Expression and regulation of the orphan receptor RDC1 and its putative ligand in human dendritic and B cells. *J Immunol*, 176(4), 2197–207.
- Insel, P.A., Tang, C.M., Hahntow, I., & Michel, M.C. (2007). Impact of GPCRs in clinical medicine: monogenic diseases, genetic variants and drug targets. *Biochim Biophys Acta*, 1768(4), 994–1005.
- Ioannidis, L.J., Nie, C.Q., & Hansen, D.S. (2014). The role of chemokines in severe malaria: more than meets the eye. *Parasitology*, 141(5), 602–13.
- Janssens, R., Struyf, S., & Proost, P. (2018). The unique structural and functional features of CXCL12. *Cellular & Molecular Immunology* volume, 15, 299–311.
- Jares-Erijman, E.A., & Jovin, T.M. (2003). FRET imaging. *Nature Biotechnology*, 21, 1387–1395.
- Jensen, J. B., Lyssand, J. S., Hague, C., & Hille, B. (2009). Fluorescence changes reveal kinetic steps of muscarinic receptor-mediated modulation of phosphoinositides and Kv7.2/7.3 K<sup>+</sup> channels. *The Journal of general physiology*, 133(4), 347–359.
- Jenssen, H., & Hancock, R.E. (2009). Antimicrobial properties of lactoferrin. *Biochimie*, 91(1), 19-29.
- Jorgensen, R., Kubale, V., Vrecl, M., Schwartz, T.W., & Elling, C.E. (2007). Oxyntomodulin differentially affects glucagon-like peptide-1 receptor  $\beta$ -arrestin recruitment and signaling through Gas. *J Pharmacol Exp Ther*, 322, 148–154.
- Jorgensen, R., Holliday, N.D., Hansen, J.L., Vrecl, M., Heding, A., Schwartz, T.W., & Elling, C.E. (2008). Characterization of G-protein coupled receptor kinase interaction with the neurokinin-1 receptor using bioluminescence resonance energy transfer. *Mol Pharmacol*, 73, 349–358.
- Jost, C.A., Reither, G., Hoffmann, C., & Schultz, C. (2008). Contribution of fluorophores to protein kinase C FRET probe performance. *ChemBiochem*, 9, 1379–1384.



- Juillerat, A., Gronemeyer, T., Keppler, A., Gendreizig, S., Pick, H., Vogel, H., & Johnsson, K. (2003). Directed Evolution of O6-Alkylguanine-DNA Alkyltransferase for Efficient Labeling of Fusion Proteins with Small Molecules in Vivo. *Chem. Biol*, 10, 313–317.
- Kalatskaya, I., Berchiche, Y.A., Gravel, S., Limberg, B.J., Rosenbaum, J.S., & Heveker, N. (2009). AMD3100 is a CXCR7 ligand with allosteric agonist properties. *Mol Pharmacol*, 75(5), 1240–7.
- Katancik, J.A., Sharma, A., & de Nardin, E. (2000). Interleukin 8, neutrophil-activating peptide-2 and GRO-alpha bind to and elicit cell activation via specific and different amino acid residues of CXCR2. *Cytokine*, 12(10), 1480–8.
- Kauk, M., & Hoffmann, C. (2018). Intramolecular and Intermolecular FRET Sensors for GPCRs- Monitoring Conformational Changes and Beyond. *Trends in Pharmacological Sciences*, 39(2), 123–135.
- Kenakin, T. (2004). Efficacy as a vector: the relative prevalence and paucity of inverse agonism. *Mol Pharmacol*, 65(1), 2-11.
- Kleemann, P., Papa, D., Vigil-Cruz, S., & Seifert, R. (2008). Functional reconstitution of the human chemokine receptor CXCR4 with G(i)/G(o)-proteins in Sf9 insect cells. *Naunyn-Schmiedeberg's archives of pharmacology*, 378(3), 261–74.
- Klein, K.R., Karpinich, N.O., Espenschied, S.T., Willcockson, H.H., Dunworth, W.P., Hoopes, S.L., & Caron, K.M. (2014). Decoy receptor CXCR7 modulates adrenomedullin-mediated cardiac and lymphatic vascular development. *Developmental cell*, 30(5), 528–540.
- Kleist, A.B., Getschman, A.E., Ziarek, J.J., Nevins, A.M., Gauthier, P.A., Chevigné, A., ... Volkman, B.F. (2016). New paradigms in chemokine receptor signal transduction: Moving beyond the two-site model. *Biochemical pharmacology*, 114, 53–68.
- Kniazeff, J., Saintot, P.P., Goudet, C., Liu, J., Charnet, A., Guillon, G., & Pin, J.P. (2004). Locking the dimeric GABA(B) G-protein-coupled receptor in its active state. *J Neurosci*, 24, 370–7.
- Kniazeff, J., Prézeau, L., Rondard, P., Pin, J.P., & Goudet, C. (2011). Dimers and beyond: The functional puzzles of class C GPCRs. *Pharmacol Ther*, 130(1), 9-25.
- Knierim, B., Hofmann, K. P., Ernst, O. P., & Hubbell, W. L. (2007). Sequence of late molecular events in the activation of rhodopsin. *Proc Natl Acad Sci USA*, 104(51), 20290–20295.
- Kochuveedu, S.T., & Kim, D.H. (2014). Surface plasmon resonance mediated photoluminescence properties of nanostructured multicomponent fluorophore systems. *Nanoscale*, 10.
- Kolakowski, L.F.J. (1994). GCRDb: a G-protein-coupled receptor database. *Receptors Channels*, 2, 1–7.
- Komolov, K.E. & Benovic, J.L. (2018). G protein-coupled receptor kinases: Past, present and future. *Cellular Signalling*, 41, 17–24.
- Krasel, C., Vilardaga, J.P., Bünemann, M., & Lohse, M.J. (2004). Kinetics of G-protein-coupled receptor signalling and desensitization. *Biochem Soc Trans*, 32, 1029–1031.
- Kristiansen, K. (2004). Molecular mechanisms of ligand binding, signaling, and regulation within the superfamily of G-protein-coupled receptors: molecular modeling and mutagenesis approaches to receptor structure and function. *Pharmacol Ther*, 103, 21–80.
- Kufareva, I., Stephens, B.S., Holden, L.G., Qin, L., Zhao, C., Kawamura, T., ... Handel, T.M. (2014). Stoichiometry and geometry of the CXC chemokine receptor 4 complex with CXC ligand 12: molecular modeling and experimental validation. *Proc Natl Acad Sci USA*, 111(50), E5363–72.

- Kufareva, I., Salanga, C.L. & Handel, T.M. (2015). Chemokine and chemokine receptor structure and interactions: implications for therapeutic strategies. *Immunol Cell Biol*, 93(4), 372–83.
- Kumar, A., Kremer, K.N., Dominguez, D., Tadi, M., & Hedin, K.E. (2011). Gα13 and Rho mediate endosomal trafficking of CXCR4 into Rab11+ vesicles upon stromal cell-derived factor-1 stimulation. *Journal of immunology*, 186(2), 951–8.
- Lacy, M., Kontos, C., Brandhofer, M., Hille, K., Gröning, S., Sinitski, D., ... Kapurniotu, A. (2018). Identification of an Arg-Leu-Arg tripeptide that contributes to the binding interface between the cytokine MIF and the chemokine receptor CXCR4. *Scientific reports*, 8(1), 5171.
- Lagane, B., Chow, K.Y., Balabanian, K., Levoye, A., Harriague, J., Planchenault, T., ... Bachelierie, F. (2008). CXCR4 dimerization and beta-arrestin-mediated signaling account for the enhanced chemotaxis to CXCL12 in WHIM syndrome. *Blood*, 112(1), 34–44.
- Lao, J., He, H., Wang, X., Wang, Z., Song, Y., Yang, B., ... Huang, F. (2017) Single-Molecule Imaging Demonstrates Ligand Regulation of the Oligomeric Status of CXCR4 in Living Cells. *J Phys Chem B*, 121(7), 1466–1474.
- Lash, J.A., Coates, T.D., Lafuze, J., Baehner, R.L., & Boxer, L.A. (1983). Plasma lactoferrin reflects granulocyte activation in vivo. *Blood*, 61(5), 885–8.
- Latorraca, N.R., Venkatakrisnan, A.J., & Dror, R.O. (2017). GPCR Dynamics: Structures in Motion. *Chem Rev*, 117(1), 139–155.
- Lavi, E., Kolson, D.L., Ulrich, A.M., Fu, L., & González-Scarano, F. (1998). Chemokine receptors in the human brain and their relationship to HIV infection. *J Neurovirol*, 4(3), 301–11.
- Leick, M., Catusse, J., Follo, M., Nibbs, R.J., Hartmann, T.N., Veelken, H., & Burger, M. (2010). CCL19 is a specific ligand of the constitutively recycling atypical human chemokine receptor *CRAM-B*. *Immunology*, 129(4), 536–46.
- Leng, L., Metz, C N., Fang, Y., Xu, J., Donnelly, S., Baugh, J., ... Bucala, R. (2003). MIF signal transduction initiated by binding to CD74. *The Journal of experimental medicine*, 197(11), 1467–76.
- Levoye, A., Balabanian, K., Baleux, F., Bachelierie, F., & Lagane, B. (2009). CXCR7 heterodimerizes with CXCR4 and regulates CXCL12-mediated G protein signaling. *Blood*, 113(24), 6085–6093.
- Leyton-Jaimes, M.F., Kahn, J., & Israelson, A. (2018). Macrophage migration inhibitory factor: A multifaceted cytokine implicated in multiple neurological diseases. *Exp Neurol*, 301(Pt B), 83–91.
- Libert, F., Parmentier, M., Lefort, A., Dumont, J.E., & Vassart, G. (1990). Complete nucleotide sequence of a putative G protein coupled receptor: RDC1. *Nucleic acids research*, 18(7), 1917.
- Lohse, M.J., Nikolaev, V.O., Hein, P., Hoffmann, C., Vilardaga, J.P., & Bünemann, M. (2008). Optical techniques to analyze real-time activation and signaling of G-protein-coupled receptors. *Trends Pharmacol Sci*, 29(3), 159–65.
- Lohse, M.J., Nuber, S., & Hoffmann, C. (2012). Fluorescence/bioluminescence resonance energy transfer techniques to study G-protein-coupled receptor activation and signaling. *Pharmacol Rev*, 64(2), 299–336.
- López-Cotarelo, P., Gómez-Moreira, C., Criado-García, O., Sánchez, L., & Rodríguez-Fernández, J.L. (2017). Beyond Chemoattraction: Multifunctionality of Chemokine Receptors in Leukocytes. *Trends Immunol*, 38(12), 927–941.
- Los, G.V., Encell, L.P., McDougall, M.G., Hartzell, D.D., Karassina, N., Zimprich, C., ... Wood, K.V. (2008). HaloTag: A Novel Protein Labeling Technology for Cell Imaging and Protein Analysis. *ACS Chem Biol*, 3, 373–382.

- Lourenco, S., Teixeira, V.H., Kalber, T., Jose, R.J., Floto, R.A., & Janes, S.M. (2015). Macrophage migration inhibitory factor-CXCR4 is the dominant chemotactic axis in human mesenchymal stem cell recruitment to tumors. *Journal of immunology*, 194(7), 3463–74.
- Ludeman, J.P., & Stone, M.J. (2014). The structural role of receptor tyrosine sulfation in chemokine recognition. *British journal of pharmacology*, 171(5), 1167–79.
- Luker, K.E., Gupta, M., Steele, J.M., Foerster, B.R., & Luker, G.D. (2009). Imaging ligand-dependent activation of CXCR7. *Neoplasia*, 11(10), 1022–1035.
- Luker, K.E., Steele, J.M., Mihalko, L.A., Ray, P., & Luker, G.D. (2010). Constitutive and chemokine-dependent internalization and recycling of CXCR7 in breast cancer cells to degrade chemokine ligands. *Oncogene*, 29(32), 4599–4610.
- Luker, K.E., Lewin, S.A., Mihalko, L.A., Schmidt, B.T., Winkler, J.S., Coggins, N.L., ... Luker, G.D. (2012). Scavenging of CXCL12 by CXCR7 promotes tumor growth and metastasis of CXCR4-positive breast cancer cells. *Oncogene*, 31, 4750–4758.
- Ma, Q., Jones, D., Borghesani, P. R., Segal, R. A., Nagasawa, T., Kishimoto, T., ... Springer, T.A. (1998). Impaired B-lymphopoiesis, myelopoiesis, and derailed cerebellar neuron migration in CXCR4- and SDF-1-deficient mice. *Proc Natl Acad Sci USA*, 95(16), 9448–9453.
- Mahoney, J.P., & Sunahara, R.K. (2016). Mechanistic insights into GPCR-G protein interactions. *Current opinion in structural biology*, 41, 247–254.
- Maier-Peuschel, M., Frölich, N., Dees, C., Hommers, L. G., Hoffmann, C., Nikolaev, V. O., & Lohse, M. J. (2010). A fluorescence resonance energy transfer-based M2 muscarinic receptor sensor reveals rapid kinetics of allosteric modulation. *The Journal of biological chemistry*, 285(12), 8793–8800.
- Makino, C.L., Wen, X.H., & Lem, J. (2003). Piecing together the timetable for visual transduction with transgenic animals. *Curr Opin Neurobiol*, 13, 404–412.
- Makita, S., & Tobinai, K. (2017). Mogamulizumab for the treatment of T-cell lymphoma. *Expert Opin Biol Ther*, 17, 1145–1153.
- Manglik, A., Kim, T.H., Masureel, M., Altenbach, C., Yang, Z., Hilger, D., ... Kobilka, B.K. (2015). Structural Insights into the Dynamic Process of  $\beta_2$ -Adrenergic Receptor Signaling. *Cell*, 161(5), 1101–1111.
- Miao, Z., Luker, K.E., Summers, B.C., Berahovich, R., Bhojani, M.S., Rehemtulla, A., ... Schall, T. J. (2007). CXCR7 (RDC1) promotes breast and lung tumor growth in vivo and is expressed on tumor-associated vasculature. *Proc Natl Acad Sci USA*, 104(40), 15735–40.
- Miller, R.J., Banisadr, G., & Bhattacharyya, B.J. (2008). CXCR4 signaling in the regulation of stem cell migration and development. *Journal of neuroimmunology*, 198(1-2), 31–8.
- Milligan, G., & Kostenis, E. (2006). Heterotrimeric G-proteins: a short history. *British journal of pharmacology*, 147, 46–55.
- Mischke, R., Kleemann, R., Brunner, H., & Bernhagen, J. (1998). Cross-linking and mutational analysis of the oligomerization state of the cytokine macrophage migration inhibitory factor (MIF). *FEBS Lett*, 427(1), 85–90.
- Mishra, R.K., Shum, A.K., Plataniias, L.C., Miller, R.J., & Schiltzb, G.E. (2016). Discovery and characterization of novel small-molecule CXCR4 receptor agonists and antagonists. *Sci Rep*, 6, 30155.
- Moll, N.M., & Ransohoff, R.M. (2010). CXCL12 and CXCR4 in bone marrow physiology. *Expert Rev Hematol*, 3(3), 315–22.

- Mona, C.E., Besserer-Offroy, E., Cabana, J., Leduc, R., Lavigne, P., Heveker, N., Marsault, & E. Escher, E. (2016). Design, synthesis and biological evaluation of CXCR4 ligands. *Org Biomol Chem*, 14, 10298-10311.
- Montecarlo, F.S., & Charo, I.F. (1996). The amino-terminal extracellular domain of the MCP-1 receptor, but not the RANTES/MIP-1 $\alpha$  receptor, confers chemokine selectivity. Evidence for a two-step mechanism for MCP-1 receptor activation. *J Biol Chem*, 271(32), 19084–92.
- Morand, E.F. (2005). New therapeutic target in inflammatory disease: macrophage migration inhibitory factor. *Intern Med J*, 35(7), 419–26.
- Mueller, W., Schütz, D., Nagel, F., Schulz, S., & Stumm, R. (2013). Hierarchical organization of multi-site phosphorylation at the CXCR4 C terminus. *PLoS one*, 8(5), e64975.
- Müller, A., Homey, B., Soto, H., Ge, N., Catron, D., Buchanan, M.E., ... Zlotnik, A. (2001). Involvement of chemokine receptors in breast cancer metastasis. *Nature*, 410, 50–6.
- Murphy, P.M., Baggiolini, M., Charo, I.F., Hébert, C.A., Horuk, R., Matsushima, K., ... Power, C.A. (2000). International union of pharmacology. XXII. Nomenclature for chemokine receptors. *Pharmacol Rev*, 52(1), 145–76.
- Nagasawa, T., Hirota, S., Tachibana, K., Takakura, N., Nishikawa, S., Kitamura, Y., ... Kishimoto, T. (1996). Defects of B-cell lymphopoiesis and bone-marrow myelopoiesis in mice lacking the CXC chemokine PBSF/SDF-1. *Nature*, 382, 635–8.
- Naumann, U., Cameroni, E., Pruenster, M., Mahabaleshwar, H., Raz, E., Zerwes, H. G., ... Thelen, M. (2010). CXCR7 functions as a scavenger for CXCL12 and CXCL11. *PLoS one*, 5(2), e9175.
- Nikolaev, V.O., Hoffmann, C., Bünemann, M., Lohse, M.J., & Vilardaga, J.P. (2006). Molecular basis of partial agonism at the neurotransmitter  $\alpha$ 2A-adrenergic receptor and Gi-protein heterotrimer. *J Biol Chem*, 281, 24506–24511.
- Nonaka, H., Tsukiji, S., Ojida, A., & Hamachi, I. (2007). Non-Enzymatic Covalent Protein Labeling Using a Reactive Tag. *J. Am. Chem. Soc*, 129, 15777–15779.
- Nuber, S., Zabel, U., Lorenz, K., Nuber, A., Milligan, G., Tobin, A. B., ... Hoffmann, C. (2016).  $\beta$ -Arrestin biosensors reveal a rapid, receptor-dependent activation/deactivation cycle. *Nature*, 531(7596), 661–4.
- Nuijens, J.H., Abbink, J.J., Wachtfogel, Y.T., Colman, R.W., Eerenberg, A.J., Dors, D., ... Hack, C.E. (1992). Plasma elastase  $\alpha$ 1-antitrypsin and lactoferrin in sepsis: evidence for neutrophils as mediators in fatal sepsis. *J Lab Clin Med*, 119(2), 159–68.
- Ödemis, V., Lipfert, J., Kraft, R., Hajek, P., Abraham, G., Hattermann, K., ... Engele, J. (2012). The presumed atypical chemokine receptor CXCR7 signals through G(i/o) proteins in primary rodent astrocytes and human glioma cells. *Glia*, 60(3), 372–381.
- Oldham, W.M., & Hamm, H.E. (2008). Heterotrimeric G protein activation by G-protein-coupled receptors. *Nature Reviews Molecular Cell Biology*, 9, 60–71.
- O'Reilly, C., Doroudian, M., Mawhinney, L., & Donnelly, S.C. (2016). Targeting MIF in Cancer: Therapeutic Strategies, Current Developments, and Future Opportunities. *Med Res Rev*, 36(3), 440–60.
- Pakianathan, D.R., Kuta, E.G., Artis, D.R., Skelton, N.J., & Hébert, C.A. (1997). Distinct but overlapping epitopes for the interaction of a CC-chemokine with CCR1, CCR3 and CCR5. *Biochemistry*, 36(32), 9642–8.
- Palmer, M. Biochemical Pharmacology, lecture notes, University of Waterloo. <http://watcut.uwaterloo.ca/webnotes/Pharmacology/downloads/pharma-notes.pdf>

- Patel, H.H., Murray, F., & Insel, P.A. (2008). G-protein-coupled receptor-signaling components in membrane raft and caveolae microdomains. *Handb Exp Pharmacol*, 186, 167–184.
- Pawig, L., Klasen, C., Weber, C., Bernhagen, J., & Noels, H. (2015). Diversity and Inter-Connections in the CXCR4 Chemokine Receptor/Ligand Family: Molecular Perspectives. *Frontiers in immunology*, 6, 429.
- Pello, O.M., Martínez-Muñoz, L., Parrillas, V., Serrano, A., Rodríguez-Frade, J.M., Toro, M.J., ... Mellado, M. (2008). Ligand stabilization of CXCR4/delta-opioid receptor heterodimers reveals a mechanism for immune response regulation. *Eur J Immunol*, 38(2), 537–549.
- Percherancier, Y., Berchiche, Y.A., Slight, I., Volkmer-Engert, R., Tamamura, H., Fujii, N., ... Heveker, N. (2005). Bioluminescence resonance energy transfer reveals ligand-induced conformational changes in CXCR4 homo- and heterodimers. *J Biol Chem*, 280(11), 9895–903.
- Philo, J.S., Yang, T.H., & LaBarre, M. (2004). Re-examining the oligomerization state of macrophage migration inhibitory factor (MIF) in solution. *Biophys Chem*, 108(1-3), 77–87.
- Poluri, K.M., Joseph, P.R., Sawant, K.V., & Rajarathnam, K. (2013). Molecular basis of glycosaminoglycan heparin binding to the chemokine CXCL1 dimer. *The Journal of biological chemistry*, 288(35), 25143–53.
- Qin, L., Kufareva, I., Holden, L.G., Wang, C., Zheng, Y., Zhao, C., ... Handel, T.M. (2015). Crystal structure of the chemokine receptor CXCR4 in complex with a viral chemokine. *Science*, 347, 1117–2210.
- Quoyer, J., Janz, J. M., Luo, J., Ren, Y., Armando, S., Lukashova, V., ... Bouvier, M. (2013). Peptidic targeting of the C-X-C chemokine receptor type 4 acts as a biased agonist favoring activation of the inhibitory G protein. *Proc Natl Acad Sci USA*, 110(52), E5088–97.
- Rajagopal, S., Kim, J., Ahn, S., Craig, S., Lam, C.M., Gerard, N.P., ... Lefkowitz, R.J. (2010). Beta-arrestin- but not G protein-mediated signaling by the "decoy" receptor CXCR7. *Proc Natl Acad Sci USA*, 107(2), 628–32.
- Rajasekaran, D., Gröning, S., Schmitz, C., Zierow, S., Drucker, N., Bakou, M., Kohl, K., ... Bernhagen, J. (2016). Macrophage Migration Inhibitory Factor-CXCR4 Receptor Interactions: EVIDENCE FOR PARTIAL ALLOSTERIC AGONISM IN COMPARISON WITH CXCL12 CHEMOKINE. *The Journal of biological chemistry*, 291(30), 15881–95.
- Ray, P., Lewin, S.A., Mihalko, L.A., Leshner-Perez, S.C., Takayama, S., Luker, K.E., & Luker, G.D. (2012a). Secreted CXCL12 (SDF-1) forms dimers under physiological conditions. *The Biochemical journal*, 442(2), 433–42.
- Ray, P., Mihalko, L. A., Coggins, N. L., Moudgil, P., Ehrlich, A., Luker, K. E., & Luker, G. D. (2012b). Carboxy-terminus of CXCR7 regulates receptor localization and function. *The international journal of biochemistry and cell biology*, 44(4), 669–78.
- Reiner, S., Ambrosio, M., Hoffmann, C., & Lohse, M.J. (2010). Differential signaling of the endogenous agonists at the beta2-adrenergic receptor. *The Journal of biological chemistry*, 285(46), 36188–36198.
- Rochais, F., Vilardaga, J.P., Nikolaev, V.O., Bünemann, M., Lohse, M.J., & Engelhardt, S. (2007). Real-time optical recording of beta1-adrenergic receptor activation reveals supersensitivity of the Arg389 variant to carvedilol. *J Clin Invest*, 117, 229–235.
- Rosenkilde, M.M., Gerlach, L.O., Jakobsen, J.S., Skerlj, R.T., Bridger, G.J., & Schwartz, T.W. (2004). Molecular mechanism of AMD3100 antagonism in the CXCR4 receptor: transfer of binding site to the CXCR3 receptor. *J Biol Chem*, 279, 3033–41.
- Saaber, S., Schütz, D., Miess, E., Abe, P., Desikan, S., Kumar, P.A., ... Stumm, R. (2019). ACKR3 Regulation of Neuronal Migration Requires ACKR3 Phosphorylation, but Not  $\beta$ -Arrestin. *Cell Reports*, 26, 1473–1488.

- Sadir, R., Imberty, A., Baleux, F., & Lortat-Jacob, H. (2004). Heparan sulfate/heparin oligosaccharides protect stromal cell-derived factor-1 (SDF-1)/CXCL12 against proteolysis induced by CD26/dipeptidyl peptidase IV. *J Biol Chem*, 279(42), 43854–60.
- Salazar, N., Muñoz, D., Kallifatidis, G., Singh, R.K., Jordà, M., & Lokeshwar, B.L. (2014). The chemokine receptor CXCR7 interacts with EGFR to promote breast cancer cell proliferation. *Mol Cancer*, 13, 198.
- Schiraldi, M., Raucci, A., Muñoz, L.M., Livoti, E., Celona, B., Venereau, E., ... Uguccioni, M. (2012). HMGB1 promotes recruitment of inflammatory cells to damaged tissues by forming a complex with CXCL12 and signaling via CXCR4. *The Journal of experimental medicine*, 209(3), 551–63.
- Schober, A., Bernhagen, J., & Weber, C. (2008). Chemokine-like functions of MIF in atherosclerosis. *J Mol Med*, 86(7), 761–70.
- Seifert, R., & Wenzel-Seifert, K. (2002). Constitutive activity of G-protein-coupled receptors: cause of disease and common property of wild-type receptors. *Naunyn Schmiedebergs Arch Pharmacol*, 366(5), 381–416.
- Shi, G., Partida-Sánchez, S., Misra, R. S., Tighe, M., Borchers, M.T., Lee, J.J., ... Lund, F.E. (2007). Identification of an alternative G $\alpha$ q-dependent chemokine receptor signal transduction pathway in dendritic cells and granulocytes. *The Journal of experimental medicine*, 204(11), 2705–18.
- Shi, X., Leng, L., Wang, T., Wang, W., Du, X., Li, J., ... Bucala, R. (2006). CD44 is the signaling component of the macrophage migration inhibitory factor-CD74 receptor complex. *Immunity*, 25(4), 595–606.
- Shimizu, S., Brown, M., Sengupta, R., Penfold, M.E., & Meucci, O. (2011). CXCR7 protein expression in human adult brain and differentiated neurons. *PLoS One*, 6(5), e20680.
- Sierro, F., Biben, C., Martínez-Muñoz, L., Mellado, M., Ransohoff, R.M., Li, M., ... Mackay, F. (2007). Disrupted cardiac development but normal hematopoiesis in mice deficient in the second CXCL12/SDF-1 receptor, CXCR7. *Proc Natl Acad Sci USA*, 104(37), 14759–64.
- Siqueiros-Cendón, T., Arévalo-Gallegos, S., Iglesias-Figueroa, B. F., García-Montoya, I. A., Salazar-Martínez, J., & Rascón-Cruz, Q. (2014). Immunomodulatory effects of lactoferrin. *Acta pharmacologica Sinica*, 35(5), 557–66.
- Soede, R.D., Zeelenberg, I.S., Wijnands, Y.M., Kamp, M., & Roos, E. (2001). Stromal cell-derived factor-1-induced LFA-1 activation during in vivo migration of T cell hybridoma cells requires Gq/11, RhoA, and myosin, as well as Gi and Cdc42. *J Immunol*, 166, 4293–4301.
- Sohy, D., Parmentier, M., & Springael, J.Y. (2007). Allosteric Transinhibition by Specific Antagonists in CCR2/CXCR4 Heterodimers. *J Biol Chem*, 282(41), 30062–30069.
- Sontag, J.M., Fykse, E.M., Ushkaryov, Y., Liu, J.P., Robinson, P.J., & Südhof, T.C. (1994). Differential expression and regulation of multiple dynamins. *J Biol Chem*, 269(6), 4547–54.
- Stumpf, A.D., & Hoffmann, C. (2015). Optical probes based on G protein-coupled receptors - added work or added value?. *British journal of pharmacology*, 173(2), 255–66.
- Sun, H.W., Bernhagen, J., Bucala, R., & Lolis, E. (1996). Crystal structure at 2.6-Å resolution of human macrophage migration inhibitory factor. *Proc Natl Acad Sci USA*, 93(11), 5191–6.
- Sungskaworn, T., Rieken, F., Lohse, M.J., & Calebiro, D. (2014). High-resolution spatiotemporal analysis of receptor dynamics by single-molecule fluorescence microscopy. *Journal of visualized experiments: JoVE*, (89), e51784.
- Sungskaworn, T., Jobin, M.L., Burnecki, K., Weron, A., Lohse, M.J., & Calebiro, D. (2017). Single-molecule imaging reveals receptor-G protein interactions at cell surface hot spots. *Nature*, 550(7677), 543–547.

- Suresh, P., & Wanchu, A. (2006). Chemokines and chemokine receptors in HIV infection: role in pathogenesis and therapeutics. *J Postgrad Med*, 52(3), 210–7.
- Szczuciński, A., & Losy, J. (2007). Chemokines and chemokine receptors in multiple sclerosis. Potential targets for new therapies. *Acta Neurol Scand*, 115(3), 137–46.
- Szekanecz, Z., Vegvari, A., Szabo, Z., & Koch, A.E. (2010). Chemokines and chemokine receptors in arthritis. *Front Biosci*, 2, 153–67.
- Szpakowska, M., Dupuis, N., Baragli, A., Counson, M., Hanson, J., Piette, J., & Chevigné, A. (2016). Human herpesvirus 8-encoded chemokine vCCL2/vMIP-II is an agonist of the atypical chemokine receptor ACKR3/CXCR7. *Biochem Pharmacol*, 114, 14–21.
- Szpakowska, M., Meyrath, M., Reynders, N., Counson, M., Hanson, J., Steyaert, J., & Chevigné, A. (2018). Mutational analysis of the extracellular disulphide bridges of the atypical chemokine receptor ACKR3/CXCR7 uncovers multiple binding and activation modes for its chemokine and endogenous non-chemokine agonists. *Biochem Pharmacol*, 153, 299–309.
- Tachibana, K., Hirota, S., Iizasa, H., Yoshida, H., Kawabata, K., Kataoka, Y., ... Nagasawa, T. (1998). The chemokine receptor CXCR4 is essential for vascularization of the gastrointestinal tract. *Nature*, 393, 591–594.
- Takayama, Y., Aoki, R., Uchida, R., Tajima, A., & Aoki-Yoshida, A. (2016). Role of CXC chemokine receptor type 4 as a lactoferrin receptor. *Biochem Cell Biol*, 95(1), 57–63.
- Tan, W., Martin, D., & Gutkind, J.S. (2006) The Gα13-Rho Signaling Axis Is Required for SDF-1-induced Migration through CXCR4. *J Biol Chem*, 281(51), 39542–39549.
- Tham, T.N., Lazarini, F., Franceschini, I.A., Lachapelle, F., Amara, A., & Dubois-Dalq, M. (2001). Developmental pattern of expression of the alpha chemokine stromal cell-derived factor 1 in the rat central nervous system. *Eur J Neurosci*, 13(5), 845–56.
- Tian, H., Fürstenberg, A., & Huber, T. (2017). Labeling and Single-Molecule Methods To Monitor G Protein-Coupled Receptor Dynamics. *Chem. Rev*, 117, 186–245.
- Torossian, F., Anginot, A., Chabanon, A., Clay, D., Guerton, B., Desterke, C., ... Le Bousse-Kerdilès, M.C. (2014). CXCR7 participates in CXCL12-induced CD34+ cell cycling through β-arrestin-dependent Akt activation. *Blood*, 123(2), 191-202.
- Tripathi, A., Vana, P. G., Chavan, T. S., Brueggemann, L. I., Byron, K. L., Tarasova, N. I., ... Majetschak, M. (2015). Heteromerization of chemokine (C-X-C motif) receptor 4 with α1A/B-adrenergic receptors controls α1-adrenergic receptor function. *Proc Natl Acad Sci USA*, 112(13), E1659–E1668.
- Ulvmar, M.H., Hub, E., & Rot, A. (2011). Atypical chemokine receptors. *Exp Cell Res*, 317(5), 556–568.
- Uy, G.L., Rettig, M.P., & Cashen, A.F. (2008). Plerixafor, a CXCR4 antagonist for the mobilization of hematopoietic stem cells. *Expert Opin Biol Ther*, 8(11), 1797–804.
- Valenti, P., & Antonini, G. (2005). Lactoferrin: an important host defence against microbial and viral attack. *Cell Mol Life Sci*, 62(22), 2576–87.
- Valentin, G., Haas, P., & Gilmour, D. (2007). The Chemokine SDF1a Coordinates Tissue Migration through the Spatially Restricted Activation of CXCR7 and CXCR4b. *Curr Biol*, 17(12), 1026–1031.
- Van der Strate, B.W., Beljaars, L., Molema, G., Harmsen, M.C., & Meijer, D.K. (2001). Antiviral activities of lactoferrin. *Antiviral Res*. 52(3), 225–39.

- Van Unen, J., Stumpf, A.D., Schmid, B., Reinhard, N.R., Hordijk, P.L., Hoffmann, ... Goedhart, J. (2016). A New Generation of FRET Sensors for Robust Measurement of Gai1, Gai2 and Gai3 Activation Kinetics in Single Cells. *PLoS ONE*, 11(1), e0146789.
- Veerapathiran, S. & Wohland, T. (2018). Fluorescence techniques in developmental biology. *J Biosci*, 43(3), 541–553.
- Vila-Coro, A.J., Rodríguez-Frade, J.M., Martín De Ana, A., Moreno-Ortiz, M.C., Martínez-A, C., & Mellado, M. (1999). The chemokine SDF-1alpha triggers CXCR4 receptor dimerization and activates the JAK/STAT pathway. *FASEB J*, 13(13), 1699–1710.
- Vilardaga, J.P., Bünemann, M., Krasel, C., Castro, M., & Lohse, M.J. (2003). Measurement of the millisecond activation switch of G protein-coupled receptors in living cells. *Nat Biotechnol*, 21, 807–812.
- Vilardaga, J.P., Nikolaev, V.O., Lorenz, K., Ferrandon, S., Zhuang, Z., & Lohse, M.J. (2008). Conformational cross-talk between  $\alpha_{2A}$ -adrenergic and  $\mu$ -opioid receptors controls cell signaling. *Nat Chem Biol*, 4, 126–131.
- Vilardaga, J.P., Bünemann, M., Feinstein, T.N., Lambert, N., Nikolaev, V.O., Engelhardt, S., ... Hoffmann, C. (2009). GPCR and G proteins: drug efficacy and activation in live cells. *Molecular endocrinology*, 23(5), 590–9.
- Vilardaga, J.P., Agnati, L.F., Fuxe, K., & Ciruela, F. (2010). G-protein-coupled receptor heteromer dynamics. *Journal of cell science*, 123(24), 4215–20.
- Vilardaga J.P. (2011a). Recording kinetics of adrenergic receptor activation in live cells. *Current topics in membranes*, 67, 101–111.
- Vilardaga J.P. (2011b). Studying ligand efficacy at G protein-coupled receptors using FRET. *Methods in molecular biology (Clifton, N.J.)*, 756, 133–148.
- Waadt, R., Schlücking, K., Schroeder, J.I., & Kudla, J. (2014). Protein fragment bimolecular fluorescence complementation analyses for the in vivo study of protein-protein interactions and cellular protein complex localizations. *Methods in molecular biology*, 1062, 629–658.
- Walenkamp, A.M.E., Lapa, C., Herrmann, K. & Wester, H.J. (2017). CXCR4 Ligands: The Next Big Hit?. *J Nucl Med*, 58, 77S-82S.
- Wang, H., Beaty, N., Chen, S., Qi, C.F., Masiuk, M., Shin, D.M., & Morse, H.C. 3rd (2012). The CXCR7 chemokine receptor promotes B-cell retention in the splenic marginal zone and serves as a sink for CXCL12. *Blood*, 119(2), 465–468.
- Wang, J., He, L., Combs, C.A., Roderiquez, G., & Norcross, M.A. (2006). Dimerization of CXCR4 in living malignant cells: control of cell migration by a synthetic peptide that reduces homologous CXCR4 interactions. *Mol Cancer Ther*, 5(10), 2474–2483.
- Wang, J., Shiozawa, Y., Wang, J., Wang, Y., Jung, Y., Pienta, K.J., ... Taichman, R.S. (2008). The role of CXCR7/RDC1 as a chemokine receptor for CXCL12/SDF-1 in prostate cancer. *J Biol Chem*. 283(7), 4283–94.
- Wang, J.F., Liu, Z.Y., & Gropman, J.E. (1998). The alpha-chemokine receptor CXCR4 is expressed on the megakaryocytic lineage from progenitor to platelets and modulates migration and adhesion. *Blood*, 92, 756–764.
- Wang, J.F., Park, I.W., & Gropman, J.E. (2000) Stromal cell-derived factor-1alpha stimulates tyrosine phosphorylation of multiple focal adhesion proteins and induces migration of hematopoietic progenitor cells: roles of phosphoinositide-3 kinase and protein kinase C. *Blood*, 8, 2505–2513.
- Watts, A.O., van Lipzig, M.M., Jaeger, W.C., Seeber, R.M., van Zwam, M., Vinet, J., ... Vischer, H.F. (2013). Identification and profiling of CXCR3-CXCR4 chemokine receptor heteromer complexes. *British journal of pharmacology*, 168(7), 1662–74.



- Wescott, M.P., Kufareva, I., Paes, C., Goodman, J.R., Thaker, Y., Puffer, B.A., ... Doranz, B.J. (2016). Signal transmission through the CXCR4 chemokine receptor 4 (CXCR4) transmembrane helices. *Proc Natl Acad Sci USA*, 113(35), 9928–33.
- Whorton, M.R., Jastrzebska, B., Park, P.S., Fotiadis, D., Engel, A., Palczewski, K., & Sunahara, R.K. (2007). Efficient coupling of transducin to monomeric rhodopsin in a phospholipid bilayer. *The Journal of biological chemistry*, 283(7), 4387–94.
- Woollard, S.M., & Kanmogne, G.D. (2015). Maraviroc: a review of its use in HIV infection and beyond. *Drug Des Devel Ther*, 9, 5447–5468.
- Wright, S.C., Alonso Cañizal, M.C., Benkel, T., Simon, K., Le Gouill, C., Matricon, P., ... Hoffmann, C. (2018). FZD5 is a Gαq-coupled receptor that exhibits the functional hallmarks of prototypical GPCRs. *Sci. Signal*, 11, eaar5536.
- Wu, B., Chien, E.Y., Mol, C.D., Fenalti, G., Liu, W., Katritch, V., ... Stevens, R.C. (2010). Structures of the CXCR4 chemokine GPCR with small-molecule and cyclic peptide antagonists. *Science*, 330(6007), 1066–71.
- Yagi, H., Tan, W., Dillenburg-Pilla, P., Armando, S., Amornphimoltham, P., Simaan, M., ... Gutkind, J.S. (2011). A synthetic biology approach reveals a CXCR4-G13-Rho signaling axis driving transendothelial migration of metastatic breast cancer cells. *Science signaling*, 4(191), ra60.
- Yang, F., Moss, L.G., & Phillips, G.N.J. (1996). The molecular structure of green fluorescent protein. *Nat Biotechnol*, 14(10), 1246–51.
- Zabel, B.A., Wang, Y., Lewén, S., Berahovich, R.D., Penfold, M.E., Zhang, P., ... Schall, T.J. (2009). Elucidation of CXCR7-mediated signaling events and inhibition of CXCR4-mediated tumor cell transendothelial migration by CXCR7 ligands. *J Immunol*, 183(5), 3204-11.
- Zhang, X.C., Liu, J., & Jiang, D. (2014). Why is dimerization essential for class-C GPCR function? New insights from mGluR1 crystal structure analysis. *Protein & cell*, 5(7), 492–495.
- Zhao, H., Guo, L., Zhao, H., Zhao, J., Weng, H., & Zhao, B. (2015). CXCR4 over-expression and survival in cancer: a system review and meta-analysis. *Oncotarget* 6, 5022–5040.
- Zheng, Y., Han, G.W., Abagyan, R., Wu, B., Stevens, R.C., Cherezov, V., ... Handel, T.M. (2017). Structure of CC Chemokine Receptor 5 with a Potent Chemokine Antagonist Reveals Mechanisms of Chemokine Recognition and Molecular Mimicry by HIV. *Immunity*, 46(6), 1005–1017.
- Ziegler, N., Bätz, J., Zabel, U., Lohse, M.J., & Hoffmann, C. (2011). FRET-based sensors for the human M(1)-, M(3)-, and M(5)-acetylcholine receptors. *Bioorg Med Chem*, 19, 1048–1054.
- Zlotnik, A., & Yoshie, O. (2000). Chemokines: a new classification system and their role in immunity. *Immunity*, 12(2), 121–7.
- Zou, Y.R., Kottmann, A.H., Kuroda, M., Taniuchi, I., & Littman, D.R. (1998). Function of the chemokine receptor CXCR4 in haematopoiesis and in cerebellar development. *Nature*, 393, 595–9.
- Zürn, A., Zabel, U., Vilardaga, J.P., Schindelin, H., Lohse, M.J., & Hoffmann, C. (2009). Fluorescence resonance energy transfer analysis of alpha 2a-adrenergic receptor activation reveals distinct agonist-specific conformational changes. *Mol Pharmacol*, 75(3), 534-41.

## 8. CURRICULUM VITAE

**Name:** Cristina Perpiñá Viciano

**Nationality:** Spanish

**Date of birth:** 09.09.1991

**Place of birth:** Valencia (Spain)

---

### RESEARCH EXPERIENCE

---

- **PhD graduate student at Institute of Pharmacology, University of Würzburg, Germany**  
 September 2015 - December 2018  
 Supervisors: Prof. Dr. Carsten Hoffmann, Prof. Dr. Elke Butt-Dörje, Prof. Dr. Martin J. Lohse  
 Fellowship: Marie Curie, Initial Training Network "ONCORNET"  
  
 Title of PhD thesis: Study of the activation mechanisms of the CXC chemokine receptor 4 (CXCR4) and the atypical chemokine receptor 3 (ACKR3).
- **Visiting PhD student at Vrije University, Amsterdam, The Netherlands**  
 January 2018 - February 2018  
 Supervisor: Prof. Dr. Martine J. Smit
- **Research student at Centre for Molecular Biology Severo Ochoa, CSIC, Madrid, Spain**  
 January 2015 - August 2015  
 Supervisor: Prof. Dr. Luis Blanco, Dr. Guillermo Sastre-Moreno  
  
 Project: Influence of the metal cofactors Mn<sup>2+</sup> and Mg<sup>2+</sup> on the activity of PrimPol primase/polymerase.
- **Research internship at Australian Centre for Plant Functional Genomics, University of Adelaide, Adelaide, Australia**  
 February 2014 - July 2014  
 Supervisor: Prof. Dr. Diane Mather  
  
 Project: Molecular mapping of markers linked to Cre8 locus in wheat. Resistance to the nematode *Heterodera avenae*.
- **Research student at University of Valencia, Valencia, Spain**  
 September 2013 - January 2014  
 Supervisor: Prof. Dr. Marcel·lí del Olmo  
  
 Project: Development of new systems of Yeast Surface Display.
- **Research internship at University of Salford, Manchester, United Kingdom**  
 June 2012 - August 2012  
 Supervisor: Prof. Dr. Rhoderick Elder  
  
 Project: Characterization of DNA glycosylases from the Neil-like (NEIL) family involved in DNA repair.

---

**EDUCATION**

---

- **Master degree in Molecular and Cell Biology** | September 2014 - July 2015  
Autonomous University of Madrid (Spain)  
Ramón Areces Foundation Fellowship 2014/2015
- **Degree in Biotechnology** | September 2009 - July 2014  
University of Valencia (Spain)  
International Program Fellowship | University of Adelaide (Australia) | February 2014 - August 2014  
Erasmus Fellowship | University of Salford (Manchester, UK) | September 2011 - August 2012

---

**SKILLS**

---

- **Language skills**
  - Spanish - Native language
  - Catalan - Native language
  - English - Advanced
  - French - Basic
  - German - Basic

- **Organizational skills**

Supervision of visiting PhD students during their research stay in the University of Würzburg.

Supervision in Pharmacology exams for students of Pharmacy and Biomedicine at the University of Würzburg.

Collaboration in the organization of the ONCORNET symposium 2018 (Amsterdam, The Netherlands).

---

Date and signature

---

**PUBLICATIONS**

---

1. Calvo, P.A., Sastre-Moreno, G., **Perpiñá, C.**, Guerra, S., Martínez-Jiménez, M.I., & Blanco, L. (2019). The invariant glutamate of human PrimPol DxE motif is critical for its Mn<sup>2+</sup>-dependent distinctive activities. *DNA Repair*, 77, 65–75.
2. Heuninck, J\*., **Perpiñá Viciano, C\***., Işbilir, A\*. Caspar, B., Capoferri, D., Briddon, S.J., Durroux, T., Hill, S.J., Lohse, M.J., Milligan, G., Pin, J.P., & Hoffmann, C. (2019). Context-dependent signalling of CXC chemokine receptor 4 (CXCR4) and atypical chemokine receptor 3 (ACKR3). *Mol Pharmacology*, 96. \*Shared first authorship.
3. Adlere, I., Sun, S., Zarca, A., Roumen, L., Gozelle, M., **Perpiñá Viciano C.**, Caspar, B., Arimont, M., Bebelman, J.P., Briddon, S.J., Hoffmann, C., Hill, S.J., Smit, M.J., Vischer, H.F., Wijtmans, M., de Graaf, C., de Esch, I.J.P., & Leurs, R. (2018). Structure-based exploration and pharmacological evaluation of N-substituted piperidin-4-yl-methanamine CXCR4 chemokine receptor antagonists. *Eur J Med Chem*, 162, 631–649.
4. Oehler B., Mohammadi M., **Perpiñá Viciano C.**, Hackel D., Hoffmann C., Brack A., & Rittner HL. (2017). Peripheral Interaction of Resolvin D1 and E1 with Opioid Receptor Antagonists for Antinociception in Inflammatory Pain in Rats. *Front Mol Neurosci*, 10.
5. **Perpiñá, C.**, Vinaixa, J., Andreu, C., & del Olmo, M. (2014). Development of new tolerant strains to hydrophilic and hydrophobic organic solvents by the yeast surface display methodology. *Appl Microbiol Biotechnol*, 99, 775–789.

## 9. ACKNOWLEDGMENTS

This journey would not have been possible without the support of my supervisors, colleagues, family, and friends. Firstly, I would like to express my gratitude to my primary supervisor Prof. Dr. Carsten Hoffmann for giving me the opportunity to perform the PhD in his group, for his supervision and advice during these years and for establishing interesting collaborations with other labs that have helped me grow as a researcher. Thanks to Prof. Dr. Martin J. Lohse for recruiting me for being part of ONCORNET, for his feedback during each of our meetings and for the valuable discussions about this project. Thanks to Prof. Dr. Elke Butt-Dörje for being always available to review the developments made in this project, for providing feedback, and for our collaboration. All of you transmitted me enthusiasm and encourage me to pursue this project.

I would also like to thank all former and present members of the AG Hoffmann group for sharing this experience with me. Special thanks to Dr. Consuelo Alonso Cañizal for her friendship and constant support, for endless discussions, for reviewing this thesis, and for sharing so many experiences and memories with me. Thanks to Nelly Rüttiger for her help translating the “Zusammenfassung” and Nicole Ziegler for her help in the lab. Thanks to Dr. Ulrike Zabel for her continuous support in cloning techniques and Christine Salomon for her assistance in administrative matters.

I am very grateful to all the members of ONCORNET, from whom I have learned so much. The personal and professional relationships forged in these years will stay with me forever, as well as the good times we spent together throughout Europe. I would like to thank all the people I had the chance to collaborate with during this time, allowing me to contribute into their projects or helping me make this project grow. Special thanks to Prof. Dr. Martine Smit and Aurélien Zarca for their time, support and assistance during my stay in their lab in Amsterdam, for our collaboration and for sharing plasmids that have been used in this thesis. Thanks to Prof. Dr. Rob Leurs and Ilze Adlere for our various collaborations and for providing ACKR3 agonists that have been used in this thesis. Thanks to Françoise Bachelerie and Carmen Gallego for sharing plasmids used in this project. Also, thanks to Prof. Dr. Steve Hill, Prof. Dr. Steve Briddon, Birgit Caspar and Laura Kilpatrick for their collaboration.

I wish to thank my family for their unconditional support and encouragement throughout this learning journey, for their advice and for believing in me. *Gràcies a la meua família, especialment als meus pares i al meu germà, pel suport incondicional durant tot aquest període d'aprenentatge. Pels vostres consells i per creure en mi inclús quan jo no podia.* Last, special thanks to Ben for following me in this adventure and for being always by my side.

The author acknowledges the use of the following figures in this thesis:

- Figures 7 and 10 of this thesis are modified from Figure 1 of the following publication:  
Pawig, L., Klasen, C., Weber, C., Bernhagen, J., and Noels, H. (2015). Diversity and Inter-Connections in the CXCR4 Chemokine Receptor/Ligand Family: Molecular Perspectives. *Frontiers in immunology*, 6, 429.  
<https://www.frontiersin.org/articles/10.3389/fimmu.2015.00429/full#h1>  
Copyright: © 2015 Pawig, Klasen, Weber, Bernhagen and Noels. Open-access article distributed under the terms of the Creative Commons Attribution License (CC BY).
- Figure 5 of this thesis is reproduced from Figure 2 of the following publication:  
Hughes, C.E., and Nibbs, R.J.B. (2018). A guide to chemokines and their receptors. *FEBS J.*  
<https://febs.onlinelibrary.wiley.com/doi/full/10.1111/febs.14466>  
Copyright: © 2018 Hughes and Nibbs. Open access article under the terms of the Creative Commons Attribution License (CC BY 4.0).
- Figures 20 and 34 of this thesis have been adapted from GPCRdb database (<http://www.gpcrdb.org>).

Required permissions for the use of the following figures in this thesis were obtained via RightsLink:

- Figure 2 of this thesis has been adapted from Figure 2 of the following publication with permission.  
"Reprinted (adapted) with permission from (Glukhova, A., Draper-Joyce, C.J., Sunahara, R.K., Christopoulos, A., Wootten, D., & Sexton, P.M. (2018). Rules of engagement: GPCRs and G proteins. *ACS Pharmacology & Translational Science*, 1(2), 73–83). Copyright (2018) American Chemical Society."
- Figure 9 of this thesis has been adapted from Figure 1 of the following publication with permission.  
From [Wu, B., Chien, E.Y., Mol, C.D., Fenalti, G., Liu, W., Katritch, V., ... Stevens, R.C. (2010). Structures of the CXCR4 chemokine GPCR with small-molecule and cyclic peptide antagonists. *Science*, 330(6007), 1066–71.]. Reprinted with permission from AAAS."
- Figure 11 of this thesis has been adapted from Figure 2 of the following publication with permission.  
Republished with permission of Biochemistry and cell biology, from [A structural perspective on lactoferrin function, Heather M. Baker and Edward N. Baker, 90, 2012]; permission conveyed through Copyright Clearance Center, Inc.
- Figure 14A of this thesis has been adapted from Figure 1 of the following publication with permission.  
Adapted by permission from Springer Nature Customer Service Centre GmbH: Springer Nature, Nature Methods; A FIAsh-based FRET approach to determine G protein-coupled receptor activation in living cells; Carsten Hoffmann, Guido Gaietta, Moritz Bünemann, Stephen R Adams, Silke Oberdorff-Maass, Björn Behr, Jean-Pierre Vilardaga, Roger Y Tsien, Mark H Ellisman & Martin J Lohse. Copyright (2005).